Geochemical Characterization of Groundwaters, Surface Waters and Water-Rock Interaction in an Area of Continuous Permafrost Adjacent to the Greenland Ice Sheet, Kangerlussuaq, Southwest Greenland

by

Emily Henkemans

A thesis
presented to the University of Waterloo
in fulfillment of the
thesis requirement for the degree of
Doctor of Philosophy
in
Earth Sciences

Waterloo, Ontario, Canada, 2016

AUTHOR'S DECLARATION

I hereby declare that I am the sole author of this thesis. This is a true copy of the thesis, including any required final revisions, as accepted by my examiners.

I understand that my thesis may be made electronically available to the public.

Abstract

Continental scale glaciations, such as those that covered much of Canada and Northern Europe during the last glacial maximum (26,000 to 19,000 y BP), can be expected to cause large disturbances to both the surficial and subsurface environments. The Greenland Ice Sheet (GrIS) provides a modern, natural analogue for past continental scale glaciations, allowing the extent and nature of the impact on ground and surface waters in the vicinity of the ice sheet to be studied. Currently, geochemical and isotopic information concerning groundwater chemistry and movement adjacent to a continental scale ice sheet is very limited. In areas of continuous permafrost, available knowledge is based on springs, open pingos and fluids from underground openings such as mines. Properly instrumented boreholes can provide additional insight into geochemical processes affecting groundwaters in cryogenic environments next to ice sheets.

As part of the Greenland Analogue Project (GAP), three deep, inclined boreholes were drilled in crystalline bedrock in the Kangerlussuaq Region of southwest Greenland and two of these were successfully instrumented with sampling systems: i) Borehole DH-GAP01 intercepting a talik beneath a lake located less than 2 km from the Greenland ice sheet; and ii) Borehole DH-GAP04 was completed adjacent to the ice sheet in order to sample groundwaters from the bedrock below the ice. Drill core from the GAP boreholes was used to study fracture mineralogy, matrix pore fluids and whole rock chemistry. Geochemical studies were conducted on the borehole groundwaters and aimed to determine the depth of meltwater penetration beneath the ice sheet and the relative impact of cryogenic processes such as in-situ freeze out versus water-rock interaction on groundwater salinity. Surface water studies, including lakes and meltwaters in the Kangerlussuaq region, were also undertaken. Understanding the role of taliks, unfrozen conduits through the permafrost, in the groundwater system was an important goal of both surface and groundwater studies.

Groundwater discharge significant enough to impact lake chemistry was not observed in any of the lakes studied, suggesting little groundwater-surface water interaction occurs in the study area. Recharge conditions between lakes and the groundwater system could also be an ongoing process and therefore help explain the lack of observable groundwater discharge into lakes. Evaporation is a key process impacting surface water chemistry. Lakes had enriched $\delta^{18}O/\delta^{2}H$

isotopic signatures and fall along local evaporation lines. Consistent with previous work (e.g. Blum & Erel, 1995) on increased biotite weathering in glaciated environments, $^{87}Sr/^{86}Sr$ isotopic ratios were found to be more radiogenic (>0.73) in lakes in more recently glaciated terrain. In more recently deglaciated areas, sulfide oxidation was the main source of sulfur (as sulfate) in lakes, while the influence of marine aerosols and bacterial sulfate reduction increased further away from the ice sheet around Søndre Strømfjord.

Groundwater sampled beneath the margin of the ice sheet (DH-GAP04) had highly depleted isotopic signatures ($\delta^{18}O$ -23.5 to -24.4‰), similar to values observed for some regional meltwaters (-23.4 to -30.5‰). Meltwater recharging beneath the ice evolves from dilute Ca, Na, K-HCO_3 type waters to the brackish Ca-Na-SO_4 waters observed in the DH-GAP04 borehole. Gypsum is found as a ubiquitous fracture and rock matrix infilling in some borehole sections and has an isotopic composition of 3.2 to 10.7‰($\delta^{34}S_{SO4}$), 4.5 to 9.1‰ ($\delta^{18}O_{SO4}$) and $^{87}Sr/^{86}Sr$ ratios of 0.7022 to 0.7093. Recharging meltwater interacts with gypsum resulting in groundwaters with SO_4^{2-} concentrations up to 1880 mg/L and groundwaters had similar isotopic signatures to fracture infillings: $\delta^{34}S_{SO4}$ (4.5 to 5.0‰), $\delta^{18}O_{SO4}$ (2.9 to 5.9‰) and $^{87}Sr/^{86}Sr$ (0.7033 to 0.7075). The origin of the gypsum is believed to be due to an older hydrothermal event and not related to solute exclusion during freezing of fracture and matrix fluids. The continued presence of such a soluble mineral phase suggest that ice sheet induced meltwater circulation has not disturbed large sections of the rock matrix porosity and parts of the groundwater system sufficiently to dissolve gypsum and activate gypsum sealed fractures. Isotopic evidence for bacterial sulfate reduction was not observed. Groundwater from the talik lake borehole had a more enriched isotopic signature ($\delta^{18}O$ -21.6‰) than the deeper groundwaters obtained from DH-GAP04, reflecting mixing with evaporatively enriched surface water. Solute exclusion due to permafrost formation was not observed to impact groundwater or matrix porewater chemistry.

A perennially flowing spring located at the front of nearby Leverett Glacier was found to be geochemically unique from the borehole groundwaters. The source of the spring water could not be confirmed but was isotopically enriched (average $\delta^{18}O$ -18.5‰) relative to meltwaters and the borehole groundwaters. High abundances of rare earth elements in the spring waters suggest a higher temperature origin for the spring.

Acknowledgements

As part of the Greenland Analogue Project, I had the assistance of many great colleagues. I will have very fond memories of my time spent in Kangerlussuaq with Timo Ruskeeniemi, Lillemor Claesson Liljedahl, Anne Lehtinen, Jon Engström, Knud-Eric Klint and many others associated with the GAP. I will be forever thankful for the opportunity to work in such a beautiful and amazing place as Greenland. Thanks to Emma Johansson, Tobias Lindborg and team GRASP for your help with everything around Two Boat Lake and giving me access to the tube wells. Thanks to Rickard Pettersson for your work at Leverett, even though the spring remains a bit of a mystery.

I would like to thank the Nuclear Waste Management Organization (NWMO) for financial support both for the GAP as well as for an Industrial NSERC and additional project funding. I would also like to thank those at NWMO with whom I had the opportunity to work in the field and whom also provided valuable feedback on my thesis chapters: Monique Hobbs, Sarah Hirschorn, Jennifer McKelvie and Laura Kennell.

I would like to thank everyone who read the groundwater and lakes chapters and gave valuable feedback including those at NWMO mentioned above as well as Lillemor, Anne, Timo, Petteri Pitkanen, Mark Jensen and Ignasi Puigdomenech. I would like to give a separate acknowledgement of the help of John Anderson for his assistance with Chapter 2, including fieldwork, sending me old samples and giving me access to lake chemistry datasets.

There are numerous people to thank at the University of Waterloo. First, everyone at the Environmental Isotope Laboratory with a special mention to Rhys Gwynne. Sue Fisher and Lorraine Albrecht in the office for putting up with Shaun and I. Richard Elgood for helping me with many random requests. Bill Annable for coming to Greenland on a moment's notice and being of great help in the field there. Bob Ingleton and Paul Johnson for all your assistance with field equipment and generally just being great, helpful guys. Lori Labelle for being a great friend and office mate and helping me stay sane through this process. I would especially like to thank Mike Makahnouk for all the strontium analyses and for helping with many other jobs along the way. Cameron Drever was also invaluable in running samples through the SELFRAG machine. Thanks to my committee, Dave Rudolph, Ed Sudicky, and Bill Annable for your help, feedback and constructive comments.

Thanks to my parents for all the support through this degree, I really can't thank you enough. Lots of thanks, appreciation and love to Jim, Max and Clara for hanging in there with me. Thanks for your love and support through this. Thanks to Dom for being my friend and digital office mate.

A big thanks to my supervisor Shaun Frape for all the adventures in Greenland, conferences and travel and for slogging your way through all the thesis edits. Thanks for always being available to answer my questions and for giving me the opportunity to work on such an interesting project.

I am thankful to all the GAP partners, NWMO, Canada, Posiva Oy, Finland and Svensk Kärnbränslehantering AB (SKB), Sweden, for planning and funding this crazy project to drill next to an ice sheet. Additional funding was provided by a Natural Sciences and Engineering Research Council (NSERC) grant to Shaun Frape and an Industrial NSERC to Emily Henkemans. I also appreciate the additional assistance from the Bob Farvolden Scholarship.

Table of Contents

AUTHOR'S DECLARATION ..... **ii**

Abstract ..... **iii**

Acknowledgements ..... **v**

Table of Contents ..... **vii**

List of Figures ..... **xii**

List of Tables ..... **xvii**

Chapter 1 Introduction **1**

1.1 Introduction 1

1.2 Background on Hydrogeology and Geochemistry in Cryogenic Environments 6

1.3 Detailed site Description 8

1.3.1 Location 8

1.3.2 Climate 8

1.3.3 Regional Geology 9

1.3.4 Permafrost and Glacial History 11

1.4 Methods 13

1.4.1 Description of Site Activities 13

1.4.2 Description of Drilling and Borehole Instrumentation 13

1.4.3 Geochemical and Isotopic Methods 18

1.5 Borehole Lithology, Fracture Systems and Hydrogeology 19

1.5.1 DH-GAP01 Lithology and Fracture Systems 20

1.5.2 DH-GAP03 Lithology and Fracture Systems 20

1.5.3 DH-GAP04 Lithology and Fracture Systems 21

1.5.4 Hydrogeology Background 21

1.5.5 DH-GAP01 Hydrogeology 22

1.5.6 DH-GAP04 Hydrogeology 25

1.5.7 Leverett Spring 28

1.6 Contributions 28

Chapter 2 Geochemical Characterization of Lakes in the Kangerlussuaq Region,Southwest Greenland: An Isotopic Approach 31
2.1 Introduction 31
2.2 Background on Lake Chemistry in Cold Climates 35
2.3 Study Area 37
2.4 Methods 38
2.4.1 Geochemical and Isotopic Analyses 40
2.5 Results 41
2.5.1 Geochemical Results 41
2.5.2 Isotopic Results 44
2.6 Discussion 49
2.6.1 Evaporation and Salts 50
2.6.2 Permafrost and Shallow Groundwater Flow 57
2.6.3 Weathering and Water Rock Interaction 60
2.6.4 Sulfur Oxidation and Reduction 64
2.6.4.1 Oxidation of Sulfides 65
2.6.4.2 Sulfate Reduction and Marine Sulfate 68
2.6.4.3 Bedrock Gypsum 71
2.6.5 Aeolian Inputs 72
2.6.6 Marine Influence 72
2.6.7 Evidence for Deep Groundwater Discharge 74
2.7 Conclusions 75
Chapter 3 Geochemical Characterization of Groundwaters in an Area of Continuous Permafrost Adjacent to the Greenland Ice Sheet, Kangerlussuaq, Southwest Greenland 78
3.1 Introduction 78
3.2 Study Area 81
3.2.1 Geology 81
3.2.2 Permafrost 82
3.3 Methods 83
3.3.1 Surface Water Sampling 83

3.3.2 Boreholes 83
3.3.3 Isotopic and Geochemical Analyses 86
3.3.4 Fracture Mineral Analyses 86
3.3.5 Gas Sampling at Leverett 86
3.4 Results 87
3.4.1 Isotopic Results 87
3.4.2 Geochemical Results 90
3.5 Discussion 94
3.5.1 Oxygen-18 and Deuterium 94
3.5.1.1 Leverett Spring 94
3.5.1.2 Groundwater and Taliks 96
3.5.1.3 Meltwater Infiltration 98
3.5.1.4 In Situ Freezing and Cryogenic Concentration 100
3.5.2 Sulfur Concentrations and Isotopic Signatures 101
3.5.3 Calcium, Sodium and Strontium Concentrations and Isotopic Signatures 103
3.5.4 Bromine and Chlorine Concentrations and Isotopic Signatures 106
3.5.5 Hydrogeology 109
3.5.5.1 DH-GAP01 110
3.5.5.2 DH-GAP04 110
3.5.5.3 Leverett Spring 111
3.6 Summary, Conceptual Model and Conclusions 112
3.6.1 Evolution of Groundwater Salinity 112
3.6.2 Meltwater Infiltration 113
3.6.3 Conceptual Model 114
3.6.4 Leverett Spring 116
3.6.5 Key Conclusions 116
Chapter 4 Water Rock Interaction in the Bedrock Subsurface Adjacent to the Greenland Ice Sheet, Kangerlussuaq, Southwest Greenland 118
4.1 Introduction 118
4.2 Methods 120

4.3 Results 121
4.3.1 Rock Matrix: Chemical and Isotopic Composition and Mineralogy 121
4.3.1.1 Major Elements 121
4.3.1.2 Trace Elements 123
4.3.1.3 Mineralogical Investigations 125
4.3.1.4 Isotopic Results 128
4.3.2 Fracture Mineral Observations, Chemistry and Isotopic Composition 129
4.3.2.1 Chemical and Isotopic Composition of Gypsum 132
4.3.3 Matrix Porewater Composition 135
4.3.3.1 DH-GAP04 Out diffusion 135
4.3.3.2 DH-GAP01, DH-GAP03 and DH-GAP04 Crush and Leach 140
4.3.3.3 Isotopic Results 146
4.4 Discussion 150
4.4.1 Cold Climate Conditions and In-Situ Freeze-Out Background 150
4.4.2 Evidence for Freeze-Out in the GAP Study Area 153
4.4.2.1 Isotopic Evidence 153
4.4.2.2 Depth Profiles in Boreholes 155
4.4.2.3 Precipitation of Secondary Mineral Phases 156
4.4.3 Gypsum: Hydrothermal Origins and Impact on Groundwater Chemistry 157
4.4.3.1 Rare Earth Elements 159
4.4.3.2 Strontium Background and Whole Rock Strontium Isotopic Composition 161
4.4.3.3 Strontium Isotopic Composition of Gypsum 164
4.4.3.4 Sulfur and Oxygen Isotopic Composition of Gypsum 165
4.4.3.5 Impact of Gypsum Dissolution and Sulfide Oxidation on Groundwater 167
4.4.4 Matrix Porewaters and Water Rock Interaction 169
4.5 Summary and Conclusions 174
5. Conclusions 177
References 181
Appendix A. Analytical Data Quality Assesment 203
Appendix B. Geochemical and Isotopic Datasets 207

Appendix C. Drill Core Investigation Methods 278

Appendix D.X-Ray Diffraction Patterns 297

List of Figures

Figure 1.1. Map overview of the Greenland Analogue Project study area. (a) The location of Kangerlussuaq in the southwest of Greenland. (b) a topographic map showing the GAP borehole locations and the key land terminated lobes of the Greenland Ice Sheet found in the study area. (b) A geological map of the study area adapted from Klint et al. (2013). 2

Figure 1.2 (a) The Nagssugtoqidian orogen (orange) and the location of map in (b) are displayed on a map of Greenland. (b) Regional geology of southwest Greenland and outline of the study area. Adapted from Garde and Hollis (2010) and Klint et al. (2013). 11

Figure 1.3 Glacial history of the study area from the last glacial maximum (LGM) (a). The ice extent during stages 3 and 4 are shown in (b). Adapted from Funder et al. (2011). 12

Figure 1.4 Map of the study area showing all surface water sampling and field measurement locations. 14

Figure 1.5. Schematic of the borehole DH-GAP01 which was drilled at an angle to intercept the talik beneath a large lake (Lake L26). Figure from Harper et al. (2015a)..... 16

Figure 1.6 (a) Equipment installed in the DH-GAP04 borehole. (b) Orientation and deflection of the DH-GAP04 drill hole and its position relative to the ice margin of Isunnguata Sermia. Aerial photo is from 2006. (c) Schematic of the DH-GAP04 borehole showing depths of important features as meters borehole length (m BHL) on the left and as elevations on the right. Figures (a) and (b) are adapted from Harper et al. (2015a). 17

Figure 1.7 Record of fluid pressure (barometrically corrected), electrical conductivity (µS/cm divided by100) and temperature (°C) from downhole sensors in DH-GAP01 presented as daily averages from June 2009 to August 2013. From Harper et al. (2015a)..... 23

Figure 1.8. A comparison of hydraulic head (meters relative to top of casing (TOC)) in DH-GAP01 compared to water level in Lake L26 (Harper et al., 2015a). Lake level data was provided by Johansson et al., (2015). 24

Figure 1.9. Daily average hydraulic heads (m.a.s.l.) in the DH-GAP04 sampling intervals (upper, mid and lower) compared to surface meltwater runoff from the Kangerlussuaq sector of the Greenland ice sheet (Hasholt et al., 2012; van As et al., 2012; Mikkelsen, 2014; Harper et al., 2015a). 26

Figure 1.10. Daily average hydraulic heads (m.a.s.l.) in the DH-GAP04 sampling sections. 27

Figure 1.11. Photos depicting the Leverett Spring at various times of the year. 29

Figure 2.1. (a) Location of study area in the south west of Greenland. (b) Transect of studied lakes extending to coast. (c) Map detailing sampling locations (a) and (b) are adapted from Anderson and Brodersen (2001). 32

Figure 2.2. (a) Isotopic composition of lakes with local evaporation lines adapted from Leng and Anderson (2003) and local meteoric water lines for Grönnedal and Thule. (b) Isotopic composition of lakes compared to groundwaters and meltwaters from Kangerlussuaq Region. 45

Figure 2.3. Map of tube well locations around L26 (Talik Lake). The wells, along with a comprehensive meteorological and hydrological data set, are described in Johansson et al. (2014 and 2015). 46

Figure 2.4. Salt crusts observed covering vegetation near Lake L32 (Store Saltsø). 52

Figure 2.5. Comparing the meq of Na^+ to Cl^- shows most lakes fall along a 1:1 equilibrium line indicative of marine and/or terrestrial halite dissolution. 53

Figure 2.6. (a) $\delta^{37}Cl$ compared to $\delta^{18}O$ isotopic composition. $\delta^{81}Br$ values compared to (b) $\delta^{18}O$ isotopic values and (c) $\delta^{37}Cl$ isotopic values. 54

Figure 2.7. Relationship between Na/Ca ratios compared to Cl/SO_4 ratios indicates the relative importance of processes such as sulfate reduction, sulfide oxidation and $CaCO_3$ precipitation. 56

Figure 2.8. Oxygen-18 of lake waters versus (a) electrical conductivity and (b) tritium. 58

Figure 2.9. The $^{87}Sr/^{86}Sr$ signature of lakes increases towards the ice sheet where weathering of biotite becomes increasingly important. 62

Figure 2.10. Comparison of the ratio of (Mg+K)/Na to $^{87}Sr/^{86}Sr$ isotope ratios for all lake types. The ratio of Mg^{2+} and K^{+} to Na^{+} increases with increasingly radiogenic $^{87}Sr/^{86}Sr$ isotopic ratios. 63

Figure 2.11. (a) the isotopic composition ($\delta^{34}S$ and $\delta^{18}O$) of sulfate in lakes and groundwaters as well as gypsum found as a fracture mineral in the bedrock. (b) A comparison of the $\delta^{34}S$ of sulfate in lakes to the Cl/SO_4 ratio. 66

Figure 2.12. The $\delta^{18}O$ isotopic composition of sulfate ($\delta^{18}O_s$) derived from the oxidation of sulfides. 67

Figure 2.13. Comparison of sulfate concentrations and $\delta^{34}S$ (SO_4) in lakes with Rayleigh distillation curves for enrichment in $\delta^{34}S$ due to bacterial sulfate reduction. 70

Figure 3.1.(a) Outline of Greenland indicating the town of Kangerlussuaq as well as locations where springs and open pingos have been studied. (b) Locations of GAP boreholes, the Leverett Spring and lakes L25 (Drilling Water Lake) and L26 (Talik Lake). (c) Study area geology modified from Engström and Klint (2014) 79

Figure 3.2. $\delta^{18}O$ and $\delta^{2}H$ of ground and surface waters. The local meteoric water line for Grønnedal is also included. 88

Figure 3.3. Piper plot showing ground and surface water ionic compositions. 91

Figure 3.4. A comparison of $\delta^{18}O$ isotopic values and chloride concentrations in ground and surface waters studied for the GAP compared to Canadian and Fennoscandian shield brines. 98

Figure 3.5. $\delta^{34}S$ and $\delta^{18}O$ isotopic composition of SO_4^{2-} in groundwaters, surface waters and fracture fillings 102

Figure 3.6. (a) $^{87}Sr/^{86}Sr$ isotopic ratios compared to sulfate concentrations (b) Groundwater Sr^{2+} vs SO_4^{2-} concentrations. 105

Figure 3.7. Meq ratios of Br/Cl and Na/Cl for ground and surface waters. 107

Figure 3.8. Chloride concentrations and isotopic composition for groundwaters and surface waters. 108

Figure 3.9. Conceptual model of groundwater evolution based on the DH-GAP01 and DH-GAP04 boreholes. 114

Figure 4.1. Lithological composition of DH-GAP01, DH-GAP03 and DH-GAP04 boreholes. Adapted from Pere (2015). 121

Figure 4.2. Chemical composition of the rock with depth in the DH-GAP04 borehole with the borehole log for comparison. 122

Figure 4.3. Chondrite normalized REE composition of DH-GAP04 rock matrix. 124

Figure 4.4. Eu and Ce anomalies and La/Lu with depth for rock matrix (coded by rock type) and fracture gypsum. 125

Figure 4.5. A selection of images from Eichinger and Waber (2013) shows the presence of gypsum in pore space and microfractures within the rock matrix. 127

Figure 4.6. A selection of photographs of fracture infillings in DH-GAP01. 131

Figure 4.7. (a) Chondrite normalized REE profiles of DH-GAP04 fracture gypsum. (b) Chondrite normalized REE profiles for hydrothermal anhyrite samples (Morgan & Wandless, 1980) and gypsum from the Eye Dashwa Lakes pluton (Mungall et al., 1987). 133

Figure 4.8. Porewater concentrations of SO_4^{2-} and Cl^- based on crush and leach experiments in DH-GAP01, DH-GAP03 and DH-GAP04. 142

Figure 4.9. Changes in porewater ion concentrations with depth in DH-GAP01 based on crush and leach experiments. 143

Figure 4.10. Changes in porewater ion concentrations with depth in DH-GAP03 based on crush and leach experiments. 144

Figure 4.11. Changes in porewater ion concentrations with depth in DH-GAP04 based on crush and leach experiments. 145

Figure 4.12. Chloride concentrations in porewaters in DH-GAP04 based on (a) out diffusion experiments (b) crush and leach experiments. 146

Figure 4.13. The isotopic composition ($\delta^{34}S$ and $\delta^{18}O$) of sulfate in porewaters, groundwaters and fracture filling gypsum. 148

Figure 4.14. $\delta^{37}Cl$ isotopic composition of porewaters, groundwaters and fracture gypsum with depth in DH-GAP04. 155

Figure 4.15. Groundwater REE profiles for boreholes and Leverett Spring compared to intermediate and felsic rock compositions. 160

Figure 4.16. Evolution of the $^{87}Sr/^{86}Sr$ signature over time for a granitic rock and its major mineral phases. From McNutt et al. (1990). 162

Figure 4.17. Strontium isotopic composition of DH-GAP04 for (a) whole rock, altered wall rock and gypsum, (b) porewaters and (c) groundwaters. 163

Figure 4.18. The range of potential isotopic values for $\delta^{18}O$ (SO_4) derived from oxidation of sulfides and the corresponding % of sulfate in groundwater derived from oxidation of sulfides. 168

Figure 4.19. Br/Cl vs Na/Cl ratios in groundwaters and porewaters, categorized by lithology. 170

Figure 4.20. Isotopic composition and concentration of chloride in groundwater, surface waters and porewaters. 173

List of Tables

Table 1.1. Regional tectonic history of the Kangerlussuaq region adapted from Wilson et al. (2006) and Klint et al. (2013). 10

Table 1.2. Results of Posiva Flow Log and hydraulic testing in the DH-GAP01 and DH-GAP04 boreholes. 25

Table 2.1. Summary (min, max, average) of major geochemical and isotopic results for lake water groups. 42

Table 2.2. Summary of representative chemistry and isotopic results for lake waters. 43

Table 2.3. Summary of results from ice-dammed lake (L38) springs and from lake L38. 44

Table 2.4. $^{87}Sr/^{86}Sr$ ratios for waters from soil pipes installed around Lake L26 (SS903). The pipes were installed along drainage routes into (A to C) and out of (D) the lake (Johansson et al., 2014). 47

Table 2.5. Results of $\delta^{37}Cl$ and $\delta^{81}Br$ analyses on lakes and borehole groundwaters. 48

Table 2.6. Isotopic composition and concentration of sulfate in surface waters and groundwaters. Sulfate minerals (predominantly gypsum) from fracture infillings and sulfide minerals from the rock matrix are included from the DH-GAP01 and DH-GAP04 cores. 49

Table 3.1. Lengths and depth of the three sampling sections of the borehole DH-GAP04 and the locations of corresponding pressure, temperature and conductivity sensors. .. 85

Table 3.2. Isotopic composition of groundwaters and of the Talik Lake(L26) and Lake L25. 90

Table 3.3. Chemistry of groundwaters and relevant surface waters. 92

Table 3.4. Range of isotopic composition for fracture filling gypsum and rock matrix sulfides. 93

Table 3.5. Composition of gas samples from the Leverett Spring. 93

Table 3.6. Isotopic composition of two gas samples from the Leverett Spring in 2011. 94

Table 4.1. Summary of analyses and methods performed on drill core from DH-GAP01, DH-GAP03 and DH-GAP04. 120

Table 4.2. Average chemical compositions for each major rock type in DH-GAP04. Chemistry of mafic, intermediate and felsic rock types from crystalline rock environments from Frape et al. (2014)(adapted from Hyndman, 1985) is given for comparison. 123

Table 4.3. Mineralogical composition of selected samples representative of the rock types found in borehole DH-GAP04 based on XRD results. 126

Table 4.4. Summary of whole rock mineralogy adapted from Eichinger and Waber (2013).... 128

Table 4.5. $^{87}Sr/^{86}Sr$ isotopic signatures for whole rock and mineral separates from GAP boreholes (DH-GAP01, DH-GAP03 and DH-GAP04). 129

Table 4.6. Summary of the occurrence of fracture infilling minerals in the GAP boreholes. Data from Pere, 2014. 130

Table 4.7. Fracture Filling XRD results for fracture filling mineral samples from a selection of DH-GAP04 fracture depths. 132

Table 4.8. Isotopic composition for $\delta^{34}S$, $\delta^{18}O$ and $^{87}Sr/^{86}Sr$ of fracture filling gypsum from DH-GAP01 and DH-GAP04. 134

Table 4.9. Major cation and anion concentrations in fracture filling mineral samples dissolved in ultrapure water expressed per mg of dissolved solid material. The major mineral dissolved was gypsum. 135

Table 4.10. Summary of calculated porewater Cl^- and Br^- concentrations in 4 sections of DH-GAP04 core (Eichinger and Waber, 2013). 136

Table 4.11. Major element chemistry of the final eluate solution from out diffusion experiments and crush and leach analyses on core previously used for GAP04-E to -H out diffusion experiments. 138

Table 4.12. Calculated porewater concentrations of Cl^- in GAP04-A to -H. 140

Table 4.13. Porewater chemistry based on crush and leach experiments on DH-GAP01, DH-GAP03 and DH-GAP04. 141

Table 4.14. Isotopic results for out diffusion experiments on DH-GAP04 core and crush and leach experiments performed on GAP04 E to GAP04 H after completion of the out diffusion experiments. 147

Table 4.15. Isotopic results from crush and leach experiments performed on DH-GAP01, DH-GAP03 and DH-GAP04 core. 149

1. Introduction

1.1. Introduction

Continental scale glaciations, such as those that covered much of Canada and Northern Europe during the last glacial maximum (26,000 to 19,000 y BP), can be expected to cause large disturbances to both the surficial and subsurface environments. The Greenland Ice Sheet (GrIS) provides a modern analogue with which to examine the effects of continental scale glaciations on surface and groundwater geochemistry. Periglacial conditions, the unique characteristics of glacial sediments, cold climate, and large volumes of meltwater effect the evolution of lakes in the vicinity of an ice sheet. The groundwater system can likewise experience strong perturbations during glaciation. Ice may be kilometers thick, causing isostatic depression. The weight of the ice on the subglacial meltwater system may induce a strong hydraulic pressure gradient with the potential to increase advective flow rates under and adjacent to the ice sheet (Piotrowski, 2006). Meltwaters infiltrating into the subsurface are initially extremely dilute and oxygenated and have characteristic depleted isotopic signatures ($\delta^{18}O/\delta^{2}H$) (Siegel, 1991; Clark et al., 2000; Ma et al., 2004; Hammer, 2006; Piotrowski, 2006; Stotler et al., 2012). While permafrost is absent under the ice sheet, allowing the potential for meltwater infiltration, it becomes an important barrier to groundwater flow and groundwater-surface water interaction in the periglacial environment (Vidstrand, 2003; Piotrowski, 2006; Lemieux et al., 2008; Person et al., 2012).

The Greenland Analogue Project (GAP) was initiated in 2008 to answer a number of important questions (see below) regarding the impact of continental scale glaciation on the groundwater system in a crystalline rock environment. The project was motivated by the general lack of real-world data concerning flow and chemistry of groundwaters under the influence of a modern,

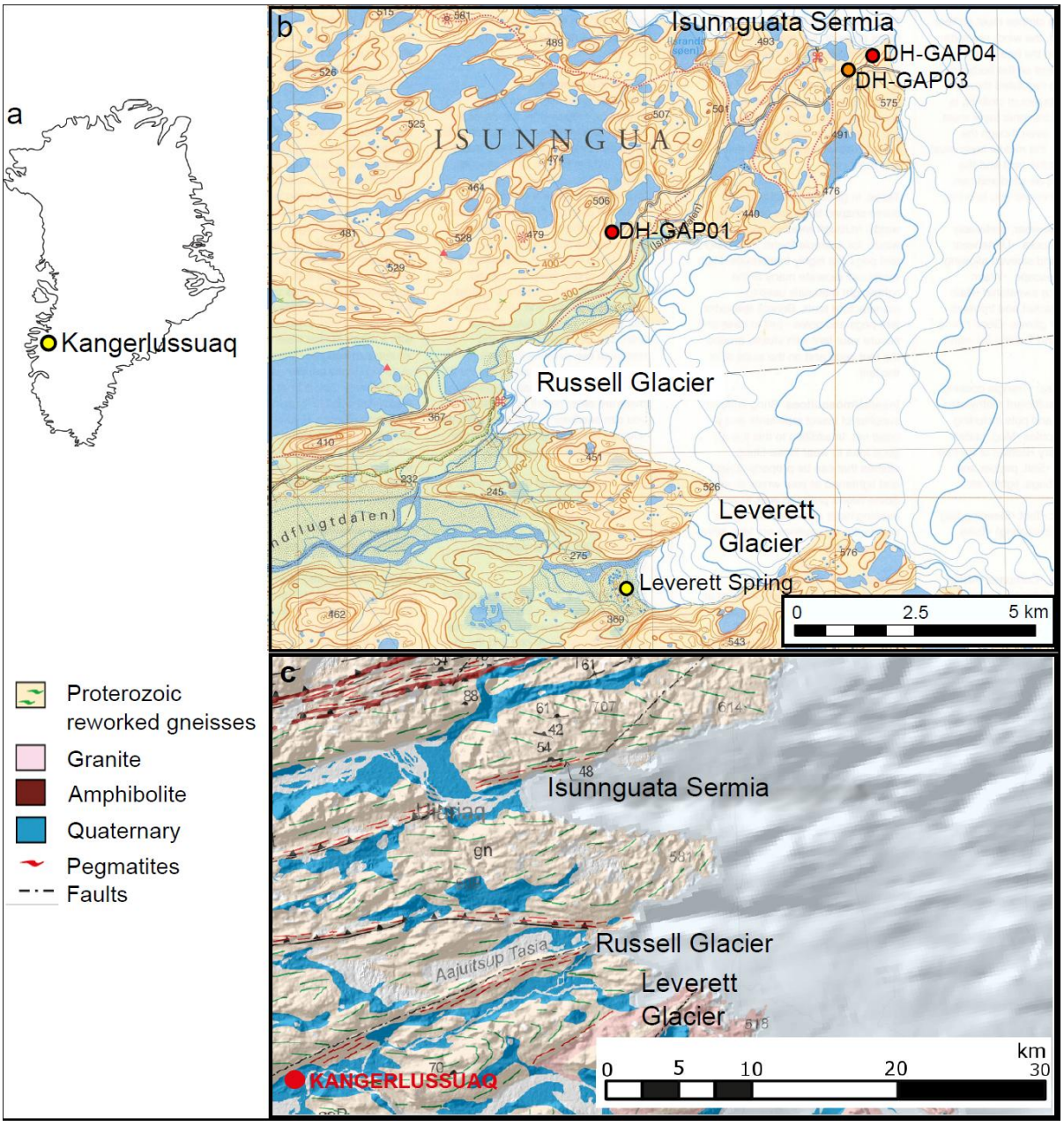

Figure 1.1. Map overview of the Greenland Analogue Project study area. (a) The location of Kangerlussuaq in the southwest of Greenland. (b) a topographic map showing the GAP borehole locations and the key land terminated lobes of the Greenland Ice Sheet found in the study area. (b) A geological map of the study area adapted from Klint et al. (2013)

.

continental scale ice sheet. The GAP was funded by the Finnish (Posiva), Swedish (SKB) and Canadian (NWMO) nuclear waste management companies in order to better understand the perturbations future glaciations may cause to deep geological repositories in crystalline rock. The Greenland Analogue Project (GAP) also aims to resolve some of the uncertainty involved in ice sheet modeling by using the Kangerlussuaq area of Western Greenland as a modern, natural analogue for ice age conditions. For example, the GAP sought to provide data on groundwater pressures at the front of the ice she sheet, the depth of meltwater penetration into the bedrock and the pressures experienced in subglacial meltwater at the bedrock-ice interface. This data adds to the current body of knowledge on glacial processes and their impact on the surface and subsurface environment (Claesson-Lilljedahl et al., 2015).

Studies under the GAP were divided into three subprojects (A, B and C) and involved multiple organizations and Universities from Europe, the United States and Canada. Subproject A studied the GrIS bedrock topography under the ice sheet and ice thickness in the study area using geophysical and remote sensing methods. Subproject B utilized hot water drilling to examine the subglacial drainage system including the subglacial water pressure, water chemistry and sediments. Subproject C, which this study is a part of, involved bedrock drilling and surface water sampling to examine the groundwater system, groundwater surface water interaction and lake evolution in close proximity to the GrIS (Figure 1.1).

This study explores the geochemical evolution of ground and surface waters under the influence of a modern, continental scale ice sheet in the Kangerlussuaq Region of southwest Greenland (Figure 1.1). The following questions examined, and to varying degrees answered, by this study were considered important to the research goals of the Greenland Analogue Project: (1) What is the role of taliks in the hydrologic system? (2) How deep do meltwaters penetrate into the subsurface?

(3) Are recharging meltwaters oxygenated at depth? (4) What is the impact of permafrost/solute exclusion on groundwater and porewater chemistry? A further breakdown of the research objectives for surface water studies (Chapter 2), groundwater geochemistry (Chapter 3) and water-rock interaction studies (Chapter 4) are given below.

Chapter 2: Geochemical characterization of lakes in the Kangerlussuaq region, southwest Greenland: an isotopic approach

Surface water studies were undertaken primarily to determine whether evidence for groundwater discharge could be observed in the lake chemistry or isotopic signature. A secondary goal of surface water studies was to use isotopic tools ($\delta^{18}O$, $\delta^{2}H$, ^{3}H, $^{87/86}Sr$, $\delta^{37}Cl$, $\delta^{81}Br$ and $\delta^{34}S$ and $\delta^{18}O$ of SO_4) to examine the geochemical evolution of lakes in a permafrost and glacially impacted environment.

Objectives:

- What is the impact of glaciation and/or permafrost on surface water chemistry?
- What is the impact of the active layer and storage of water as ground ice on lake water isotopic composition?
- Is there evidence of landscape (i.e. development of soil and vegetation) and weathering evolution after deglaciation?
- What is the impact of the climatic gradient between the coast (warmer, wetter) and the ice sheet (colder, dryer)?
- What is the extent of groundwater-surface water interaction in this environment and what is the role of taliks in the groundwater system? Is there evidence for groundwater discharge as is predicted by several models during ice sheet retreat (Boulton et al.,

1996; Lemieux et al., 2008)? Is there evidence for the upwelling of highly saline water such as is predicted by the model of salinity evolution proposed by Starinsky and Katz (2003)?

Chapter 3: Geochemical characterization of groundwaters in an area of continuous permafrost adjacent to the Greenland Ice Sheet, Kangerlussuaq, southwest Greenland

Chapter 3 characterizes the groundwater chemistry in the GAP boreholes as well as a spring found at Leverett Glacier (Figure 1.1). The borehole DH-GAP01 also aimed to provide further information on the role of taliks in the groundwater system.

Objectives:

- To what depth does glacial meltwater penetrate beneath a continental ice sheet?
- What is the impact of glaciation and/or permafrost on groundwater geochemistry?
- Characterization of redox conditions, microbial activity, and water-rock interaction in groundwaters.
- What is the extent of groundwater-surface water interaction in this environment and what is the role of taliks in the groundwater system?

Chapter 4: Water-rock interaction and hydrothermal and cryogenic processes in the subsurface adjacent to the Greenland Ice Sheet, Kangerlussuaq, southwest Greenland

Matrix porewater studies, whole rock analyses and fracture mineral studies were used to examine what aspects of the groundwater salinity could be attributed to cold climate conditions compared to salinity from long term water-rock interaction and hydrothermal processes. Defining the origin of gypsum, which occurred frequently as both a fracture infillings and in the rock matrix

below 300 m BHL in DH-GAP04, was particularly significant to understanding the role of cold climate, cryogenic geochemical evolution versus long term geological processes.

Objectives:

- What geochemical characteristics of groundwaters are a result of cryogenic conditions versus long term geological features and water-rock interaction?
- Is there evidence of low temperature, cryogenic or recent precipitation processes in the fracture mineralogy or are the minerals present from older tectonic or hydrothermal processes?
- Does porewater chemistry indicate solute exclusion and concentration due to freeze out or long term water-rock interaction?

1.2. Background on Hydrogeology and Geochemistry in Cryogenic Environments

There is little available information on groundwater in Greenland, or elsewhere in glacial dominated terrain, mainly limited to springs and open pingos (e.g. Cruickshank and Colhoun, 1965; Allen et al., 1976; Worsley and Gurney, 1996; Scholz and Baumann, 1997; Pollard et al., 1999). However, other locations impacted by both modern and past glaciations and permafrost have been examined in more detail (e.g. Cartwright and Harris, 1981; Alexeev and Alexeeva, 2003; Lyons et al., 2005; Shouakar-Stash et al., 2007; Stotler et al., 2012). A number of processes and features related to cold-climate conditions at other locations provide a framework with which to evaluate groundwaters in the GAP study area. The processes summarized below are explored in more detail within the relevant chapters.

(1) Cryogenic Concentration of Seawater

Starinsky and Katz (2003) proposed that highly saline (up to 300 g L^{-1}) brines found in the Canadian Shield were created during Pleistocene glacial periods in North America. Starinsky and Katz (2003) suggest that seawater may infiltrate to and become trapped between the ice margin and the foreland bulge where it becomes highly concentrated due to sea ice formation. The cryogenically concentrated brines, which have characteristic geochemical signatures (Herut et al., 1990; Starinsky & Katz, 2003) then infiltrated into the subsurface due to density driven flow. As the ice sheet retreats, the flow direction is reversed (e.g. Lemieux et al., 2008) and brine discharge should occur in the ice marginal area (Starinsky & Katz, 2003). The Starinsky and Katz (2003) model suggests that the GAP should observe cryogenically concentrated brines evolved from seawater composition and discharge of saline waters in the periglacial area. The validity of this theory as applied to surface waters (evidence for saline groundwater discharge) and groundwaters examined by the GAP in the Kangerlussuaq region of Greenland is explored in Chapters 2 and 3.

(2) In-Situ Freeze-Out

During permafrost aggradation, the formation of ice excludes solutes, which are then concentrated in the remaining water. In-situ freeze-out or solute exclusion may potentially create a saline, supercooled cryopeg within and/or at the base of the permafrost (Laaksoharju et al., 1999; Gascoyne, 2000; Alexeev & Alexeeva, 2003; Vidstrand, 2003). Evidence for in-situ freeze out may include increasing salinity with depth, the formation of fracture infilling minerals, such as calcite and sulfates, and characteristic changes in the isotopic and geochemical composition of groundwaters (e.g. increasing Cl^- concentration with depletion of $\delta^{18}O$)(Anisimova, 1980; Chizhov, 1980; Alexeev & Alexeeva, 2002, 2003; Zhang & Frape, 2003; Stotler, 2008; Stotler et al., 2012). Understanding the potential impact of in-situ freeze out was an important research objective in both Chapters 3 and 4.

(3) Meltwater Infiltration into Subsurface

Ice sheets are capable of producing large volumes of subglacial meltwater. Meltwater may infiltrate hundreds of meters into the subsurface even in crystalline rock environments where overall transmissivity is low. Meltwaters are characterized by depleted isotopic ($\delta^{18}O/\delta^{2}H$) signatures, extremely low TDS and the possibility for high concentrations of dissolved oxygen (Siegel, 1991; Smellie & Frape, 1997; Glynn et al., 1999; Laaksoharju & Rehn, 1999; Clark et al., 2000; Rasilainen et al., 2003; Piotrowski, 2006). The depth of meltwater penetration was a key objective of the GAP and is addressed in Chapter 3.

1.3. Detailed Site Description

1.3.1. Location

Kangerlussuaq, southwest Greenland, was chosen as the site for the Greenland Analogue Project due to the logistical benefits of an international airport, science support, a shipping port and a semi-maintained road from the town to the ice sheet. Kangerlussuaq is located above the Arctic Circle at 67° N and 57° W and is approximately 125 km from the coast at the head of Kangerlussuaq Fjord (Søndre Strømfjord in Danish) (Figure 1.1). The GrIS terminates on land in this region. The landscape is dominated by WSW-ENE trending ridges, bare gneissic bedrock, glacial moraines and sparse vegetation. Large meltwater rivers and their associated valleys are also a significant feature of the landscape. Further from the ice sheet, towards the town of Kangerlussuaq and along the fjord towards the coast, vegetation is more extensive.

1.3.2. Climate

Kangerlussuaq has a dry, subarctic climate with a mean annual precipitation, as measured over the period of 1977-2011, of 173 mm. The GrIS exerts a strong control over both the precipitation

and winds around Kangerlussuaq, with strong katabatic winds coming from the ice sheet. The temperature in Kangerlussuaq ranges from -40°C in winter to temperatures of 18-20°C in summer with an average annual temperature of -5.1°C (Cappelen, 2012). Towards the coast the climate becomes low-arctic maritime with cooler summer temperatures and increased precipitation (383 mm/year longer term normal from 1961-1990).

Permafrost at the town of Kangerlussuaq was reported to be approximately 100 - 150 m thick (Van Tatenhove & Olesen, 1994). Closer to the ice sheet, continuous permafrost was found to be greater than 300 m thick (Kern Hansen, 1990). Permafrost thickness around 300 m was corroborated by this study. The active layer thickness decreases sharply from 1.7 m thick near the town of Kangerlussuaq to 0.15 m thick near the ice margin (Van Tatenhove & Olesen, 1994).

Warming related to climate change is projected to impact polar regions with more extreme temperature increases than those projected for global surface warming. Since 2000, the five highest melt seasons on record have been observed for the Greenland Ice Sheet (Tedesco et al., 2013). Increased temperatures will impact the volume of meltwater, solute and nutrient export from the GrIS as well as increased melting of permafrost, changes in timing and volume of snowmelt and the related changes in active layer hydrology (Wolfe et al., 2011; Bouchard et al., 2013; Tedesco et al., 2013; Hawkings et al., 2015). Studies undertaken at least partly for the GAP were able to observe extensive surface meltwater discharge during a record warm year (2010) (van As et al., 2012).

1.3.3. Regional Geology

Past tectonic history and stress fields in the study area have been fairly well established in the literature (van Gool et al., 2002; Wilson et al., 2006; Garde & Hollis, 2010). Additional outcrop to regional scale mapping of faults, fractures, lineaments and structures undertaken for GAP has been interpreted in Engström et al. (2012). The study area is located in the most south-eastern part of

the Southern Nagssugtoqidian orogen (Figure 1.2). The 300 km wide Nagssugtoqidian orogen consists mainly of Archean orthogneisses (Figure 1.1c) that have been reworked during Palaeoproterozoic orogenesis (van Gool et al., 2002).

Table 1.1. Regional tectonic history of the Kangerlussuaq region adapted from Wilson et al. (2006) and Klint et al. (2013).

	Event	Sub-events
1.	Formation of Archean gneisses (>2.5 Ga)	
2.	Continental rifting and intrusion of Kangamiut dyke swarm (2.04 Ga)	
3.	Continental collision: Nagssugtoqidian orogen (1.92 to 1.75 Ga)	a. Large scale folding (1.92 to 1.87 Ga) b. Pegmatite intrusion, large scale folding and tilting during peak metamorphism (1.87 to 1.92 Ga) c. Shearzone formation, thrust faulting (E-W) (1.84 to 1.82 Ga) d. rotation of maximum stress direction to NW-SE. Sinistral shears, conjugated thrust faulting in this orientation (1.82 to 1.78 Ga)
4.	20 - 25 km uplift causing various stress conditions. Fracturing and reactivation of fractures (1.78 Ga to present)	
5.	Seafloor spreading causes faulting (NNE-SSW) (100 to 50 Ma)	
6.	Glaciations cause erosion, subsidence and then rebound on the order of 100s of meters (last 2 Ma)	

Large scale folding is observed at DH-GAP03 and DH-GAP04 (Figure 1.1). DH-GAP03 is located in the limb of a large scale, synform fold while DH-GAP04 is located at the hinge of the fold (Klint et al., 2013). However, this folding may have occurred during the Archean rather than being associated with 3 a or b above (Table 1.1). A second fold system that folds the Kangamiut dyke swarm has been noted that corresponds with 3 a or b above (Klint et al., 2013) (Table 1.1). Consequently the foliation and one of the main fracture sets observed in DH-GAP03 is sub-vertical while in DH-GAP04 the foliation and the dominant fracture sets are sub-horizontal to horizontal. In the region of DH-

GAP01, E-W oriented semi-ductile shear zones are observed which correspond to the events described in 3 c (Table 1.1). Klint et al. 2013 found that the sinistral and conjugate dextral strike slip fault systems associated with 4 (Table 1.1) were likely the primary hydraulic zones.

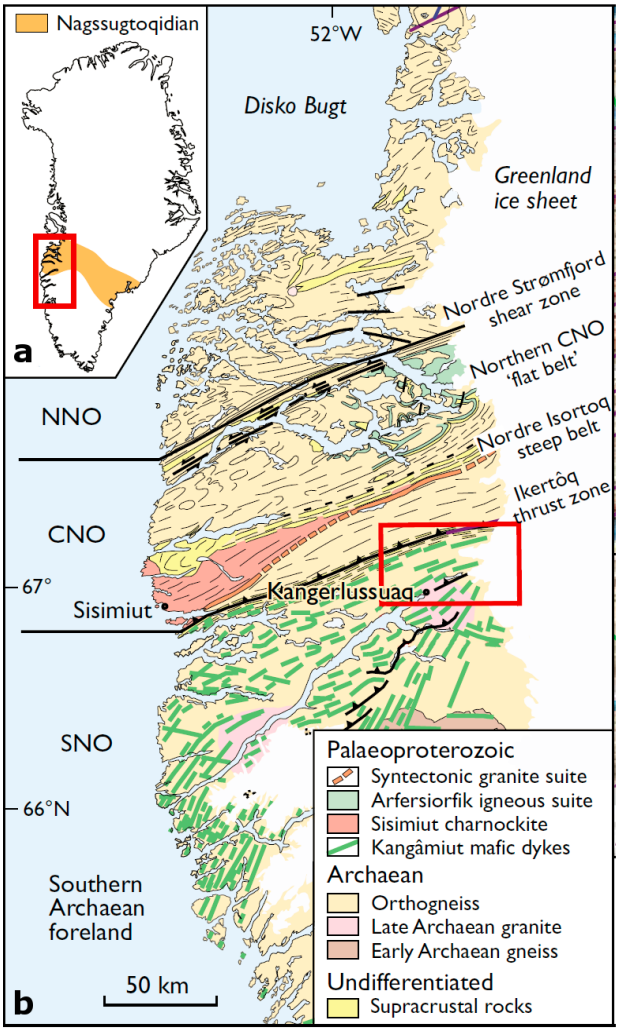

Figure 1.2 (a) The Nagssugtoqidian orogen (orange) and the location of map in (b) are displayed on a map of Greenland. (b) Regional geology of southwest Greenland and outline of the study area. The Nagssugtoqidian orogen is divided into the northern (NNO), central (CNO) and southern (SNO) sections. Adapted from Garde and Hollis (2010) and Klint et al. (2013).

1.3.4. Permafrost and Glacial History

Glacial conditions have been present on Greenland for the past 18 million years and the study area has been glaciated for much of that time period (Thiede et al., 2010; Funder et al., 2011). Long periods of glacial conditions were interrupted by the relatively shorter interstadial periods when the GAP site would be free of glacial ice and dominated by periglacial climate conditions. Figure 1.3 describes and illustrates the timeline of ice retreat since the last glacial maximum (LGM). During the LGM, the Greenland ice sheet (GrIS) extended offshore and was considerably larger than its current margins (Funder & Hansen, 1996) (Figure 1.3a). The ice began to retreat at the beginning of the Holocene.

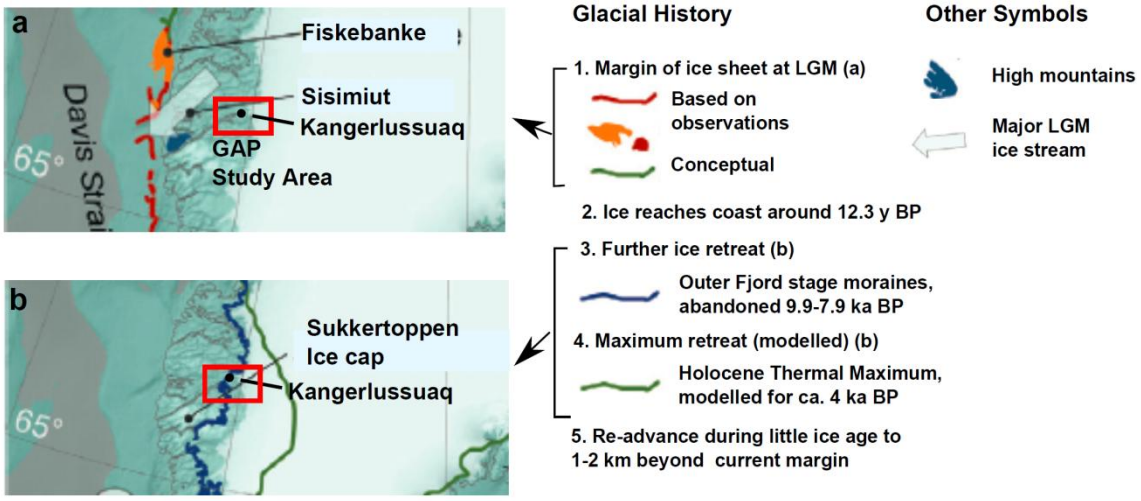

Figure 1.3 Glacial history of the study area from the last glacial maximum (LGM) (a). The ice extent during stages 3 and 4 are shown in (b). Adapted from Funder et al. (2011).

The ice margin had reached the coastal area of southwest Greenland by around 12, 300 y BP (Funder & Hansen, 1996) (Figure 1.3). The ice margin retreated beyond its current margin around 6000 years B.P. (Figure 1.3b) before re-advancing during the Little Ice Age (Van Tatenhove, 1996; Funder et al., 2011). The re-advance extended approximately 1-2 km beyond the current position of the ice margin near Kangerlussuaq. Forman et al (2007) reported that the current thinning of the ice margin has occurred over the past 100 years.

The GAP study site is located in an area of continuous permafrost. Permafrost depths of 100-150 m were reported at the airport in the town of Kangerlussuaq near the head of Sondre Stromfjord (Van Tatenhove, 1996). Closer to the ice sheet, permafrost depths of 300 to 350 m were measured at the GAP boreholes (Harper et al., 2011, 2015a). The temperature profile in the DH-GAP04 borehole indicates that the 0 degree isotherm occurs at around 400 m of borehole length (BHL) or 375 m vertical depth (see Figure 1.6). Thermal modeling conducted for the GAP determined that approximately 20% of the many lakes located in the region were of suitable size (>400 m) to maintain a through talik connecting the subpermafrost groundwater system to the

surface. Advance and retreat of the GrIS and changes in lake coverage in the study area suggest that the extent and depth of permafrost would have aggraded and degraded with time as well (Harper et al., 2015a).

1.4. Methods

Methods that are common across the Chapters of this thesis are included here to avoid extensive repetition in Chapter content. Borehole drilling and instrumentation and geochemical and isotopic methods are given here while the Chapters contain methods specific to the material presented within that Chapter.

1.4.1. Description of Site Activities

Field work in Kangerlussuaq was initiated in 2008 and consisted of preliminary surface water sampling as well as geological mapping. In 2009, the Greenland Analogue Project officially began and included a wide variety of research activities both on and in front of the GrIS. This study focuses on research on surface waters and groundwaters in front of the ice sheet. Samples were acquired from 47 lakes between 2008 to 2013 as part of GAP with additional lakes analyzed for field parameters (pH and EC) (Figure 1.4). Glacial meltwaters were also sampled from supraglacial and subglacial flows (Figure 1.4). Four boreholes were drilled, three in 2009 (DH-GAP01, DH-GAP02 and DH-GAP03) and one (DH-GAP04) in 2011. DH-GAP02 failed and was abandoned after hitting a crush zone. DH-GAP01, DH-GAP03 and DH-GAP04 are described in more detail below.

1.4.2. Description of Drilling and Borehole Instrumentation

More detailed descriptions of the drilling and instrumentation of the GAP boreholes can be found in Chapter 3 and GAP reports (SKB, 2010; Harper et al., 2011, 2015a; b; Pere, 2014; Claesson Liljedahl et al., 2015). A brief description of each borehole is included below. Boreholes were drilled using diamond drill bits while hot water was circulated within the borehole to keep it from freezing

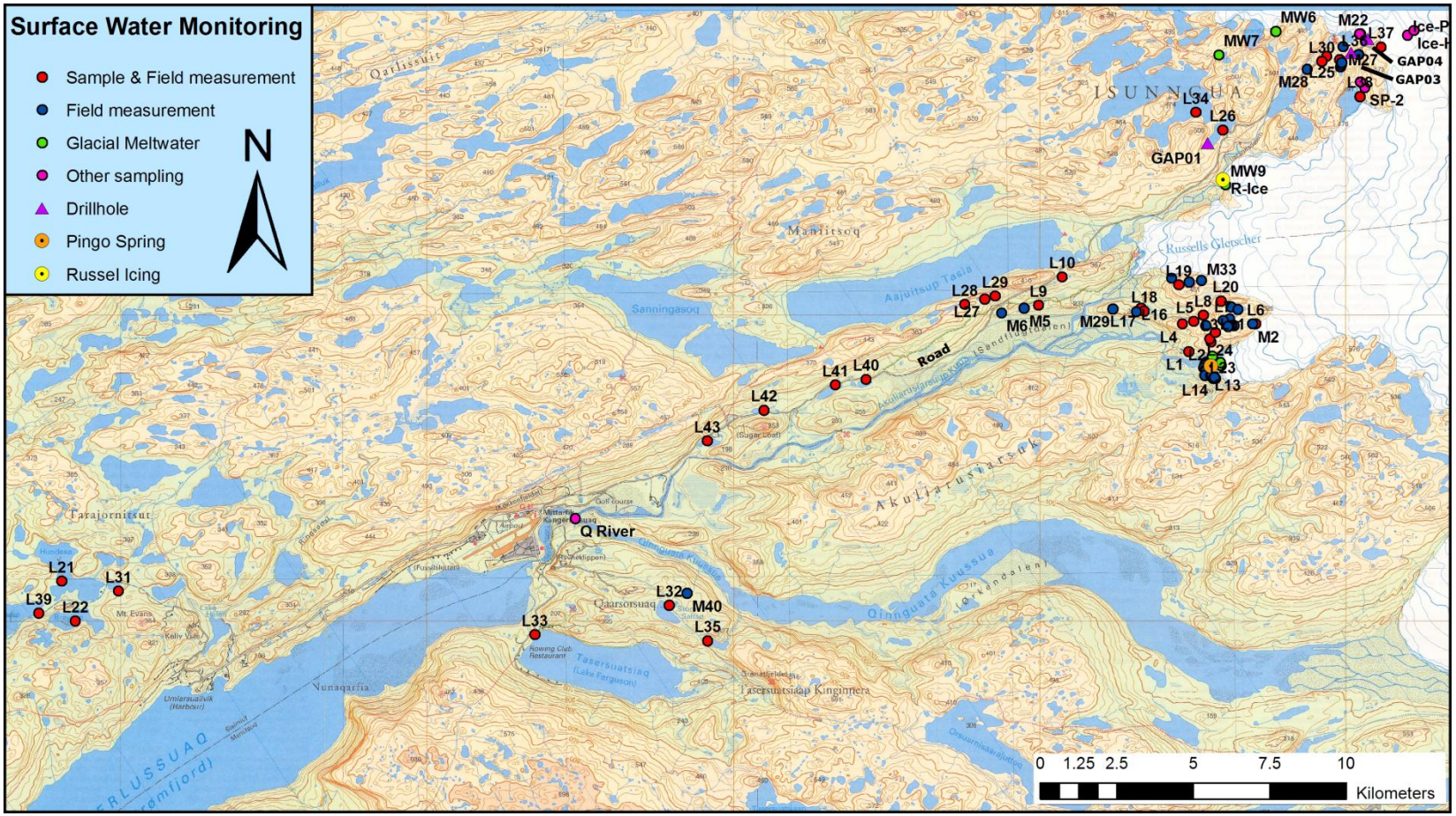

Figure 1.4 Map of the study area showing all surface water sampling and field measurement locations. The GAP boreholes and the Leverett Spring are indicated here and in Figure 1.1.

A tracer (sodium fluorescein) was added to the drilling water in order to determine the proportion of drilling fluid lost to the rock and contained in borehole groundwater samples. Core was extracted and logged in detail (Pere, 2014). Locations are indicated on Figures 1.1 and 1.4.

DH-GAP01

DH-GAP01 was drilled in 2009 to a length of 221 m (vertical depth of 130 m) (Figure 1.5) with a diameter of 56.8 mm. The borehole was drilled at a plunge of 60° to the NNE. DH-GAP01 was drilled next to a lake that was considered to be of suitable size to support a through talik that fully penetrates the permafrost (Figure 1.5) (Harper et al., 2015b). The borehole intercepts the talik and is equipped with a nitrogen push, U-tube sampler (Freifeld et al., 2005) to sample the groundwater system within the talik. A packer at 150 m borehole length (BHL) isolates the lower 71.6 m of borehole length as the sampling section (Figure 1.5). DH-GAP01 is further equipped with fibre optic cables to measure the temperature profile of the borehole as well as an Aqua TROLL 200 to measure absolute pressure, temperature and conductivity at 140 m vertical depth (SKB, 2010). DH-GAP01 was successfully cleared of drilling water contamination by May 2010.

DH-GAP03

DH-GAP03 was drilled in 2009 at a plunge of 70° to the NNW. The total borehole length of DH-GAP03 is 341 m (vertical depth of 320 m) with a diameter of 56.8 mm. DH-GAP03 was equipped with fibre optic cables to measure the temperature profile of the borehole as well as an Aqua TROLL 200 to measure absolute pressure, conductivity and temperature. The Aqua TROLL in DH-GAP03 stopped functioning shortly after installation. No sampling system is installed in DH-GAP03.

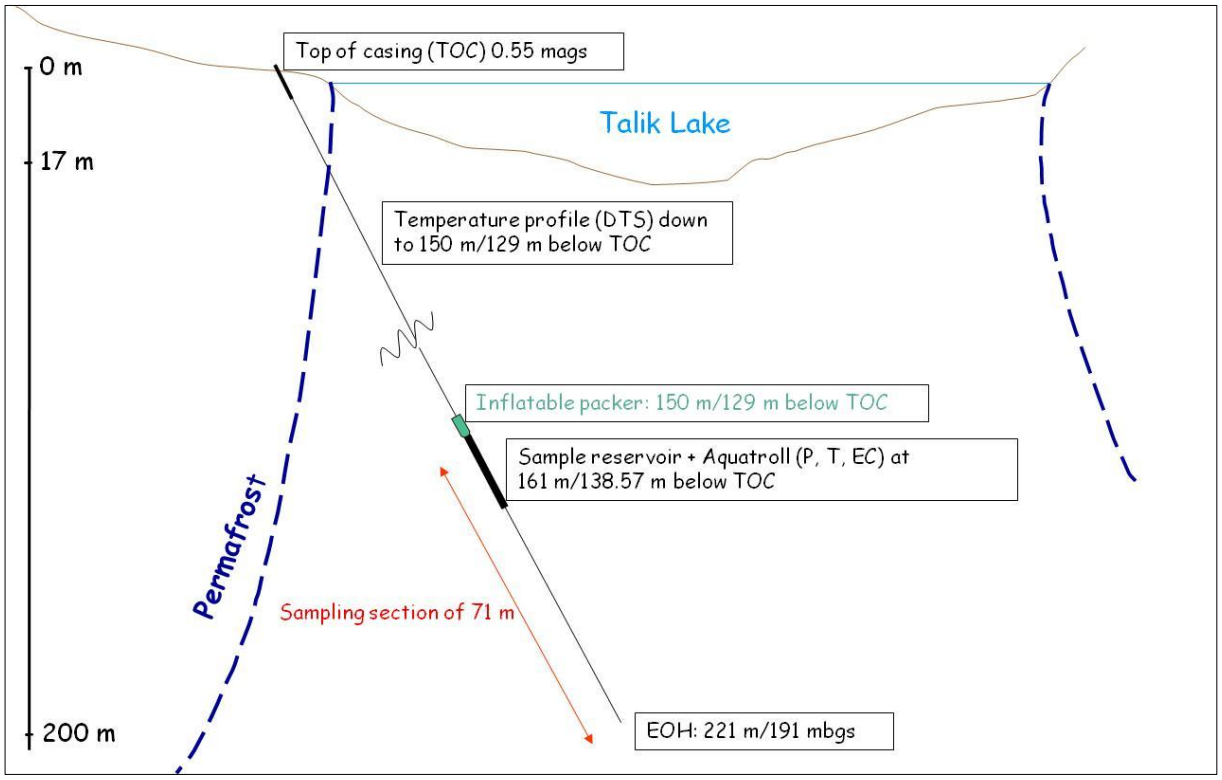

Figure 1.5. The borehole DH-GAP01 was drilled at an angle to intercept the talik beneath a large lake (Lake L26). the borehole instrumentation is shown here relative to the top of casing (TOC), which is 0.55 m above ground surface. The end of hole (EOH) is shown relative to ground surface (mbgs = meters below ground surface). Figure from Harper et al. (2015a). Horizontal axis not to scale. Borehole extends approximately 100 m underneath the lake.

DH-GAP04

In 2011, DH-GAP04 was completed next to Isunnguata Sermia glacier. DH-GAP04 was drilled at a plunge of 70° toward the ice sheet (NNE) (Figure 1.6b) and has a diameter of 76 mm. DH-GAP04 is 687 m in length (vertical depth of 649.1 m) (Figure 1.6c). DH-GAP04 is equipped with a nitrogen push, U-tube sampling system designed by GeoSigma (Sweden) as well as sensors for pressure, temperature and conductivity (Figure 1.6a). Fibre optic cables measure the temperature profile in the borehole (Figure 1.6a). The Posiva Flow Log (PFL) system was used to catalogue the location and transmissivity of fractures in the borehole in order to determine the best placement for

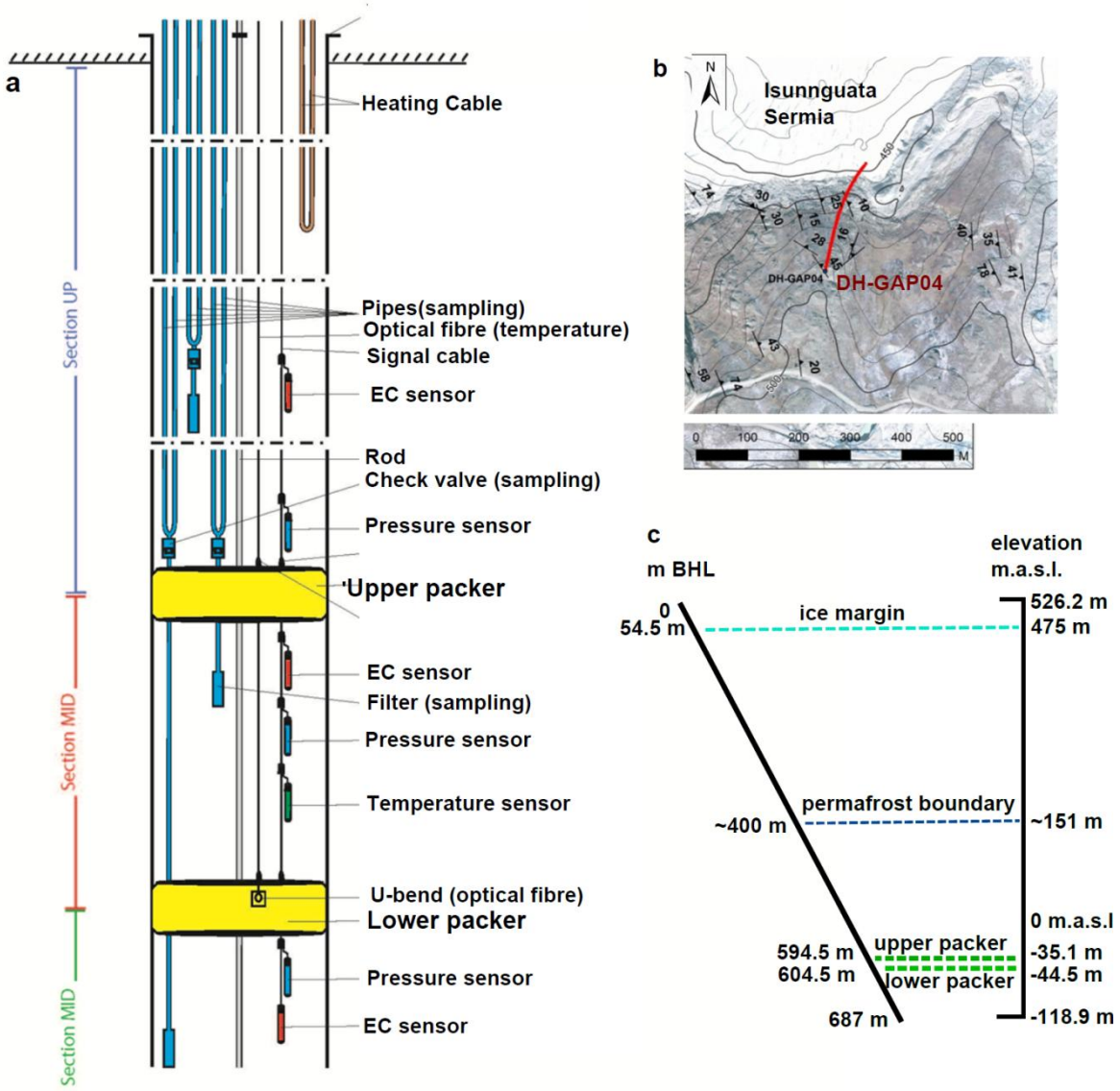

Figure 1.6 (a) Equipment installed in the DH-GAP04 borehole. (b) Orientation and deflection of the DH-GAP04 drill hole and its position relative to the ice margin of Isunnguata Sermia. Aerial photo is from 2006. (c) Schematic of the DH-GAP04 borehole showing depths of important features as meters borehole length (m BHL) on the left and as elevation (meters above sea level (m.a.s.l.) using datum D-WGS84) on the right. Elevations and borehole lengths are relative to top of casing. Ground elevation is at 525.64 m. The upper section is considered to extend from the base of the permafrost to the upper packer while the lower section extends from the lower packer to the bottom of the hole. Figures (a) and (b) are adapted from Harper et al. (2015a).

the packer system (Pöllänen et al., 2012). Technical problems with thawing the upper sections of the sampling equipment prevented sampling from early 2012 to September 2013. In 2013, the lowest section of the borehole was successfully cleared of drilling fluid contamination. However, the upper and middle sections of DH-GAP04 were still contaminated with 33 and 29% drilling fluid, respectively, in September 2014.

1.4.3. Geochemical and Isotopic Methods

Surface and groundwater samples were analyzed at Labtium Oy and the TVO (Teollisuuden Voima Oy) laboratories in Finland. Geochemical analyses were performed using the following methods at Labtium Oy: alkalinity was measured using a titrimetric determination; anions were measured by Ion Chromatography (IC); and, cation multi-element determination was performed by a combination of Inductively Coupled Plasma Mass Spectrometry (ICP-MS) and Inductively Coupled Plasma Atomic Emission Spectroscopy (ICP-AES). At TVO, multi-element analyses were performed using Inductively Coupled Plasma Optical Emission Spectrometry (ICP-OES) and ICP-MS analysis. Geochemical results that exceeded a charge balance error of 10% were not considered.

Isotope analyses were performed at the University of Waterloo Environmental Isotope Laboratory. Tritium pre-analysis was determined using the electrolytic enrichment method of Taylor (1977). After enrichment, samples were counted in a LKB Wallac 1220 Quantalus liquid scintillation counter with a detection limit of 0.8 ±0.8 TU. Deuterium determinations were made following the Cr reduction method outlined by Morrison et al. (2001) and analyzed on an Isoprime IRMS coupled to a Eurolectron elemental analyzer. Oxygen isotope analysis was performed on an IsoPrime continuous flow isotope ratio mass spectrometer (CF-IRMS) using the preparation procedures of Epstein and Mayeda (1953) with Moser's modification (Moser, 1977). Results for $\delta^{18}O$ and $\delta^{2}H$ are reported based on standard corrections to VSMOW (Vienna Standard Mean Ocean Water) and

VSLAP (Vienna Standard Light Antarctic Precipitation) from the International Atomic Energy Agency (IAEA). Analytical reproducibility of $\delta^{18}O$ and $\delta^{2}H$ are ±0.2‰ and ±0.8‰, respectively.

Sulphate is extracted using $BaCl_2$ and converted to SO_2 by combustion with Nb_2O_5 and analyzed on a Micromass IsoChrom-IRMS (±0.3‰) (Rees, 1984; Morrison et al., 1996). For analysis of ^{18}O in SO_4^{2-}, the $BaSO_4$ is combusted to produce CO_2 and analyzed in a GVI IsoPrime-IRMS (±0.5‰) (Morrison, 1997). ^{18}O and ^{34}S are corrected to $BaSO_4$ IAEA-SO5, IAEA-SO-6 and NBS-127.

Chlorine and bromine stable isotope determinations are performed by first precipitating Cl^- or Br^- as AgCl or AgBr using $AgNO_3$. Analyses for ^{37}Cl and $\delta^{81}Br$ are carried out on CH_3Cl and CH_3Br, respectively, after reacting the silver chloride/bromide with methyl iodide. ^{37}Cl and $\delta^{81}Br$ were analyzed using continuous flow technology on a Micromass IsoPrime IRMS (±0.2‰) using the methods outlined in Eggenkamp, 1994; Kaufmann et al., 1984; and Shouakar-Stash et al., 2005a, 2005b. The reference material used for $\delta^{37}Cl$ analysis is Standard Mean Ocean Chloride (SMOC) and for $\delta^{81}Br$ analysis is Standard Mean Ocean Bromide (SMOB).

Analysis of $^{87}Sr/^{86}Sr$ isotopic ratios was performed using thermal ionization mass spectrometry (TIMS). Samples are passed through a strontium specific resin. The isolated strontium is loaded onto a double rhenium filament and analyzed using a Thermo Finnegan Scientific TRITON TIMS and calibrated against the NBS international standard material NIST SRM 987 (Dicken, 2000).

An analysis of data quality and consistency can be found in Appendix A.

1.5. Borehole Lithology, Fracture Systems and Hydrogeology

The following sections describing the geological and hydrogeological aspects of the GAP boreholes comprise work that was a part of Subproject C but was outside the scope of this study.

However, in order to understand and interpret the groundwater and porewater chemistry and the occurrence of fracture infilling minerals, it is necessary to have some background on the local geological and hydrogeological setting.

The descriptions of the GAP borehole geology and fracture systems are summarized from the following GAP reports: Harper et al. (2011); Pere, (2014); Harper et al. (2015a). Detailed hydrogeological results and analyses can be found in the yearly and final GAP reports (SKB, 2010; Harper et al., 2011, 2015a; b; Pere, 2014; Claesson Liljedahl et al., 2015) as well as several hydrology papers (Bosson et al., 2013; Johansson et al., 2014, 2015).

1.5.1. DH-GAP01 Lithology and Fracture Systems

DH-GAP01 is composed predominantly of felsic gneiss. The main fracture set is composed of sub-vertical fractures trending to the NNE-SSW. Apart from the main fracture set, most of the remaining fractures dip at various angles towards the west. The overall fracture freqeuncy in the borehole is 2.2 fractures/meter and fracture infillings are dominated by calcite, chlorite, unspecified clays and kaolinite. Two brittle fault zones intersect the borehole at 84.30 - 89.55 meters and 203.72 - 0 206.20 meters..

1.5.2. DH-GAP03 Lithology and Fracture Systems

Lithologically DH-GAP03 is divided between felsic and mafic gneiss, with the majority of the felsic gneiss occurring in the upper 200 meters of the borehole. Two dominant fracture sets were observed. The first fracture set consists of sub-horizontal fractures trending to the NE-SW. The second set of fractures are sub-vertical and trend to the NW-SE. Fracture frequency in DH-GAP03 is 3.4 fractures per meter. Below 330.86 meters of core length, the core becomes highly fractured with a freacture frequency estimated at over 35 fractures/meter. Four brittle fault zones intersect

the core: 89.90-92.70, 246.06-246.75, 296.98-300-40 and 326.87-341.20 m. Fracture infillings are predominantly calcite, chlorite and unspecified clays. Iron hydroxides also occur in two zones, above 50 m and below 300m with the deeper occurrence associated with a brittle fault zone.

1.5.3. DH-GAP04 Lithology and Fracture Systems

The lithology of the DH-GAP04 borehole is mainly intermediate gneiss (47%) followed by mafic gneiss (41%). Mafic gneiss is found in the upper 300 meters of the core while the intermediate gneiss is predominantly found below 300 m. Felsic gneiss composes only 11 % of the core. Pegmatitic veins cross cut the gneissic material. A diatexitic gneiss was also logged as a section of irregularly deformed rock. Fractures are predominantly horizontal to sub-horizontal and dip gently to the NW, beneath the ice sheet. The shallow dip of the fractures is likely due to its position at the apex of a fold. Water conductivity in the DH-GAP04 borehole is related to the sub-horizontal fractures. Fracture frequency in DH-GAP04 was 2.0 fractures/meter. Seven brittle fault zones were mapped in DH-GAP04: 102.67-103.08 m, 262.98-264.59 m, 368.85-371.50 m, 565.10-567.07 m, 582.51-586.75 m, 594.79-601.72 m and 636.40-637.15 m. Fracture infilling minerals are predominantly chlorite, calcite, gypsum and unspecified clays. The amount of gypsum increases significantly below 300 meters in the core and is observed only occasionally in the DH-GAP01 and DH-GAP03 cores. Iron hydroxides are mainly observed above 300 m.

1.5.4. Hydrogeology Background

Advective groundwater flow in crystalline rock environments occurs through fractures while solute transport in the rock matrix is dominated by molecular diffusion. Water conducting features in crystalline rock are generally generated by brittle deformation processes and groundwater flow is governed by the geometric and structural attributes of these features at various scales. The geochemical composition of groundwaters in crystalline rocks is thus dependent on the

mineralogical and geochemical attributes of water conducting fractures. A thorough background on the hydrogeology of crystalline rocks can be found in Mazurek (2000) and Stober and Bucher (2006).

Hydraulic parameters can be described on the scale of individual water conducting features up to rock mass values for blocks extending hundreds of meters. In general, short term hydraulic testing on boreholes as geographically separated as DH-GAP01 and DH-GAP04 will provide information only on the rock immediately surrounding the individual boreholes. Fracture mapping and knowledge of structural features such as folds and faults are important for understanding flow in crystalline rock environments. Information on the regional structures and borehole fracture systems can be found in the GAP reports (Engström et al., 2012; Pere, 2014; Harper et al., 2015a) as well as several published papers (Klint et al., 2013; Engström & Klint, 2014).

1.5.5. DH-GAP01 Hydrogeology

Interpretation of the physical hydrogeology of the GAP boreholes was outside the scope of this study but are summarized here from various reports and papers (see Section 1.5) to provide a hydrogeological context for the geochemical studies. DH-GAP01 was successfully drilled into a talik beneath what was referred to as the Talik Lake (Lake L26) in 2009. Downhole sensors (In-Situ Inc. Aqua TROLL® 200) have provided long term monitoring of pressure, temperature and conductivity (Figure 1.7). Monitoring by downhole sensors (EC, P, T) indicated that the borehole had recovered from drilling by summer 2010, with the EC stabilizing around 800 μS/cm (Figure 1.7). Concentrations of the sodium fluorescein drilling tracer fell below 5% of the original concentration by the May 2010 sampling period, indicating that purging of drilling fluid contamination was completed at that time.

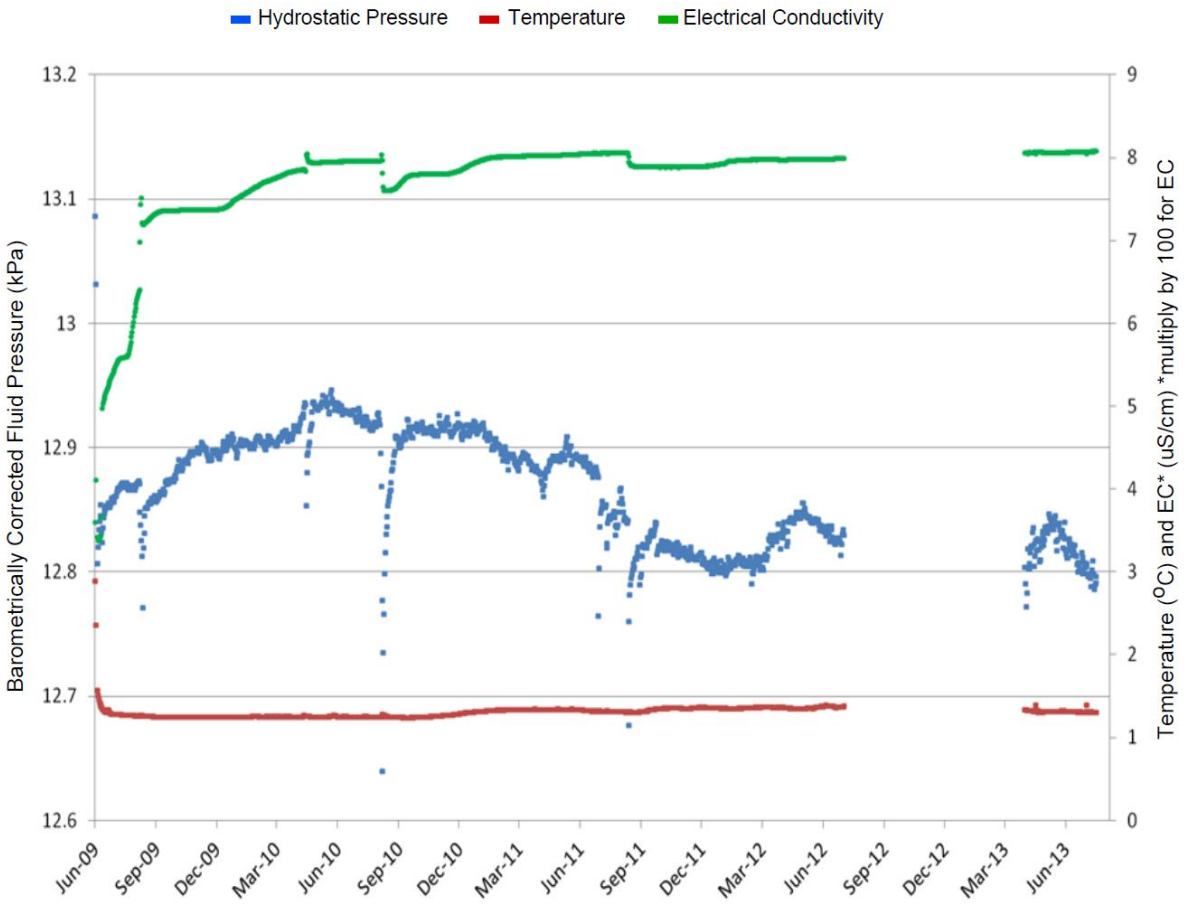

Figure 1.7 Record of fluid pressure (barometrically corrected), electrical conductivity (µS/cm divided by100) and temperature (°C) from downhole sensors in DH-GAP01 presented as daily averages from June 2009 to August 2013. Technical issues with the power supply caused the GAP in the data from July, 2012, to April, 2013. Borehole purging (June-09, Sep-09, May-10, Sep-10 and Sep-11) is apparent as large pressure drops during these sampling campaigns. The frequency of measurements has varied over time from 1 minute to 6 hours depending on data needs. For example, measurement frequency was increased during purging to monitor the pressure response. From Harper et al. (2015a).

Posiva Flow Log (PFL) testing was not performed on DH-GAP01, and thus there is limited data on the nature of water conducting fractures in the 71 m testing section. Hydraulic testing was conducted by Subproject C and reported in Harper et al. (2011). Pressure recovery data collected during sample acquisition in September 2010 was used to estimate the total fracture transmissivity in the sampling section (130-191 m vertical depth). The short duration of the hydraulic testing implies that the calculated transmissivity and conductivities are related to the rock immediately surrounding the borehole. The total fracture transmissivity represents the sum of all fracture

transmissivities in the sampling section. The pressure recovery data was analyzed using methods for slug tests with the results summarized below. A total transmissivity of 10^{-6} m^2/s is estimated which yields a rock mass hydraulic conductivity of approximately 10^{-8} m/s (Harper et al., 2011).

Pressure monitoring in DH-GAP01 and the lake was carried out by the Greenland Analogue Surface Project (GRASP) (Johansson et al., 2014, 2015; Harper et al., 2015a). Lake levels were observed to be higher than groundwater hydraulic head in DH-GAP01 (Figure 1.8). While the lake and groundwater had similar variations in water level/hydraulic head, the magnitude of change was greater in the borehole

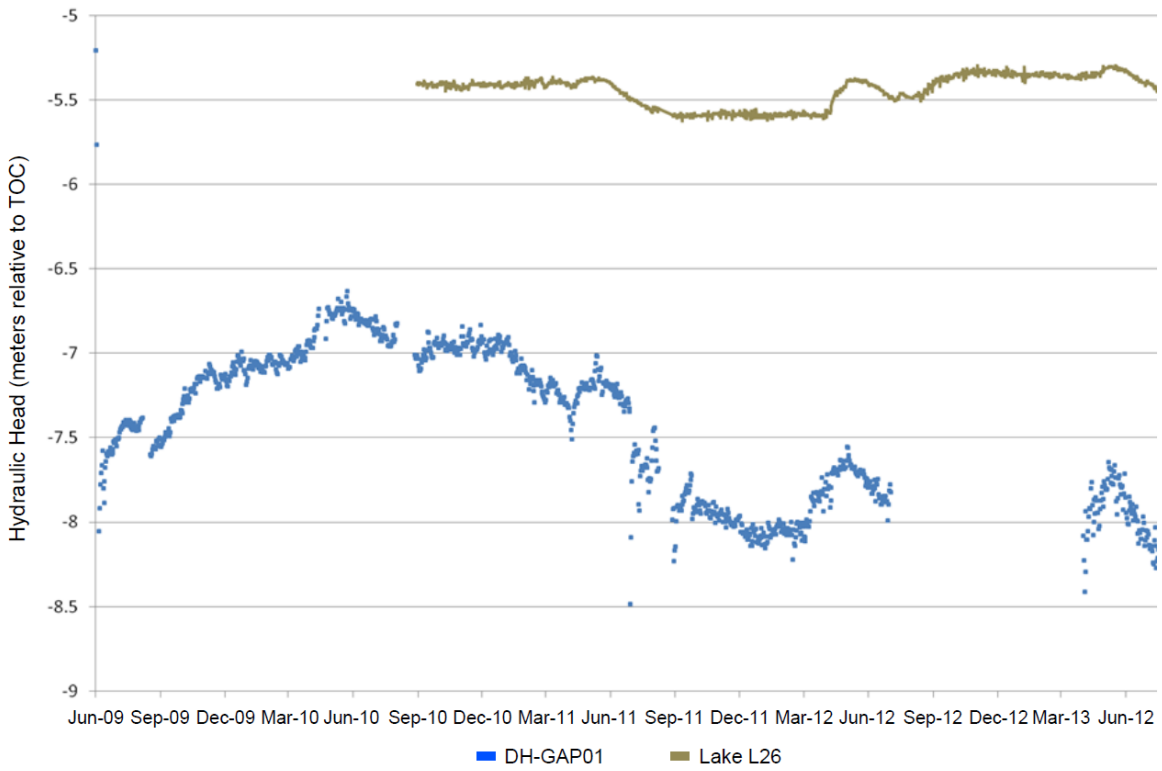

Figure 1.8. A comparison of hydraulic head (meters relative to top of casing (TOC)) in DH-GAP01 compared to water level in Lake L26 (Harper et al., 2015a). Hydraulic head values are daily averages during undisturbed conditions (i.e. hydraulic heads during pumping were excluded but borehole recovery data was included). The hydraulic head record for DH-GAP01 covers June 2009 to August 2013 while the lake level record covers September 2010 to august 2013. Technical issues with the power supply caused the GAP in the data from July, 2012, to April, 2013. Lake level data was provided by Johansson et al., (2015).

than the changes observed in the lake level (Figure 1.8). At no time did the lake level (relative to the top of casing of DH-GAP01) fall below that of the groundwater hydraulic head relative to TOC (Figure 1.8). The difference between the lake level and groundwater hydraulic head indicates that at the present time the lake is recharging the talik. Taliks may be transient in nature due to changes in the regional hydrology (e.g. elevation, drainage, groundwater pressures, permafrost) induced by the retreat and advance of the ice sheet (Johansson et al., 2015).

1.5.6. DH-GAP04 Hydrogeology

The Posiva Flow Log (PFL) method of hydraulic testing was used on DH-GAP04 immediately following drilling in 2011. Detailed results of the testing are described in Pöllänen et al. (2012). Nine, two m long intervals were found to contain water conducting fractures and the associated range of transmissivities are described in Table 1.2. The transmissive features measured by the PFL system are related to single fractures or several fractures, closely spaced (Harper et al., 2015a).

Table 1.2. Results of Posiva Flow Log and hydraulic testing in the DH-GAP01 and DH-GAP04 boreholes. Hydraulic testing of DH-GAP01 reported in Harper et al. (2011) and represents total fracture transmissivity (sum of all fracture transmissivities in the borehole). PFL transmissivities are described in Pöllänen et al. (2012) and hydraulic testing of the low section of DH-GAP04 in SKB (2015).

Section	Method	Transmissivity (m^2/s)	Comment
DH-GAP04 Upper	PFL	10^{-6} to 10^{-9}	Fracture transmissivities
DH-GAP04 Middle	PFL	10^{-6} to 10^{-8}	Fracture transmissivities
DH-GAP04 Lower	PFL	10^{-8} to 10^{-9}	Fracture transmissivities
	Hydraulic Testing	10^{-7}	Total fracture transmissivity
DH-GAP01	Slug Test	10^{-6}	Total fracture transmissivity

Pressure monitoring in DH-GAP04 shows strong variations in pressure in the upper and middle sections of DH-GAP04. These variations appear to be seasonal in nature and show a delayed

response to increasing and decreasing meltwater volumes (Figure 1.9). The lower section of DH-GAP04 does not show the strong, seasonal pressure response of the upper and middle sections, though some minor cyclic changes can be noted (Figure 1.9). The relationship between the hydraulic head variations in the upper and middle sections of DH-GAP04 and the meltwater runoff volumes (Figure 1.9) is interpreted to illustrate a coupling between the borehole pressure response

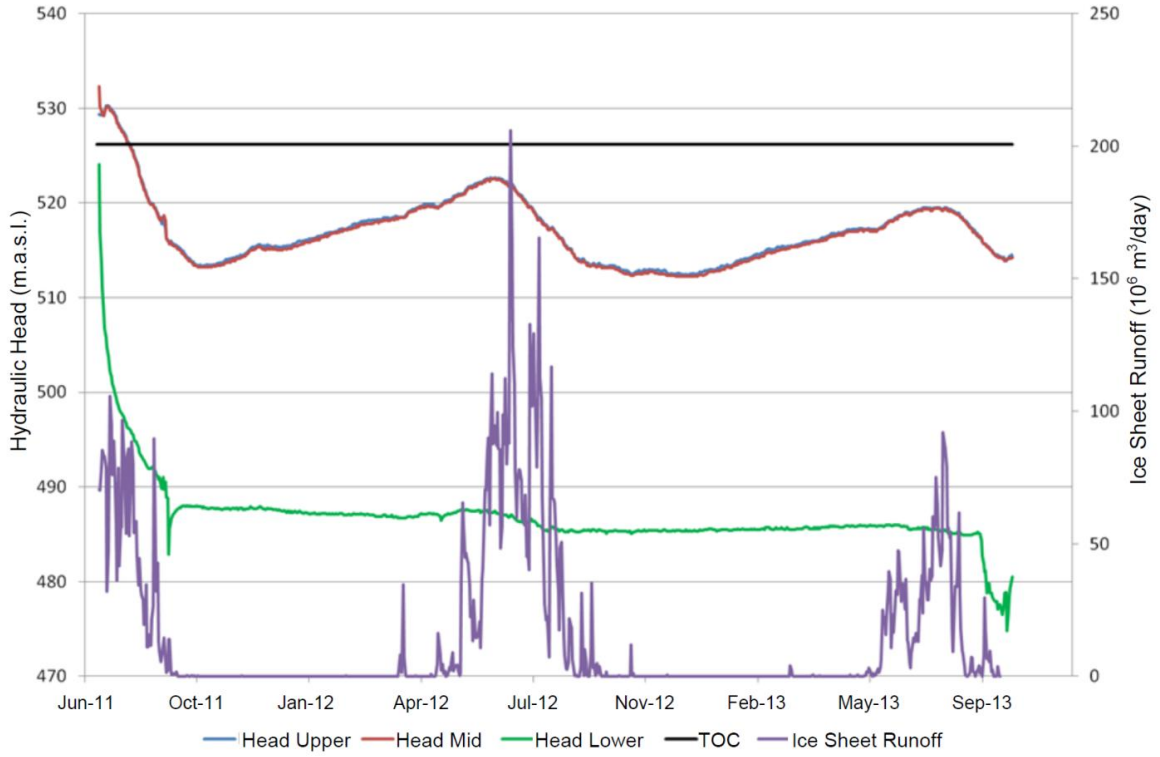

Figure 1.9. Daily average hydraulic heads in m.a.s.l. (D-WGS84) in the DH-GAP04 sampling intervals (upper, mid and lower). Hydraulic heads are compared to surface meltwater runoff from the Kangerlussuaq sector of the Greenland ice sheet (Hasholt et al., 2012; van As et al., 2012; Mikkelsen, 2014; Harper et al., 2015a) presented in 10^6 * m^3/day.

and the glaciohydrological processes (Harper et al., 2015a). The seasonal nature of the hydraulic head variations in the upper and middle sections of DH-GAP04 suggest a connection to the subglacial drainage system beneath the warm based (at or above freezing at the ice-rock interface) parts of the Isunnguata Sermia glacier. The recharge area for subglacial meltwaters beneath the ice sheet is potentially very large and cannot be pinpointed with the available information. Work by the

GAP suggests that wet based conditions with significant volumes of surface melt input exist at the ice bed as far as 100 km inland from the ice margin (Harper et al., 2015a). The temperature profile in DH-GAP04 suggests that permafrost exists at the ice margin (see Section 1.3.4). Whether subglacial recharge is directed beneath the permafrost or over the permafrost to discharge channels will depend on the orientation and geometry of water conducting structural features in the recharge area (i.e. horizontal vs. vertical fractures) (Harper et al., 2015a).

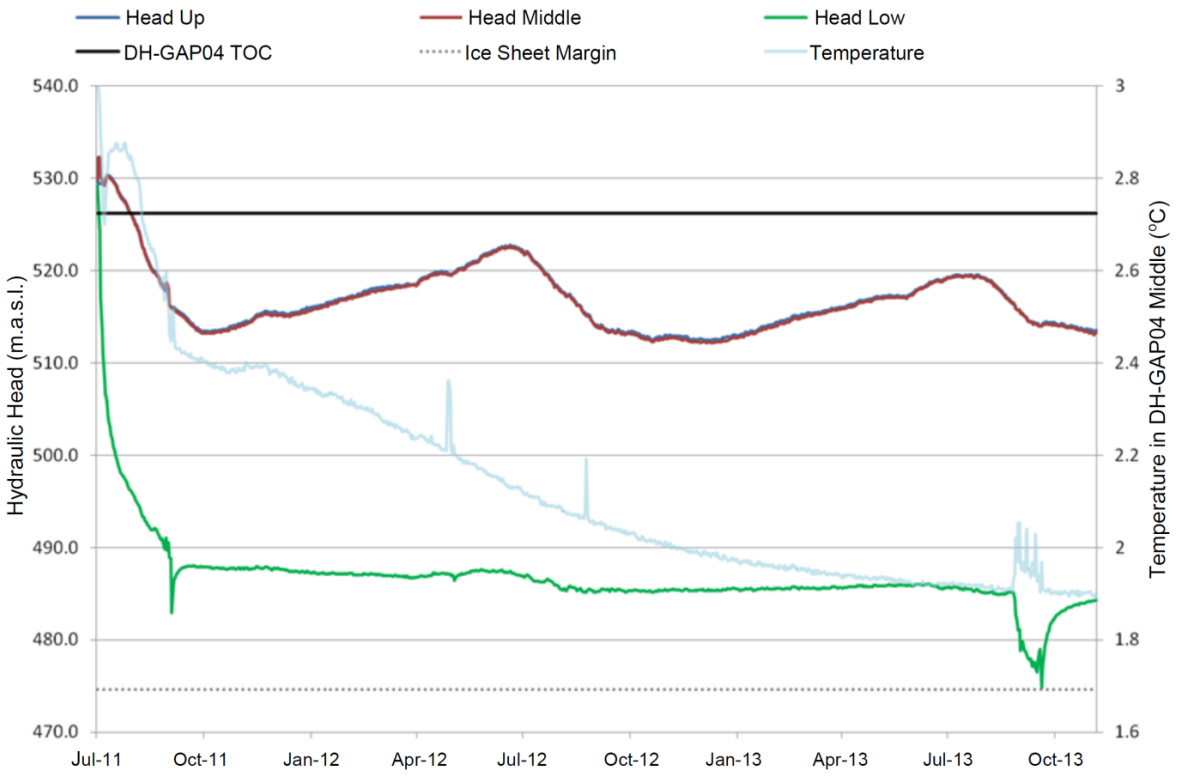

Figure 1.9. Daily average hydraulic heads in m.a.s.l. (D-WGS84) in the DH-GAP04 sampling section: upper (sect Up), mid (Sect mid) and low (sect lo) from July, 2011 to November, 2013. Top of casing of DH-GAP04 is 526.17 m,. The dashed line represents the elevation of the ice sheet margin. From Harper et al. (2015a).

Hydraulic head in all three sections of DH-GAP04 are well above the ground surface at the ice sheet margin, indicating the potential for artesian conditions to exist (Figure 1.10). The permafrost, which is around 350 m thick at the DH-GAP04 site creates an effective barrier to upward flow. The hydraulic heads in the lower section of DH-GAP04 are 25-35 m lower than those observed in the

upper and middle sections, suggesting downward flow would occur along transmissive, vertical fractures.

1.5.7. Leverett Spring

The Leverett Spring indicates that artesian conditions exist in front of the Leverett Glacier. The spring was first noted and studied by Scholz and Baumann (1997). They referred to it as an open pingo and suggested a hydrothermal origin for the waters. During the summer, the spring forms a pond within the pingo crater (Figure 1.11a and c). The water takes on a rust-red colour as the iron in the spring water is oxidized at surface (Figure 1.11c). The spring flows year round, forming a large mound of ice overtop of the spring outlet during the winter (Figure 1.11b). Similar to the the DH-GAP04 borehole at Issunguata Sermia, artesian conditions appear to be present along the ice margin at Leverett Glacier (Figure 1.1 and 1.11). Drilling through the ice mound in the winter results in pressurized water flowing up out of the drill hole (Figure 1.11d). The pressurized winter flow is clear, suggesting that reducing conditions prevail in the subsurface and oxidation occurs at the surface. The Leverett spring is discussed in more detail in Chapters 3 and 4.

1.1. Contributions

The work presented in this thesis is a part of the much larger Greenland Analogue Project. The project was a team effort involving a core group of colleagues collecting the field data and providing feedback on the data synthesis and analysis. Original text was initially written by Emily Henkemans with supervisory edits by Shaun Frape. Additional feedback was provided by representatives from the funding agencies (NWMO, Posiva and SKB). As such, the author acknowledges the contributions of colleagues and presents below an estimate of the author's personal contributions. Potential co-authors and affiliates are listed for each chapter to acknowledge the contributions of these individuals.

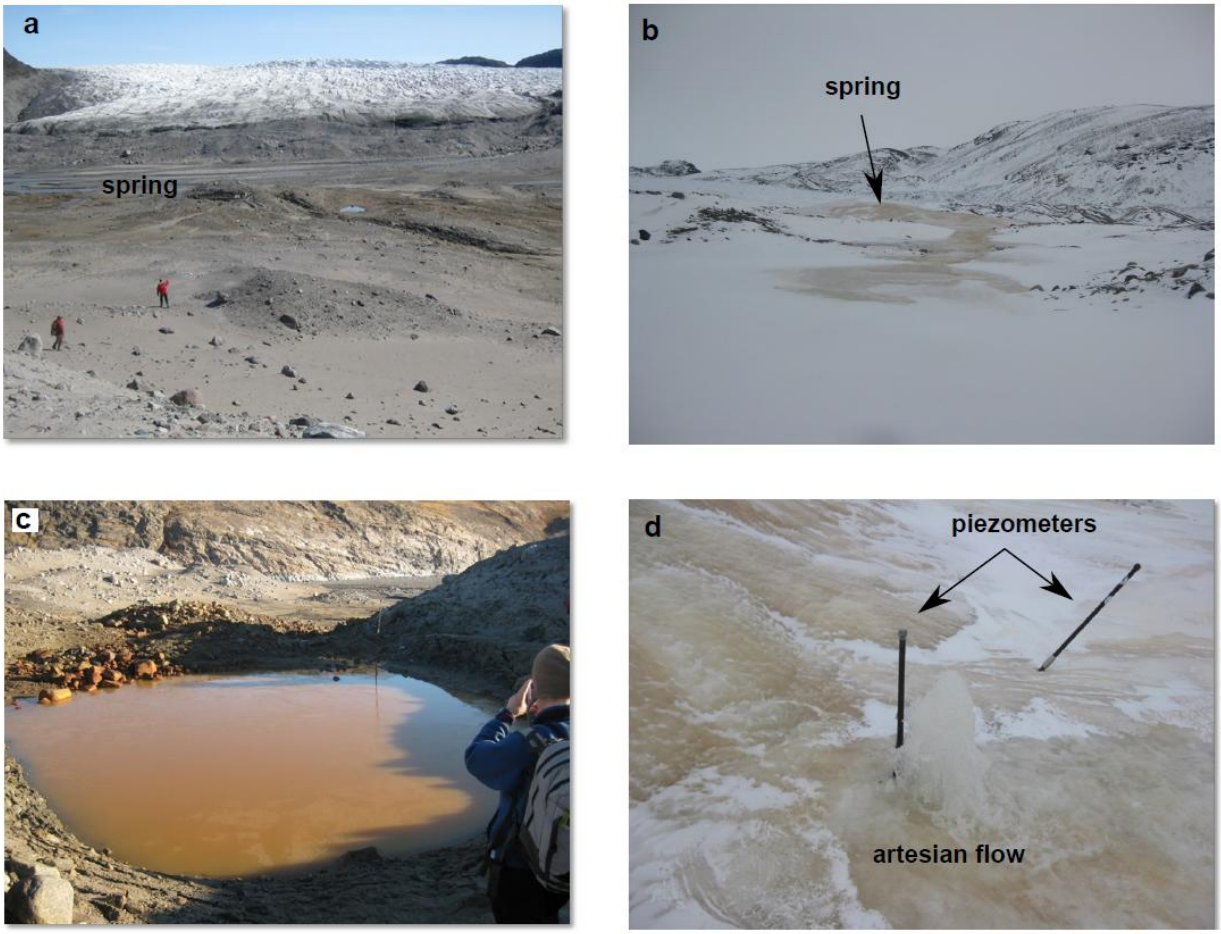

Figure 1.10 Photos depicting the Leverett Spring. (a) view of the frozen mound where the spring emerges with Leverett Glacier in the background. In the winter the spring continues to flow, producing a large mound of ice (c): a pond forms in the spring crater during the summer months. (d) drilling through the ice covering the spring outlet in the winter produces strong artesian flow that is clear and lacking in oxidized iron. Piezometers were installed in the spring pond, however they were destroyed over winter by ice formation.

Chapter 2. Surface waters: Data collection, synthesis and analysis: %85

Authors and affiliates: Shaun Frape, John Anderson, Monique Hobbs, Lillemor Claesson-Liljedahl, Anne Lehtinen, and Timo Ruskeeniemi.

Chapter 3. Groundwaters: Data collection, synthesis and analysis: %80

Authors and affiliates: Shaun Frape, Timo Ruskeeniemi, Lillemor Claesson-Liljedahl, Anne Lehtinen and William Annable.

Chapter 4. Water-rock interaction: data collection, synthesis and analysis: %85

Authors and affiliates: Shaun Frape, Timo Ruskeeniemi, Jon Engstrom, Tuomas Pere, Florian Eichinger, Nick Waber, Lillemor Claesson-Liljedahl and Anne Lehtinen.

2. Geochemical Characterization of Lakes in the Kangerlussuaq Region, Southwest Greenland: an Isotopic Approach

2.1. Introduction

Lakes in periglacial environments provide a unique opportunity to study the geochemical evolution and primary succession of water bodies under changing climatic conditions (Engstrom et al., 2000; Leng et al., 2012; Fritz & Anderson, 2013). Climate can impact Arctic lakes directly through processes such as precipitation and evaporation, as well as indirectly through catchment inputs (Anderson et al., 2001). In many ways, changing temperatures can influence lake basins, water chemistry and biota in these environments, including changes in soil stability, vegetation cover, duration and depth of snow cover, and chemical and physical weathering (Birks et al., 2004). On longer time scales, lakes in deglaciated areas can provide a chronosequence of lake evolution (Engstrom et al., 2000) and provide insight into how variation in the factors listed above affect lake chemistry over the time since deglaciation.

In the Kangerlussuaq region of south west Greenland, a series of lakes, from the coast to the ice front, were sampled between 2001 and 2013, with the majority of sampling occurring between 2008 and 2012 (Figure 2.1). In lieu of age estimates, the distance from the current ice margin is used as a proxy for time since deglaciation. Despite periods of ice re-advancement, distance from the ice margin provides a rough comparison between recently deglaciated areas and those which have been ice free for longer time periods. The coastal areas were ice covered until 11,000 years BP (Van Tatenhove, 1996) and the ice retreated further than its current extent by ~6,000 to 4,000 years BP before re-advancing (Rinterknecht et al., 2009)(see Figure 1.3). In the area around the head of

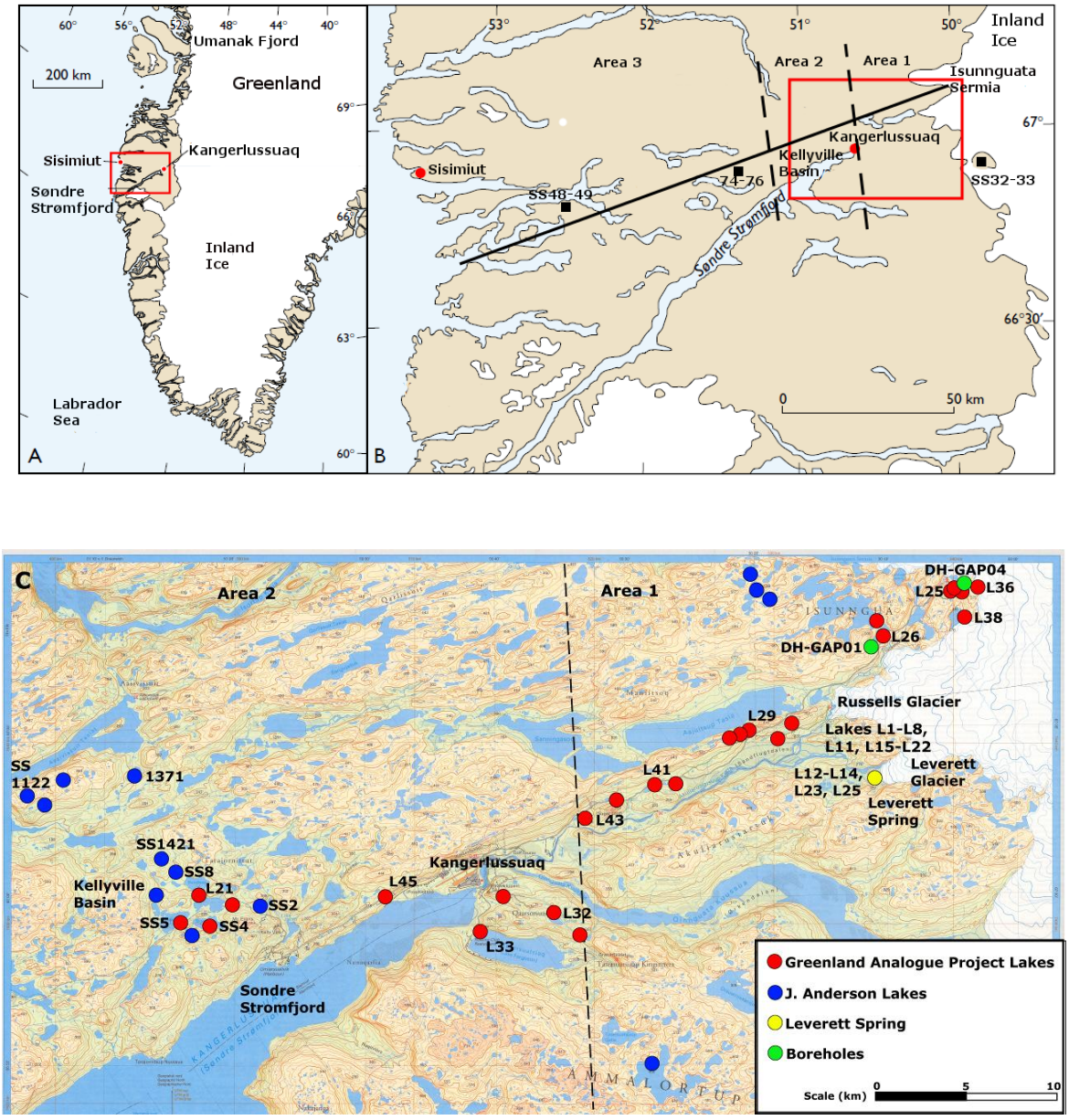

Figure 2.1. (a) Location of study area in the south west of Greenland. (b) Transect of studied lakes extending to coast. (c) Map detailing most heavily sampled area and indicating which lakes were sampled for the Greenland Analogue Project and which were sampled by Dr. John Anderson. The study area is divided into 3 regions: ice marginal (area 1), upper fjord (area 2) and coastal (area 3). (a) and (b) are adapted from Anderson and Brodersen (2001).

Søndre Strømfjord and the Kellyville basin lakes, deglaciation occurred around 8,500 years BP (Anderson et al., 2008; Aebly & Fritz, 2009). Currently the ice is approximately 160 km from the coast (Figure 2.1). Previous studies have examined lake chemistry, paleolimnological history and ecology in the Kangerlussuaq region (Jensen, 1889; Bocher, 1949; Fredskild, 1977; Williams, 1991; Eisner et al., 1995; Anderson et al., 2001, 2008; McGowan et al., 2003; Leng & Anderson, 2003; Anderson & Leng, 2004; Aebly & Fritz, 2009; Leng et al., 2012; Olsen et al., 2013; Fritz & Anderson, 2013). Additional insight into lake evolution can be gained by using novel isotopic tools, such as $\delta^{37}Cl$ and $\delta^{81}Br$, in combination with more traditional geochemical and isotopic analyses ($\delta^{18}O$, $\delta^{2}H$, ^{3}H, $\delta^{34}S/\delta^{18}O$ (SO4) and $^{87}Sr/^{86}Sr$).

Lakes in this region are fresh (<1,000 mg/L) to brackish (1,000 - 10,000 mg/L), based on the classification of Davis (1964). However, previous literature on lakes in the region have used a classification of <800 µS/cm (approximately 500 mg/L TDS) as dilute and >800 µS/cm as "saline"; thus, saline is used in a relative sense when comparing the more brackish lakes to the dilute lakes (Anderson et al., 2001; Leng & Anderson, 2003). The convention of referring to lakes with EC > 800 µS/cm as "saline" will be used in this paper. Most lakes have an electrical conductivity of less than 800 µS/cm. In general, the Kangerlussuaq Region of Greenland lacks the very high TDS lakes (TDS > 10,000 mg/L) that may be found in other polar environments, such as the Canadian Arctic (Ouellet et al., 1989) and Antarctica (e.g., Lyons et al., 2002; Matsubaya et al., 1978). Saline lakes in the Kangerlussuaq region are often closed basin lakes where evaporation has concentrated salts in the lake water over the last 6-11k years since deglaciation. The majority of lakes included in the current study are located above the elevation at which seawater intrusion may have occurred, about 100 m above the present day sea level (Aebly & Fritz, 2009) and, thus, are not impacted directly by seawater salts. This does not discount other forms of marine input such as marine aerosols and aeolian transport of marine sediments deposited around the fjord (e.g. Anderson et al., 2001).

Differences between catchment processes, such as evapotranspiration and active layer hydrology, as well as differences in precipitation rates due to orographic and continental effects can create large geochemical and isotopic variations among lakes (Anderson et al., 2012).

In deglaciated areas of continuous permafrost, taliks provide one of the few pathways for groundwater-surface water interaction. Taliks are created in permafrost environments by lakes that do not freeze to the bottom during the winter, resulting in warming of the ground around the lake bottom to temperatures above zero degrees Celsius. Taliks have been documented beneath lakes in permafrost environments in both the Arctic (Burn, 2002; Kokelj et al., 2009) and Antarctic (Matsubaya et al., 1979; Cartwright & Harris, 1981). Subpermafrost waters may only receive recharge from lakes with taliks that fully penetrate the permafrost (through taliks), and from subglacial meltwaters where permafrost is absent. Subpermafrost groundwater discharge will occur in lakes with through taliks, or as discharge into the ocean (e.g. DeFoor et al., 2011). Isotopic tracers such as $\delta^{18}O$ and $\delta^{2}H$, as well as $^{87}Sr/^{86}Sr$ and $\delta^{34}S$-$\delta^{18}O$ (SO_4) can reveal whether groundwater discharge is providing a significant component of the water balance within a lake catchment. Two boreholes drilled as part of the Greenland Analogue Project (GAP) provide information on the geochemical and isotopic composition of groundwaters in the study area (see Chapter 3). The GAP was initiated by three nuclear waste management agencies: the NWMO (Canada), Posiva (Finland) and SKB (Sweden). The goal of the GAP was to study the properties of subglacial recharge into the subsurface and potential permafrost and glacial impacts on deep geological repositories for nuclear waste storage or disposal (Claesson Liljedahl et al., 2015).

Closed basin lakes have been useful in paleaoclimate research (Fritz, 1996; Anderson et al., 2001; Aebly & Fritz, 2009). Several studies in the Kangerlussuaq region (Leng et al., 2012; Fritz & Anderson, 2013; Olsen et al., 2013) have examined lake ontogeny since deglaciation using lake

sediment records. The concepts discussed here support the results of these previous studies using a novel isotopic approach to analyzing lake water chemistry. Use of these isotopic parameters has provided increased understanding of evaporation, the extent and timing of permafrost, glaciation/deglaciation, weathering, aeolian transport, marine inputs, groundwater-surface water interaction and microbial processes in the study area. Previous findings from the Kangerlussuaq region, and other cold climates, regarding the aforementioned processes were also used to support the isotopic and chemical evidence for lake geochemical evolution.

2.2. Background on Lake Chemistry in Cold Climates

In the Kangerlussuaq Region, dilute lakes are of the Ca,Mg-HCO_3 type with increasing percentage of Cl^- towards the coast, while more saline lakes (EC >800 μS/cm) are of the Na or Mg-HCO_3,Cl type (Williams, 1991; Anderson et al., 2001). Anderson et al. (2001) found that higher altitude lakes tended to be more dilute due to lack of vegetation and lower weathering rates. Nesbitt and Young (1996) suggest chemical weathering is limited by cold temperatures in glacial environments. However, Hall et al. (2002) suggests that the availability of moisture is the main control on chemical weathering rates. The lack of vegetation around the higher altitude lakes leads to reduced snow cover due to wind loss (Turner et al., 2010; Bouchard et al., 2013), leading to limited availability of moisture and reduced chemical weathering. Slope direction in relation to both the dominant wind direction as well as the sun also exert strong controls on moisture availability.

Together with the balance between evaporation and precipitation, the presence of a lake outlet appears to be the main control on lake salinity. Lakes can be isolated during periods of low precipitation as lake levels fall and eventually become cut off from drainage routes, forming closed basin lakes where salinity increases over time due to evaporation (Williams, 1991; Anderson et al., 2001; Leng & Anderson, 2003; Aebly & Fritz, 2009). While deglaciation of the saline lakes around

the head of Søndre Strømfjord may have occurred over 8000 years ago, climate variability over this time period has led to both periods of evaporation, resulting in decreasing lake levels, and periods of increased precipitation, humidity and lake level rise (e.g., Aebly and Fritz, 2009), resulting in lower salinity than would be expected of a purely evaporative environment. Saline lakes (>800 µS/cm) resulting from closed basin, evaporative conditions are reported around the heads of a number of fjords in Greenland including Søndre Strømfjord as well as Umanak Fjord (Figure 2.1) and Independence Fjord, which are located in the north east area of Greenland (Williams, 1991). On a shorter time scale (<100 years), the chemistry of the saline lakes tends to remain fairly constant (Williams, 1991). Evaporation within closed basin lakes is also an important process in creating the very saline lakes (TDS > 10 g/kg) found in the McMurdo Dry Valleys, Antarctica (e.g. Matsubaya et al., 1978; Gooseff et al., 2006). Compared to the lakes in the Kangerlussuaq region (<4 g/kg), salinity in the Dry Valley lakes can be much higher – with Cl^- concentrations exceeding 100 g/kg (Matsubaya et al. 1978) – and receive an influx of saline groundwater that is apparent in the lake geochemistry (e.g. Takamatsu et al., 1998; Green and Lyons, 2008).

Groundwater discharge into lakes may also influence surface water chemistry. For example, several of the Dry Valley lakes in Antarctica, such as Don Juan pond and Lake Vanda, are fed by saline groundwaters (Matsubaya et al., 1979; Green & Canfield, 1984). It has been previously assumed that groundwater discharge into lakes in the Kangerlussuaq region is insignificant (e.g. Anderson et al., 2001). However, a number of conceptual and numerical models for groundwater flow under and adjacent to continental scale ice sheets predict significant groundwater discharge at the front of the ice sheet (e.g. Boulton et al., 1996; Lemieux et al., 2008), with the potential for highly saline groundwater discharge (Starinsky & Katz, 2003). Determining the extent of groundwater discharge into lakes in the study area was an important objective of surface water studies. Tatenhove and Olesen (1994) estimate that in the Kangerlussuaq area, lakes with diameters

greater than 30 m do not freeze completely during the winter and, thus, are capable of supporting a closed talik. Thermal modeling may be used to predict the size of lake necessary to create a through or closed talik (e.g., Burn, 2002). Thermal modeling performed as part of the GAP indicated that lakes with a width greater than 200 m have the potential to form a through talik while lakes that are at least 100 m wide may support closed taliks (Harper et al., 2011). Thermal modeling also indicated that taliks may form over only a few hundred years (Harper et al., 2011). The relatively short time scale on which taliks may form implies that the majority of lakes capable of supporting a through talik have had sufficient time to form the talik.

2.3. Study Area

The study area centers on the town of Kangerlussuaq, located about 125 km inland from the west coast on Søndre Strømfjord and 25 km east of the Greenland ice sheet. Originally, lake samples were taken for the Greenland Analogue Project (GAP) in the area from around the head of Søndre Strømfjord and extending to the ice sheet (Figure 2.1). Samples for the GAP were acquired between 2008 and 2013. The aim of GAP was to study the impact of a modern ice sheet on the groundwater system. During the initial phase of the study, the lake sampling program was designed to examine the potential for groundwater discharge to, or recharge from, lakes in the periglacial area. Additional samples provided by Dr. John Anderson (Loughborough University) greatly extended the study area to complete a transect of lakes from the ice sheet to the coast in the vicinity of Søndre Strømfjord (Figure 2.1). The samples provided by Dr. Anderson consisted of historical samples (2001 to 2012) from previous studies in the region. The possibility of sample deterioration in the older samples provided by Dr. Anderson was considered; however, for the isotopic analyses used in this study it was considered unlikely that sample deterioration was an issue.

The study area encompasses both a low-arctic maritime climatic regime in the coastal region to a low-arctic continental inland regime (Anderson et al. 2001). Inland, continuous permafrost may be greater than 300 m thick near the ice sheet (Chapter 1; Kern Hansen, 1990; Harper et al., 2015a), while closer to the head of the fjord it is reported to be ~100 - 150 m thick (Van Tatenhove & Olesen, 1994). Near the town of Kangerlussuaq, the active layer is ~1.7m thick, on average, and the thickness decreases toward the ice sheet margin to reach a minimum of 0.15 m (van Tatenhove & Olesen, 1994). Mean annual temperature (measured 1977 - 2011) at Kangerlussuaq is -5.1°C and varies from -40°C in winter to 18-20°C in summer, with an annual precipitation of 173 mm (Cappelen, 2012). In coastal areas, summer temperatures are cooler and mean annual precipitation is higher: 383 mm/year on the coast at Sisimiut (Figure 2.1) (long term normal 1961 - 1990) (Cappelen, 2012).

Local geology consists of Archean gneisses reworked in the Paleoproterozoic with an ENE structural trend. The area is structurally complex, having gone through several episodes of deformation (Engström & Klint, 2014) with lakes often occurring along structural lineaments and within closed basins. Mafic dykes of the Paleaoproterozoic Kangamiut dyke swarm (2040-2050 Ma) intrude the Archean gneisses and are NNE trending (van Gool et al., 2002). The dominant rock type is quartzo-feldspathic gneiss that is quartz rich and commonly biotite-bearing. Mafic intrusions are generally garnet-bearing amphibolites. Pegmatites are quartz and feldspar rich and frequently contain biotite.

2.4. Methods

Data collected as part of this study and the GAP includes surface water samples, subpermafrost groundwater samples, spring water samples and samples of glacial meltwater taken from sub and supra glacial flow at Isunnguata Sermia, Russells Glacier and Leverett Glacier (Figure 2.1). Shallow

groundwater samples were acquired from tube wells installed for detailed lake basin studies at L26 (Johansson et al., 2014, 2015).

Water samples from lakes collected for the GAP were generally taken from the shoreline using nalgene bottles. Care was taken to sample in deeper locations to avoid poorly mixed shallow waters. In some instances, samples were taken at various depths, either from a boat or from holes drilled through ice (depending on the time of year). Sample depths are indicated in the sample name for samples not acquired from the surface. Samples taken at depth were acquired using a kemerer or kayak sampler. pH, conductivity and lake temperature were measured in the field using a portable Oakton pH/conductivity meter. Cation samples were filtered (0.45 μm) and acidified in the field while anion and isotope samples were untreated. Samples were refrigerated at approximately 4 °C, except for brief periods during shipping.

Two research boreholes installed for the GAP have provided subpermafrost and talik groundwater samples with which to compare the surface waters (Claesson Liljedahl et al., 2015; Harper et al., 2015a; see Chapters 1 and 3). DH-GAP01 was drilled to intersect a talik beneath lake L26 (SS903; see Figure 2.1) and is a total of 221.6 m long and 191 m deep (vertical depth). DH-GAP04 was drilled at the edge of the ice margin at Isunnguata Sermia glacier. DH-GAP04 is 687 m long and has a vertical depth of 645 m. DH-GAP04 has three sampling sections between the base of the permafrost, at 400 m borehole length, and the bottom of the borehole. The lowest section (604.5 to 687 m borehole length) of the DH-GAP04 borehole is free of drilling water contamination while the upper and middle sections still contained significant drilling water contamination (33 and 29 % respectively) at the time of sampling in 2014. $\delta^{18}O$ and $\delta^{2}H$ results presented here for the upper and middle sections of DH-GAP04 are calculated using a linear mixing model and drilling fluid tracer concentrations. Other isotopic results for these sections ($\delta^{34}S$-$\delta^{18}O$ of SO_4. $\delta^{37}Cl$, $\delta^{81}Br$ and

$^{87}Sr/^{86}Sr$) can be considered representative of groundwater isotopic values due to much higher concentrations of these ions in the groundwaters.

The highly soluble mineral gypsum ($CaSO_4 \bullet 2H_2O$) was found as an abundant fracture infilling mineral in the DH-GAP04 core, predominantly below 300 m of borehole length (Pere, 2014; Harper et al., 2015a; see Chapter 4). Samples of fracture gypsum were obtained using dental tools under a binocular microscope and analyzed for $\delta^{34}S$ and $\delta^{18}O$ of SO_4 as well as $^{87}Sr/^{86}Sr$. Sulfide minerals, pyrite (FeS_2) and chalcopyrite [$(CuFe)S_2$], from gneissic bedrock from the DH-GAP01 borehole were extracted and analyzed for $\delta^{34}S$.

Samples of salt crusts that had formed on soils near lake L21 (Hunde Sø) and Lake L32 (Store Saltsø) were preserved in sample bags and analyzed by X-ray Diffraction (XRD). XRD was used to determine what salts formed these crusts.

2.4.1. Isotopic and Geochemical Analyses

Isotope analyses were performed at the University of Waterloo Environmental Isotope Laboratory. Methods for isotopic analyses are included in Chapter 1. Geochemistry samples were analyzed at Labtium Oy (via Geological Survey of Finland) in 2008 and 2010-2013 and the TVO (Teollisuuden Voima Oy) laboratory in Finland in 2009 (see Chapter 1). Results with charge balances exceeding 10% were either discarded with the exception of the sample from Lake L20 (01/07/2008) which had a charge balance error of -12.5%. Cl^- and $SO4^{2-}$ concentrations from the 2008 L20 sample (L20-1 in Appendix B) are used in order to include L20 $\delta^{34}S$ and $\delta^{18}O$ (SO_4) isotopic values in Figures 2.11 and 2.13. Sampling and analytical methods for historical samples acquired from Dr. Anderson are documented in Anderson et al. (2001).

2.5. Results

2.5.1. Geochemical

The dilute lakes were generally Ca or Mg -HCO_3 or Ca or Mg-HCO_3-SO_4 type, while the more saline lakes tended to be Na or Mg-HCO_3,Cl type waters. A small subset of lakes contained a high percentage of anions as sulfate: Lake L20 from the GAP and Lakes SS70-76 in Anderson et al. (2001). Lake L20 was highly acidic, with a pH of 3.5, whereas the majority of lakes had pH >7.

Lakes were divided into 4 categories based on size, salinity and water source. (1) Ponds are lakes that are approximately 2 m deep or less, and may evaporate completely in the summer or freeze to the bottom in the winter. Ponds may show seasonal salinity variations due to evaporation. For example, Lake L20 had an electrical conductivity of 354 μS/cm when sampled in early June, 2008, and 1750 μS/cm when sampled in early September, 2010. Lake L20 had visibly shrunk by a significant amount when sampled in 2010. (2) Dilute lakes are those that were unlikely to freeze to the bottom in winter (>2 m deep) and had conductivities of <800 μS/cm, following the classification of Anderson et al. 2001. (3) Saline lakes were also of sufficient size to not freeze to the bottom in winter and had conductivities >800 μS/cm. In general, saline lakes are located in closed basins with no visible outflow. (4) Meltwater/thaw lakes include glacial meltwater fed lakes (e.g., Lake L6).

Also included are the thaw lakes deriving water from melting of frozen till and precipitation, such as Lakes L12-L14 and L23-L24, all of which are located on the till plain in front of Leverett glacier (Figure 2.1). While the thaw lakes are likely to be more geochemically evolved than the meltwater-fed lakes, they are similar in terms of low conductivity, depleted $\delta^{18}O$ isotopic signatures (Table 2.1) and access to relatively fresh glacial sediment. Meltwater and thaw lakes tend to plot together in many of the figures.

Table 2.1. Summary of major geochemical and isotopic results. Alkalinity is expressed as mmol/L as $CaCO_3$. Meltwater lakes, lakes which receive meltwater directly, and the thaw lakes on the Leverett till plain are separated here to illustrate the similarity between these two groups.

Group		EC uS/cm	pH	$\delta^{18}O$ ‰ VSMOW	$\delta^{2}H$ ‰ VSMOW	^{3}H TU	Ca mg/L	Mg mg/L	K mg/L	Na mg/L	Cl mg/L	SO_4 mg/L	Alk mmol/L
Ponds n=8	**Avg**	845	7.8	-10.5	-107.9	10.2	84.5	46.7	16.7	17.8	21.4	360	1.6
	Min	164	3.4	-16.2	-134.1	9.4	3.5	1.1	1.7	0.9	1.4	6.1	0.2
	Max	1797	9.2	-5.2	-84.5	12.0	210	135	45	78	102	949	3.0
Dilute Lakes n = 26	**Avg**	256	8.2	-11.0	-109.0	9.5	16.5	13.8	6.9	13.5	17.7	7.2	1.8
	Min	50	7.2	-15.1	-131.6	7.4	2.7	2.2	0.7	1.3	1.7	0.0	0.1
	Max	616	9.6	-6.8	-91.9	12.9	42	36	28	53	69	88	4.5
Saline Lakes n=14	**Avg**	2848	8.9	-8.8	-99.9	10.5	25.9	161	113.9	350	487	174	14.0
	Min	902	8.2	-11.4	-113.2	8.2	4.0	57.3	35.3	74.2	121	18.2	6.6
	Max	4500	9.2	-6.5	-93.9	13.2	108	254	190	590	782	403	22
Melt-water Lakes	**L6**	223	7.7	-15.1	-128.8	10.5	25.5	9.3	3.4	3.1	3.0	43.6	1.23
	L36 (P660)	62	6.8	-18.1	-145.5	9.4	5.9	3.3	0.4	1.8	1.8	3.3	0.43
Thaw Lakes n = 5	**Avg**	238	8	-14	-130	8	32.7	5.0	6.3	4.2	2.6	57.2	0.9
	Min	61	7	-15	-136	7	7.2	0.9	1.7	1.1	0.9	12.0	0.3
	Max	327	8.4	-13.1	-127.2	10.5	46	7.3	8.5	5.2	3.8	77	1.6

Table 2.2. (next page) Summary of representative chemistry and isotopic results. P = pond, DL = dilute lake, SL = saline lake and MW = meltwater lake. * indicates the results for dissolved chemical species are average results over multiple years as measured by John Anderson (ex. Anderson et al. 2001). Alkalinity is expressed as mg/L as $CaCO_3$. NM = not measured.

.

	Location	Name	Sample Date	Lake Type	EC uS/cm	pH	Ca mg/l	Mg mg/l	K mg/l	Na mg/l	Cl mg/l	SO4 mg/l	Alk mg/L	Sr µg/l	Br µg/l	$\delta^{18}O$ ‰ VSMOW	$\delta^{2}H$ ‰ VSMOW	^{3}H TU	$^{87/86}Sr$
Ice Marginal	L8		2008-06-28	P	342	7.9	32	20	2	3.5	2	132	76	62	36	-16.2	-134	10	NM
	L20 2	Acid Lake	2010-09-05	P	1750	3.4	182	74	29	17	14	949	<2	217	123	-10.6	-107	10	NM
	L18		2008-07-01	P	1797	8.9	130	135	45	78	102	725	304	540	420	-5.2	-85	10	0.7459
	L1		2008-06-27	DL	381	8.4	27	19	11	19	31	2	303	94	156	-11.0	-111	11	0.7553
	L15		2008-06-30	DL	74	8.0	5	4	1	1.8	2	1	57	15	16	-14.8	-132	8	0.7536
	L26 26m	Talik Lake	2010-05-11	DL	232	7.7	18	11	6	6.7	10	3	190	63	40	-12.9	-118	10	0.7385
	L41		2011-09-12	DL	550	8.6	26	36	18	29	40	<1	451	93	141	-7.5	-95	9	0.7487
	L43		2011-09-12	DL	150	7.7	12	7	3	6.9	9	3	112	40	84	-12.5	-115	8	0.7439
	SS32		2003-08-21	DL	51	7.3	4	3	1	2	2	1	<1	NM	NM	NM	NM	NM	0.7557
	L17		2008-07-01	DL	902	9.0	23	85	35	74	121	24	816	72	277	-11.4	-113	10	0.7510
	L29		2010-09-04	SL	1250	9.2	15	85	88	105	152	<1	859	70	79	-6.5	-96	10	NM
	L6		2008-06-28	MW	223	7.7	26	9	3	3.1	3	44	123	52	40	-15.1	-129	11	0.7514
	L12		2008-06-29	TH	297	7.8	40	6	8	4.9	4	71	130	130	27	-13.6	-128	7	0.7533
Upper Fjord	L33	Lake Ferguson	2010-09-04	DL	66.1	7.6	7	3	2	2.6	3	2	57	41	21	-12.7	-112	12	0.7187
	SS2*		2003-08-20	DL	321	7.9	26	13	4	18	15	3	NM	NM	NM	NM	NM	NM	0.7353
	SS8/L46		2012-09-03	DL	236	8.9	23	15	11	21	28	2	237	96	103	-10.2	-95	7	0.7310
	L45		2012-08-28	SL	3470	8.3	108	150	80	340	722	384	656	883	1960	-9.0	-101	9	0.7267
	L21	Hunde Sø		SL	4030	8.8	16	203	182	545	797	180	2060	574	980	-10.1	-101	15	0.7298
	L32	Store Saltsö	2010-09-04	SL	3110	8.9	21	155	181	343	372	18	1880	238	667	-9.9	-104	8	0.7540
	L22/SS4	Braya Sø	2011-09-10	SL	3000	8.9	20	149	128	362	493	91	1560	356	759	-8.9	-95	12	0.7295
	L39/SS5	Limnea Sø	2011-09-10	SL	4500	9.0	15	233	190	588	782	190	2230	337	944	-7.7	-93	11	NM
	SS1122*			SL	3167	8.8	58	141	156	418	664	243	NM	NM	NM	NM	NM	NM	0.7275
	SS1421 2m*		2004-06-23	SL	2690	9.1	18	155	4181	337	415	175	NM	NM	NM	NM	NM	NM	0.7314
Coastal	SS48*			DL	29.1	6.6	3	1	<1	2	4	2	NM	NM	NM	NM	NM	NM	0.7154
	SS76*		12.08.03	DL	345.5	7.7	42	10	3	9	13	88	NM	NM	NM	NM	NM	NM	0.7410
	SS75*		12.08.03	DL	226.3	5.0	16	7	1	6	7	76	NM	NM	NM	NM	NM	NM	NM

A breakdown of average, minimum and maximum values for concentrations of dissolved species, EC, pH, alkalinity as well as a subset of isotopic results are presented in Table 2.1. Results for a representative subset of lakes for each of the areas (ice marginal, upper fjord and coastal) described in Figure 2.1 are given in Table 2.2.

A large ice-dammed lake (lake L38) located along Russell Glacier (Figure 2.1) was observed to drain abruptly in 2011, exposing three springs on the lake bottom. The ice-dammed lake springs were dilute (97 and 155 μS/cm), Ca-Mg-HCO_3-SO_4 type waters, similar to the dilute lakes, but were isotopically ($\delta^{18}O/\delta^{2}H$) depleted relative to most of the other lake waters in the study area (Table 2.3).

2.5.2. Isotopic Results

When considering the isotopes of water, lakes fall along local evaporation lines (LELs) similar to those described by Leng and Anderson (2003) for lakes close to the ice (zone 5) and lakes around the upper fjord (zone 4)(Figure 2.2a). Meltwater lakes tend to show greater isotopic depletion and lower deuterium-excess (D-excess) values than those predicted by the LELs described by Leng and Anderson (2003) (Figure 2.2a). The precipitation average of $\delta^{18}O$ was estimated to be -19‰ by Leng and Anderson (2003) based on the interception of the LELs with the GMWL and Kangerlussuaq's position between the International Atomic Energy Agency (IAEA) monitoring stations at Grönnedal and Thule. A snowfall sample taken July 1st, 2009, near the ice sheet had a $\delta^{18}O$ of -20.16 ‰.

Table 2.3. Summary of results from ice-dammed lake (L38) springs and from lake L38. Alkalinity is presented as mg/L as $CaCO_3$. Charge balance error on IDL spring 2 exceeds 10%.

	EC	pH	δ18O	δ2H	^3H	Ca	Mg	K	Na	Cl	SO_4	Alk	NO3
	uS/cm		‰ VSMOW		TU	mg/L	mg/L	mg/L	mg/L	mg/L	mg/L	mg/l	mg/L
IDL Spring 2	97	7.3	-21.8	-165.4	7.6	7.1	3.2	1.8	1.3	1.7	11.6	30	5.4
IDL Spring 3	155	8.3	-24.4	-186.0	4.8	13.4	5.6	2.9	1.4	0.8	26.0	70	3.6
Lake L38	19	7.8	-28.2	-217.0	1.0	chemistry not analyzed							

IDL = ice-dammed lake

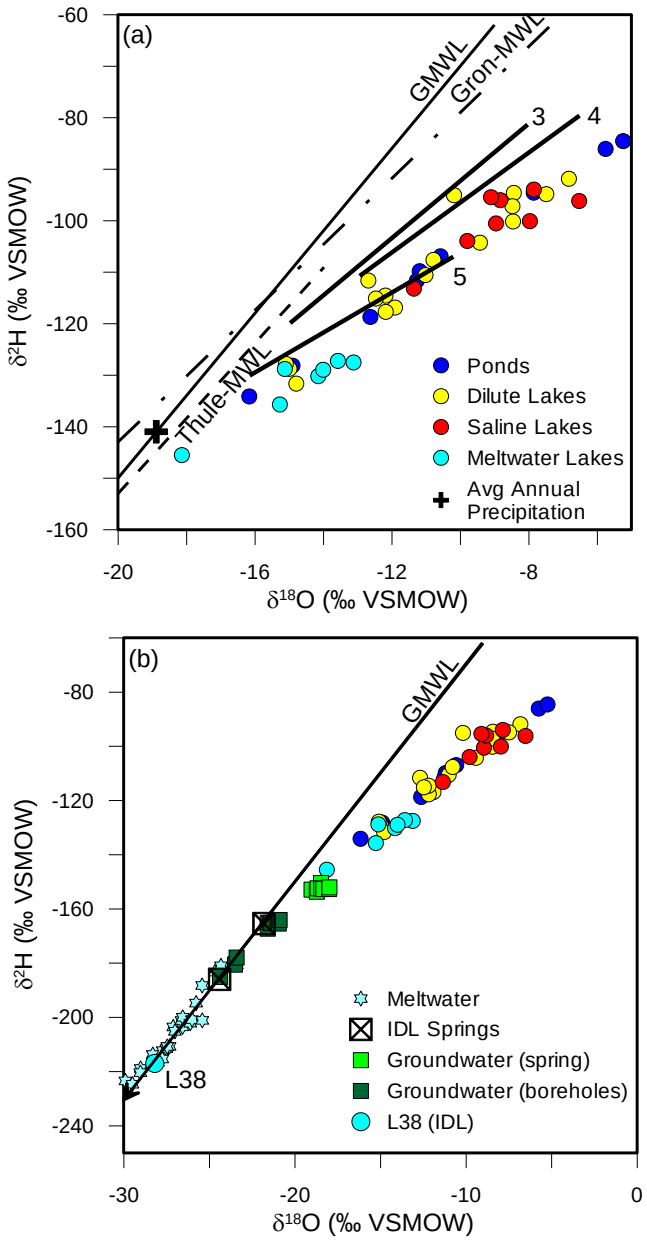

Figure 2.2. (a) Isotopic composition of lakes. Local evaporation lines are adapted from Leng and Anderson (2003) for zones 3 - Mid fjord, 4 - upper fjord and 5 - close to ice sheet. The zones from Leng and Anderson (2003) correspond to area 3 (zone 3), area 2 (zone 4), and area 1 (zone 5). Average annual precipitation estimated from intercept of LEL with GMWL. Local meteoric water lines for Grönnedal and Thule were generated using isotopic monitoring data from IAEA stations. (b) Isotopic composition of lakes compared to groundwaters and meltwaters from Kangerlussuaq Region.

Tritium analyzed in summer snow sampled in 2009 had a tritium concentration of 13.8 TU. Lakes had a wide range of tritium concentrations, 6.6 to 13.2 TU, with an overall average of 9.6 TU for all lakes where tritium was measured. Average, minimum and maximum tritium concentrations are broken down for each lake grouping in Table 2.1.

$^{87}Sr/^{86}Sr$ isotopic ratios in lakes have a large range of values from 0.7154 to 0.7580 (subset of results in Table 2.2). As well, $^{87}Sr/^{86}Sr$ isotopic ratios were analyzed for soil water samples. PVC tube wells were installed around lake L26 (SS903) (Figure 2.3) as part of a detailed hydrological and geochemical study of the lake basin. The hydrological characterization of this study was published by Johansson et al. (2014, 2015). An overview of the installation methods can be found in Johansson et al., (2014), which describes the extensive hydrological dataset acquired around lake L26. The $^{87}Sr/^{86}Sr$ isotopic ratios measured in the soil waters are presented in Table 2.4.

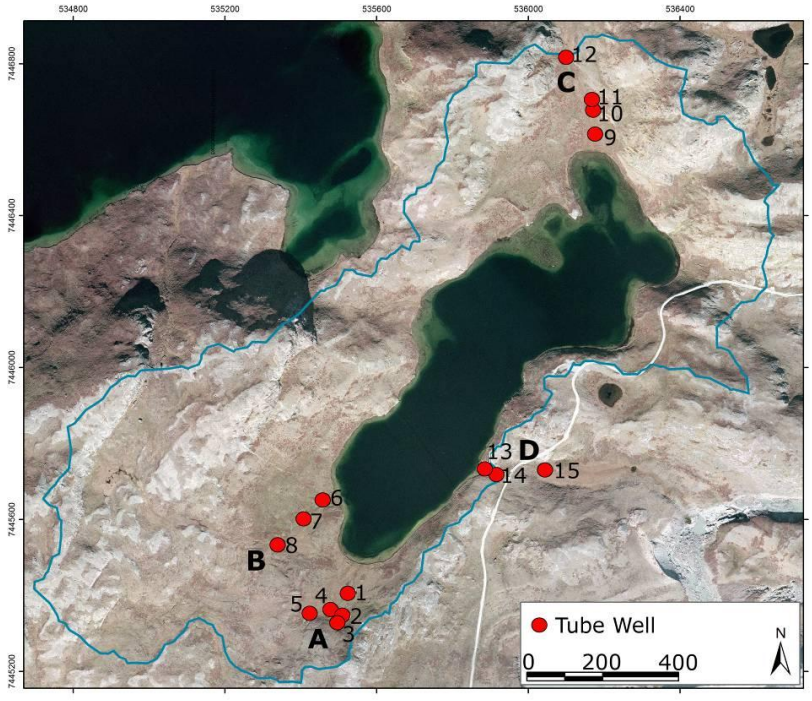

Figure 2.3. Map of tube well locations around L26 (Talik Lake). The wells, along with a comprehensive meteorological and hydrological data set, are described in Johansson et al. (2014 and 2015).

Table 2.4. $^{87}Sr/^{86}Sr$ ratios for waters from soil pipes installed around Lake L26 (SS903). The pipes were installed along drainage routes into (A to C) and out of (D) the lake (Johansson et al., 2014).

A	87Sr/86Sr	B	87Sr/86Sr	C	87Sr/86Sr	D	87Sr/86Sr	Lake	87Sr/86Sr
P1	0.7542	**P6**	0.7470	**P9**	0.7433	**P14**	0.7318	**L26-5m**	0.7385
P3	0.7548	**P7**	0.7307	**P10**	0.7425	**P15**	0.7365	**L26-8m**	0.7385
P4	0.7565			**P11**	0.7396			**L26-28m**	0.7385
P5	0.7552			**P12**	0.7437				

$\delta^{37}Cl$ and $\delta^{81}Br$ are measured against standard mean oceanic chloride (SMOC) and bromide (SMOB), respectively, and thus, marine chlorine and bromine have isotopic signatures of 0‰. Fifteen lakes were analyzed for $\delta^{37}Cl$, which ranged from -0.41 to +0.04‰ (Table 2.5). Six lakes were analyzed for $\delta^{81}Br$, which ranged from -0.06 to +1.76‰ (Table 2.5).

Groundwaters tend to be of Ca-Na-SO_4 type and are depleted in $\delta^{18}O$ and $\delta^{2}H$ relative to lake waters. DH-GAP01 intersects the talik beneath lake L26 (SS903). Pressure measurements indicating a downward gradient in hydraulic head suggest recharge conditions in the talik (Johansson et al., 2015). $\delta^{18}O$ and $\delta^{2}H$ isotopic values that are more enriched than the DH-GAP04 groundwaters and plot below the GMWL further support recharge and mixing of lake water into the talik (Figure 2.2b). Groundwater from DH-GAP04 indicates that subpermafrost groundwater at the ice margin is brackish to a depth of 450 m and contains concentrations of sulfate up to 1900 mg/L and Cl concentrations of 176 mg/L. $^{87}Sr/^{86}Sr$ ratios of groundwater (0.7033 to 0.7075) reflect that of fracture minerals, such as gypsum (0.7023-0.7080), and are less radiogenic than surface waters (0.7154 to 0.7580) (Chapters 3 & 4).

Lake sulfate values have a much larger range of $\delta^{34}S$ and $\delta^{18}O$ (SO_4) values than groundwaters or sulfide and sulfate minerals. Full results for $\delta^{34}S$ and $\delta^{18}O$ (SO_4) are given in Table 2.6.

Table 2.5. Results of $\delta^{37}Cl$ and $\delta^{81}Br$ analyses on lakes and borehole groundwaters. Analytical uncertainty on $\delta^{37}Cl$ and $\delta^{81}Br$ is ±0.2 ‰. Locations with * next to the name indicate average lake chemistries. NM = not measured.

Location	Cl mg/l	Br µg/l	$\delta^{37}Cl$ ‰ SMOC	$\delta^{81}Br$ ‰ SMOB
L32	372	667	-0.2	-0.1
L22/SS4	493	759	0.0	0.8
SS1122 8m*	664	NM	0.0	0.9
L29	152	79	-0.3	1.0
L41	40	141	0.0	1.7
SS1421 18m*	415	NM	-0.5	1.8
SS1421 2m	NM	NM	-0.3	NM
SS1421	NM	NM	0.1	NM
SS3*	669	NM	-0.6	NM
L18	102	420	-0.4	NM
L21	797	980	-0.2	NM
SS6*	567	NM	-0.2	NM
L26 5m	10	40	-0.1	NM
SS5 0.5m	782	944	0.0	NM
SS1164 8m*	173	NM	0.0	NM
L12	4	27	0.0	NM
DH-GAP01	8	90	-0.1	0.3
DH-GAP04U	94	1260	0.3	0.4
DH-GAP04M	109	1520	0.2	NM
DH-GAP04L	173	2390	0.4	0.6

Salt crusts collected from the vicinity of L21 (Hunde Sø) and L32 (Störe Saltsö) were analyzed by X-ray Diffraction. Salts around Lake L21 included antarcticite ($CaCl_2 \bullet 6H_2O$), calcite ($CaCO_3$) and hydrohalite ($NaCl \bullet 2H_2O$) while around L32 (Store Saltsø) the salt crust was composed primarily of gypsum ($CaSO_4 \bullet 2H_2O$).

Table 2.6. Isotopic composition and concentration of sulfate in surface waters and groundwaters. Sulfate minerals (predominantly gypsum) from fracture infillings and sulfide minerals from the rock matrix are included from the DH-GAP01 and DH-GAP04 cores. Gypsum was found abundantly as a fracture filling below a depth of 300 m in the DH-GAP04 borehole, while only one occurrence of gypsum was noted in the DH-GAP01 borehole. NM is not measured due to insufficient sample material. NA is not applicable.

Location	Sample Type	$\delta^{34}S$ SO_4	$\delta^{18}O$ SO_4
		‰ CDT	‰ VSMOW
L20 2	pond	-0.7	-3.0
L20 1	pond	0.4	-3.9
L18	pond	1.1	3.4
SS75	dilute lake	1.2	-2.2
L43	dilute lake	12.5	-1.0
L45	saline lake	14.1	NM
SS5	saline lake	19.3	8.1
SS5	saline lake	20.2	8.0
SS4	saline lake	22.9	5.5
SS4	saline lake	23.3	4.6
L21	saline lake	23.4	5.3
1371	saline lake	28.5	7.8
L12 1	thaw lake	3.8	-11.0
DH-GAP01	Groundwater BH	4.9	5.9
DH-GAP04-Up	Groundwater BH	5.0	3.9
DH-GAP04-Mid	Groundwater BH	4.5	3.1
DH-GAP04-Low	Groundwater BH	5.0	2.9
Leverett Spring	Groundwater Spr	10.9	5.9
DH-GAP01	Sulfide Minerals	2.3 - 3.7	NA
DH-GAP04	Fracture Sulfate	2.6 - 10.7	4.5 - 9.1

2.6. Discussion

The lakes sampled represent a transect (Figure 2.1) from the coast north of Søndre Strømfjord to the ice sheet east of Kangerlussuaq. The transect represents both a climatic gradient from maritime to continental interior (Anderson et al., 2012; Leng et al., 2012), as well as a chronosequence of lake and lake catchment development since glacial retreat (Fritz & Anderson, 2013). The lakes along this transect can be roughly divided into the three areas shown on Figure 2.1b. The first area (1) is from the ice margin to the head of the fjord (ice marginal). The second (2)

is the area around the head of the fjord that Leng and Anderson (2003) termed "upper fjord", and the third area (3) is coastal and covers from the head of the fjord to the west coast (Figure 2.1). The three areas represent increasing distance from the present ice margin and increasing time since deglaciation. The division of the transect into three areas helps to provide a framework in which to discuss the impact of glaciation on lake evolution and the effect of landscape evolution post glaciation.

From the coastal to ice marginal areas, the processes that affect the chemical evolution of lakes vary in importance. Evaporation decreases toward the coast as humidity increases (Leng & Anderson, 2003; Anderson et al., 2012). Weathering rates decrease in the less vegetated, cooler and dryer areas close to the ice sheet (Anderson et al., 1997, 2001). Microbial activity, most significantly sulfate reducing bacteria, increases in the warmer temperatures around the upper fjord. Toward the coast there is increased influence of marine aerosols (Anderson et al., 2001). These processes and others are discussed in detail below.

2.6.1. Evaporation and Salts

The influence of distance from the coast, which controls marine inputs and the relative influence of evaporation versus precipitation, is apparent in several isotopic systems related to lake water composition (Leng and Anderson, 2003). Inland, evaporation increases as humidity and precipitation decrease. Anderson et al. (2001) indicate that the change to negative effective precipitation occurs at approximately 52° W (Figure 2.1).

Evaporation is a major influence on the isotopic signature ($\delta^{18}O/\delta^{2}H$) of lakes in the region. Leng and Anderson (2003) analyzed $\delta^{18}O$ and $\delta^{2}H$ in lakes from the coast to the ice sheet and found that lakes fall along local evaporation lines (LELs) which vary in slope by region (Figure 2.2a). Coastal lakes have an LEL with a slope (s = 5.4-5.5) closest to the slope of the GMWL (s = 8), while in the dry,

low precipitation regions, close to the ice sheet, the slope was much lower (s = 3.9). Depending on the volume of precipitation, surface area and lake depth, the $\delta^{18}O$ isotopic signature can vary annually by over 2‰ (Leng & Anderson, 2003). The lakes sampled for the GAP show similar trends to those sampled by Anderson et al. (2001) (Figure 2.2a). Evaporative effects are greatest in the ice marginal lakes (area 1) and decrease toward the coast (area 3). Lakes for the GAP were sampled in the ice marginal (area 1) and upper fjord (area 2) regions, which coincide with areas 4 and 5 in Leng and Anderson (2003) (Figure 2.2a). Correspondingly, the lakes sampled for the GAP tend to fall along the LELs described for the ice marginal (4) and upper fjord (5) areas (see Figure 2.2a). A departure from the local evaporation lines described by Leng and Anderson (2003) can be seen in the $\delta^{18}O/\delta^{2}H$ isotopic signature of the meltwater lakes (Figure 2.2a). The majority of lakes whose main water source is glacial meltwater have a lower D-excess and plot below the LEL for the ice marginal lakes (area 1) (shown as line 5 in Figure 2.2a). The initial source of water for the meltwater lakes would have the more depleted isotopic signature observed for meltwaters (Figure 2.2b). Thus, a lower D-excess would be expected in the meltwater sourced lakes.

Turner et al. (2010) and Bouchard et al. (2013) found that shallow subarctic lakes were vulnerable to evaporation and desiccation when runoff from snowmelt was low, either because of the lack of snow accumulation in the basin or due to years of reduced snowfall. Ponds in the ice marginal area are rapidly impacted by evaporation and, similar to shallow lakes in the Canadian Arctic, may see increased desiccation if snowfall decreases due to climate change.

Evaporation in shallow areas around lakes or from soils can lead to salt crust formation. Lake and soil salts crusts have both been observed in the study area (figure 2.4). Salt crusts may be redissolved during precipitation events or snowmelt, contributing to lake salinity. Salts may also be removed by wind and transported with prevailing winds further inland. XRD analysis of salt crusts

from around L21 (Hunde So) showed the presence of antarcticite and hydrohalite: chloride salts that occur in cold climate conditions. Antarcticite was discovered as a crystalline salt in the Don Juan Pond in the Dry Valleys of Antarctica (Torii & Ossaka, 1965; Takamatsu et al., 1998). The presence of chloride salts reflects the relatively high chloride concentrations (797 mg/L) found in Lake 21. Interestingly, the salt crust found near Lake L32 (Store Saltsø) was composed entirely of gypsum despite the relatively low concentration of SO_4^{2-} (18 mg/L) relative to Cl^- (372 mg/L) in the lake waters. It may be that the salt crust sampled is reflective of salts found within the soils surrounding the lake.

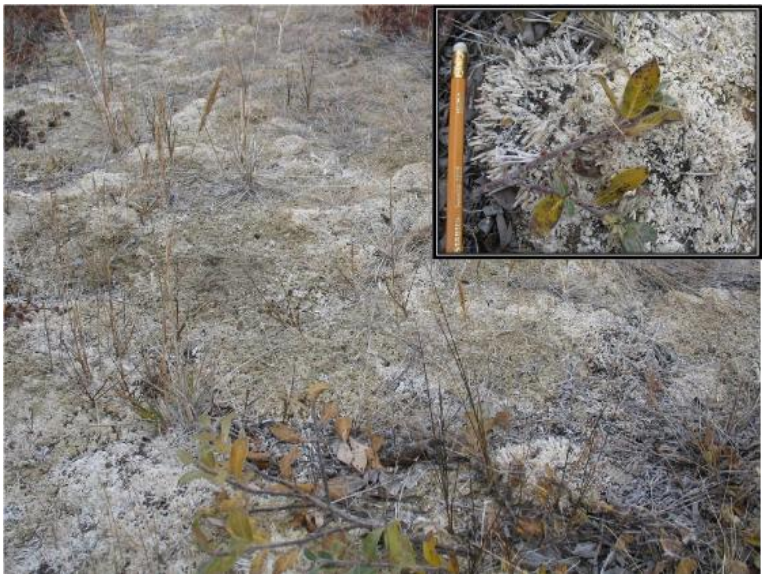

Figure 2.4. Salt crusts observed covering vegetation near Lake L32 (Store Saltsø). Evaporation of brackish lake waters from shallow areas leads to precipitation of salts.

Lakes that receive chloride primarily from halite, whether marine or terrestrial, tend to have a Na:Cl equivalent ratio of 1. Figure 2.5 indicates that most lakes fall on or close to a 1:1 meq ratio of Na^+ to Cl^- and generally do not have an excess of Cl^-, with the notable exception of lake L45, which is discussed later. Seawater and seawater aerosols will have a Na:Cl molar ratio of 0.86 . Sources of additional Na^+ are addressed further in later sections.

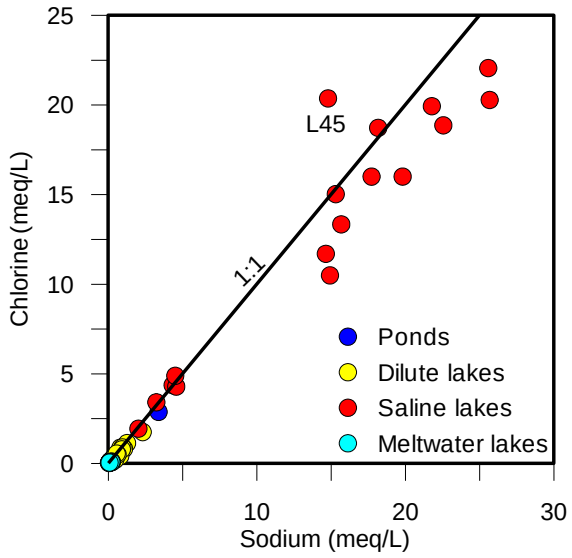

Figure 2.5. Comparing the meq of Na^+ to Cl^- shows most lakes fall along a 1:1 equilibrium line indicative of marine and/or terrestrial halite dissolution.

The stable isotopic ratio of chlorine (chloride), $^{37/35}Cl$, can be used to identify sources of chloride salts and processes. Chlorine-37 is preferentially incorporated into the solid phase during halite precipitation causing the residual solution to become progressively lighter as halite precipitates (Magenheim et al., 1995; Wood et al., 2005). In a closed system, where halite is precipitated and then re-dissolved, the $\delta^{37}Cl$ signature should not change significantly from the initial value. In the case of the lakes in the Kangerlussuaq region, Cl^- is likely to be of marine origin from sea salt aerosols and have a value around 0‰ (Eggenkamp, 1994; Eggenkamp et al., 1995; Zhang et al., 2007). In an open system, for example if halite is removed by aeolian activity, $\delta^{37}Cl$ should be depleted relative to the marine value, yielding negative isotopic signatures. Alternatively, lakes with positive $\delta^{37}Cl$ values may be receiving $\delta^{37}Cl$ enriched chloride, deflated from halite precipitated from waters whose initial chloride input was marine.

$\delta^{81}Br$ follows the opposite trend to $\delta^{37}Cl$, becoming more enriched in the residual solution (Hanlon, 2015). In the Sand Hills of Nebraska, $\delta^{81}Br$ was found to be more enriched than $\delta^{37}Cl$ in the

waters, while $\delta^{37}Cl$ in salt crusts was found to be more enriched than $\delta^{81}Br$. $\delta^{37}Cl$ in salts crusts was slightly enriched relative to $\delta^{37}Cl$ in waters, while $\delta^{81}Br$ in salt crusts was depleted relative to the waters (Frape et al., 2013; Hanlon, 2015).

Lakes analyzed for $\delta^{37}Cl$ and $\delta^{81}Br$ are within areas 1 and 2, as the dilute coastal lakes (area 3) had insufficient concentrations of halides to perform the analyses. Both the ice marginal and upper fjord areas were predicted to show isotopic depletion of $\delta^{37}Cl$ values and enrichment in $\delta^{81}Br$ due to evaporation (Magenheim et al., 1995; Wood et al., 2005; Frape et al., 2013). Two trends in the $\delta^{37}Cl$-$\delta^{18}O$ isotopic results are indicated on Figure 2.6a. The first trend (1) describes the evaporative enrichment of $\delta^{18}O$, which is correlated with depletion of $\delta^{37}Cl$. The second group (2) of samples includes two saline and one dilute lake (L41, SS4 and 1122) maintaining a marine $\delta^{37}Cl$ isotopic signature (0 ‰) despite evaporative enrichment of $\delta^{18}O$. However, Lakes L41, SS4 and 1122 do have enriched $\delta^{81}Br$ values indicative of salt deflation (Figure 2.6b).

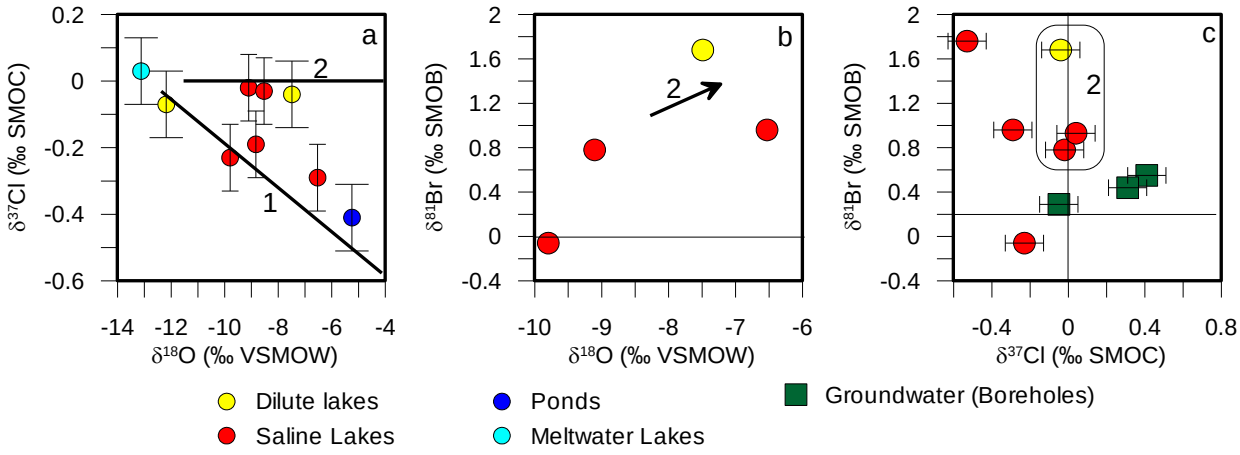

Figure 2.6. (a) $\delta^{37}Cl$ compared to $\delta^{18}O$ isotopic composition. $\delta^{81}Br$ values compared to (b) $\delta^{18}O$ isotopic values and (c) $\delta^{37}Cl$ isotopic values. Analytical error corresponds to symbol size except where otherwise indicated by error bars.

The majority of lake samples analyzed for $\delta^{81}Br$ are positive, as predicted (see Figure2.6b). However, a comparison plot of the $\delta^{37}Cl$ and $\delta^{81}Br$ results shows a poor correlation. That is, the most depleted $\delta^{37}Cl$ values do not necessarily correspond to the most enriched $\delta^{81}Br$ values (Figure 2.6c). It is clear that the impact of evaporation on $\delta^{37}Cl$ and $\delta^{81}Br$ signatures is complex and the limited data provided here are only a first attempt at understanding $\delta^{37}Cl$ and $\delta^{81}Br$ processes in Arctic lake environments.

The dissolution of soil salts can be an important process for lake chemistry. Weathering of soils and bedrock by rainwater or snowmelt, followed by evaporation, produces salts that are later re-dissolved and carried into surface waters. In some case, these soil salts can be a dominant control on lake chemistry (Garrels & Mackenzie, 1967; Drever & Smith, 1978). Drever and Smith (1978) found that soil salts dissolved in a specific order, with Na^+ and Cl^- as the first salts to enter solution, followed by K^+, SO_4^{2-}, Mg^{2+} and Ca^{2+} and then SiO_2, resulting in solutions that were enriched in Na^+ and Cl^- relative to Ca^{2+}, Mg^{2+} and SO_4^{2-}. The selective dissolution of soil salts may be a plausible mechanism to enrich lake waters in Cl^- relative to SO_4^{2-} and Na^+ relative to Ca^{2+} (Figure 2.7). Cation exchange in the lake catchment soils, where Ca^{2+} displaces Na^+ from exchange sites, may also enrich lakes in Na^+ relative to Ca^{2+}.

The majority of ponds and dilute lakes fall along a trend of increasing Cl^- compared to SO_4^{2-} and increasing Na^+ compared to Ca^{2+} (Figure 2.7). Ponds, meltwater lakes and runoff tend to have higher SO_4^{2-} relative to Cl^- and higher Ca^{2+} relative to Na^+. Sulfide oxidation in the lake basin will contribute SO_4^{2-} as well as increase acidity. Low pH promotes carbonate dissolution, increasing input of Ca^{2+}. The ponds and meltwater lakes sampled were located in the ice marginal area and, as such, most likely have decreased input of marine Cl^- and limited or no removal of SO_4^{2-} by sulfate reduction.

Winds in the ice marginal area are dominantly katabatic winds from the ice sheet (Aebly & Fritz, 2009) which may limit marine Cl^- inputs.

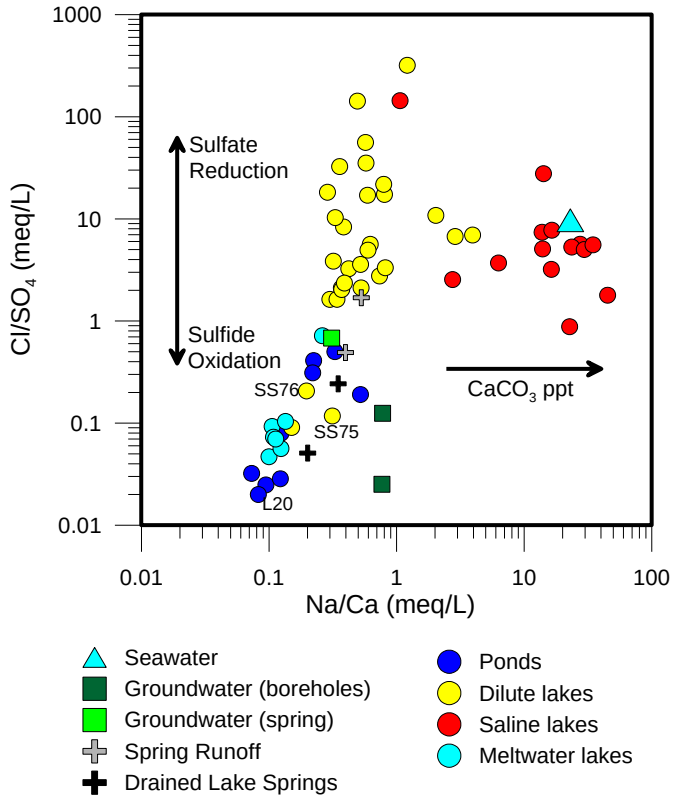

Figure 2.7. Relationship between Na/Ca ratios compared to Cl/SO_4 ratios indicates the relative importance of processes such as sulfate reduction, sulfide oxidation and $CaCO_3$ precipitation.

Saline lakes tend to have excess Na^+ versus Ca^{2+} when compared to the dilute lakes. As lake salinity increases through evaporation or by salt exclusion during winter ice formation, $CaCO_3$ saturation may be reached and $CaCO_3$ will precipitate, removing Ca^{2+} and increasing the Na/Ca ratio. $CaCO_3$ rich layers can be observed in lake cores around Søndre Strømfjord (Bennike, 2000; Anderson et al., 2001, 2002; McGowan et al., 2003), supporting the precipitation of $CaCO_3$ as a mechanism for Ca^{2+} depletion in saline lakes. Anderson et al. (2002) also suggest that $CaCO_3$ precipitation may occur during the summer months when pH is increased due to photosynthesis.

2.6.2. Permafrost and Shallow Groundwater Flow

Flow through the active layer toward Arctic lakes can be a complex process (Bursey, 1990; Bursey et al., 1991) . Flow rates could be vastly different over short distances and water may be stored in frozen soil over the winter season. Quinton and Marsh (1999) found that most runoff occurs during summer in the shallow subsurface rather than as overland flow. The depth of the active layer and its permeability will depend strongly on soil type. Flow could be rapid through the active layer, following inter-hummock channels and soil pipes. In general, the mineral soils of the hummocks are less permeable than the peat between hummocks, allowing for faster inter-hummock flow (Carey & Woo, 1998; Quinton & Marsh, 1999; Quinton et al., 2000; Vidstrand, 2003). Uneven thaw of the active layer also can contribute to complex shallow groundwater flow, allowing for subsurface flow that does not directly match surface topography (Woo & Steer, 1983). The possibility for storage as shallow permafrost, coupled with complex active layer flow, can have direct influence on the $\delta^{18}O/\delta^{2}H$, conductivity, $^{87}Sr/^{86}Sr$ and ^{3}H of waters entering lakes.

During evaporation, salinity (conductivity) increases. Evaporation also causes $\delta^{18}O$, $\delta^{2}H$ and ^{3}H to enrich as the lighter isotopes are preferentially incorporated into the vapour phase. Figure 2.8 indicates that the correlation between these parameters in the studied lakes is not straightforward and is likely complicated by the factors discussed above. Storage, as shallow permafrost/ground ice, would allow for ^{3}H decay while permafrost melt re-introduces water with a tritium content lower than that of modern precipitation to the shallow flow system, and ultimately to surface water bodies. Tritium has been found in the upper meter to several meters of permafrost due to temperature-induced water migration (Chizhov et al., 1985; Romanov et al., 1986; Burn & Michel, 1988). We do, in fact, see poor correlation between these parameters (^{3}H, EC and $\delta^{18}O$), which should be related through evaporative processes (Figure 2.8). Dilute lakes show a wide range of $\delta^{18}O$ values that do not reflect a common initial $\delta^{18}O$ value similar to modern precipitation (-19‰).

Enrichment of $\delta^{18}O$ can be observed in the saline lakes; however, the most saline lakes are not those which are most enriched in $\delta^{18}O$. The upper fjord lakes follow a different evaporative pathway than the ice marginal lakes in terms of $\delta^{18}O$ and conductivity (Figure 2.8a). The reason for this is unclear, but may be related to lake basin size, lower relative humidity in the ice marginal area, temperature difference, contribution of meltwaters or to differences in active layer flow and permafrost melt contributions in the warmer upper fjord area compared to the ice marginal area. As discussed above, the impact of climatic differences, especially humidity, between the ice marginal and upper fjord lakes is also apparent in the local evaporation lines described by these two areas (Figure 2.2a). At lower humidities, there is increased fractionation in $\delta^{18}O$ relative to the fraction of water lost through evaporation (Gonfiantini, 1986). Thus, we would expect to see greater enrichment in $\delta^{18}O$ in the ice marginal area for a given increase in conductivity.

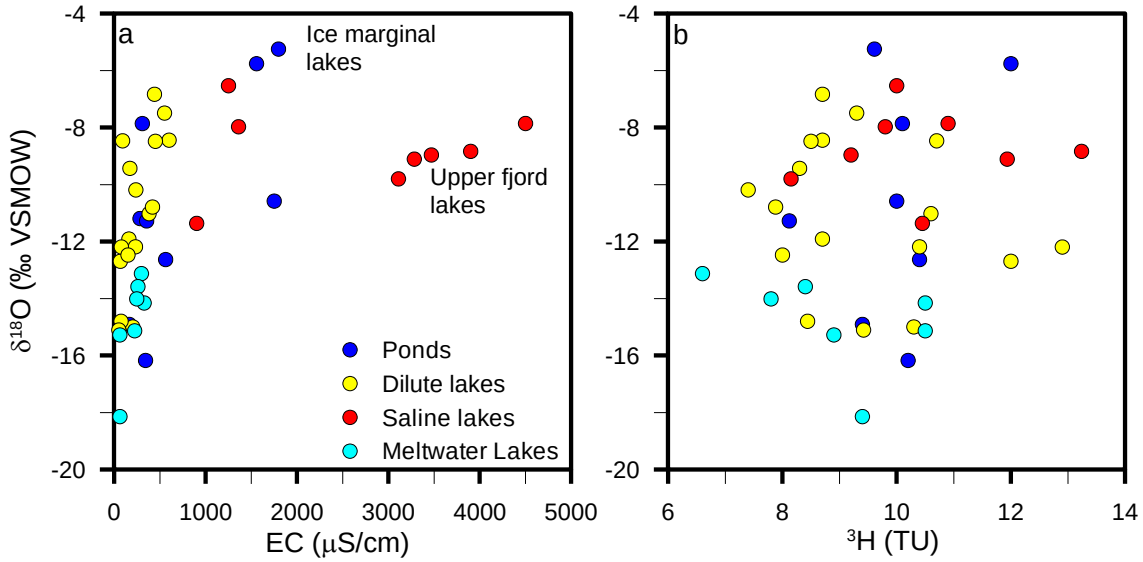

Figure 2.8. Oxygen-18 and (a) electrical conductivity and (b) tritium are often related through evaporative processes. Evaporation causes an enrichment in the $\delta^{18}O$ isotopic signature, increased conductivity and higher tritium concentrations. However, shallow groundwater flow and permafrost melt can complicate the relationship between these 3 parameters.

In almost all lakes, tritium concentrations are below those observed in summer precipitation samples (13.8 TU) acquired from freshly fallen snow on July 1st, 2009. Fourre et al. (2006) determined that by 1990, tritium levels in Greenland had returned to background levels measured in Thule before thermonuclear testing, between 10 and 20 TU. Many lakes also fall below the lower end (10 TU) of the range of tritium values given for Greenland by Fourre et al. (2006). This occurs even in ponds that dry completely on a yearly basis and receive a fresh influx of modern precipitation each spring. A secondary, less tritiated source, such as old ground ice trapped for long periods of time in or near the active layer, may be contributing to lake waters during warmer time periods. Lake basins that retain more snowfall tend to be larger, more vegetated and away from the arid conditions and high winds present in the ice marginal area. These lake basins, which receive higher inputs of spring melt containing more modern levels of tritium, are likely to have higher tritium concentrations: for example, the large Kellyville basin lakes have tritium concentrations higher than 10 TU.

Permafrost degradation and an increase in active layer thickness is predicted to occur with climate warming (Anisimov et al., 1997; Kokelj et al., 2002, 2009; Keller et al., 2007). Permafrost melt can cause an increased ionic input into surface waters (Kokelj et al., 2002, 2009; Keller et al., 2007) as previously frozen materials are exposed to weathering. With warming Arctic temperatures, an increase in permafrost degradation is expected and is predicted to drive change in chemical conditions and water quality of lakes in permafrost affected areas (Osterkamp & Romanovsky, 1999; Kokelj et al., 2009). Isotopic changes, such as a dilution of lake ^{3}H concentrations with permafrost melt that is ^{3}H poor, may also be expected.

The springs exposed after drainage of the ice-dammed lake (lake L38) corresponded to drainage pathways on the lake basin slopes and were interpreted to be shallow groundwater flow.

Supportive of this interpretation are the relatively high concentrations of nitrate (3.6 to 5.4 mg/L) compared to the lakes and groundwater, which generally did not have detectable concentrations of nitrate. During a shallow groundwater monitoring program in front of the Mittivakkat Glacier in southeast Greenland, higher concentrations of NO_3^- were observed in shallow wells located closest to valley walls (Kristiansen et al., 2013). Atmospheric deposition of nitrate, and subsequent accumulation due to lack of biologic degradation, has been observed in other cold arid climates such as the Atacama Desert in Chile (Michalski et al. 2004) and the soils and regolith of the Antarctic Dry Valleys (Michalski et al., 2004; McLeod et al., 2008). Similar to the Atacama Desert and Dry Valleys, limited nitrogen cycling may be occurring in the lake catchment. Additionally, spring waters had appreciable tritium concentrations(4.8 and 7.6 TU), further supporting a shallow source for the springs rather than deep groundwater discharge. Groundwaters measured in the GAP boreholes did not have detectable concentrations of tritium or nitrate (Chapter 3).-

Lake 38 is fed predominantly by glacial runoff and has a stable isotopic signature (-28.2/-217.0 ‰ $\delta^{18}O/\delta^{2}H$) that reflects a meltwater source (Figure 2.2b). The shallow groundwater flow in the ice-dammed lake springs reflects both a meltwater and modern meteoric source and, as such, falls between those two end members. Spring 3, located closest to the ice, has proportionally more meltwater than Spring 2, and this is reflected by a greater depletion in $\delta^{18}O$ (-24.41 compared to -21.81 ‰) and lower tritium concentrations (4.8 compared to 7.6 TU). It is likely that shallow groundwater flow reflects a more modern meteoric signature in lake basins that do not receive glacial meltwater input.

2.6.3. Weathering and Water Rock Interaction

The $^{87}Sr/^{86}Sr$ isotopic ratios can be a useful tool for tracing the sources of salinity as the isotopes do not fractionate during mineral dissolution and precipitation (McNutt et al., 1990; Frape et al.,

2014). In Antarctica, $^{87}Sr/^{86}Sr$ isotopic ratios in lake waters were often observed to be similar to the $^{87}Sr/^{86}Sr$ isotopic ratios found in soil salts, derived from the weathering of silicates in the nearby bedrock and regolith (Jones & Faure, 1978). Green and Canfield (1984) demonstrated that the Onyx River derived a significant fraction of its salts from interaction with soils in the Wright Valley, Antarctica.

Work on strontium in glacial and proglacial environments suggests that biotite weathering may have a strong influence on $^{87}Sr/^{86}Sr$ ratios, especially in recently exposed glacial sediments (Anderson et al., 1997; Blum & Erel, 1997; Sharp et al., 2002). Generally, during chemical weathering, feldspars, specifically palgioclase and K-feldspar, are initially weathered (Grant, 1963; Nesbitt & Young, 1996). However, in glacial environments, where biotite is enriched in fine grained sediment, biotite weathering occurs rapidly (Blum & Erel, 1995, 1997; Nesbitt & Young, 1996). Biotite weathering also decreases rapidly over a fairly short time scale (10 ky) due to the loss of reactive mineral surfaces (Eggleston et al., 1989; Blum & Erel, 1995, 1997; Taylor & Blum, 1995; Anderson et al., 1997). The large range of $^{87}Sr/^{86}Sr$ isotopic ratios covered by ice marginal lakes represents the relative influence of minerals such as biotite during weathering versus feldspar weathering (McNutt et al., 1990; Blum & Erel, 1997).

A plot comparing the $^{87}Sr/^{86}Sr$ isotopic ratio in lake waters with increasing distance from the coast (shown as Eastings, which represents the distance east from the coast towards the ice margin) shows that lakes becoming increasingly radiogenic with distance from the coast (Figure 2.9). The regional geology in the Kangerlussuaq area is dominated by felsic and intermediate gneisses and amphibolite facies mafic intrusions. These rock types are rich in biotite and feldspars and provide a potential source for a radiogenic strontium signature. $^{87}Sr/^{86}Sr$ isotopic ratios of bedrock minerals can be found in Chapter 4, Table 4.7). In the current study, the $^{87}Sr/^{86}Sr$ isotopic signature of the ice

marginal lakes exceeded 0.73 and is dominated by weathering of soil and rock material recently released from the melting ice. Many of these lakes surrounded by relatively fresh glacial sediment can have a highly radiogenic strontium isotope signature approaching 0.76 (Figure 2.9). For example, lakes L12, L13 and L14 are located in non-vegetated till in front of Leverett Glacier (Figure 2.1). Lakes L12 and L14 have $^{87}Sr/^{86}Sr$ ratios of 0.7533 and 0.7576, respectively. Ice marginal (area 1) lakes, with $^{87}Sr/^{86}Sr$ approaching values of 0.73, are probably less influenced by biotite weathering with a corresponding increase in the relative contribution of feldspar weathering. This is likely due to either the absence of glacial sediment (bare rock) or reduced biotite weathering surfaces due to sediment and soil aging with time.

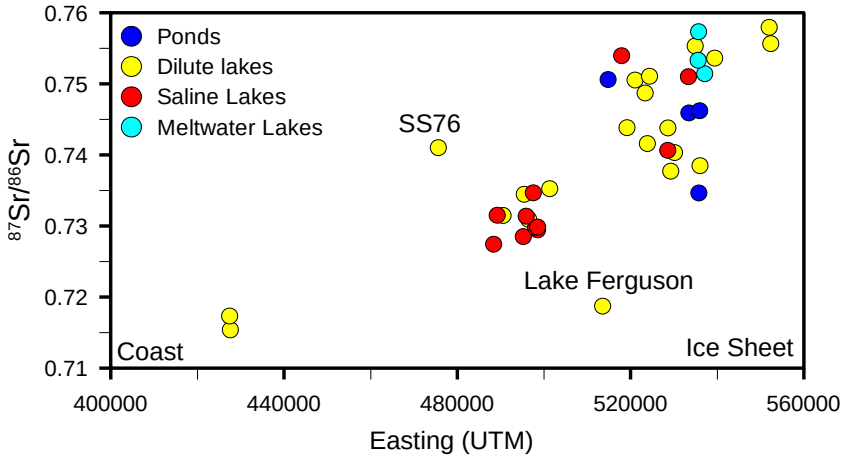

Figure 2.9. The $^{87}Sr/^{86}Sr$ signature of lakes increases towards the ice sheet where weathering of biotite becomes increasingly important.

In the upper fjord and coastal areas, highly radiogenic $^{87}Sr/^{86}Sr$ ratios are not observed and the influence of marine aerosols or deflated marine sediments becomes more significant (Figure 2.9). Marine inputs are discussed further below. Overall, a trend of decreasing $^{87}Sr/^{86}Sr$ can be observed with distance from the ice sheet, or decreasing Easting values (Figure 2.9), reflecting the reduced impact of biotite, or other radiogenic mineral, weathering with time since deglaciation (Blum & Erel, 1997), and an increased marine input closer to the coast. The influence of biotite weathering on

$^{87}Sr/^{86}Sr$ ratios can also be observed on a plot of $(Mg^{2+} + K^{+})/Na^{+}$ (Figure 2.10). Biotite weathering will contribute Mg^{2+} and K^{+} to the lake chemistry while feldspar weathering and marine input will contribute Na^{+}. Thus we see a pattern of increasing Mg^{2+} and K^{+} relative to Na^{+} with increasingly radiogenic $^{87}Sr/^{86}Sr$ values. Ponds and meltwater lakes show a large range of high $(Mg^{2+} + K^{+})/Na^{+}$ ratios and radiogenic $^{87}Sr/^{86}Sr$ isotopic ratios, suggesting biotite weathering is a key process for these water bodies. Two outliers exist in Figure 2.10: L33 (Lake Ferguson) is impacted by marine $^{87}Sr/^{86}Sr$ as discussed above. Lake L11 had high $(Mg^{2+} + K^{+})/Na^{+}$, possibly a result of removal of Na^{+} through halite precipitation or due to local geology (mafic material in surrounding rock).

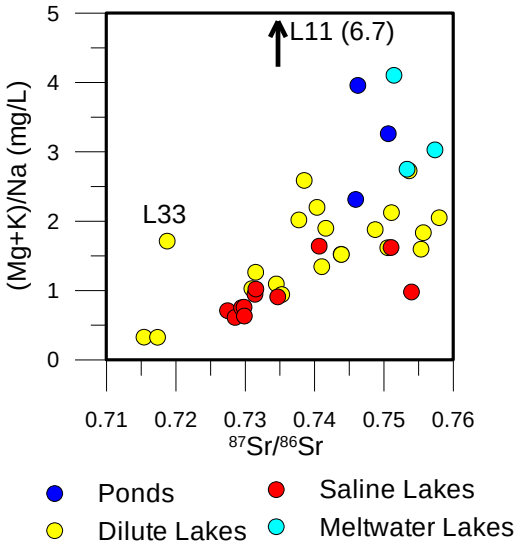

Figure 2.10. Comparison of the ratio of (Mg+K)/Na to $^{87}Sr/^{86}Sr$ isotope ratios for all lake types. The ratio of (Mg+K) to Na increases with increasingly radiogenic $^{87}Sr/^{86}Sr$ isotopic ratios.

Within a lake basin, $^{87}Sr/^{86}Sr$ of shallow groundwater flow can vary greatly. $^{87}Sr/^{86}Sr$ isotopic ratios were measured in soil waters in the basin of lake L26. The $^{87}Sr/^{86}Sr$isotopic ratio of active layer flow in the lake L26 basin ranged from 0.7307 to 0.7565, with similar isotopic values observed within each drainage route studied (Figure 2.3, Table 2.4). Variations in flow path length, vegetation, soil development and weathering between the four flow routes result in large variations

in $^{87}Sr/^{86}Sr$. As well, the oscillation of ice may rework soil profiles and preferred drainage pathways. The outflow route (D- see Table 2.4, Figure 2.3) is dominated by the lake water $^{87}Sr/^{86}Sr$ signature, while the three inflow transects (A-C, Figure 2.3), which move through rapidly weathering sediments, tend to be more radiogenic (Table 2.4).

It has been proposed that increased weathering of glacially comminuted sediments during continental scale glaciations may have affected the marine $^{87}Sr/^{86}Sr$ record over short and longer time periods (Hodell et al., 1991; Anderson et al., 1997; Zachos et al., 1999). With an increase in glacial melting due to climate warming and the potential for enhanced geochemical loading to the oceans, further understanding of processes that affect $^{87}Sr/^{86}Sr$ in this proglacial environment will aid in the study of the interaction between the marine $^{87}Sr/^{86}Sr$ signature and glaciation.

2.6.4. Sulfur Oxidation and Reduction

The variability in $\delta^{34}S$ and $\delta^{18}O$ of sulfate (Figure 2.11) in the lakes of the Kangerlussuaq region could be indicative of several processes: sulfide oxidation, sulfate reduction and mixing with marine sulfate. Sulfide oxidation may cause a slight depletion of sulfur-34 (approximately 2 to 5.5‰) in the resulting sulfate (Toran & Harris, 1989) or may result in no discernible fractionation between sulfide and sulfate (Gavelin et al., 1960; Nakai & Jensen, 1964; Seal et al., 2000). Sulfate reduction that is mediated by sulfate reducing bacteria causes enrichment in the remaining $\delta^{34}S$ (SO_4), as the bacteria preferentially use the lighter sulfur isotopes due to their lower activation energy, which maximizes the energy yield for bacterial metabolic processes (Kaplan & Rittenberg, 1963; Clark & Fritz, 1997). Finally, marine sulfate may be a significant source of sulfate close to the coastal regions (area 3) and the head of the fjord (area 2).

2.6.4.1 Oxidation of Sulfides

The $\delta^{18}O$ of the sulfate produced during sulfide oxidation is a mixture of atmosphere $\delta^{18}O$ (+23‰) and the $\delta^{18}O$ of the water present during oxidation. The relative importance of atmospheric $\delta^{18}O$ versus water $\delta^{18}O$ depends on the degree of water saturation. With increasing saturation, the $\delta^{18}O$ isotopic signature of the sulfate will more closely resemble that of the water, while in relatively dryer conditions the $\delta^{18}O$ isotopic signature of the sulfate will more closely resemble that of the atmospheric O_2 (Clark & Fritz, 1997). van Everdingen and Krouse (1985) developed an equation (2.1) to calculate the $\delta^{18}O$ of sulfate ($\delta^{18}O_s$) derived from sulfide oxidation:

$$\delta^{18}O_s = Y(\delta^{18}O_w + \varepsilon_w)+(1-Y)[0.875(\delta^{18}O_a + \varepsilon_a)+0.125(\delta^{18}O_w + \varepsilon_w)] \qquad [2.1]$$

Where $\delta^{18}Ow$ represents the $\delta^{18}O$ contents of water and $\delta^{18}Oa$ represents that of dissolved and/or atmospheric oxygen present. Y represents the proportion of SO_4^{2-} derived using oxygen from H_2O versus O_2 described in equations 2.2 and 2.3:

$$(1)\ FeS_2 + 14\ Fe^{3+} + 8\ H_2O = 15\ Fe^{2+} + 2\ SO_4^{2-} + 16\ H^+ \qquad [2.2]$$

$$(2)\ FeS_2 + 7/2\ O_2 + H_2O = Fe^{2+} + 2SO_4 + 2\ H+ \qquad [2.3]$$

The enrichment factors between the $\delta^{18}O$ of sulfate and water and sulfate and oxygen are given by e_w (4.1) and e_a (-11.2) respectively. $\delta^{18}Oa$ is +23.5 ‰ (atmospheric). Figure 2.12 illustrates the relationships derived by varying Y from 0.1 to 1 and testing several potential $\delta^{18}Ow$ values consistent with the $\delta^{18}O$ isotopic composition of subglacial meltwaters (~-24 ‰), modern precipitation (-19 ‰) and a highly evaporated lake water (-5 ‰) (Figure 2.12). Figure 2.12 illustrates that a broad range of $\delta^{18}O$ (SO_4) values are attainable under various saturations and water types, the implications of which are discussed further below.

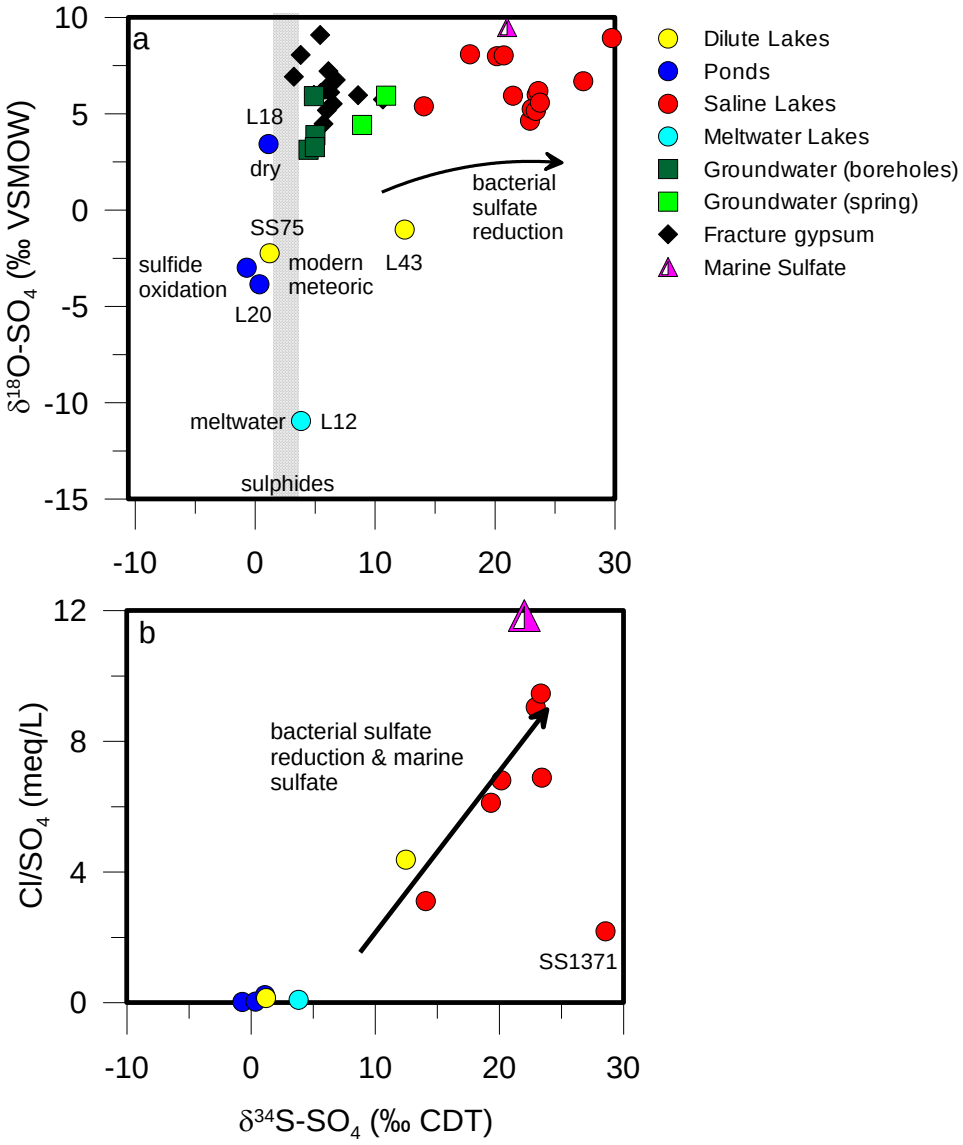

Figure 2.11. (a) the isotopic composition ($\delta^{34}S$ and $\delta^{18}O$) of sulfate in lakes and groundwaters as well as gypsum found as a fracture mineral in the bedrock. $\delta^{34}S$ of sulfide minerals found in the bedrock are indicated by the stippled area. (b) A comparison of the $\delta^{34}S$ of sulfate in lakes to the Cl/SO_4 ratio shows that as $\delta^{34}S$ is enriched during bacterial sulfate reduction, sulfate is removed and the Cl/SO_4 ratio increases.

A similar effect on the $\delta^{34}S$ and $\delta^{18}O$ of SO_4^{2-} as that produced by the oxidation of inorganic sulfide minerals may be caused by oxidation of organic sulfur compounds (Clark & Fritz, 1997; Canfield, 2001a). However, the extent of SO_4^{2-} derived from organic sulfur may be limited in the ice marginal area where vegetation is fairly sparse and cold, dry conditions limit productivity.

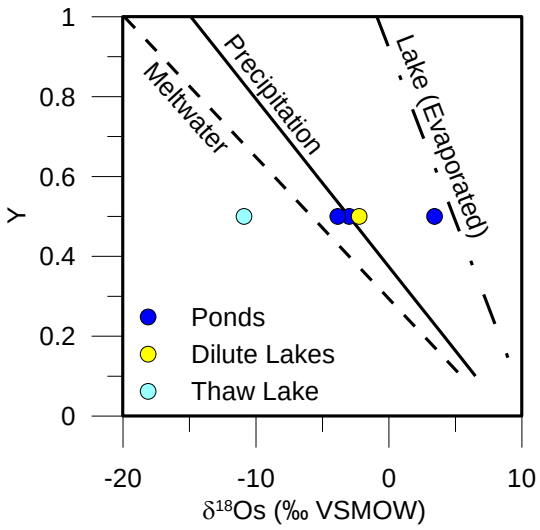

Figure 2.12. The $\delta^{18}O$ isotopic composition of sulfate ($\delta^{18}O_s$) derived from the oxidation of sulfides. Y is varied from 0.1 to 1, which represents increasing proportions of $\delta^{18}Os$ derived from $\delta^{18}Ow$ and is a proxy for increasing saturation. Lake $\delta^{18}O$ signatures are displayed along an arbitrary Y of 0.5 for comparison. From left to right the lakes are L12, L20 2008, L20 2011, SS75 and L18. $\delta^{18}Ow$ values used are: meltwaters (~-24 ‰), modern precipitation (-19 ‰) and lake (evaporated) (-5 ‰).

Sulfide minerals, including pyrite and chalcopyrite, from the bedrock core obtained during drilling of the research borehole DH-GAP04 (Figure 2.1) have a $\delta^{34}S$ of 2.3 to 3.7‰ (Figure 2.11a) (Table 2.6). A dilute lake (lake SS75) and a large, acidic (pH 3.4) pond (lake L20) have $\delta^{34}S$-$\delta^{18}O$ signatures indicative of sulfate produced during oxidation of sulfide in the presence of modern meteoric water and atmosphere (Figure 2.11a). That is, the $\delta^{34}S$ (SO_4) values of Lake 20 and Lake SS75 (-3.0 to -3.9 ‰ respectively) are slightly depleted relative to that of the sulfides (2.4 to 3.7 ‰). The $\delta^{18}O$ (SO_4) of Lake 20 and Lake SS75(-0.7 to 1.2 ‰ respectively) reflects the oxidation of sulfide in the presence of meteoric water (~-19‰) and atmospheric oxygen (+23.5 ‰) as discussed above (Figure 2.12). Lake L20, SS75 and SS76 have low Cl/SO_4 ratios (Figure 2.7), high SO_4^{2-} as percentage of anions, and low alkalinity. Local geology is likely responsible for these anomalous lakes. Anderson et al. (2001) observed highly weathered and friable, orange-reddish rocks (gossans) on the slopes around lakes SS75 and SS76 which are presumed to be similar to the weathered sulfide-rich rocks that were observed around lake L20 (personal observation). Weathering of these sulfide-rich

rocks would contribute increased sulfate concentrations (lower Cl/SO_4 ratios). Sulfide oxidation generates H^+, resulting in low alkalinity and low pH (Lake L20 had a pH of 3.5).

A thaw lake located within the till at the front of Leverett Glacier (L12) has a similar $\delta^{34}S$ (SO_4) and depleted $\delta^{18}O$ (SO_4) to the lakes indicated above – where sulfide oxidation occurred in the presence of modern meteoric water (Figure 2.11a; Figure 2.12). In the case of L12, the $\delta^{18}O$ (SO_4) is a mixture between glacial meltwater or melt from frozen till, which has highly depleted $\delta^{18}O$ and atmospheric oxygen, resulting in sulfate with depleted $\delta^{18}O$ relative to sulfate produced from modern precipitation (Figure 2.12).

Compared to lakes L12, L20 and SS75, lake L18 has sulfate with a similar $\delta^{34}S$ (SO_4) but also an enriched $\delta^{18}O$ (SO_4) isotopic signature (Figure 2.11a). L18 is a shallow pond that may completely evaporate over the summer. Sulfate in lake L18 is likely derived from sulfide oxidation occurring in the presence of minimal water and, thus, has an $\delta^{18}O$ (SO_4) value (3.4 ‰) with increased influence of atmospheric $\delta^{18}O$ (23.5 ‰). As well, the $\delta^{18}O$ of the water present may have a more enriched isotopic signature due to heavy evaporation, similar to the L18 lake water ($\delta^{18}O$ -5.2 ‰). Figure 2.12 shows that such highly enriched $\delta^{18}O$ (SO_4) values may be achieved through sulfide oxidation of an evaporated water source or under very dry (low Y) conditions.

2.6.4.2 Sulfate Reduction and Marine Sulfate

Sulfide oxidation is the main process affecting lakes in close proximity to the ice sheet (area 1). Further from the ice sheet, in the upper fjord area (area 2), sulfate reducing bacteria and sea spray have a significant effect on lake chemistry and the isotopic composition of sulfate. Sulfate reducing bacteria (SRB) have been observed in other cold climate areas, such as Antarctica, where SRB were observed in lakes in the McMurdo Dry Valleys (Green et al., 1988), as well as in the Canadian Arctic (Burton & Barker, 1979). Leng et al. (2012) theorized that in a coastal lake (area 3), sulfur was

derived from both the catchment (oxidation of pyrite) and sea salt aerosols. In the lake studied by Leng et al. (2012), sulfate reduction was identified as an important process, especially during warmer climatic conditions when lake productivity was highest. Sulfate reduction is likely to occur in lake sediments, during iced over conditions or deep in the water column if anoxic conditions prevail (Holmer & Storkholm, 2001).

The effects of both marine sulfate and sulfate reducing bacteria can be seen on a plot comparing the Cl/SO_4 ratio and $\delta^{34}S$ (SO_4) (Figure 2.11b). Bacterial sulfate reduction removes sulfate from lakes by reducing SO_4^{2-} it to H_2S. H_2S may then react with metal ions to precipitate metal sulfides such as FeS. H_2S may also be utilized by purple sulfur bacteria which oxidize the sulfide to elemental sulfur (Fry et al., 1988). Purple sulfur bacteria were observed in lakes in the Kellyville Basin (Figure 2.1). Removal of SO_4^{2-} by sulfate reducing bacteria increases the Cl/SO_4 ratio as well as enriching the remaining sulfate in $\delta^{34}S$ (SO_4). Addition of marine sulfate creates a similar effect due to the higher Cl/SO_4 ratio of seawater (Figure 2.11b). The enrichment of $\delta^{34}S$ (SO_4) beyond that of seawater indicates that sulfate reduction is occurring along with mixing with marine sulfate. The saline lakes around the head of the fjord are the most impacted by SRB enrichment of $\delta^{34}S$ (SO_4). Surface water environments become less hostile to microbial communities with distance from the ice sheet due to warmer temperatures and increased time for the evolution and development of communities. For example, cooler temperatures around 8200 years BP caused a definitive decrease in productivity in a lake close to the head of the fjord near Kangerlussuaq, based on isotopic and fossil records from a lake core (Anderson et al., 2008). The cooler, dryer conditions around 8200 years BP and the reduction in productivity may be related to the close proximity of the ice sheet to the lake at that time (Anderson et al., 2008).

The effect of sulfate reducing bacteria on $\delta^{34}S$ (SO_4) can be described by a Rayleigh distillation curve (Canfield, 2001b):

$$\delta^{34}S_{SO4-res} = (\delta^{34}S_{SO4-in} + 1000) * f_{SO4}^{(1-\alpha)} - 1000 \qquad [2.4]$$

Where $\delta^{34}S_{SO4\text{-}res}$ is the $\delta^{34}S$ (SO_4) of the residual sulfate, $\delta^{34}S_{SO4\text{-}in}$ is the initial isotopic composition of the sulfate, f is the fraction of the initial sulfate pool remaining and α is the fractionation factor. Using L18 ($\delta^{34}S_{SO4\text{-}in}$ 1.1 ‰ and SO_4^{2-} 725 mg/L) as a representative lake whose initial sulfate source was the oxidation of sulfides and in which sulfate has been concentrated through evaporation yields the Rayleigh distillation curve presented in Figure 2.13. The fairly good agreement between the Rayleigh distillation curve and the $\delta^{34}S$ (SO_4) enriched lakes at the head of the fjord (Figure 2.13) suggests that the highly enriched $\delta^{34}S$ (SO_4) values observed in these lakes can be caused by sulfate reducing bacteria.

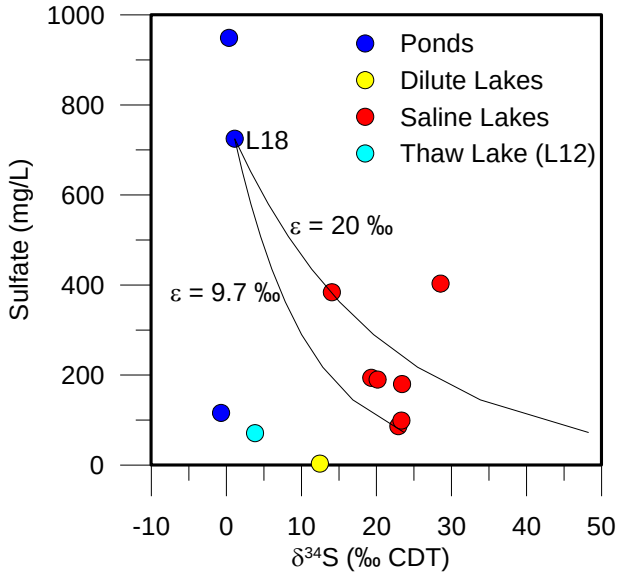

Figure 2.13. Comparison of sulfate concentrations and $\delta^{34}S$ (SO_4) in lakes. Two Rayleigh distillation curves for enrichment in $\delta^{34}S$ due to bacterial sulfate reduction are displayed using L18 as an example initial composition. An ε of 20 ‰ is based on Clark and Fritz (1997) and an ε of 9.7 ‰ is from Strebel et al. (1990).

Sulfate reducing bacteria have significantly less impact on the $\delta^{18}O$ (SO_4) of the residual sulfate pool. Balci et al. (2006) found that $\delta^{18}O$ (SO_4) changed by <4 ‰ despite large fractionations in $\delta^{34}S$ (SO_4). Strebel et al. (1999) found an isotopic enrichment factor of 6 ‰. The majority of the lakes studied had $\delta^{18}O$ (SO_4) of less than 0 ‰ while the SRB impacted lakes at the head of the fjord ranged from 4.6 to 8.1 ‰ (Table 2.6). The enriched $\delta^{18}O$ values in the saline lakes at the head of the fjord suggest that either bacterial sulfate reduction has proceeded to very low residual fractions (f in equation 2.4) or that mixing with marine sulfate is also occurring.

2.6.4.3 Bedrock Gypsum

The possibility of sulfate dissolution from a bedrock source was also considered as a source of sulfate in the area 2 saline lakes, which are enriched in $\delta^{34}S$ (SO_4) and $\delta^{18}O$ (SO_4) and plot in the upper right of Figure 2.11a. Gypsum is found extensively in the DH-GAP04 borehole below a depth of 300 m borehole length (BHL). Based purely on the sulfate isotopic signature of these saline lakes, it seems possible that the original source of sulfur could be dissolution of gypsum similar to that observed as fracture minerals in the GAP boreholes (Table 2.6; see Chapters 3 and 4), which has then been subsequently enriched in $\delta^{34}S$ (SO_4) by sulfate reducing bacteria. However, comparing the $^{87}Sr/^{86}Sr$ isotopic signature of these lakes, which ranges from 0.727 to 0.735, to the $^{87}Sr/^{86}Sr$ isotopic signature of the fracture sulfate minerals (0.702-0.708), dissolution of bedrock gypsum is not supported as the source of sulfur nor is such a soluble mineral phase likely to have been preserved in rock fractures around the lake catchment. The upper fjord saline lakes fall along the trend of decreasingly radiogenic $^{87}Sr/^{86}Sr$ ratios with distance from the ice sheet and do not indicate mixing with another, less radiogenic $^{87}Sr/^{86}Sr$ source (Figure 2.9).

2.6.5. Aeolian Inputs

Aeolian dust can provide a significant chemical flux, especially in glacial environments where a large amount of sediment with small particle size is available (Lamoureux et al., 2002; Lawrence & Neff, 2009). The rate of dust deposition has been shown to be greatest during glacial maxima (Lambert et al., 2008) though the Kangerlussuaq region would have been covered in ice at this time. Mineralogical composition of dust can be variable, depending on local geology, but generally contains silicate minerals such as quartz, feldspars and phyllosilicates (Schütz & Sebert, 1987). Winds in the Kangerlussuaq area are dominantly katabatic winds from the east, coming off the ice sheet; however, coastal storms from the west do occur (Aebly and Fritz, 2009). Easterly winds coming from the ice sheet pick up dust from the exposed glacial sediments, the ice surface and large sand flats present in front of the ice sheet (personal observation).

Anderson et al. (2001) suggest that the enrichment in Na^+ relative to Cl^- compared to seawater (Na/Cl 0.858) or halite (Na/ Cl 1) may be attributed to loess deflation. A Na/Cl ratio greater than 1 can be observed in a number of lakes in the study area (Figure 2.5). Aeolian loess deposits can be found throughout the area around Søndre Strømfjord (Anderson et al. 2001). Eisner et al. (1995) report continuous deposition of aeolian sand in a lake near the Sandflugtdalen floodplain east of Kangerlussuaq. Anderson et al. (2012) found that the impact of aeolian activity increased inland due to local aridity. Weathering within the lake catchment and cation exchange also are likely to contribute additional Na^+.

2.6.6. Marine Influence

Marine aerosols have been found to impact lake chemistry in both the Arctic and Antarctic. In the MacKenzie delta in the Northwest Territories of Canada, Cl^- concentrations were correlated to distance from the coast (Kokelj et al., 2009). Increasing Cl^- near the coast was attributed to an

increase in marine aerosols (Kokelj et al. 2009). In the Taylor Valley in Antarctica, the $^{87}Sr/^{86}Sr$ ratio of soil salts were found to decrease toward the coast, indicating an increase in marine ^{87}Sr either from sea salt aerosols or as a relic from marine incursion (Jones & Faure, 1978). In the Dry Valleys of Antarctica, soil salts such as mirabilite ($Na_2SO_4 \bullet 10H_2O$) can accumulate due to long term marine aerosol deposition and are an important source of salinity in shallow groundwater seeps and surface waters (e.g. Keys and Williams, 1981; Green and Canfield, 1984; Lyons et al., 2005; Harris et al., 2007). Anderson et al. (2001) found that the percentage of Cl^- in lakes increased toward the west coast of Greenland. In southeast Greenland, an increased influence of marine-derived Na^+ and Cl^- was found in shallow groundwater toward the coast (Kristiansen et al., 2013). Kristiansen et al. (2013) found that both present day salt spray and Holocene marine sediment deposits contributed to the marine Na^+ and Cl^- in the shallow groundwater. Similar to the other near coastal environments discussed above, several lines of evidence indicate that marine aerosols affect lake chemistry in the Kangerlussuaq region:

- Chloride from marine aerosols has a Na:Cl equivalent ratio of 1 and an initial $\delta^{37}Cl$ signature of 0‰. Many of the sampled lakes have Na:Cl ratios that fall along or close to the 1:1 line (Figure 2.5). Some excess Na^+ is observed, likely due to weathering or aeolian inputs (Anderson et al. 2001). Many of the dilute lakes as well as several saline lakes analyzed for stable chlorine isotopes have a $\delta^{37}Cl$ isotopic value that is within analytical error of 0‰, providing further evidence of marine Cl^- input (Figure 2.6) throughout the study area.
- As discussed in Section 2.6.4.2. The enriched $\delta^{34}S$-$\delta^{18}O$ of SO_4^{2-} found in many of the upper fjord lakes, which trend towards a marine signature, indicate mixing with marine sulfate (Figure 2.11a); however, it is difficult to separate this effect from enrichment due to microbial sulfate reduction.

- $^{87}Sr/^{86}Sr$ ratios show a pattern of decreasing radiogenic Sr toward the coast (Figure 2.9). While some of the decrease in $^{87}Sr/^{86}Sr$ ratios may be explained by a shift from biotite dominated weathering with distance from the ice sheet, it is likely that marine aerosols (with a $^{87}Sr/^{86}Sr$ signature of ~0.7092) are also a factor.

The majority of lakes are above the marine limit (approximately 100 m above modern sea level) (Anderson et al. 2001)(Funder & Hansen, 1996; Anderson et al., 2001). The marine limit is the maximum elevation at which relict marine shorelines are observed and thus lakes above this elevation are unlikely to contain relict seawater. A prominent exception is Lake Ferguson (L33) (Figure 2.1), which is located below the marine limit. The $^{87}Sr/^{86}Sr$ ratio of Lake Ferguson (0.7187) is atypical for its distance from the coast (Easting) (Figure 2.9) and is closer to that of seawater (0.7092). Lake L45 (Figure 2.1), is also below the marine limit at 96 m elevation. The $^{87}Sr/^{86}Sr$ isotopic ratio of Lake L45 (0.7267) is typical of lakes at similar distance from the coast (Figure 2.9), suggesting that the lake salinity is derived from local weathering processes and aeolian activity rather than relic seawater. Lake L45 is unique in its high concentration of Cl^- relative to Na^+ (Figure 2.5) and has a Na/Cl ratio of 0.73. The Na/Cl ratio of Lake L45 is less than that of seawater (0.86), suggesting either an additional removal mechanism for Na^+ or an additional source of Cl^-.

2.6.7. Evidence for Deep Groundwater Discharge

Deep (subpermafrost) groundwaters measured by the GAP boreholes tend to have $\delta^{18}O/\delta^{2}H$ isotopic signatures that fall along the GMWL and are depleted relative to surface waters (Section 3.4.1 and Figure 3.2). The subpermafrost groundwaters are similar in composition to glacial meltwaters (Figure 2.2b). These groundwaters have high sulfate concentrations with a characteristic $\delta^{34}S/\delta^{18}O$ of SO_4 (Figure 2.11). Groundwaters do not contain tritium and have low strontium isotopic signatures (<0.71). Significant discharge of groundwater into lakes via a through

talik would cause the lake chemistry and isotopic signature to shift towards the groundwater end member. i.e., anomalously low $\delta^{18}O$, $\delta^{2}H$, ^{3}H and $^{87}Sr/^{86}Sr$ isotopic values. None of the lakes sampled in the ice marginal area (area 1) show evidence of groundwater discharge (e.g. Figures 2.2 & 2.9) and have $^{87}Sr/^{86}Sr$ isotopic ratios greater than 0.73.

In area 2 (head of fjord), the geochemical and isotopic composition of the Kellyville basin lakes bear some similarities to groundwater, such as high chloride concentrations, less radiogenic $^{87}Sr/^{86}Sr$ ratios and enriched $\delta^{18}O$ of sulfate; however, alternative explanations have been presented for these characteristics earlier in the paper. The most compelling argument against significant groundwater discharge into lakes in the region is the lack of a mixing trend with a more depleted ($\delta^{18}O/\delta^{2}H$) groundwater source (Figure 2.2b). If groundwater discharge is occurring, volumes are too small to affect the lake isotopic composition or other geochemical parameters of the lake waters discussed in this paper.

2.7. Conclusions

Understanding the impact of climate and glaciation on lake chemistry was an important goal of surface water studies (see research objectives, Section 1.1). A number of key processes, such as evaporation, weathering and microbial activity, were found to vary relative to lake distance from the coast and ice margin, providing insight into the role that climatic gradients and glacial processes play in lake geochemical evolution.

Evaporation is one of the main processes affecting the geochemical evolution of lakes in this study, especially in the inland areas close to the ice sheet. Evaporation in closed basin lakes is interpreted to be responsible for the higher, though still brackish, salinities (>800 µS/cm) observed in a number of the Kangerlussuaq region lakes. $\delta^{37}Cl$ and $\delta^{81}Br$ provide new insight into the importance of salt precipitation and recycling in soils and shallow lake areas. Chlorine and bromine

isotopes provide further evidence that evaporation and salt precipitation are important processes to lake geochemistry.

Highly radiogenic $^{87}Sr/^{86}Sr$ ratios indicate that biotite weathering is enhanced in more recently deglaciated catchments. Marine aerosols and feldspar weathering become increasingly important with distance from the ice sheet and with proximity to the coast. These findings support previous work (Blum & Erel, 1995, 1997; Anderson et al., 1997; Sharp et al., 2002) on enhanced biotite weathering in proglacial environments and indicate that these theories are applicable to deglaciated areas of Greenland. The findings from the Kangerlussaq study area may have implications for the impact of glaciation and climate warming on the marine $^{87}Sr/^{86}Sr$ signature (Hodell et al., 1991; Anderson et al., 1997; Zachos et al., 1999). With the increased observed (e.g. van As et al., 2012) and predicted melting of the ice cap, increased runoff rates and the potential increase in solute loadings to the ocean (Anderson et al., 1997; Hasholt et al., 2012), increased radiogenic strontium from glaciated and recently deglaciated terrain will enter the ocean, potentially shifting the marine $^{87}Sr/^{86}Sr$ signature.

In more recently deglaciated areas, sulfide oxidation is the main source of sulfate in lakes, while the influence of marine aerosols increases around the fjord. The impact of sulfide oxidation under varying conditions (saturation, water source) is apparent in the $\delta^{18}O$ signature of the resulting sulfate. Bacterial sulfate reduction does not appear to be an important process in most of the lakes in close proximity to the ice sheet, but, in the warmer, more productive lakes around the head of the fjord, significant $\delta^{34}S$ enrichment due to microbial sulfate reduction is observed. However, it is difficult to separate the impact of sulfate reduction from mixing with marine aerosols. This study provides new information on the extent of bacterial sulfate reduction in lakes in the Kangerlussuaq area and the relationship between SRB and landscape evolution after de-glaciation.

An important objective of the GAP surface water studies was to determine the role of taliks in the groundwater system and the extent of groundwater-surface water interaction. Previously, studies of lakes in the area had assumed little interaction between groundwater and surface water (e.g., Leng and Anderson, 2003). Consistent with this assumption, a comparison of surface and groundwater isotopic ($\delta^{18}O$, $\delta^{2}H$, ^{3}H, $\delta^{34}S$ and $\delta^{18}O$) and geochemical data collected as part this study found no evidence for significant groundwater discharge within the sampled lakes. The lack of observable groundwater discharge may indicate low discharge volumes and little groundwater-surface water interaction or recharge conditions such as those observed between L26 and the DH-GAP01 borehole.

3. Geochemical Characterization of Groundwaters in an Area of Continuous Permafrost Adjacent to the Greenland Ice Sheet, Kangerlussuaq, Southwest Greenland

3.1. Introduction

There is little information available on groundwater flow and chemistry in Greenland. The information that is available focuses on springs and open pingos, which offer insight into the groundwater system without necessitating expensive and logistically challenging drilling programs (Pedersen, 1926; Muller, 1959; Cruickshank & Colhoun, 1965; Halliday et al., 1974; Allen et al., 1976; Worsley & Gurney, 1996; Yoshikawa et al., 1996; Scholz & Baumann, 1997). The Greenland Analogue Project (GAP) was initiated by the nuclear waste management agencies: NWMO, Posiva and SKB. The goal of the GAP was to study the properties of subglacial recharge into the subsurface and potential permafrost and glacial impacts on deep geological repositories for nuclear waste storage or disposal. The bedrock drilling component of the GAP aimed to provide data on the depth of meltwater penetration beneath a continental ice sheet, the impact of glaciation and permafrost on groundwater geochemistry, and the extent of groundwater-surface water interaction in this environment (Claesson Liljedahl et al., 2015). The Kangerlussuaq Region, southwest Greenland (Figure 3.1), was chosen to represent a modern, natural analogue to future glaciations in Canada, Finland and Sweden. Ice extended to the coastal area of southwest Greenland until ~11,000 years BP (Van Tatenhove, 1996). By ~6000 to 4000 years BP, the ice had retreated farther than its current extent before re-advancing over the study area (Rinterknecht et al., 2009). In this region, the current margin of the Greenland Ice Sheet is located approximately 160 km from the coast.

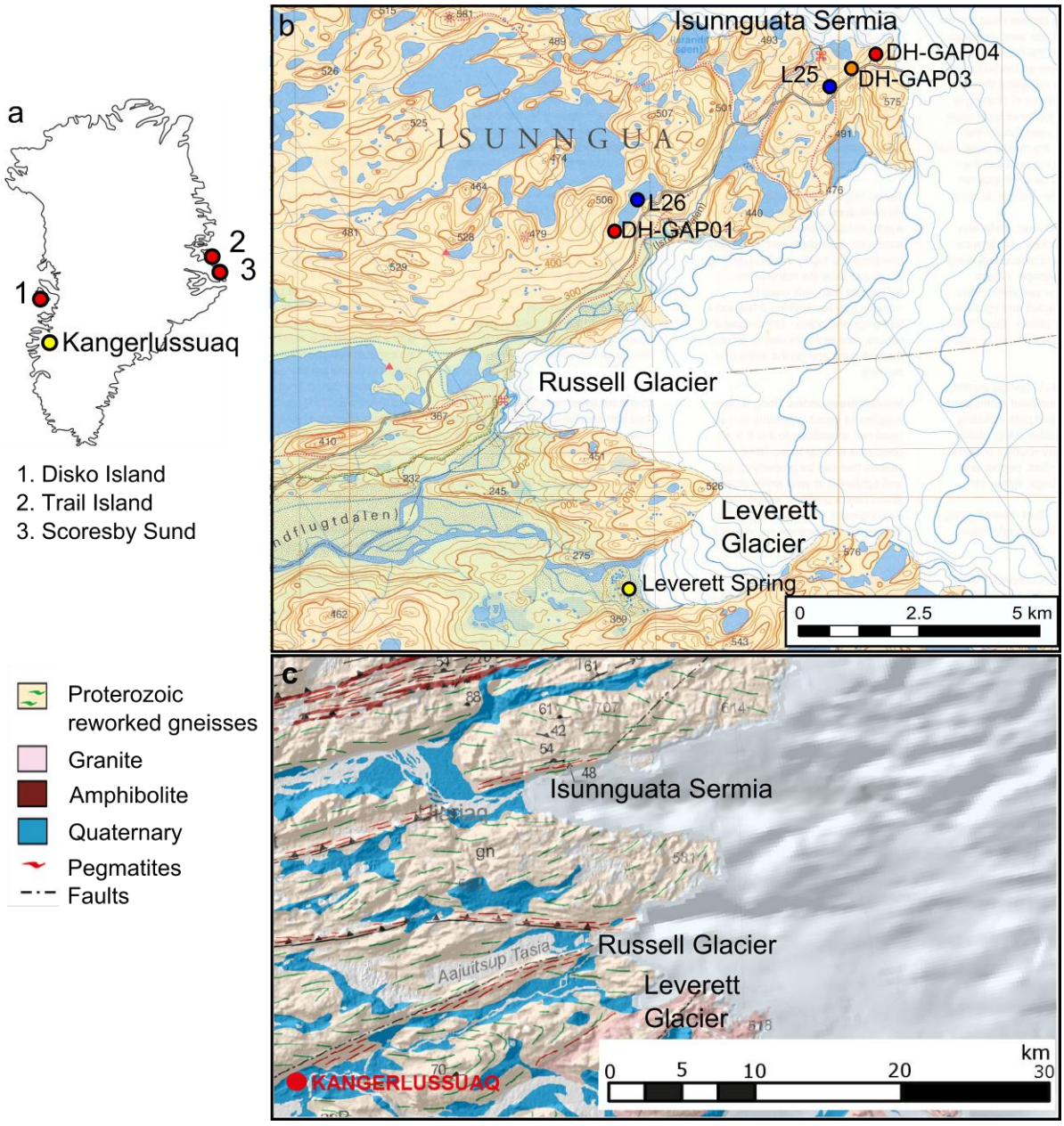

Figure 3.1.(a) Outline of Greenland indicating the town of Kangerlussuaq as well as locations where springs and open pingos have been studied. (b) Locations of GAP boreholes, the Leverett Spring and lakes L25 (Drilling Water Lake) and L26 (Talik Lake). (c) Study area geology modified from Engström and Klint (2014).

In the Kangerlussuaq Region there is one open pingo, previously studied by Scholz and Baumann (1997), which is revisited here and referred to as Leverett Spring. In addition, data and samples have been acquired from two bedrock boreholes (DH-GAP01 and DH-GAP04). DH-GAP01 was drilled in 2009. It is a 220 m long, angled borehole that intersects a through talik (an unfrozen conduit through permafrost beneath a lake) located to the North of Russell Glacier (Figure 3.1) (SKB, 2010;

Harper et al., 2011). A second borehole, DH-GAP04, was drilled in 2011 and is a 687 m long, angled borehole directed toward Isunnguata Sermia Glacier, a part of the Greenland Ice Sheet (Figure 3.1). DH-GAP04 extended approximately 18 m beneath the glacier after completion of drilling in 2011. These boreholes provide new and unique datasets on groundwater in taliks and below the permafrost in the immediate vicinity of the Greenland Ice Sheet.

In addition to the direct study of groundwater sampled from Leverett spring and the GAP boreholes, a study was conducted to characterize surface water bodies in the region around Kangerlussuaq. Surface water studies were undertaken in order to determine the extent of groundwater-surface water interaction (Chapter 2). Lakes and meltwaters were analyzed for their geochemical composition, as well as for multiple isotopes: $\delta^{18}O_{(H2O)}$, $\delta^{2}H_{(H2O)}$, ^{3}H, $\delta^{87}Sr$, $\delta^{37}Cl$, $\delta^{81}Br$, $\delta^{34}S_{(SO4)}$ and $\delta^{18}O_{(SO4)}$. Previous work on the chemistry of the lakes in the region has included geochemical and isotopic studies ($\delta^{18}O$, $\delta^{2}H$ and $\delta^{13}C$) (Anderson et al., 2001, 2008; Leng & Anderson, 2003; Olsen et al., 2013). There have been no previous studies focused on groundwater composition in the Kangerlussuaq region. The study adds to the body of knowledge of groundwater evolution under cryogenic conditions (i.e., permafrost and glacial) as well as groundwater chemistry in crystalline rock at depths of several hundred meters on the margin of a continental scale ice sheet.

Groundwater studies in shield environments in permafrost-affected areas of the Canadian Arctic have provided insights into the evolution of saline brines found beneath the permafrost. The source of the very high salinities (up to 300 g/L) found in shield brines (Frape et al., 2004, 2013; Stotler et al., 2012) is still debated, with possible explanations including cryogenic concentration of seawater during glaciations (Herut et al., 1990; Bottomley et al., 1999; Starinsky & Katz, 2003) and a variety of in situ processes such as methane hydrate formation, freeze-out and water rock interaction (e.g.,

Frape et al., 1984; Pollard et al., 1999; Andersen et al., 2002; Grasby et al., 2003a; Grasby et al., 2003b; Frape et al., 2004; Stotler et al., 2009; Stotler et al., 2010; Stotler et al., 2011; Stotler et al., 2012). Groundwaters occurring in cold climate areas, such as the Canadian Arctic (Beschel, 1963; Pollard et al., 1999; Andersen et al., 2002; Grasby et al., 2003a; Grasby et al., 2003b; Frape et al., 2004; Stotler et al., 2009; Stotler et al., 2010; Stotler et al., 2011; Stotler et al., 2012), Antarctica (Cartwright & Harris, 1981; Carlson et al., 1990; Takamatsu et al., 1998; Lyons et al., 2005; Green & Lyons, 2008; Frank et al., 2010) and the Siberian Platform (e.g., Shvartsev, 1998; Alexeev & Alexeeva, 2002; Alexeev & Alexeeva, 2003; Alexeev et al., 2007; Shouakar-Stash et al., 2007), may be impacted to varying degrees by such processes. The processes affecting the groundwaters examined by the GAP are discussed and compared in the context of these processes known to occur in other cold climate environments.

3.2. Study Area

Kangerlussuaq is located above the Arctic Circle at 67°00' N and has a dry, subarctic climate. The GAP boreholes are located approximately 150 km from the southwestern coast. The Greenland Ice Sheet to the east exerts a dominant control over both precipitation and winds in the study area. Mean annual precipitation, as measured over the period of 1977-2011, was 173 mm. Average annual temperature at Kangerlussuaq is -5.1°C, with temperatures ranging from lows of -40°C in winter to temperatures of 18-20°C in summer (Cappelen, 2012).

3.2.1. Geology

A more detailed description of the local geology, borehole lithology and the regional tectonic history of the Kangerlussuaq region can be found in Chapter 1 (Sections 1.3.3 and 1.5). Local geology consists of Archean gneisses, reworked in the Paleoproterozoic, with an ENE structural trend. Mafic dykes of the Paleaoproterozoic Kangamiut dyke swarm (2050-2040 Ma) intrude the

Archean gneisses and are NNE trending (van Gool et al., 2002). The dominant rock type is quartzo-feldspathic gneiss that is quartz rich and commonly biotite-bearing. Mafic intrusions are generally garnet-bearing amphibolites. Pegmatites are quartz and feldspar rich and frequently contain biotite.

DH-GAP01 (total length 221 m, 60° plunge to NNE) (Figure 1.5) shows moderate to sub-vertically dipping fractures, with an average fracture frequency of 2.44 fractures/m, and contains completely intact sections (SKB 2010). DH-GAP04 (total length 687 m, 70° plunge to N)(Figure 1.6) is drilled into an open fold with a NNW-trending and shallowly plunging (ca. 14°) synform. Fractures in DH-GAP04 are primarily sub-vertical at depths <100 m, transitioning to sub-horizontal fractures below 300 m where sub-vertical fractures become rare. The greatest fracture frequency occurs between 500 and 600 m of borehole length in DH-GAP04 and this section also contains the most water conductive fractures (Pöllänen et al., 2012). Aside from this 100 m thick interval, DH-GAP04 is evenly fractured throughout, with an average fracture frequency of 1.97 fractures/m. Hydraulic testing at DH-GAP01 suggests a rock mass hydraulic conductivity of approximately 10^{-8} m s^{-1} (Harper et al., 2011). The local geology, including surface mapping and information from boreholes DH-GAP01 and DH-GAP03 (did not penetrate permafrost and was not instrumented for sampling), is described in detail in Engström et al. (2012) and Engström and Klint, (2014) .

3.2.2. Permafrost

The study area is located in a region of continuous permafrost, with permafrost depths of 100–150 m reported for the town of Kangerlussuaq (Van Tatenhove & Olesen, 1994). Closer to the ice margin, the GAP study confirms a permafrost depth of greater than 300 m using the distributed temperature sensing (DTS) technique and optical fibres in DH-GAP03 and DH-GAP04 (Harper et al., 2011, 2015a). DH-GAP01 provides direct evidence of a talik beneath lake L26 (herein referred to as

the Talik Lake; see Figure 3.1); DTS measurements in DH-GAP01 indicate the absence of permafrost below 20 m of borehole length, which corresponds to the shoreline of the lake.

3.3. Methods

3.3.1. Surface Water Sampling

Sampling of surface waters in the Kangerlussuaq Region for the GAP began in June 2008 with the sampling of lakes, meltwaters and a spring (referred to here as Leverett Spring; reported on in an earlier study by Scholz and Baumann, 1997). Water samples for isotopic analyses were collected in plastic Nalgene bottles. Cation samples were filtered with 0.45 μm filters and acidified with ultra-pure nitric acid. pH and electrical conductivity were measured in the field. Eh of Leverett Spring was also measured at surface by inserting an Eh field probe into a hole drilled through the ice that covers the spring in winter. Spring water flows out through the hole under pressure and thus the spring's redox potential can be measured before the spring water contacts atmospheric conditions. Meltwater samples were acquired from supraglacial, subglacial flow and glacial meltwater rivers at Isunnguata Sermia, Russells Glacier and Leverett Glacier. Additional samples of subglacial meltwaters were acquired from the beneath Isunnguata Sermia by hot water drilling. Detailed results of subglacial meltwater chemistry and weathering are reported in Graly et al. (2014). Due to their dilute nature, the majority of the meltwater samples had high charge balance errors. Only samples with charge balance errors of less than 10% were utilized in plots.

3.3.2. Boreholes

In June-July 2009, two boreholes (DH-GAP01 and DH-GAP03) were drilled with a diameter of 56.8 mm. Flushing water was drawn from local lakes and heated to a temperature of 30 to 60°C to allow drilling in the frozen ground without the addition of antifreeze chemicals (SKB 2010). Water was also heated to allow time for the instrumentation of the boreholes before freezing downhole

could occur. Sodium fluorescein was used as a tracer in the drill water at a target concentration of 250 μg/L, and a measured average concentration of 221 μg/L for DH-GAP01 and 194 μg/L for GAP03, respectively. Water from Lake L26 (Talik Lake) was used to drill DH-GAP01 and water from lake L25 (Drill Water Lake) was used during the drilling of DH-GAP03 (as well as DH-GAP04) (Figure 3.1). Sections 1.4.2. and 1.5 describe the boreholes in detail, including instrumentation, lithology and hydrogeology.

The first hole, DH-GAP01, was drilled next to the Talik Lake (L26, see Figure 3.1), considered to be of suitable size to support a through talik that fully penetrates the permafrost. DH-GAP01 was drilled at a plunge of 60° to a total depth of 221 m and a vertical depth of 191 m. DH-GAP01 intersects a talik beneath the lake after 20 m. The instrumentation of DH-GAP01 is described in section 1.4.2.

A discussion of the hydrogeology of DH-GAP01 can be found in several papers published by the Greenland Analogue Surface Project (GRASP) (Bosson et al., 2013; Johansson et al., 2014, 2015). Lake levels (as elevation) in the Talik Lake were approximately 369 m and varied by less than one meter while hydraulic head in the borehole varied between 366 and 368 m. Elevations were measured relative to the reference ellipsoid D-WGS84 (a standard reference ellipsoid for GPS measurements) unless otherwise indicated. Lake level in the Talik Lake was always higher than the hydraulic head of the borehole, indicating a downward gradient and suggesting recharge.

From June 17th to July 7th, 2011, DH-GAP04 was completed next to Isunnguata Sermia Glacier (Figure 3.1). Water pumped from nearby surface water bodies was heated to 60°C and circulated through the borehole during drilling to prevent freezing. The drilling water was spiked with sodium fluorescein (average concentrations of 229 μg/L) to help monitor recovery of the natural flow system after drilling. DH-GAP04 has a diameter of 76 mm, is 687 m in length, and has an angle of

plunge of 70° toward the ice sheet for a total vertical depth of 649.1 m from top of casing. The instrumentation of DH-GAP04 is described in Section 1.4.2. and Table 3.1.

Table 3.1. Lengths and depth of the three sampling sections of the borehole DH-GAP04 and the locations of corresponding pressure, temperature and conductivity sensors. The elevation of the top of casing (TOC) is 526.17 m.a.s.l. (D-WGS84).

Sampling Section	Borehole length (m)	Depth below TOC (m)	Pressure sensor (m borehole length)	Temperature sensor (m borehole length)	Conductivity sensor (m borehole length)
Upper	400-594.5	375-561.3	592.01	n/a	541.32
Middle	594.5-604.5	561.3-570.7	596.74	597.47	595.70
Lower	604.5-687	570.7-646	606.90	n/a/	607.52

Detailed results and methodologies of the PFL measurements are described in (Pöllänen et al., 2012) and summarized in Chapter 1 (Section 1.5.6). Transmissivities in DH-GAP04 ranged from 10^{-6} to 10^{-9} m^2 s^{-1}. The most transmissive fractures were observed in the upper and middle sections (10^{-6} m^2 s^{-1}). Hydraulic testing was performed in both DH-GAP01 and DH-GAP04 during pumping of the boreholes for sampling. Hydraulic testing in DH-GAP01 gave a total fracture transmissivity of 10^{-6} m^2 s^{-1} over the testing interval of 130 to 191 m vertical depth.

Hydraulic heads in all sections of DH-GAP04 are above the ground surface elevation at the edge of Isunnguata Sermia Glacier (475 m). The upper and middle sections of DH-GAP04 have similar head values (512 to 523 m) from 2011 to 2014 with the maximum head value observed in 2012. The lower section has the lowest hydraulic head. The initial hydraulic head in the low section was 529 m directly after drilling followed by a rapid drop to approximately 487 m and has since varied between 485 -487 m (excluding sampling events) (Harper et al., 2015a).

3.3.3. Isotopic and Geochemical Analyses

Isotope analyses were performed at the University of Waterloo Environmental Isotope Laboratory. Methods for isotopic analyses are included in Chapter 1. Geochemistry samples were analyzed at Labtium Oy and the TVO (Teollisuuden Voima Oyj) laboratories in Finland (methods in Chapter 1). Geochemical results that exceeded a charge balance error of 10% were not considered.

3.3.4. Fracture Mineral Analyses

Samples of gypsum present as fracture infilling minerals in the DH-GAP04 core, as well as one sample from the DH-GAP01 core, were removed using dental tools under microscope. Sulfide samples from a section of DH-GAP04 were hand separated under microscope. Gypsum samples were analyzed for $\delta^{34}S$ and $\delta^{18}O$ of SO_4^{2-} as well as $^{87}Sr/^{86}Sr$. Sulfide samples were analyzed for $\delta^{34}S$. A more comprehensive look at the fracture filling minerals can be found in Chapter 4.

3.3.5. Gas Sampling at Leverett Spring

Gas bubbles were observed in the outlet pond of the Leverett Spring, focused around the spring outlet. A number of gas samples were acquired from the spring and analyzed for composition and isotopic analyses. Gas samples were taken under water using a large funnel feeding into a glass sample bottle. The sample bottle was first filled with water which was displaced as the spring gases filled the bottle. The sample bottles were capped under water with a teflon septum equipped cap. Gas samples were transported in an inverted position. Further steps were taken in 2011 to ensure sample quality: samples were transported cooled and inverted with the caps sitting in a layer of water. Results from the 2011 samples are believed to be more representative due to these improved methods. Gas samples from the Leverett Spring were analyzed at the University of Waterloo Organic Geochemistry Laboratory on a Fisher/Hamilton Model 29 gas chromatograph for oxygen, nitrogen, carbon dioxide and methane.

3.4. Results

DH-GAP01 was successfully cleared of drilling waters, based on sodium fluorescein concentrations <5% intial, by May 2010 and subsequent sampling has yielded consistent chemical and isotopic results. During sampling in September 2013, the lower section of DH-GAP04 was rapidly cleared of drilling water contamination; however, in September 2014, the upper and middle sections of DH-GAP04 still contained 33 and 29% drilling fluid, respectively, based on the measured sodium fluorescein concentrations. Results from the upper and middle sections of DH-GAP04 are useful despite the drilling contamination, especially for isotopes such as $^{34}S_{(SO4)}$, $^{18}O_{(SO4)}$, ^{87}Sr, ^{37}Cl and ^{81}Br, where concentrations of dissolved chemical species in the groundwater are many times higher than in the drilling water. For $\delta^{18}O$, $\delta^{2}H$ and Cl^-, a linear mixing model can be used to predict the groundwater composition based on the concentration of drilling tracer in the samples.

3.4.1. Isotopic Results

Stable isotopic composition ($\delta^{2}H$, $\delta^{18}O$) of groundwaters, meltwaters and the Talik Lake waters are shown in Figure 3.2. Modern local precipitation is interpreted to have a yearly average $\delta^{18}O$ of -19‰, based on IAEA monitoring data from stations in Thule to the north and Grønnedal to the south (Leng & Anderson, 2003). The local meteoric water line (LMWL) for Grønnedal is included in Figure 3.2. Lake waters fall along a local evaporation line (LEL) with a slope of 4.5. Meltwaters, including supraglacial flow, subglacial flow and meltwater rivers, are depleted in $\delta^{18}O$ by up to 11.5‰ when compared to modern precipitation, and fall on or slightly above the GMWL. These findings are consistent with previous research on the $\delta^{18}O/\delta^{2}H$ composition of lakes in the Kangerlussuaq Region by Leng and Anderson (2003). Lakes have $\delta^{37}Cl$ isotopic signatures that range from -0.6 to 0.4‰ with an average value of -0.1‰. Lakes tend to have highly radiogenic strontium signatures 0.709 to 0.758 with an average of 0.738.

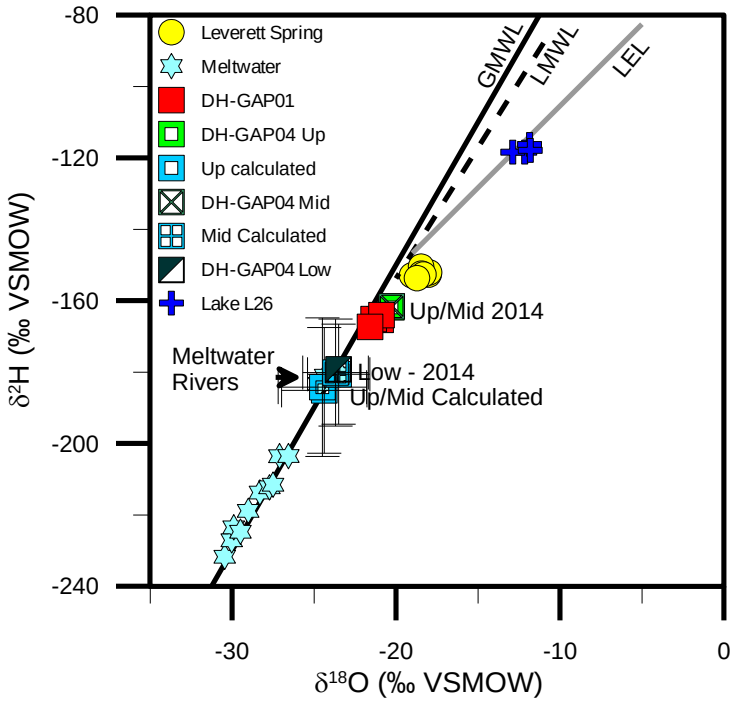

Figure 3.2. $\delta^{18}O$ and $\delta^{2}H$ of ground and surface waters. Calculated values for the upper and middle sections of DH-GAP04 were determined using a linear mixing model (equation 1). The local meteoric water line for Grønnedal is also included. Note that the label "meltwater rivers" shows additional meltwater sampling points located on the GMWL at the location indicated. Error bars are given for the calculated compositions of the middle and upper sections of DH-GAP04.

Groundwaters from DH-GAP04, and to a lesser extent from DH-GAP01, are depleted in $\delta^{18}O$ and $\delta^{2}H$ relative to modern meteoric values (Figure 3.2). DH-GAP01 samples fall slightly to the right of the GMWL. The Leverett Spring water falls to the right of the GMWL and is slightly enriched relative to modern meteoric values.

Based on the fluorescein tracer, the upper and middle sampling sections of DH-GAP04 still contained significant drilling fluid in September 2014. However, groundwater isotopic compositions in DH-GAP04 upper and middle sections (δ_A) can be calculated using the following linear mixing model:

$$\delta_{sample} = \chi\delta_A + (1-\chi)\delta_B \qquad [3.1]$$

where χ is the portion of uncontaminated waters (δ_A) in the sample, δ_B is the known isotopic composition of the drilling fluid. The results of this calculation are indicated as Up and Mid Calculated in Figure 3.2. Based on the actual (lower section) and predicted (upper and middle sections) results, DH-GAP04 groundwaters fall on the GMWL and isotopic compositions of the upper and middle sections of DH-GAP04 (calculated using Equation 3.1) were the same, within the range of analytical uncertainty, for the 2013 samples and the 2014 samples.

Error in the calculated values, included as error bars in plots, are based on a 10% variation in fluorescein concentrations in the drilling fluid. Error in the calculated values of $\delta^{18}O$ ranged between 1.9 to 2.7‰ and in $\delta^{2}H$ was 14 to 19‰. While errors in calculated values are significant, it seems likely that the calculations are fairly accurate based on: (1) similar results between 2013 and 2014 (both are shown in Figure 3.2) (2) results falling on the GMWL (3) results similar to measured isotopic values in the low section of DH-GAP04 (Figure 3.2).

Groundwaters generally do not contain ^{3}H, with the exception of the DH-GAP04 upper and middle section samples – which were still contaminated with drilling waters in 2014 and contain 2.4 and 1.6 TU, respectively. It is likely that, similar to DH-GAP04 low, uncontaminated samples in the upper and middle sections will also be free of tritium. By comparison, lakes in the region have an average ^{3}H concentration of 10 TU and a sample of summer snow from a storm in July 2009 had a ^{3}H concentration of 13.8 TU. A summary of isotopic results for groundwaters and relevant surface waters is provided in Table 3.2.

Table 3.2. Isotopic composition of groundwaters and of the Talik Lake(L26) and Lake L25. The sample from the Talik Lake was taken at 25 m depth. For the groundwater from the boreholes, the percentage of contamination with drilling fluid, based on the concentration of the tracer, from the most recent sample is given. Calculated results (italics) are based on the 2014 measured values.

	Sample	δ18O	δ2H	δ34S	δ18O	$\delta^{37}Cl$	$\delta^{81}Br$	$^{87}Sr/^{86}Sr$	^{3}H	Drill Water
	Date	‰ VSMOW	‰ VSMOW	SO_4 (‰ CDT and VSMOW)		‰ SMOC	‰ SMOB		TU	%
L25 (Drill Water Lake)	6/25/2011	-11.9	-117						8.7	
L26 (GAP01 Talik Lake)	11/05/2010	-12.9	-118			-0.1		0.73847	10.1	
DH-GAP01	09/2010	-21.6	-167	4.9	5.9	-0.1		0.70753		<5
DH-GAP04 Upper	09/2013	-19.7	-160	5.0	3.9	0.3	0.4	0.70334	2.9	38
DH-GAP04 Upper	09/2014	-20.3	-162						2.4	33
DH-GAP04 Upper (calc)	2014	*-24.4*	*-185*							
DH-GAP04 Middle	09/2013	-19.7	-160	4.5	3.1	0.2		0.70407	2.5	33
DH-GAP04 Middle	09/2014	-20.3	-162						1.6	29
DH-GAP04 Middle (calc)	2014	*-23.5*	*-181*							
DH-GAP04 Low	09/2013	-23.2	-176	5.0	2.9	0.4	0.6	0.70440	<0.8	<5
DH-GAP04 Low	09/2014	-23.5	-179						<0.8	<5
Leverett Spring	29/06/2008	-18.7	-152	8.9	4.4	0.0		0.74283	1.2	
	27/06/2009	-18.0	-153					0.73249	<0.8	
	05/09/2009	-19.0	-153						<0.8	
	10/05/2010	-18.5	-150	10.9	5.9				<0.8	
	05/09/2010	-18.5	-152			0.06			<0.8	
	14/04/2011	-18.3	-153						<0.8	
	11/09/2014	-18.7	-154						<0.8	

3.4.2. Geochemical Results

Groundwaters sampled from DH-GAP04 and DH-GAP01 are brackish (Davis, 1964), Ca-Na-SO_4 type waters (Figure 3.3). Surface waters in the area are dilute to brackish, and those brackish lakes with the highest salinity fall into either HCO_3-SO_4 or HCO_3-Cl end members. Meltwaters are HCO_3^- type waters with variable proportions of Ca^{2+}, K^+ and Na^+ and are extremely dilute, with conductivities generally lower than 50 μS/cm and ranging from 2 to 121 μS/cm.

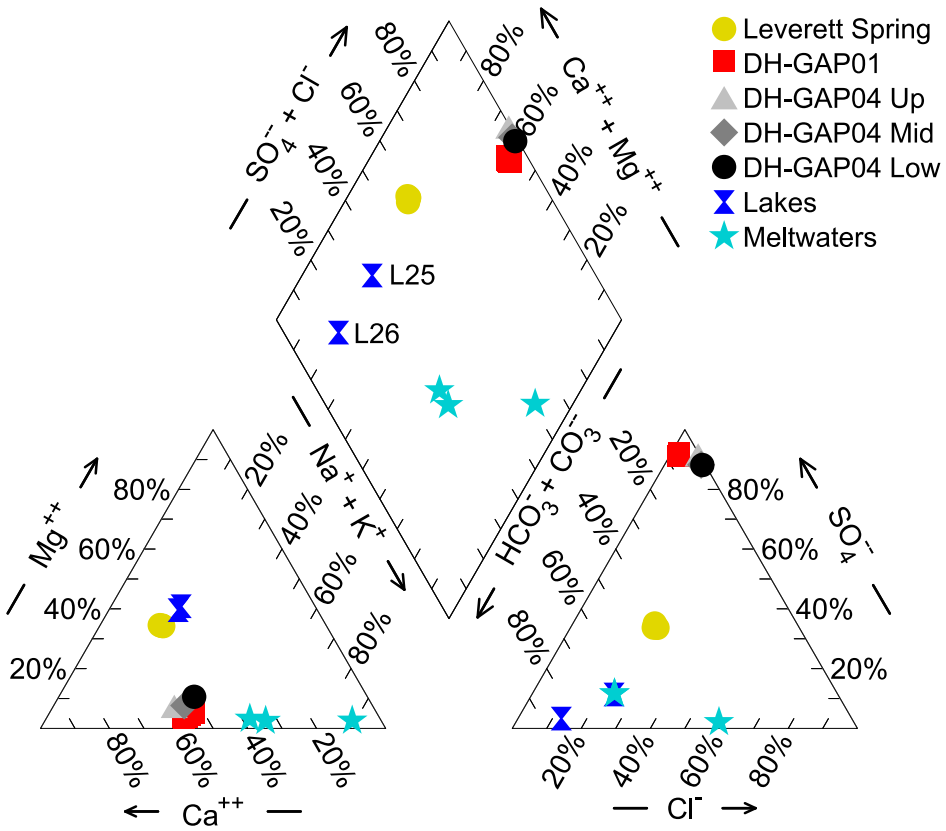

Figure 3.3. Piper plot showing ground and surface water ionic compositions. Borehole groundwaters from DH-GAP01 and DH-GAP04 have similar, SO4-dominated compositions. The Leverett Spring has a chemical composition that differs from the borehole groundwaters. Note that neither the Leverett Spring nor borehole groundwaters resemble the chemical composition of meltwaters.

The most saline groundwaters, at electrical conductivity values of 3670 µS/cm, are found in the lower section of DH-GAP04, while the most dilute groundwaters are found in DH-GAP01 (800 µS/cm). The upper and middle sections of DH-GAP04, which tend to respond in unison to pressure changes (Harper et al., 2015a), have conductivities between 2500 to 2560 µS/cm. The saturation index for gypsum (calculated using PHREEQC) in the low section of DH-GAP04 in 2013 indicates that the low section is at equilibrium with respect to gypsum. The low section of DH-GAP04 is undersaturated with respect to calcite (-0.85) and celestite (-0.16).

Table 3.3. Chemistry of groundwaters and relevant surface waters. The sample from the Talik Lake(L26) was taken at 25 m depth. For the boreholes, the 2013 sampling results are given along with the percentage of drilling contamination.

	Sample Date	Ca mg/L	Mg mg/L	K mg/L	Na mg/L	Cl mg/L	SO_4 mg/L	Alk mmol/L	Br µg/L	Sr µg/L	Drill Water %
L25 (Drill Water Lake)	6/25/2011	12	7.9	3.7	5.2	5.9	3.8	0.46	36	37	
L26 (Talik Lake)	11/05/2010	18	11	6.4	6.7	9.9	3.5	1.90	40	63	
DH-GAP01	09/09/2011	96	3.5	2.2	76	7.7	347	0.49	90	2670	<5
DH-GAP04 Upper	22/09/2013	368	23	3.6	257	94	1310	0.32	1260	6490	33
DH-GAP04 Middle	23/09/2013	325	28	5.6	255	109	1230	0.35	1520	6120	29
DH-GAP04 Low	24/09/2013	459	59	5.9	409	173	1880	0.40	2390	8170	<5
Leverett Spring	11/09/2011	40.8	18	4.7	16	36	68	1.80	1040	118	

The isotopic and major ion chemistry results for the DH-GAP01 and DH-GAP04 groundwaters, the Talik Lake and Drill Water (L25) lakes, as well as Leverett Spring, are given in Tables 3.2 and 3.3. A comprehensive table of geochemical results can be found in Appendix B. In Leverett Spring, iron concentrations of up to 14.8 mg/L are observed, while the borehole groundwaters contain less than 1 mg/L of iron. The geochemical composition of Leverett Spring was similar to that measured by Scholz and Baumann (1997) with the exception of fluoride. Scholz and Baumann (1997) measured fluoride concentrations of 0.55 mg/L while spring samples taken for the GAP had fluoride concentrations of 0.1 mg/L or less.

The linear mixing model (Equation 1), used to predict the groundwater isotopic composition of the upper and middle sections of DH-GAP04, can also be used to predict chloride concentrations in the uncontaminated groundwater. The upper and middle sections of DH-GAP04 are predicted to have approximate chloride concentrations of 147 (± 26) and 159 (± 21) mg/L, respectively. Sulfate concentration in DH-GAP04 was likely to have been impacted by dissolution of fracture gypsum by mixing of dilute drilling waters with abundant fractures containing the mineral.

Selected isotopic results from mineralogical studies that are relevant to the characterization of groundwaters are given in Table 3.4. Chapter 4 contains a more comprehensive look at the fracture filling gypsum, its origin and impact on groundwater chemistry.

Table 3.4. Range of isotopic composition for fracture filling gypsum and rock matrix sulfides. NM = not measured. NA = not applicable.

	Number of Samples	δ34S (SO4) ‰ CDT	δ18O (SO4) ‰ VSMOW	$^{87}Sr/^{86}Sr$
DH-GAP01 Sulfate	n=3	2.63-4.90	NM	0.7075(n=1)
DH-GAP04 Sulfate	n=31	3.22-10.65	4.48-9.09	0.7017-0.7093
DH-GAP04 Sulfide	n=3	2.26-3.73	NA	NA

Gas samples from the Leverett Spring are dominated by nitrogen. The spring gas composition is similar to atmospheric but with a reduced proportion of oxygen and a greater proportion of carbon dioxide(Table 3.5). The 2011 samples indicate that methane concentrations are likely higher than those observed in previous samples. $\delta^{13}C$ of the methane samples was highly depleted (-69.3 and -71.6‰) (Table 3.6). The gas samples from the spring contained small concentrations of O_2 (Table 3.5) that had a depleted isotopic signature (-22.4 and -23.5 ‰) (Table 3.7).

Table 3.5. Composition of gas samples from the Leverett Spring. Improved sampling methods in 2011 yielded what are likely the most representative results.

	% O_2	% N_2	% CO_2	% CH_4	Total %
Atmosphere	20.95	78.08	0.04	0	99.07
Spring 2008	10.96	85.52	0.36	ND	96.83
Spring 2009 (Avg)	1.26	92.29	0.92	0.11	94.59
Spring 2010 (Avg)	1.53	93.69	1.88	0.03	97.13
Spring 2011(Avg)	**1.83**	**88.7**	**0.625**	**0.65**	**91.81**
Spring 2011 (Range)	**1.56 - 2.10**	**86.9 - 90.5**	**0.60 – 0.65**	**0.65 – 0.65**	**90.25 – 93.36**

Table 3.6. Isotopic composition of two gas samples from the Leverett Spring, September 2011.

	$\delta^{18}O$ O_2	$\delta^{15}N$ N_2	$\delta^{13}C$ CH_4	$\delta^{13}C$ CO_2
Spring 2011 1	-23.5	0.05	-71.6	-23.7
Spring 2011 2	-22.4	0.12	-69.3	-22.9

3.5. Discussion

3.5.1. Oxygen-18 and Deuterium

3.5.1.1. Leverett Spring

The Leverett Spring is located at an elevation of 230 m, within a moraine complex at the front of Leverett Glacier (Figure 3.1). The presence of Leverett Spring (pingo) is unique in the Kangerlussuaq area despite similar glacial sediment filled valleys at the forefront of other glacial lobes nearby. The spring flows year round, forming a large mound of ice overtop of the spring location during the winter and a small pond in the spring crater during the summer. The water in the spring pond is rust red in colour, as are the surrounding rocks and till. After drilling through several meters of ice in winter, pressurized spring water flows up out of the drill hole. The water that flows out during winter is clear, with iron in a reduced state and an Eh value of -120 mV. The highest concentrations of iron (14.8 mg/L) in the spring water were observed in the winter, presumably because Fe is not removed by the precipitation of iron oxyhydroxides. Thus, the spring water appears to be under reducing conditions with oxidation occurring at the surface within the pond.

Isotopically, Leverett Spring is distinct from the borehole groundwaters – being more enriched in both $\delta^{18}O$ and $\delta^{2}H$, as well as plotting further to the right of the GMWL (Figure 3.2). This suggests that there may be some component of evaporatively enriched surface water in the spring water. Geothermal waters also may plot to the right of the GMWL (Craig, 1963; Truesdell & Hulston, 1980)

due to high temperature exchange of ^{18}O between minerals and water. This generally requires temperatures above 100 °C, necessitating a large degree of cooling to reach the low 0.5 – 3°C temperatures of the Leverett Spring waters. It is important to note that while the spring is located within 200 meters of the Leverett Glacier, the $\delta^{18}O/\delta^{2}H$ of the spring water does not have the characteristic depleted isotopic signature of meltwaters (Figure 3.2).

In terms of the source water for Leverett Spring, four possible end members are considered. The spring water likely represents a mixture between two or more of these end members.

(1) Shallow flow in a permeable layer beneath the ice is emerging at this location after mixing with some source of surface water. This hypothesis would be consistent with other open-system pingos in Greenland which are associated with intra or subpermafrost flow and artesian conditions (Cruickshank & Colhoun, 1965; Allen et al., 1976; Worsley & Gurney, 1996).

(2) Dilute, isotopically depleted glacially meltwaters recharging beneath the GrIS.

(3) Deep groundwater that has evolved through water-rock interaction, possibly flowing along the geological boundary between the deformed gneisses of the Nagssuqtoqidian and the undeformed Archean block (Figure 3.1).

(4)Deep groundwater that is hydrothermal in origin. Scholz and Baumann (1997) suggest that the spring waters are hydrothermal in origin, citing high fluoride concentrations (0.55 mg/L) as evidence. However, over multiple years of sampling for the GAP, fluoride concentrations were observed to be much lower (0.1 mg/L or less). Springs and pingos related to geological structures or geothermal conditions have been observed on Disko Island, West Greenland (Yoshikawa et al., 1996), in the Scoresby Sund area of Eastern Greenland (Pedersen, 1926; Haliday et al., 1974) and on Axel Heiberg Island in the Canadian Arctic (Pollard et al., 1999; Grasby et al., 2003a; b).

Deep groundwaters may have mixed with some component of evaporated surface water to impart an enriched $\delta^{18}O$ isotopic signature that falls below the GMWL. Alternatively, deep, geothermal groundwaters with an enriched $\delta^{18}O/\delta^{2}H$ isotopic signature may be mixing with dilute glacial meltwaters with a depleted isotopic signature. Interaction of the spring water with the valley sediment imparts a unique chemistry compared to groundwaters obtained from DH-GAP boreholes. The following sections further discuss the spring chemistry.

Gas sampled from the Leverett Spring contained methane with a depleted $\delta^{13}C$ isotopic signature (-69.3 and -71.6 ‰) characteristic of methane that is biogenic in origin (Barker & Fritz, 1981). One possible source of the spring gases is the release of air trapped as bubbles in the ice found within the till around the Leverett pond. The moraine units at Leverett contain abundant layers and lenses of ice rich in atmospheric gas bubbles (Waller & Tuckwell, 2005). This hypothesis explains the similarity of the Leverett Spring gas samples to atmospheric composition and suggests that the source of oxygen is shallow. Oxygen would likely be consumed by redox reactions such as the precipitation of the iron oxide minerals observed in and around the spring pond. Biogenic methane production may be occurring in the pond sediments after oxygen has been consumed. It is unknown at this time why the $\delta^{18}O$ isotopic signature of the oxygen (-22 to -24 ‰) is so depleted relative to atmospheric oxygen (+23.5 ‰).

3.5.1.2. Groundwater and Taliks

Permafrost acts as an aquitard (Woo & Steer, 1983; Vidstrand, 2003), restricting hydraulic conductivity and groundwater flow between the surface and subpermafrost aquifers (King-Clayton et al., 1997). The presence of continuous permafrost prevents recharge, except where unfrozen conduits (taliks) exist between the surface and subpermafrost aquifer and in those areas beneath ice sheets where permafrost is absent (e.g., Cutler et al., 2000). Taliks may penetrate fully through

permafrost or may be closed at one end and, thus, do not connect the surface to the subpermafrost aquifer (e.g., van Everdingen, 1990). Thermal modeling suggests that lakes larger than 200 m across could be capable of supporting taliks through the permafrost in the Kangerlussuaq area (Harper et al., 2011). Taliks may be either recharging or discharging, or may also be recharging in one part of the lake and discharging in another (Vidstrand, 2003; Bosson et al., 2010). Taliks were reported in Antarctica where groundwater discharge into Lake Vanda and Don Juan Pond can be identified by isotopic means, such as δ^{36}Cl and δ^{7}Li, as well as geochemical parameters (Harris & Cartwright, 1981; Green & Canfield, 1984; Carlson et al., 1990; Lyons et al., 1998; Green & Lyons, 2008; Witherow et al., 2010).

Hydraulic head in the DH-GAP01 borehole was, at all times, lower than water levels in the Talik Lake (Section 1.5.5; Figure 1.8), suggesting that the lake is recharging into the talik (Bosson et al., 2013; Johansson et al., 2015). A comparison of the δ^{18}O/δ^{2}H values for DH-GAP01 and DH-GAP04 with that of the lake waters indicates that it is possible that DH-GAP01 groundwaters may represent a mixture of groundwaters similar to those present at DH-GAP04 and lake waters. Based on a simple linear mixing model (Equation 1), using the groundwater isotopic composition of DH-GAP04-Up (calculated), DH-GAP01 may contain up to 25% lake water. However, a mixing scenario between DH-GAP04 groundwaters and lake waters cannot account for the low chloride concentrations (7.7 mg/L) found in DH-GAP01 groundwaters (Figure 3.4). It is considered more likely that the fluid represents mixing with a dilute groundwater end member that has undergone less water rock interaction, either due to reduced residence time compared to DH-GAP04 or to differences in local geology. Geologically, DH-GAP01 is situated in more felsic-type bedrock than DH-GAP04 (Pere, 2014). As well, gypsum was found very infrequently as a fracture infilling mineral in the DH-GAP01 core when compared to the DH-GAP04 core. However, the upper 200 m of the DH-GAP04 core, which corresponds to the depth of DH-GAP01, also contains little gypsum mineralization. The

shallow systems of DH-GAP01 and DH-GAP04 may not be directly comparable due to the distance (6 km) and differences in structural geological setting and elevation. There may have been little gypsum in the shallow bedrock to begin with, or it was present and subsequently dissolved. Understanding the origin of the gypsum in the DH-GAP04 core was an important objective of this study and is covered in detail in Chapter 4.

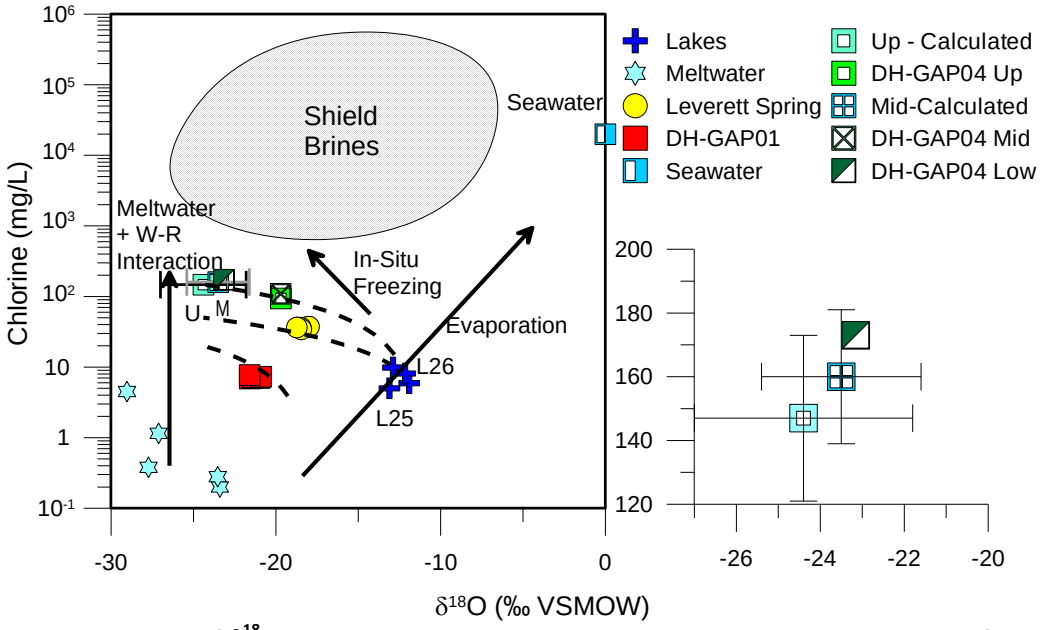

Figure 3.4. A comparison of δ^{18}O isotopic values and chloride concentrations in ground and surface waters studied for the GAP compared to Canadian and Fennoscandian shield brines. The evaporation line described the evolution of lake salinity and isotopic composition. In-situ freezing causes increasing chloride concentrations with depletion in δ^{18}O. Dashed lines represent various mixing scenarios calculated using the linear mixing model described by equation 1 and various surface water and groundwater end members. Infiltrating meltwaters would maintain a depleted δ^{18}O isotopic signature while increasing in salinity through low temperature water-rock interaction.

3.5.1.3. Meltwater Infiltration

Continental ice sheet meltwaters have been reported to have δ^{18}O that is significantly more depleted than modern meteoric waters at a similar latitude (e.g., Siegel, 1991; Clark et al., 2000; Ma et al., 2004; Hammer, 2006). Meltwaters in Kangerlussuaq were analyzed from a variety of sources, including subglacial and supraglacial runoff along the ice margin, as well as from the large terminal rivers flowing from the Isunnguata Sermia and Leverett glaciers. Figure 3.2 shows meltwaters have

a large range of isotopic values, making it difficult to describe a "typical" meltwater end member with which to calculate mixing scenarios. $\delta^{18}O$ values in cores of the Greenland Ice Sheet show large variations with depth and latitude that are reflected along the ice margin and in meltwater signatures (Dansgaard et al., 1993; Reeh et al., 2002). Waters from DH-GAP04 represent the most depleted groundwaters found in the region and are similar in terms of $\delta^{18}O$ and $\delta^{2}H$ to the large meltwater streams at the termini of the Isunnguata Sermia and Leverett glaciers. Due to the wide range of isotopic values for meltwaters (Figure 3.2), it is difficult to determine whether DH-GAP04 groundwater represents purely a recharging meltwater endmember. DH-GAP04 groundwaters are at the upper range of isotopic values for the meltwaters sampled and it cannot be ruled out that recharging meltwaters are mixing with another, deeper, groundwater end member.

Meltwater infiltration during Pleistocene glaciation has been inferred from the presence of groundwaters depleted in $\delta^{18}O$ and $\delta^{2}H$ in Greenland (DeFoor et al., 2011) as well as in rocks from North America and Europe in both crystalline (Smellie & Frape, 1997; Glynn et al., 1999; Laaksoharju & Rehn, 1999; Blomqvist et al., 2000; Clark et al., 2000; Douglas et al., 2000; Pitkanen et al., 2001, 2004; Stotler et al., 2012) and sedimentary environments (Desaulniers et al., 1981; Siegel & Mandle, 1984; Siegel, 1991; Remenda et al., 1994; Martini et al., 1998; Grasby et al., 2000; Vaikmae et al., 2001; McIntosh & Walter, 2005, 2006; Raidla et al., 2009; McIntosh et al., 2011).

Work by Stotler et al. (2012) has highlighted the need for caution when interpreting depleted $\delta^{18}O$ values as glacial meltwater. In situ freezing processes as well as methane hydrate formation also can result in depleted $\delta^{18}O$ values similar to those commonly attributed to glacial meltwater. The possible impact of in situ freezing on the isotopic composition of the GAP borehole groundwaters is evaluated below.

3.5.1.4. In Situ Freezing and Cryogenic Concentration

During permafrost formation, cryogenic salt exclusion tends to concentrate salts that have low eutectic temperatures, such as Cl^- salts, in the fluids, while precipitating salts that have higher eutectic temperatures, such as mirabilite ($Na_2SO_4 \bullet 10H_2O$; -3.5 to 8.2 °C)(Terwilliger & Dizio, 1970; Anisimova, 1980; Laaksoharju & Rehn, 1999; Gascoyne, 2000; Alexeev & Alexeeva, 2003; Vidstrand, 2003; Stotler, 2008). Evidence for solute exclusion during permafrost formation has been observed at a lake in the Canadian High Arctic (e.g., Ouellet et al., 1989; Mackay, 1997) and in a sedimentary environment in Russia (e.g., Anisimova, 1980; Chizhov, 1980; Fotiev, 1980; Alexeev and Alexeeva, 2002) in the form of saline waters on the order of hundreds of g/L. Such high salinities are not observed in the DH-GAP boreholes. At other crystalline rock sites in the Canadian and Fennoscandian shields, Stotler (2008) did not find conclusive evidence that in situ freezing had affected groundwaters. The Dry Valleys Drilling Project in Antarctica also found the salinity of deep groundwaters in a basaltic aquifer to be the result of water-rock interaction rather than cryogenic processes related to permafrost formation (Harris & Cartwright, 1981).

In situ freezing can produce depleted $\delta^{18}O$ values, as discussed in Stotler et al. (2012). During the freezing process, the residual water tends to be displaced above the GMWL (Zhang & Frape, 2003; Stotler et al., 2012). Stotler et al. (2012) and Zhang and Frape (2003) noted that during in situ freeze-out, Cl^- is concentrated in the residual water and more depleted $\delta^{18}O$ values correspond to greater Cl^- concentrations. In Figure 3.4 the measured (lower) and predicted (upper and middle) chloride concentrations in the DH-GAP04 borehole waters are plotted against $\delta^{18}O$, showing a trend of increasing chloride that corresponds to more enriched $\delta^{18}O$ values, the opposite of what would be expected during in situ freezing.

3.5.2. Sulfur Concentrations and Isotopic Signatures

Groundwaters from the DH-GAP boreholes are dominated by SO_4^{2-} (Figure 3.3), ranging from 400 mg/L (DH-GAP01) to 2000 mg/L (low section of DH-GAP04). Possible sources for sulfate in the borehole waters include oxidation of bedrock sulfides (Fritz et al., 1994; Stotler et al., 2009), infiltration of high sulfate surface waters, and dissolution of sulfate-bearing mineral phases such as gypsum ($CaSO_4 \bullet 2H_2O$) or mirabilite ($Na_2SO_4 \bullet 10H_2O$) (Alexeev & Alexeeva, 2003; Stotler et al., 2012). Gypsum was observed as a frequent fracture filling mineral in the DH-GAP04 core below a borehole length of 300 m and, more rarely, in the DH-GAP01 core and the upper 300 m of the DH-GAP04 core. SEM analysis revealed that gypsum and celestite ($SrSO_4$) also exist within the bedrock matrix pore space (Eichinger & Waber, 2013) and that porewaters are of Ca-Na-SO_4 type. Mirabilite was not observed in any mineralogical studies of the DH-GAP04 core (Chapter 4; Pere, 2014).

Oxidation of sulfide minerals tends to result in a sulfur isotopic signature that is similar to slightly depleted (2 – 5‰,) in $\delta^{34}S$ compared to the original sulfide value (Gavelin et al., 1960; Toran & Harris, 1989; Seal et al., 2000). Dissolution of soluble sulfate-bearing minerals is a non-fractionating process (Fry et al., 1988; Clark & Fritz, 1997). Figure 3.5 indicates that groundwater sulfate isotopic values closely resemble sulfate isotopic values for the gypsum fracture minerals throughout the core and are slightly enriched relative to sulfides. This suggests that high sulfate concentrations are derived from dissolution of gypsum and celestite. However, the $\delta^{18}O$ of SO_4^{2-} in the DH-GAP04 borehole has a slight depletion relative to the fracture gypsum from which it is primarily derived. $\delta^{18}O$ of dissolved SO_4^{2-} and $\delta^{18}O$ in the water may exchange, however the process is incredibly slow except at high temperatures or low pH. It is more likely that there is a secondary source of sulfate which could be (a) SO_4^{2-} derived from oxidation of sulfides (see Section 4.4.3.5) and (b) gypsum with a more depleted $\delta^{18}O$ (SO_4) signature present further up the flow path from the DH-GAP04 borehole. $\delta^{18}O$ (SO_4) may vary due to differences in fractionation factors between $\delta^{18}O$-H_2O

and δ^{18}O-SO_4 with temperature, post-depositional changes or separate hydrothermal events (Chiba & Sakai, 1985; Boschetti et al., 2011).

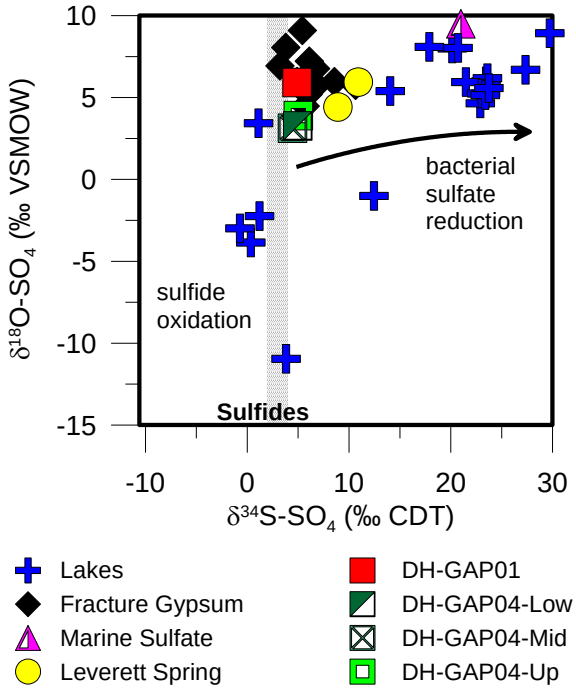

Figure 3.5. δ^{34}S and δ^{18}O isotopic composition of SO_4^{2-}. While some surface waters appear to derive sulfate from sulfide oxidation, others are enriched through bacterial sulfate reduction. Groundwaters closely resemble the isotopic composition of fracture filling gypsum while the Leverett spring shows a δ^{34}S enrichment likely caused by bacterial sulfate reduction.

Enriched sulfur-34 values, greater than 20‰, in many lake waters (Figure 3.5) are indicative of the activity of sulfur reducing bacteria (SRB). While SRB may be present and active in shield groundwaters (Fritz et al., 1994; Stotler et al., 2009) and in cold climate environments (Grasby et al., 2003a), a microbial study conducted on DH-GAP01 waters as part of the GAP did not indicate that SRB were present (Harper et al. 2010). While microbial studies have not yet been conducted on the DH-GAP04 groundwaters, the lack of sulfur-34 enrichment in DH-GAP04 compared to DH-GAP01 suggests that an active SRB community is unlikely to be present in the middle and lower sections. It should be noted, however, that during borehole purging and sampling of DH-GAP04 in 2013, a slight H_2S smell was noted during sampling of the upper section of the borehole that was not present

during initial sampling in 2011. Sulfur-34 enrichment, however, was not observed in the upper section of DH-GAP04. It may be that SRB were introduced into the borehole during drilling and/or that sulfate reduction is not a significant enough process to impact the isotopic signature of the high sulfate groundwaters in the borehole.

Redox studies for the GAP were carried out by Terralogica AB, Linnaeus University and University of Helsinki. Analysis of redox sensitive mineral phases, such as pyrite, iron-oxyhydroxides and Mn-oxides, in the cores indicates reducing conditions in the subpermafrost groundwater system. Oxidizing conditions have existed in the near surface environment, with the deepest occurrence of oxidized mineral phases such as goethite at around 260 m (Harper et al., 2015a). Below the permafrost (~400 m BHL), at least one sample has shown an indication from uranium series disequilibrium analyses that oxidizing conditions were favourable for U mobilisation in the past, however Fe(II) oxidation is not observed at this depth (Harper et al., 2015a).

Leverett Spring is enriched in $\delta^{34}S$ compared to the borehole groundwaters by 4 – 6‰. Leverett Spring continues to flow year round, resulting in formation of a significant ice mound during the winter months. When sampled during iced over conditions, the smell of H_2S is present; however, it was not possible to collect a sufficient volume of sulfur gas for analysis. As previously discussed, the redox condition of the spring waters becomes apparent in winter when the waters are isolated from the atmosphere by ice formation. Reduced iron and an Eh of -120 mV measured in the winter flow indicate reducing conditions which would favour sulfate reduction and $\delta^{34}S$ enrichment.

3.5.3. Calcium, Sodium and Strontium Concentrations and Isotopic Signatures

In granitic environments, fresh to brackish groundwaters are generally Na > Ca > Mg > K due to interaction between surface recharge and the host rock (Frape et al., 1984), including dissolution of

Na- and Ca-containing plagioclase feldspars (McNutt et al., 1990). In mafic environments, the trend is generally Ca > Mg > Na (Frape et al. 1984). Groundwaters composition in boreholes DH-GAP01 and DH-GAP04, are Ca > Na > Mg > K with a dominance of Ca^{2+} as a result of the dissolution of gypsum found in fracture infillings and the rock matrix. Sr^{2+} in groundwater is likely also mainly derived from dissolution of fracture minerals. Strontium may substitute for Ca^{2+} in gypsum or occur as celestite ($SrSO_4$), which was observed in the rock matrix (Eichinger & Waber, 2013). The slight increase in the percentage of Mg^{2+} in the DH-GAP04 groundwaters compared to the DH-GAP01 groundwater may be due to differences in geology: DH-GAP01 is located in felsic rock, while DH-GAP04 contains an abundance of intermediate gneiss.

In crystalline environments, the dissolution of plagioclase feldspar is first to affect the strontium isotope signature of groundwaters, resulting in groundwaters with $^{87}Sr/^{86}Sr$ ratios between approximately 0.703 - 0.710 (McNutt et al. 1990). Over time, alkali feldspars and micas have a greater affect on groundwater strontium isotopic composition, cause $^{87}Sr/^{86}Sr$ isotopic ratios to increase (McNutt et al., 1990). Négrel and Casanova (2005) found a broader range of $^{87}Sr/^{86}Sr$ values in groundwaters from the Canadian and Fennoscandian Shields, with $^{87}Sr/^{86}Sr$ isotopic values ranging from 0.7050 to 0.7450. The groundwaters from the GAP boreholes have $^{87}Sr/^{86}Sr$ ratios ranging from 0.7033 to 0.7075, falling within the lower range of values predicted for shield rocks (McNutt et al., 1990; Blum & Erel, 2003; Négrel & Casanova, 2005; Frape et al., 2014). Local surface waters have much more radiogenic strontium signatures, ranging from 0.7187 to 0.7580 (Figure 3.6a; Figure 2.9), likely due to the weathering of radiogenic mineral phases, for example biotite, as a result of atmospheric exposure and glacial comminution (Blum & Erel, 1995, 1997).

The extensive gypsum fracture fillings found in the DH-GAP04 core at depths below 300 m and, in much smaller amounts, in the DH-GAP01 core (to depths of 170 m), have $^{87}Sr/^{86}Sr$ isotopic ratios

ranging from 0.7017 - 0.7093 (Table 3.4), similar to groundwaters. Likely the strontium concentration and isotopic signature of the groundwater is associated with the dissolution of sulfate-bearing minerals. This hypothesis is further supported by the good correlation between strontium and sulfate concentrations in the borehole groundwaters (Figure 3.6b).

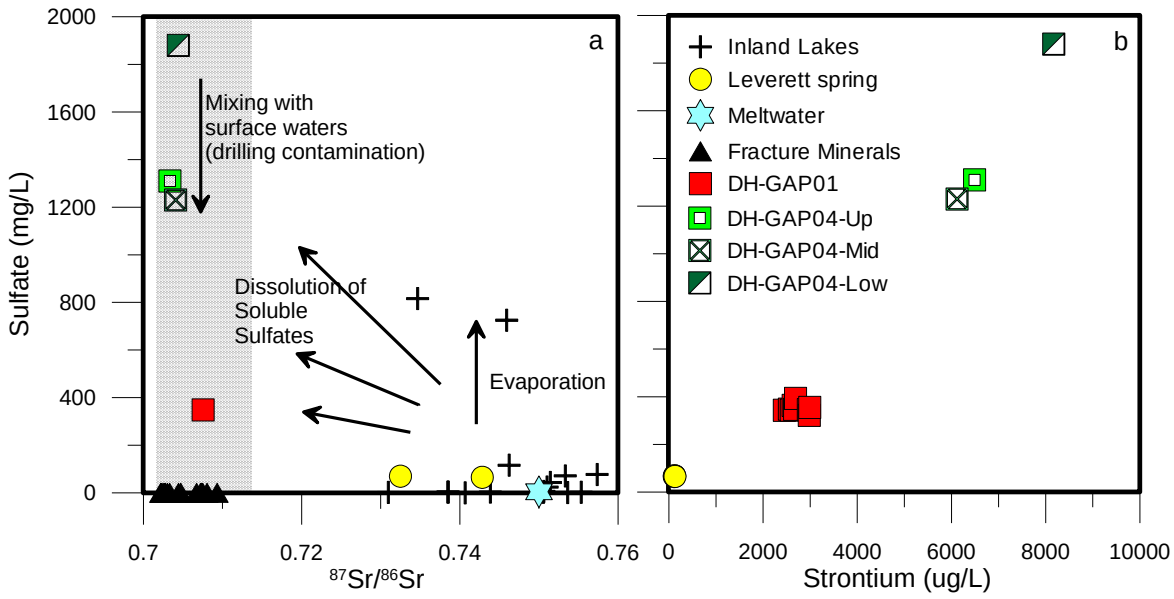

Figure 3.6. (a) $^{87}Sr/^{86}Sr$ isotopic ratios compared to sulfate concentrations indicate that Sr^{2+} in the groundwaters from the GAP boreholes is derived from dissolution of fracture infilling minerals such as gypsum. (b) Sr^{2+} and SO_4^{2-} concentrations are closely related in groundwaters.

The processes discussed above are illustrated in Figure 3.6a. Meltwaters are typically of low SO_4^{2-}, an average of 4.4 mg/L in subglacial waters, and have a radiogenic $^{87}Sr/^{86}Sr$ ratio (average 0.750). Following infiltration into the subsurface, recharging meltwaters interact with sulfate minerals to gain SO_4^{2-}, Ca^{2+} and Sr^{2+}. The $^{87}Sr/^{86}Sr$ trends toward the range described by the fracture and matrix gypsum mineralogy found in drill core, particularly from DH-GAP04 (see Chapter 4).

Water sampled from Leverett Spring (pingo) is more radiogenic than the borehole groundwaters, with a value of 0.7428, falling in a range more similar to local surface waters than groundwaters. The groundwater emerging at the spring likely flows through the glacial sediment filling the valley, interacting with comminuted material that may impart a more radiogenic signature

through alteration of more radiogenic silicate minerals with high Rb/Sr ratios. Alternatively, as suggested by the $\delta^{18}O/\delta^{2}H$ signature, which is below the GMWL, there may be a component of surface water from the active melt zone with a radiogenic $^{87}Sr/^{86}Sr$ ratio in the spring groundwaters.

3.5.4. Bromine and Chlorine Concentrations and Isotopic Signatures

The ratio of Br/Cl in groundwaters is a useful tool for evaluating the source and evolution of groundwaters. Modern seawater has a characteristic Br/Cl meq ratio of 1.53×10^{-3} and during freezing versus evaporation it was proposed by Herut (1990) that the Br/Cl ratio would evolve along different pathways as a result of differences in mineral precipitation. Starinsky and Katz (2003) used Br/Cl ratios and the theory of a distinct evolutionary pathway during freezing of seawater to theorize that shield brines were created by cryoconcentration of seawater along the margins of continental ice sheets. Subsequent work on this topic suggests that shield brines would actually evolve along different pathways during freezing as a function of the initial fluid composition (Stotler et al. 2012).

Support for the Starinsky and Katz (2003) theory of cryogenic concentration along ice sheet margins was not found in the Kangerlussuaq area. Highly saline waters, predicted to exfiltrate to the surface after ice retreat, were not found either in local lakes (Chapter 2) or groundwaters and groundwaters are not geochemically or isotopically similar to seawater.

Br/Cl ratios in borehole groundwaters are similar to those observed in other shield environments (Figure 3.7; Stotler et al., 2012). Na/Cl meq ratios in borehole groundwaters are, however, at the upper range or higher than Na/Cl ratios previously documented for shield groundwaters. For example, Stotler et al. (2012) document that Na/Cl meq ratios in groundwaters from the Canadian and Fennoscandian Shields tend to be less than 2.5, with a maximum Na/Cl ratio of 7.5 observed at the Palmottu site in Finland. Na^{+} may be derived from cation exchange or

interaction between groundwaters and plagioclase feldspar. The relationship between plagioclase feldspar and Na^+ concentrations in groundwaters and porewaters is further explored in Chapter 4 (Section 4.4.4).

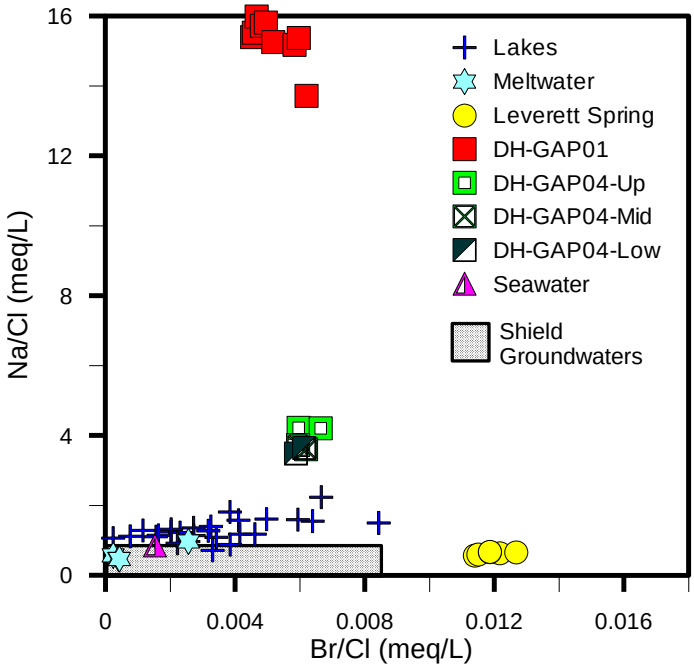

Figure 3.7. Meq ratios of Br/Cl and Na/Cl for ground and surface waters. Groundwaters from GAP boreholes have high Na/Cl ratios relative to other shield waters (stippled area) while the Leverett Spring has a high Br/Cl ratio. Ion ratios from Canadian and Fennoscandian Shield groundwaters are from Stotler et al. (2010).

Higher chloride concentrations (178 mg/L) are observed in the low section of DH-GAP04 compared to the calculated (147 and 159 mg/L) chloride compositions of the upper and middle sections respectively. While the difference is at the upper end of the potential range of error for the calculated Cl^- concentration in the middle section, the difference is still important to note and suggests that overall there is increasing salinity with depth.

Local surface waters, as well as Leverett Spring and DH-GAP01, are isotopically depleted in $\delta^{37}Cl$ (Figure 3.8). DH-GAP01 has much lower concentrations of Cl^- (7 – 10 mg/L) compared to DH-GAP04 – which has up to 173 mg/L in the lower section. The $\delta^{37}Cl$ signature of DH-GAP01 is isotopically

depleted (-0.1‰) relative to the $\delta^{37}Cl$ value of deep groundwaters from DH-GAP04 (0.2 to 0.4‰). Groundwater from DH-GAP01 (7.7 mg/L) has similar Cl^- concentrations to those found in the Talik Lake (9.9 mg/L) (Figure 3.8). The Talik Lake also has a similar $\delta^{37}Cl$ value of -0.1‰, which lends additional geochemical support that the groundwaters from the DH-GAP01 borehole are a mixture between groundwater and surface water recharging from the Talik Lake. Chloride, which is not greatly affected by the dissolution of gypsum (see Section 4.4.3.5), provides one of the few conservative tracers in this system.

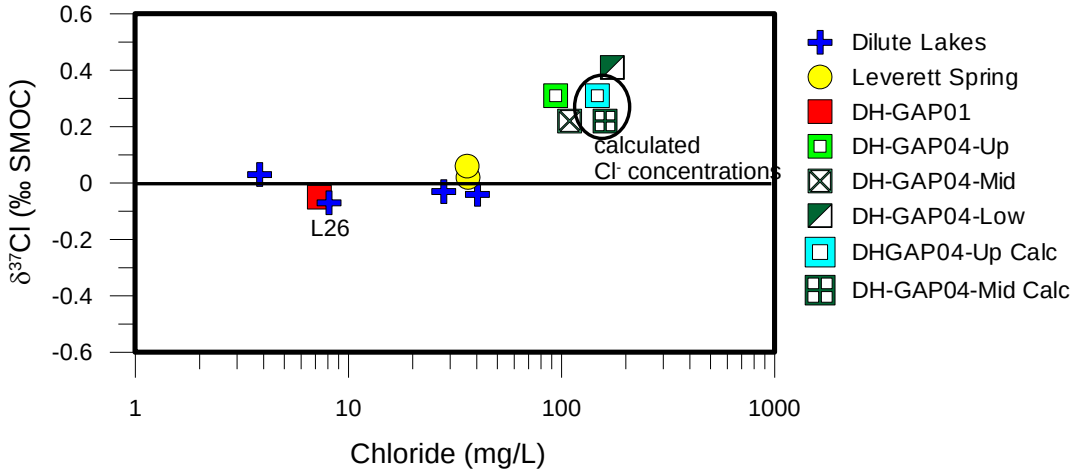

Figure 3.8. Chloride concentrations and isotopic composition for groundwaters and surfacewaters. Both the measured and calculated (see Section 3.4.2) Cl^- concentrations are shown for the upper and middle sections of DH-GAP04.

Leverett Spring has a high Br/Cl ratio relative to the groundwaters found in the boreholes and surface waters (Figure 3.7). The Na/Cl ratio of the spring is lower than that of the borehole groundwaters and more similar to surface waters. However, the majority of lakes have Na/Cl molar ratios of 1 or greater while Leverett Spring has a Na/Cl ratio <1, more similar to other shield groundwaters (Figure 3.7).

The $\delta^{37}Cl$ signatures in the DH-GAP04 borehole ranged from (0.2 to 0.4‰) (Table 3.2). As shown in Figure 3.8 there is a slight trend of $\delta^{37}Cl$ isotopic enrichment with increasing Cl^- concentration.

The trend shown in Figure 8 also corresponds to increasing Cl^- concentration and isotopic enrichment with depth. Surficial lakes, Leverett Spring and groundwaters from DH-GAP01, which have been shown to have a large component of surface water, are close to 0 ‰ in isotopic value (Figure 3.8). Long term impact of sea salt aerosols ($\delta^{37}Cl$ 0 ‰) may be a possible influence on the isotopic signature of these samples. DH-GAP04 groundwaters trend towards higher Cl^- concentrations and slightly more enriched isotopic signatures, similar to rock derived Cl^- found in other studies (Alexeev et al., 2007; Shouakar-Stash et al., 2007; Stotler et al., 2010).

During freezing, experimental results indicate that the $\delta^{37}Cl$ signature of the ice will be enriched relative to the isotopic signature of the water because the heavier isotope is preferentially incorporated into the ice phase (Zhang & Frape, 2003; Stotler et al., 2012). Zhang and Frape (2003) also noted that freezing did not create a significant change in the $\delta^{37}Cl$ isotopic signature of the water because relatively small amounts of chloride were incorporated into the ice. The positive correlation between $\delta^{37}Cl$ and $\delta^{18}O$ that occurs during freeze out (Zhang and Frape, 2003) is not observed in the DH-GAP04 groundwaters.

Canadian Shield waters have a reported $\delta^{37}Cl$ range of -0.8 to 1.0‰ and Fennoscandian Shield waters have a reported $\delta^{37}Cl$ range of -1.3 to 2.1‰ (Stotler et al., 2010). Groundwaters from DH-GAP01 and DH-GAP04 fall within the range of values reported for the Canadian and Fennoscandian Shields. The $\delta^{81}Br$ values observed in the groundwaters from the upper and lower sections of DH-GAP04 (0.4 and 0.6‰, respectively) also fall within the normal range for shield groundwaters (Stotler et al., 2010).

3.5.5. Hydrogeology

The geology of the study area is structurally complex and, as such, DH-GAP01, DH-GAP04 and Leverett Spring will be discussed separately. The physical hydrogeology was outside the scope of

this study and the summaries present here are combined from various reports and papers (See Section 1.5).

3.5.5.1. DH-GAP01

DH-GAP01 groundwaters have low chloride concentrations with $\delta^{37}Cl$ values more similar to surface water bodies (Figure 3.8), and enriched $\delta^{18}O$ and $\delta^{2}H$ isotopic signatures suggest mixing with an evaporation impacted surface water (Figure 3.2). The geochemical and hydrogeological (Johansson et al., 2015) results combined support recharge conditions. Total transmissivity of the sampling section of DH-GAP01 (10^{-6} m^2 s^{-1}) is moderate and the small hydraulic gradient (0.01) suggests that downward migration of groundwater in the talik is slow. Overall, the flow of water between the lake and talik (modeled with MIKE SHE) is small when compared to the other components of the lake basin water balance (Johansson et al., 2015).

3.5.5.2. DH-GAP04

The matching hydraulic head values between the upper and middle sections of DH-GAP04 may indicate a hydraulic connection between these sections and the similarity of many geochemical and isotopic compositions would support such a connection. Based on the calculated groundwater compositions ($\delta^{18}O$ and $\delta^{2}H$) of the upper and middle sections, the middle, packered off, section has similarities to the lower section rather than the upper section of the borehole, although overall differences are minor (Figure 3.2). Other minor differences between the middle section compared to the upper section include a more radiogenic $^{87}Sr/^{86}Sr$ isotopic ratio (Figure 3.6a), a more depleted $\delta^{18}O$ (SO_4) and a more depleted $\delta^{37}Cl$ isotopic signature (Figure 3.8) in the middle section compared to the upper section.

The lower section of DH-GAP04 has a lower and less variable hydraulic head than the upper and middle sections of DH-GAP04. Minor differences exist between the lower section and upper and

middle sections. For example, more radiogenic $^{87}Sr/^{86}Sr$ ratios in the middle and lower sections (Table 3.2; Figure 3.6a) and a more enriched $\delta^{34}S/\delta^{18}O$ of SO_4^{2-} in the low section. Geochemical differences between the lower section and upper and middle sections likely reflect differences in the isotopic composition of sulfur, oxygen and strontium in gypsum (see Chapter 4) rather than differences related to hydraulic conditions. Longer flow paths and residence times are suggested in the lower section by higher chloride concentrations and this is supported by sub-horizontal fracture sets with low transmissivity in the low section of DH-GAP04 (Section 1.5).

The extensive presence of highly soluble gypsum in DH-GAP04 below 300 m suggests that repeated advance and retreat of the ice sheet across the site of DH-GAP04 has not induced extensive flushing of the deeper bedrock/fracture network with dilute meltwaters. The continued presence of gypsum is an indicator of the long-term stability of the deep groundwater system. A secondary factor suggesting that meltwater infiltration into, and movement within, the subsurface is fairly limited is the slow recovery of the upper and middle sections of DH-GAP04. For example, drilling contamination fell by only 13% in the upper section and 14% in the middle section over two years (September 2011 to September 2013). Limited groundwater movement, as suggested by the lack of borehole recovery, indicate that while meltwater is present at this depth, its residence time is likely long. In the lower section, evidence of the rapid removal of drill fluid may not indicate faster flushing or a more active flow system, but rather that less drilling fluid entered the lower transmissivity (10^{-7} - 10^{-9} m^2/s) fractures in this section.

3.5.5.3. Leverett Spring

Little is known about the hydrogeology of Leverett Spring. Hydraulic heads observed at DH-GAP04 suggest that artesian conditions, similar to the spring, do exist in the deeper flow system at the ice margin. Open pingos found in similar glacial and cold climate environments in Greenland

have a variety of water sources and flow paths. These include shallow flow and deep circulation and are often related to local geological or geographical phenomena such as fault structures, topography, or bedrock type (Allen et al., 1976; Worsley & Gurney, 1996; Yoshikawa et al., 1996; Gurney, 1998). Numerous geochemical and isotopic parameters presented in this chapter suggest the Leverett Spring waters are a mixture of surface waters and deeper groundwaters, possibly hydrothermal fluids.

3.6. Summary, Conceptual Model and Conclusions

3.6.1. Evolution of Groundwater Salinity

Internal (water-rock interaction, in situ freeze out) and external (cryogenic concentration of seawater) sources of groundwater salinity have been proposed for shield environments. The cryogenic concentration model of salinity production in front of continental ice sheets is not supported by geochemical or isotopic evidence from the GAP. In situ freeze out is also unlikely due to lack of displacement of $\delta^{18}O$ isotopic values from the GMWL and the inverse relationship between $\delta^{18}O$ depletion and Cl^- concentration. However, this conclusion is hard to confirm due to uncertainties introduced by drilling water contamination.

The strong relationship between the isotopic composition ($\delta^{34}S$-$\delta^{18}O_{(SO4)}$ and $^{87}Sr/^{86}Sr$) of fracture-filling gypsum and groundwater suggests that highly soluble fracture- and pore-filling sulfate-bearing minerals are the cause of high sulfate concentrations in the groundwater. Aqueous sulfate found at other Canadian and Fennoscandian Shield locations has also been attributed to water-rock interaction, such as sulfide oxidation, especially where mining has introduced fresh, oxygenated water to depth (e.g., Fritz et al., 1994; Stotler et al., 2009) and enhanced sulfate mineral dissolution (Mungall et al., 1987; Fritz et al., 1994). Because water-rock interaction is responsible

for the high sulfate concentrations in DH-GAP04 and DH-GAP01, it is a site-specific phenomenon and may not directly pertain to processes related to glaciation or permafrost.

3.6.2. Meltwater Infiltration

The development of complex models coupling continental scale glaciations with hydrogeological and hydromechanical processes has seen major advancement over the past decade (Boulton et al., 1995; Bekele et al., 2003; Person et al., 2003; Hoaglund et al., 2004; Flowers et al., 2005; Bense & Person, 2008; Lemieux et al., 2008a; b; Cohen et al., 2009; Normani & Sykes, 2012). Many of the relevant papers are reviewed in Person et al. (2012). These models are generally constrained using groundwater data from areas glaciated during the last glacial maximum (~21 ka) to infer past processes. A great deal of attention has been placed on modeling anomalous porewater pressures and their impact on flow systems in sedimentary basins (Boulton et al., 1993; Piotrowski, 1997; Breemer et al., 2002; Bekele et al., 2003; Hoaglund et al., 2004; Marksamer et al., 2007; Normani & Sykes, 2012), with fewer models for crystalline rock terrains (Boulton et al., 1995; Bense & Person, 2008; Lemieux et al., 2008a; b; Vidstrand et al., 2008). The GAP work is a primary opportunity to provide data from an area of present day continental glaciation in a crystalline rock environment that can be used to compare the results of such large scale models.

Ice sheet hydrogeological models often seek to quantify the depth to which meltwater may have penetrated into the subsurface and this was one of the main objects of the GAP. Depleted $\delta^{18}O$ and $\delta^{2}H$ isotopic signatures in the upper, middle and lower sections of DH-GAP04 indicate that meltwater may penetrate to depths of greater than 570 m into the subsurface in this specific crystalline environment. Horizontal to sub-horizontal fracture sets in DH-GAP04 dip gently to the NW, beneath the ice sheet (Section 1.5), suggesting that the recharge area for this meltwater is likely distant from the borehole. Gypsum fracture fillings influence the geochemistry of recharging

meltwaters. The extensive presence of gypsum in DH-GAP04 below 300 m provides evidence that circulation of meltwaters to depth in DH-GAP04 has been limited.

3.6.3. Conceptual Model

A conceptual model for the geochemical evolution of groundwaters studied for the GAP is depicted in Figure 3.9. The advance and retreat of the ice with corresponding changes in the depth and extent of permafrost and isostatic depression and rebound create a dynamic environment. This conceptual model represents a concept of current conditions and a model for producing the observed geochemical conditions.

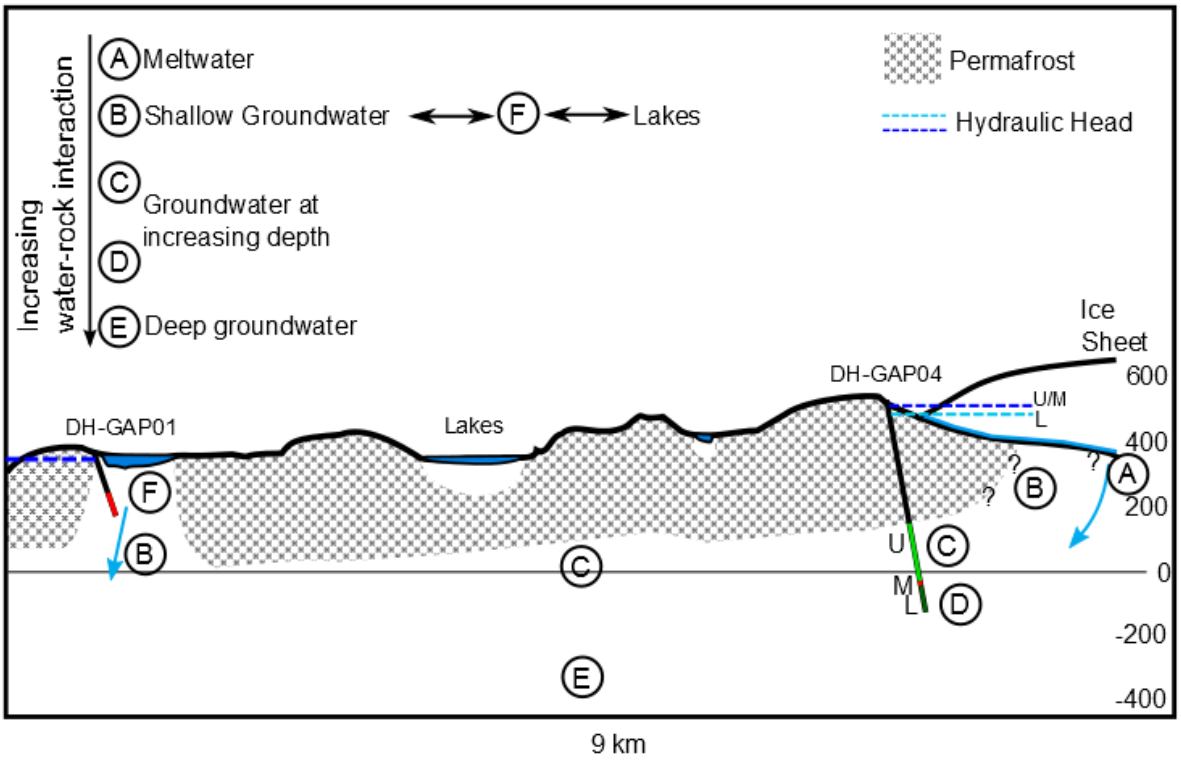

Figure 3.9. Conceptual model of groundwater evolution based on the DH-GAP01 and DH-GAP04 boreholes. Minimum values of hydraulic heads, excluding sampling events, are included. It should also be noted that while the talik at DH-GAP01 is represented as recharging at this time it may have been discharging at other times. Currently discharging taliks may be located further down the flow system and are not represented here. Question marks around subglacial recharge indicate uncertainty in where recharge is occurring beneath the ice sheet.

Meltwater (A) recharges beneath the ice sheet and is characteristically very dilute and depleted in $\delta^{18}O/\delta^{2}H$. Shallow groundwater (B) was not directly measured but, instead, the composition was inferred based on the need for a more dilute groundwater end member to exist between meltwater recharge and the deeper groundwaters observed at DH-GAP04, which are represented as evolving from the upper section to lower section composition (C to D). The evolution of a dilute groundwater end member (B) to the more brackish groundwaters (C and D) is likely a function of both residence time and the presence or absence of soluble mineral phases such as gypsum. A more dilute groundwater end member was also necessary to adequately explain a mixing scenario between groundwater and lake water that accounted for both chloride concentrations and $\delta^{18}O$ values in groundwater from DH-GAP01 (F) (Figure 3.4).

A deep groundwater end member (E) may also exist that is more saline, due to increased water-rock interaction, and less depleted in $\delta^{18}O$, similar to brines found in the Canadian and Fennoscandian Shields (Figure 3.4). Overall, groundwater evolution from meltwater to deep groundwaters involves increasing salinity, including increased Cl^{-}, Ca^{2+} and SO_4^{2-} concentrations with depth. $\delta^{18}O$ becomes more enriched with depth, except where mixing with evaporated surface waters enriches the shallow groundwaters (F). Na/Cl ratios decrease with depth (Figure 3.7). Ca and SO_4^{2-} concentrations, SO_4^{2-} isotopic composition and $^{87}Sr/^{86}Sr$ isotopic ratios are highly affected by dissolution of sulfate-bearing fracture mineral phases (Figures 3.5 & 3.6). The dissolution of soluble fracture infillings was likely impacted by drilling, when large volumes of dilute surface waters were circulated in the boreholes. It is probable that the natural in situ groundwaters are at saturation with respect to gypsum based on the fracture and rock matrix mineralogy (Chapter 4). The saturation of the lower section of DH-GAP04 with respect to gypsum suggests that this is the case. However, at this time the extent of the impact of drilling contamination cannot be easily

quantified. Recovery of the upper and middle sections of DH-GAP04 may yield a better understanding of the Ca^{2+}, Na^{+}, Sr^{2+} and SO_4^{2-} concentrations in the natural groundwater system.

3.6.4. Leverett Spring

Leverett Spring, which is geographically separate from the boreholes (Figure 3.1), bears very little geochemical and isotopic similarity to the groundwaters obtained from the boreholes drilled for the study. Spring waters appear to be influenced by interaction of valley sediments and/or mixing with surface waters and/or meltwaters, based on the radiogenic $^{87}Sr/^{86}Sr$ ratios and $\delta^{37}Cl$ isotopic results that are similar to the marine signature of 0‰ (Eggenkamp, 1994) found in the dilute lakes of the study area. The $\delta^{18}O/\delta^{2}H$ of the spring waters, which plot below the GMWL, may be impacted by an evaporative surface water or deeper, crystalline rock hydrothermal signature.

3.6.5. Key Conclusions

Groundwater geochemical studies provided new information that supported key research objectives of this study and the GAP (Section 1.1), including: the depth of meltwater penetration into the subsurface, the impact of cryogenic processes on groundwater geochemical evolution and the role of taliks in the groundwater system. The Key conclusions arising from the GAP on groundwater chemistry in a glaciated region with extensive permafrost include the following.

1. Borehole groundwaters are isotopically ($\delta^{18}O/\ \delta^{2}H$) similar to glacial meltwaters. The isotopic composition of groundwaters in the GAP study area suggests recharge of glacial meltwater to a depth of at least 570 m. The strong relationship between hydraulic head variations and ice sheet runoff volume (Section 1.5.6, Figure 1.9)(Harper et al., 2015a) further supports the connection between the subglacial meltwater system and the upper and middle sections of DH-GAP04. The actual recharge area for the meltwaters observed in DH-GAP04 is likely distant from the borehole based on the sub-horizontal nature of the

water conducting fractures in the borehole. The lack of tritium in the lower section of DH-GAP04 indicates recharge times are at least greater than 60 years, but likely much longer. The extensive presence of gypsum in fractures (below 300 m borehole length) in DH-GAP04 supports limited recharge or movement of groundwater(meltwater) within the subsurface at this site.

2. Groundwater salinity in borehole DH-GAP04 is mainly derived from the dissolution of fracture gypsum which was likely enhanced by the introduction of dilute drilling water. Overall salinity is low (brackish) and therefore does not support extensive cryogenic concentration of seawater or other fluids. Freeze-out/solute exclusion during permafrost formation was considered unlikely based on isotopic and geochemical evidence ($\delta^{18}O$, Cl^-). Sulfate reducing bacteria do not appear to be active in any groundwaters sampled from the boreholes.
3. Geochemical and hydrogeologic evidence indicated that the talik intersected by DH-GAP01 shows recharge conditions between the lake and talik. Talik groundwaters are a mixture of surface waters and a dilute or shallow groundwater end member rather than the deeper, more brackish groundwater sampled by DH-GAP04. The recharge conditions observed between the Talik Lake and DH-GAP01 as well as the lack of evidence for groundwater discharge into lakes (Chapter 2) suggests that while artesian pressure conditions are observed at the ice margin, extensive groundwater discharge is not occurring into surface water bodies at the forefront of the ice sheet.

4. Water-rock Interaction in the Bedrock Subsurface Adjacent to the Greenland Ice Sheet, Kangerlussuaq, Southwest Greenland

4.1. Introduction

In the Canadian and Fennoscandian Shields, brines (>100 g/L) exist at depths greater than 400 m (Frape et al., 2014) despite repeated glaciations that may provide significant recharge of dilute meltwaters (Smellie & Frape, 1997; Laaksoharju & Rehn, 1999; Lemieux et al., 2008; Stotler et al., 2012). In the Kangerlussuaq Region of southwest Greenland, brines were not found at depths down to 570 m and maximum salinities did not exceed brackish (1 - 10 g/L) by the classification of Davis (1964). Groundwaters were found in the previous chapter to be infiltrating glacial meltwaters heavily impacted by the dissolution of gypsum, which was found as a ubiquitous fracture infilling in one borehole, DH-GAP04, below 300 m borehole length (m BHL) (Chapter 2). This chapter examines the evidence for the impact of cryogenic processes on the geochemistry and isotopic composition of groundwater, rock matrix porewater and fracture mineralogy. It follows the work of Stotler et al. (2012) by exploring the possible impact of in-situ freeze out in an area influenced by modern glaciation and permafrost that has not been impacted by mining activities. Understanding what aspects of the groundwater salinity may be related to cryogenic processes was considered an important objective of this study.

A more in depth examination of the role of water-rock interaction on the geochemical evolution of groundwater can provide additional insight into the geochemistry of the groundwater system and the potential impact of cryogenic processes such as solute exclusion. To understand the groundwater chemistry, a more in depth examination of the rock and fracture mineralogy is

necessary to evaluate the extent of water-rock interaction. Matrix diffusion studies as well as rock leaching experiments are used to further evaluate the potential impact of pore fluids on groundwater systems. Understanding the origin of the gypsum at the GAP research site was also a key research objective and is explored further here to examine any relationship between cryogenic or recent precipitation processes and fracture mineralogy.

Groundwater geochemical studies in crystalline rock are often focused on high TDS (>100 g/L) fluids found at depth in these environments (e.g. Frape et al., 1984; McNutt et al., 1984; Starinsky & Katz, 2003). The composition and evolution of these fluids is still under some debate, with both allochthonous and autochthonous theories proposed in the literature. Salinity that is created within the rock mass (autochthonous) comes from the interaction between water and the rock: dissolution and alteration of minerals, leakage of fluid inclusions and magmatic fluids (Fritz & Frape, 1982; Frape et al., 1984, 2014; McNutt et al., 1990; Négrel & Casanova, 2005). Allochthonous sources involve salinity that is created externally to the crystalline rock mass (e.g. concentrated seawater, basinal brines, dissolution of evaporites) and then transported into the rock mass or modified after emplacement (Herut et al., 1990; Bottomley et al., 1999; Starinsky & Katz, 2003). In cold climate areas, the formation of permafrost has the potential to concentrate existing fluids within the rock by solute exclusion during permafrost aggradation (in-situ freeze-out). Some evidence for solute-exclusion has been found in the Siberian Platform, including increasing TDS with depth, precipitation of secondary minerals and isotopic fractionation of $\delta^{18}O$ and $\delta^{2}H$ (Egorov et al., 1987; Alexeev & Alexeeva, 2002, 2003). However, Stotler et al. (2012) found no conclusive evidence for solute exclusion in crystalline rock environments and were unable to separate the influence of solute exclusion from other processes listed above.

4.2. Methods

Core from the GAP boreholes was logged in detail for lithology, deformation zones, fracturing and fracture filling minerals. The details of the core logging can be found in Pere (2014). After logging, core was collected from the boreholes for matrix pore fluid out diffusion studies, crush and leach experiments, whole rock chemistry and fracture mineral analyses.

A variety of techniques were used to analyze the geochemistry of rocks, fracture minerals and porewaters, primarily from DH-GAP04. These methods are summarized in Table 4.1. Details of the analytical methods can be found in Appendix C and Chapter 1 of this thesis.

Table 4.1. Summary of analyses and methods performed on drill core from DH-GAP01, DH-GAP03 and DH-GAP04. EIL = Environmental Isotope Laboratory at the University of waterloo (UofW), GTK = Geological Survey of Finland. IC = **ion chromatography. ICP-MS = inductively coupled plasma mass spectrometry. ICP-OES = inductively coupled plasma optical emission spectrometry.**

	Type	Analyses	Method	Location
Whole rock analyses	Whole rock chemistry	Major and trace elements	ICP-OES, ICP-MS	ActLabs Inc. (Ancaster)
	Isotopic composition	$^{87}Sr/^{86}Sr$, $\delta^{34}S$ (sulfides)	TIMS, CF-IRMS	EIL
	Mineral separates	$^{87}Sr/^{86}Sr$	TIMS	EIL
	Mineralogy	Mineral components	XRD	UofW
Fracture Minerals	Fracture mineral chemistry	Major and trace elements	ICP-OES, ICP-MS	ActLabs Inc. (Ancaster)
	Isotopic composition	$^{87}Sr/^{86}Sr$, $\delta^{34}S$ (SO_4), $\delta^{18}O$ (SO_4)	TIMS, IRMS	EIL
	Dissolve gypsum chemistry	Major elements	ICP-OES, ICP-MS	ActLabs Inc. (ancaster)
	Mineralogy	Mineral components	XRD	GTK
Matrix Porewaters	Out diffusion and GAP04-E to -H crush and leach chemistry	Major and trace elements	High resolution ICP-MS, ICP-OES	ActLabs Inc. (Ancaster)
	DH-GAP01/03 crush and leach chemistry	Major and trace elements	IC, ICP-MS, ICP-OES, titration	Labtium Oy (Finland)
	DH-GAP04 crush and leach	Major elements	IC, ICP-MS	York Durham Laboratory
	Isotopic analyses	$^{87}Sr/^{86}Sr$, $\delta^{34}S$ (SO_4), $\delta^{18}O$ (SO_4), $\delta^{37}Cl$, $\delta^{81}Br$	TIMS, IRMS, CF-IRMS	EIL

4.3. Results

The data presented here represent the key results of this study. The full geochemical datasets can be found in Appendix B.

4.3.1. Rock Matrix: Chemical and Isotopic Composition and Mineralogy

The lithology of the host rock found in the DH-GAP04 borehole varies from mafic rocks in the upper 300 m BHL to intermediate and felsic gneisses below 300 m BHL (Figure 4.1). The DH-GAP01 borehole is predominantly felsic gneiss while the DH-GAP03 borehole is composed of felsic and mafic gneiss with a lesser amount of intermediate gneiss (Figure 4.1).

4.3.1.1 Major elements

Major element whole rock chemistry can be found in Appendix B and is summarized in Table 4.4. The average composition for each rock type (mafic, intermediate and felsic gneiss) are typical

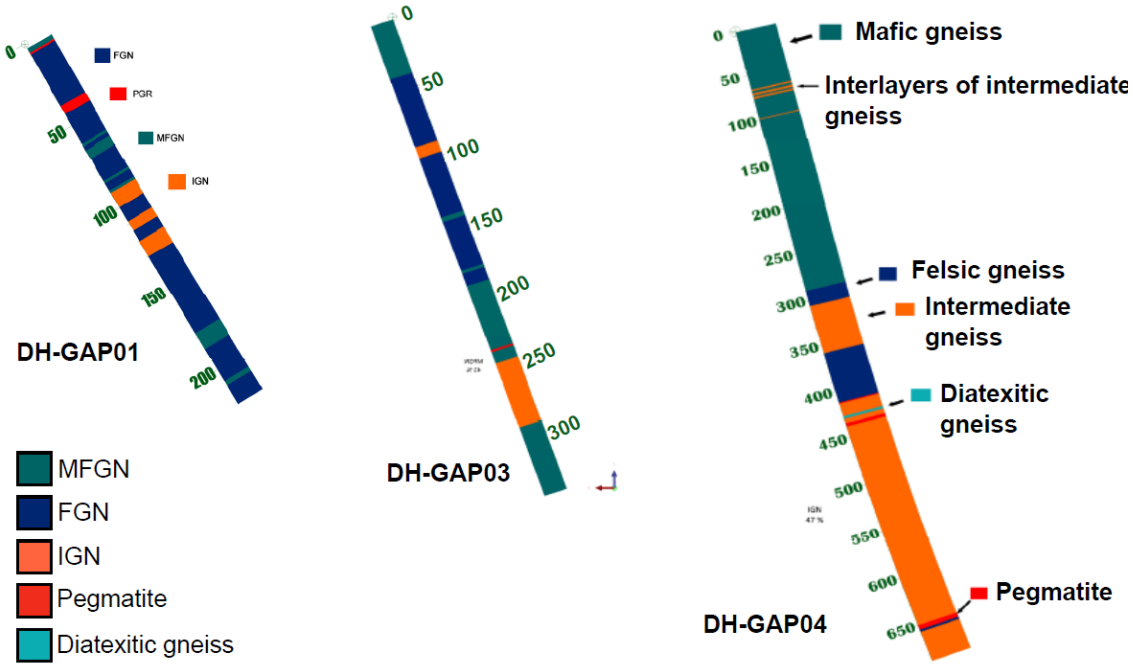

Figure 4.1. Lithological composition of DH-GAP01, DH-GAP03 and DH-GAP04 boreholes. Adapted from Pere (2015). Boreholes are represented on their respective drilling angles.

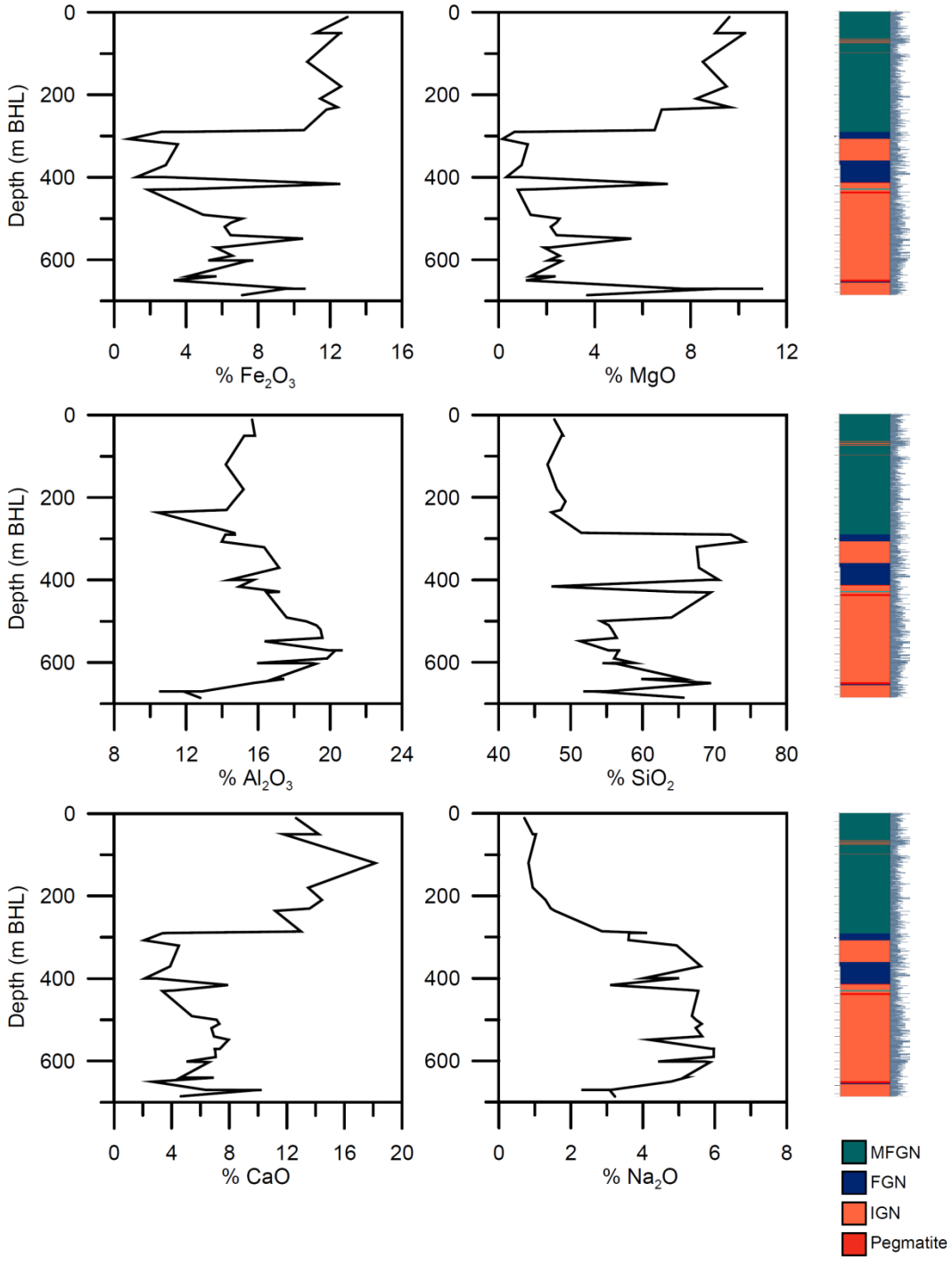

Figure 4.2. Chemical composition of the rock with depth in the DH-GAP04 borehole with the borehole log for comparison. MFGN = mafic garnet bearing gneiss, FGH = felsic gneiss, IGN = intermediate gneiss. Fracture frequency is shown along the right side of the borehole log.

for the chemistry of these rock types given for crystalline rock environments (Hyndman, 1985; Frape et al., 2014). Transitions between rock types were often gradational and this can be observed in the rock chemistry. For example, the transition from mafic to felsic gneissic compositions between 200 and 300 m BHL (Figures 4.1 & 4.2). However, often significant changes in the rock chemistry exist (Figure 4.2) that correspond to locations in the core where visible layering occurs. For example, at approximately 416 m BHL there is a sharp increase in the % Fe_2O_3, MgO, CaO and TiO_2 associated with recrystallized biotite found in narrow, cohesively brecciated sections (Figure 4.2). Pere (2014) suggests that these recrystallized sections may have formed in the time period between the original layering and metamorphism (>2.5 Ga).

Table 4.2. Average chemical compositions for each major rock type in DH-GAP04. MFGN = mafic garnet bearing gneiss. FGN = felsic gneiss. IGN = intermediate gneiss. Fe_2O_3 represents total iron. Chemistry of mafic, intermediate and felsic rock types from crystalline rock environments from Frape et al. (2014)(adapted from Hyndman, 1985) is given for comparison.

		GAP			Frape et al (2014)		
		MFGN	IGN	FGN	Mafic	Inter.	Felsic
n		11	23	4	1451	872	2485
SiO_2	%	50.6	58.3	70.0	51	59	72
Al_2O_3	%	14.4	17.0	15.4	15.9	17.0	14.4
Fe_2O_3 (T)	%	11.2	6.6	2.4	10.8	7.7	2.9
MnO	%	0.2	0.1	0.0	0.12	0.12	0.05
MgO	%	8.0	3.3	0.7	7.7	3.7	0.7
CaO	%	12.4	6.4	3.1	9.9	6.7	1.8
Na_2O	%	1.6	4.8	4.6	2.5	3.6	3.7
K_2O	%	0.3	1.3	2.4	1.0	1.8	4.1
TiO_2	%	0.5	0.7	0.2	1.2	1.0	0.3

4.3.1.1 Trace Elements

Whole rock rare earth element patterns are typical for the rock types with steeply dipping, light rare earth element (LREE) enriched patterns in the intermediate and felsic gneiss and flat to slightly heavy rare earth element (HREE) enriched mafic profiles (Figure 4.3). The more HREE enriched

mafic rare earth element (REE) profiles reflect a gradual transition from mafic to intermediate and felsic gneisses from 200 to 300 m BHL (Figure 4.4). The transition from mafic to felsic gneiss below 200 m BHL is also characterized by increasing $\%Na_2O$ and deceasing %MgO and CaO (Figure 4.2).

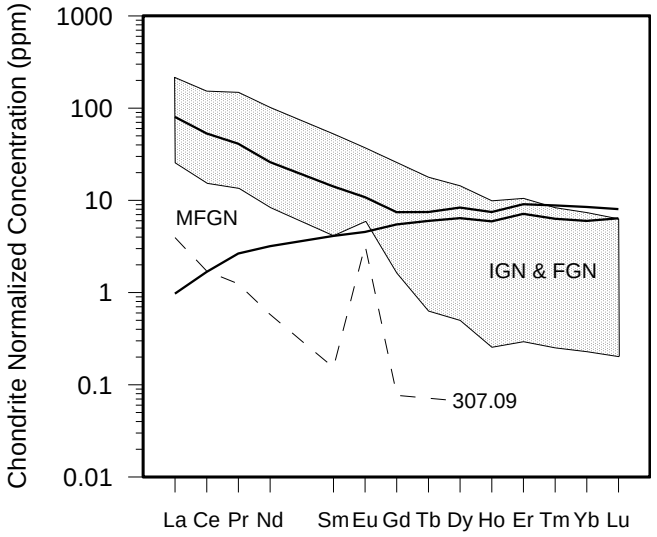

Figure 4.3. Chondrite normalized REE composition of DH-GAP04 rock matrix. The stippled area represents the range of intermediate and felsic gneiss composition. The area described by the two dark lines represents the range of mafic gneiss compositions. An intermediate gneiss outlier is also depicted (DH-GAP04 307.09 m).

Mafic and intermediate rocks sampled in DH-GAP04 had no or slightly negative Eu anomalies while felsic rocks and a small subset of intermediate rocks had positive Eu anomalies (Figure 4.4). The positive Eu anomalies are likely due to influence of feldspar, which usually has a strong positive Eu anomaly (e.g. Landström and Tullborg, 1990; Schnetzler and Philpotts, 1970). Consistently negative Ce anomalies suggest that an oxidizing fluid, at the time of crystallization or in subsequent alteration events, has not impacted the bulk rock matrix. .

Between approximately 400 and 625 m BHL depth in DH-GAP04, the intermediate gneissic rock becomes more massive and visible layering disappears. This section is characterized by little

variation in chemical composition (Figure 4.2). The upper, middle and most of the low water sampling sections in DH-GAP04 are located within this massive intermediate gneiss.

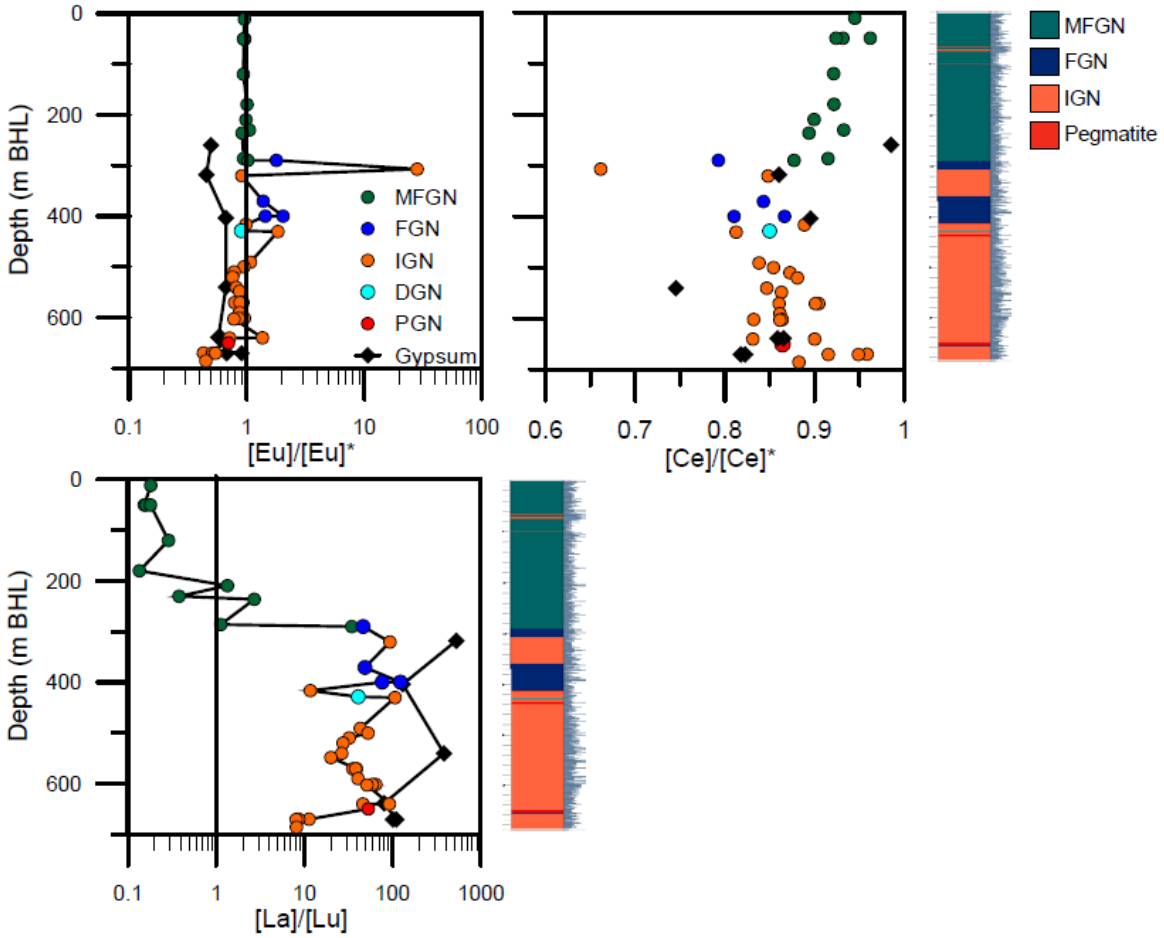

Figure 4.4. Eu and Ce anomalies and La/Lu with depth for rock matrix (coded by rock type) and fracture gypsum. MFGN = mafic garnet bearing gneiss, FGH = felsic gneiss, IGN = intermediate gneiss. Fracture frequency is shown along the right side of the borehole log.

4.3.1.2 Mineralogical Investigations

X-Ray diffraction analysis of the rock matrix is summarized in Table 4.3 and the XRD patterns are included in Appendix D. In general, DH-GAP04 mafic rocks are composed of anorthite, ferroactinolite, quartz and biotite. Intermediate and felsic gneissic samples are composed predominantly of albite and quartz with ferroactinolite, actinolite and biotite. Calcite and gypsum were also present in the matrix mineralogy of some intermediate gneissic samples. Two samples of

altered wall rock both showed similar compositions predominantly containing albite and quartz with minor calcite.

Table 4.3. Mineralogical composition of selected samples representative of the rock types found in borehole DH-GAP04 based on XRD results. MFGN = mafic garnet bearing gneiss, FGN = felsic gneiss, IGN = intermediate gneiss and AWR = altered wall rock from the wall of a fracture located at the given depth. MGN = non-garnet bearing mafic gneiss.

Sample	Composition	Comments
289.76 (MFGN)	Anorthite, quartz	
377.65 (FGN)	Quartz, albite, ferroactinolite, biotite	
399.84 (IGN)	Albite, quartz	Biotite visually observed.
557.40 (IGN)	Albite, quartz, ferroactinolite	
570.07 (AWR)	Albite, quartz, calcite ($Mg_{0.01}Ca_{0.9}$)	
570.59 (IGN)	Albite, actinolite, calcite, gypsum	
638.85 (AWR)	Albite, quartz, calcite ($Mg_{0.03}$, $Ca_{0.97}$)	
670.20 (MGN)	Anorthite, ferroactinolite, quartz, biotite	Mafic layers in intermediate section

In a parallel study, Eichinger and Waber (2013) performed mineralogical investigations on four core samples from DH-GAP04, including SEM and transmitted and reflected light microscopy analyses of thin sections. As well, a fluorescent resin (NHC-9) was used to impregnate core fragments in order to visualize pore space. Methodology and comprehensive results can be found in Eichinger and Waber (2013). A brief summary of results, that pertain to and will be used in this thesis, is given below.

A summary of the mineralogical composition of the 4 sections of DH-GAP04 core used by Eichinger and Waber (2013) is given in Table 4.4. Gypsum ($Ca_2SO_4 \bullet 2H_2O$) was found to occur in all 4 of the core sections tested and Eichinger and Waber (2013) believed it to be hydrothermal in origin based on lithological evidence. Gypsum occurred dispersed within the rock matrix (Figure 4.5a-d) and in microfractures (Figure 4.5e-g). Often gypsum occurs together with celestine ($SrSO_4$) (Figure 4.5b). Gypsum occurs as very fine-grained to fine-grained rounded crystals. Opaque ore minerals are primarily composed of iron oxides and iron sulfides (Figure 4.5c). These mineral groups are often associated with amphiboles. Fine grained pyrite (FeS_2) may also occur with gypsum.

Biotite mineralization in the matrix was found to be weakly chloritized. Biotite was more likely to be strongly chloritized in the vicinity of fractures.

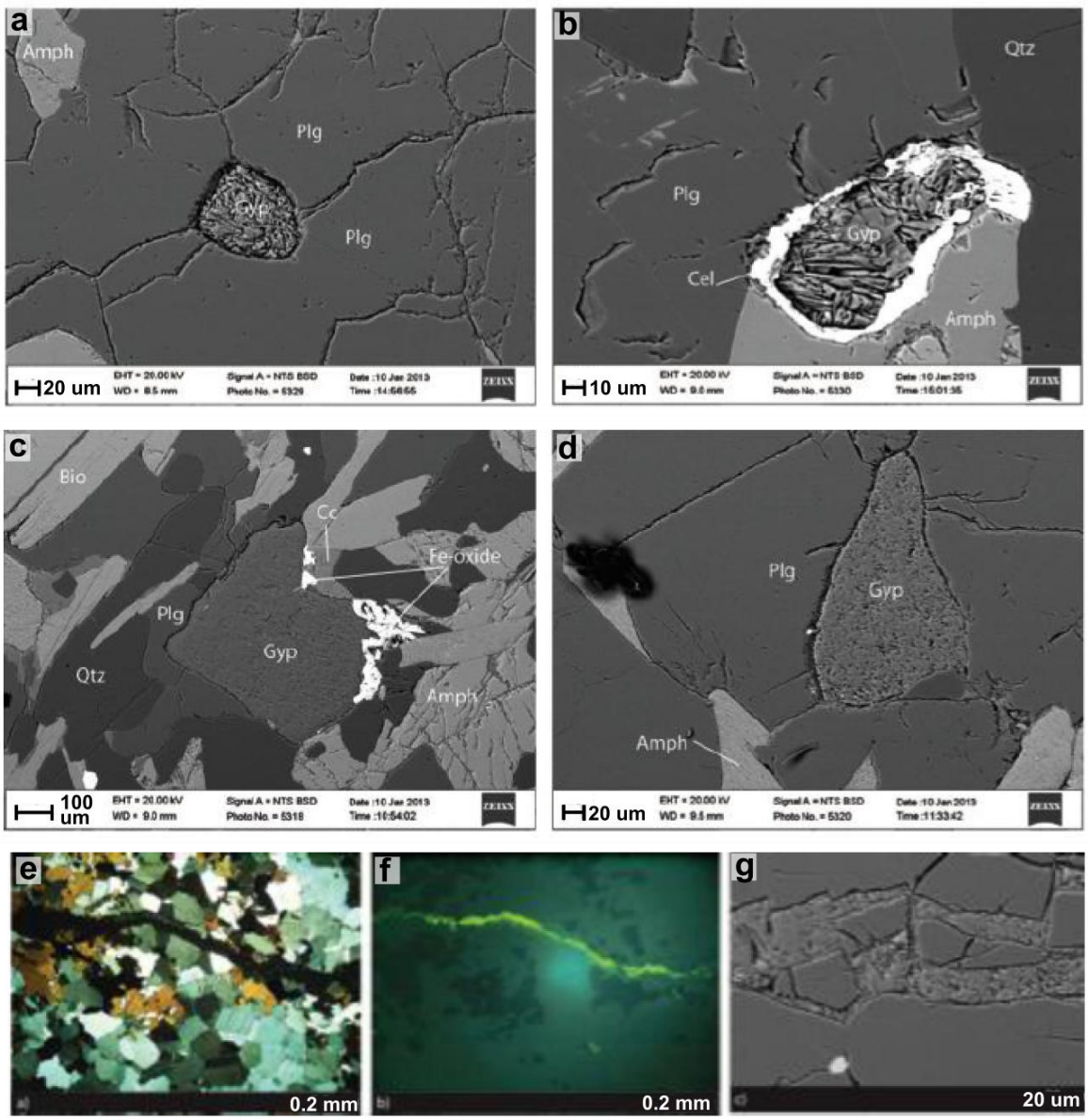

Figure 4.5. A selection of images from Eichinger and Waber (2013) shows the presence of gypsum in pore space and microfractures within the rock matrix. (a) GAP04-1 501.5 m BHL Intermediate gneiss SEM image showing dispersed gypsum in the rock matrix and (b) accompanied by celestite. (c) GAP04-2 651.9 m BHL Intermediate gneiss SEM image showing dispersed gypsum in the rock matrix with associated Fe-oxides and calcite and (d) surrounded by plagioclase. A gypsum filled microfracture in the rock matrix of GAP04-3 557.7 m BHL Intermediate gneiss is shown (e) under cross-polarized, transmitted light (f) impregnated with water-based, fluorescent resin under UV-light NHC-9 and (g) by SEM.

Table 4.4. Summary of whole rock mineralogy adapted from Eichinger and Waber (2013).

Section	Composition
GAP04-1 501.5 m BHL - IGN	Plagioclase, quartz, amphibole, biotite, opaque ore minerals and gypsum with minor smectite and apatite.
GAP04-2 651.9 m BHL - IGN	Plagioclase, quartz, amphibole, biotite, minor opaque minerals, alteration products (smectite, chlorite) and gypsum.
GAP04-3 557.7 m BHL - IGN	Plagioclase, quartz, amphibole, opaque ore minerals and biotite with minor gypsum and amphibole alteration products (smectite and chlorite). Accessory minerals include celestine, zircon, florencite, synchysite, allanite, lanthanite, calcite, rutile, apatite and muscovite.
GAP04-4 607.7 FGN	Quartz, plagioclase, K-felspar, minor opaque ore minerals, biotite, amphibole, gypsum, muscovite and apatite. Accessory minerals include zircon, lanthanite, rutile and celestine.

4.3.1.3 Isotopic Results

Rock matrix and mineral samples from DH-GAP01, DH-GAP03 and DH-GAP04 were analyzed for the $^{87}Sr/^{86}Sr$ isotopic ratio (Table 4.5). Whole rock $^{87}Sr/^{86}Sr$ ratios in DH-GAP04 varied from 0.7015 to 0.7220. Mineral separate $^{87}Sr/^{86}Sr$ isotopic ratios indicate biotite is the most radiogenic (>0.84) and plagioclase feldspar the least radiogenic (<0.72806). At 377.65 m BHL, the whole rock $^{87}Sr/^{86}Sr$ isotopic ratio (0.70371) is lower than the strontium isotopic ratio measured in plagioclase feldspar (0.70524). It may be that the handpicked plagioclase grains were not fully representative of the plagioclase signature.

Samples of sulfide minerals (predominantly pyrite and chalcopyrite) were hand separated from sections of DH-GAP04 core and analyzed for $\delta^{34}S$. Sulfide $\delta^{34}S$ (n = 3) ranged from 2.26 to 3.73 ‰ CDT.

Table 4.5. $^{87}Sr/^{86}Sr$ isotopic signatures for whole rock and mineral separates from GAP boreholes (DH-GAP01, DH-GAP03 and DH-GAP04). MFGN = mafic garnet bearing gneiss. FGN = felsic gneiss. IGN = intermediate gneiss. AR = altered wall rock. MGN = mafic gneiss, non-garnet bearing. FF = Fracture Filling. The whole rock and mineral separate $^{87}Sr/^{86}Sr$ isotopic data for DH-GAP01 and DH-GAP03 is provided for comparison from Makahnouk (unpublished).

Borehole	Depth m BHL	Rock Type	Whole Rock	Biotite	Amphiboles $^{87}Sr/^{86}Sr$	Plagioclase	K-Feldspar
DH-GAP01	74.25	FGN	0.74114	1.62802		0.72806	0.73347
	191.41	IGN	0.71175	1.62359		0.70648	
DH-GAP03	28.54	MFGN	0.71018	2.0198	0.70981	0.70638	
	208.71	IGN	0.70364	0.79054	0.71723	0.70338	
DH-GAP04	289.76	MFGN	0.709845	1.27906	0.71136	0.70524	
	377.65	FGN	0.703671	0.84835	0.71030	0.70407	
	399.84	FGN	0.709951	0.93281		0.70607	
	403.81	FF		0.84020			
	557.4	IGN	0.701512				
	570.07	AR	0.703863				
	570.59	IGN	0.70174		0.70917	0.70152	
	638	AR	0.701961				
	670.2	MGN	0.721955	1.10777	0.80345	0.70860	

4.3.2. Fracture Mineral Observations, Chemistry and Isotopic Composition

The mineralogical composition of fracture infillings varied between the three drilling locations but had some common features. The most commonly observed fracture filling minerals were calcite, chlorite, gypsum and clays. Table 4.6 summarizes the types of fracture filling minerals found in the boreholes DH-GAP01, DH-GAP03 and DH-GAP04. Detailed logging of fractures and fracture infillings in the GAP drill cores can be found in Pere (2014). The present study focuses mainly on the fracture filling gypsum (Figure 4.6), in particular the potential for this mineral to have a cryogenic or recent low temperature origin. Studies of the fracture calcite are ongoing and will be presented in the PhD thesis of Michael Makahnouk.

Table 4.6. Summary of the occurrence of fracture infilling minerals in the GAP boreholes. Data from *Pere, 2014*. n = number of fractures.

Borehole	Calcite	Gypsum	Chlorite	Unspecified Clays	Other
DH-GAP01 n= 496	286 (57.7%)	1 (<1 %)	233 (46.9%)	169 (34.1%)	Kaolinite (108), muscovite, pyrite, illite, biotite, epidote, quartz, feldspar and hematite
DH-GAP03 n = 878	522 (59.5%)	-	476 (54.2%)	212 (24.2%)	Iron hydroxides (74), pyrite, chalcopyrite, kaolinite, illite, biotite, epidote, quartz and hematite
DH-GAP04 n = 1353	623 (46%)	460 (34 %)	759 (56%)	175 (13 %)	Pyrite, pyrrhotite, chalcopyrite, kaolinite, illite, biotite, epidote, quartz and hematite

While calcite was found as a fracture filling throughout all three GAP drill cores, gypsum was found almost exclusively in the DH-GAP04. Gypsum was found primarily after 300 meters of borehole length, which is above the present permafrost boundary and corresponds to the transition from mafic to intermediate gneiss. X-Ray diffraction patterns indicate gypsum is the primary fracture filling below 300 m BHL and may occur along with calcite. Minor amounts of biotite, talc, quartz, amphibole and clay minerals also occur in some fracture fillings (Table 4.7). There is no indication that gypsum was previously extensive in the upper, mafic section of DH-GAP04 and was dissolved away by flowing water (for example, by observing open or porous fractures). Saturation indices calculated using the porewater concentrations from the crush and leach experiments indicate that matrix porewaters are likely at equilibrium with gypsum throughout the DH-GAP04 core. However, the lower concentrations of SO_4^{2-} found in the crush and leach derived porewaters from DH-GAP01, DH-GAP03 and above 300 m BHL in DH-GAP04 suggests gypsum is also less pervasive in the rock matrix above this depth (see Section 4.3.3.).

Gypsum was often found growing as fibrous crystals across fractures (Figure 4.6c-e) or as more tabular crystals (Figure 4.6a). In some fractures, silicate minerals, usually biotite (likely highly chloritized), are embedded in gypsum and/or calcite (Figure 4.6b-c). In the mafic sections of the DH-

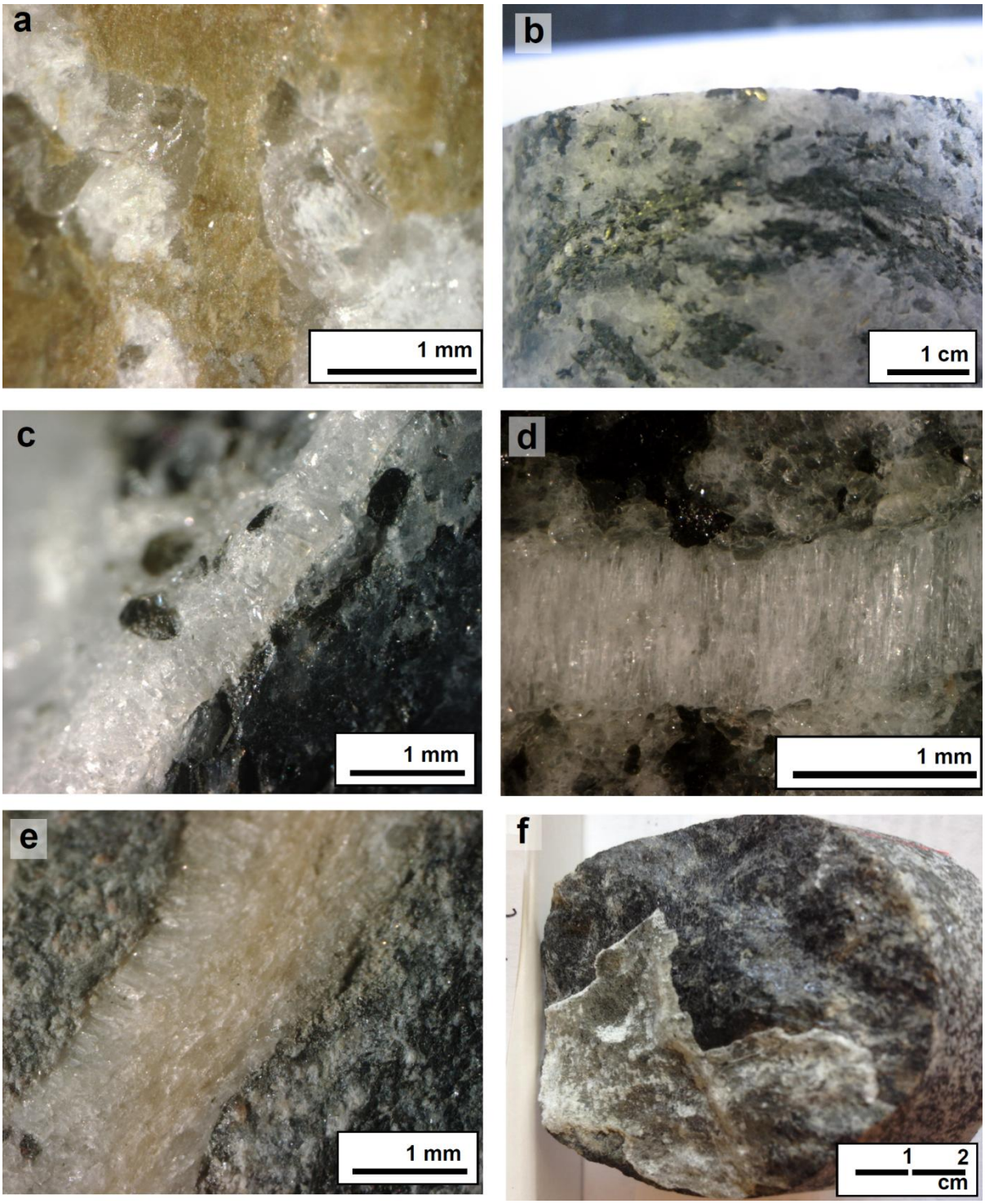

Figure 4.6. A selection of photographs of fracture infillings in DH-GAP01. (a) 259.60 m BHL gypsum and calcite with a thin coating of chlorite. (b) 403.81 m BHL sealed fracture containing gypsum with seams of recrystallized biotite. (c) 417.9 m BHL gypsum with embedded biotite flakes. (d) 556.6 m BHL gypsum crystals growing perpendicular to fracture. (e) 570.0 m BHL pink tinged gypsum running through the center of a gypsum filled fracture. (f) 670.57 m BHL gypsum infilling over chlorite.

GAP04 core, trace amounts of sulfide minerals occurred. Gypsum may occur on its own or with calcite and frequently occurs with very dark chlorite mineralization (Figure 4.6f). Chlorite is the most common fracture mineral found in the DH-GAP04 core. Gypsum is also found within the rock matrix and microfractures adjacent to the gypsum filled fractures (Figure 4.5e-g).. In some cases, fragments of the host rock appear to have separated from the fracture wall and are embedded within the fracture infilling (Figure 4.6e).

Redox studies for the GAP were carried out by Terralogica AB, Linnaeus University and University of Helsinki. The results of this study are reported in Harper et al. (2015a) and are summarized in Section 3.5.2.

Table 4.7. Fracture Filling XRD results for fracture filling mineral samples from a selection of DH-GAP04 fracture depths. The mixed clay mineral is likely a chlorite-vermiculite type mineral.

Length along Core (m BHL)	Major Components	Minor Components
67.95	Calcite and quartz	
259.60	Calcite, gypsum, talc and mixed clay mineral	
345.42	Gypsum	Quartz
416.70	Gypsum, Biotite	Amphibole
525.66	Gypsum	
675.48	Gypsum, Calcite, Quartz	

4.3.2.1 Chemical and Isotopic Composition of Gypsum

Fracture filling gypsums varied somewhat in their $\delta^{34}S/\delta^{18}O$ (SO_4) signature. $\delta^{34}S$ (SO_4) ranged from 2.6 to 6.8 ‰ and $\delta^{18}O$ (SO_4) ranged from 4.48 to 9.09 ‰. The $^{87}Sr/^{86}Sr$ ratio of the gypsum ranged from 0.70217 to 0.70932 (Table 4.8). A sample of biotite which occurred as flakes embedded into a fracture dominated by gypsum at 403.81 m BHL was found to have a highly radiogenic $^{87}Sr/^{86}Sr$ isotopic ratio of 0.84020 (Table 4.5).

Major and trace element chemistry for fracture gypsum samples can be found in Appendix B. Na^+ (as Na_2O) was found to make up <0.5 % of the analyzed fracture material. Gypsum had steep, LREE enriched REE patterns with negative Eu anomalies, similar to the intermediate gneiss in DH-GAP04 (Figures 4.4 & 4.7).

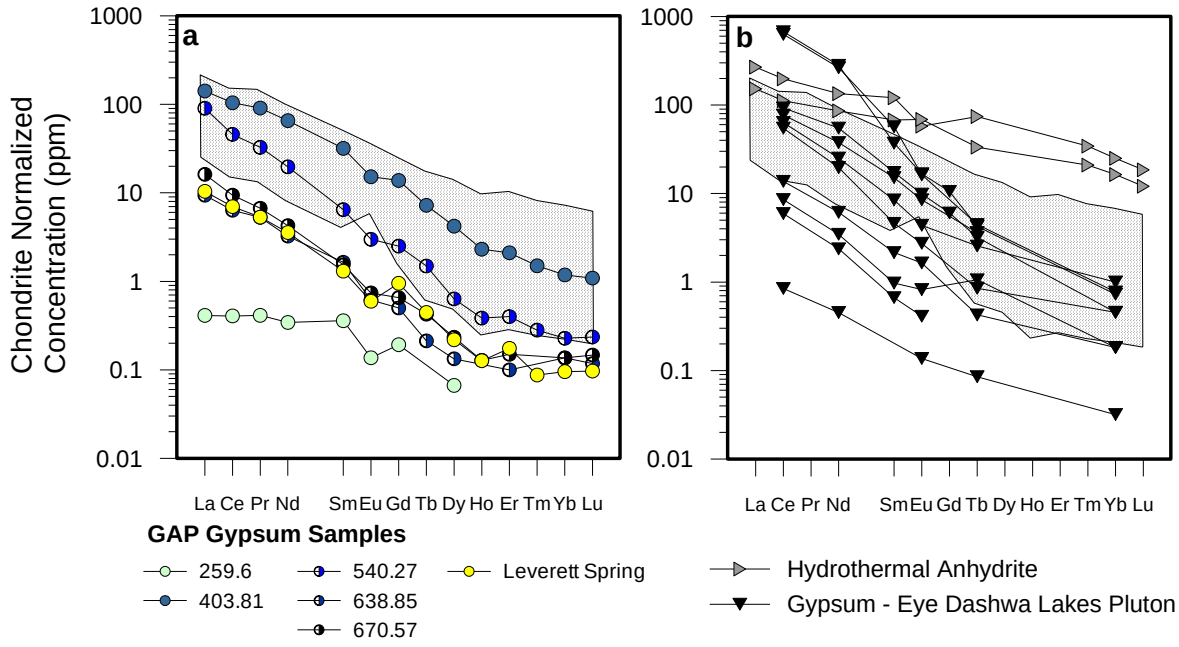

Figure 4.7. (a) Chondrite normalized REE profiles of DH-GAP04 fracture gypsum. The stippled area represents the range of REE compositions for intermediate and felsic gneisses. Groundwater from Leverett Spring is included here based on its similarity to the gypsum REE profiles. (b) Chondrite normalized REE profiles for hydrothermal anhyrite samples (Morgan & Wandless, 1980) and gypsum from the Eye Dashwa Lakes pluton (Mungall et al., 1987).

Six samples of gypsum fracture infillings from DH-GAP04 were dissolved in ultrapure water (Section C.2.1). The dissolved fracture fillings indicate that Cl^- concentrations in the readily dissolvable components of the fracture fillings (predominantly gypsum) increase slightly with depth from 3.1×10^{-3} to 1.5×10^{-2} mmol Cl^-/mmol gypsum dissolved (Table 4.9). Two samples with the highest chloride concentrations were further analyzed for $\delta^{37}Cl$ of the dissolved chloride (Table 4.9).

Table 4.8. Isotopic composition for $\delta^{34}S$, $\delta^{18}O$ and $^{87}Sr/^{86}Sr$ of fracture filling gypsum from DH-GAP01 and DH-GAP04.

Borehole	Depth	$\delta^{18}O$ (SO_4) ‰ VSMOW	$\delta^{34}S$ (SO_4) ‰ CDT	$^{87}Sr/^{86}Sr$	Lithology
DH-GAP01: gypsum	168.4		2.63		
	168.4		4.90		
	168.4			0.7075	
DH-GAP04: gypsum	67.95	NES	6.45		MFGN
	142.97	9.09	5.41	0.70735	MFGN
	259.6	8.06	3.79	0.70803	MFGN
	259.6		3.87		MFGN
	318.21	7.22	6.10	0.70443	IGN
	318.21	5.74	10.65		IGN
	334.91		6.21		IGN
	334.91		5.85		IGN
	345.38		6.20		IGN
	345.42		5.63		IGN
	394.23		4.05		FGN
	403.81			0.70932	FGN
	417.93		4.02		IGN
	479.91	5.18	5.97	0.70332	IGN
	479.91	6.12	6.25	0.70304	IGN
	483.55		5.44		IGN
	483.55		5.68		IGN
	525.66		5.90		IGN
	540.27	5.97	8.57	0.70217	IGN
	553.11		6.10		IGN
	553.11		6.17		IGN
	556.62	6.76	6.72	0.70248	IGN
	556.62	5.52	6.46	0.70228	IGN
	556.62		6.78		IGN
	570.07	4.48	5.69	0.70262	IGN
	570.07	6.27	5.84	0.70264	IGN
	570.07	6.09	5.47	0.70277	IGN
	637.07	NES	5.87		IGN
	638.85	6.52	6.22	0.70472	IGN
	652.59	6.93	3.22	0.70721	PGR/MFGN
	670.57	5.98	4.89	0.70672	MFGN

Table 4.9. Major cation and anion concentrations in fracture filling mineral samples dissolved in ultrapure water expressed per mg of dissolved solid material. The major mineral dissolved was gypsum.

Borehole	Length Along Core	Diss-olved Mass	Ca	K	Mg	Na	Cl	SO4	Cl/mmol gypsum	δ^{37}Cl	
	mbgs	mg	mg/mg-solid	mg/mg-solid	mg/mg-solid	mg/mg-solid	mg/mg-solid	mg/mg-solid	mmol/ mmol	SMOC Result	± 0.1‰ Stdv
DH-GAP04	217.57	61	3.6	3.6E-02	5.7E-02	2.4E-01		10.9			
	318.21	96	5.3	2.9E-03	1.6E-03	4.4E-03		14.3			
	370.43	114	2.7	6.7E-03	4.6E-03	8.7E-03	1.5E-02	13.2	3.1E-03		
	417.93	96	5.2	3.4E-02	9.0E-04	4.3E-03	1.3E-02	13.1	2.7E-03		
	556.62	110	4.8	1.6E-03	7.0E-04	2.9E-03	5.2E-02	13.1	1.1E-02	-0.09	0.04
	638.85	105	4.4	1.2E-03	3.2E-03	4.2E-03	7.2E-02	12.9	1.5E-02	0.30	0.08

4.3.3. Matrix Porewater Composition

4.3.3.1 DH-GAP04 Out diffusion

University of Bern Out Diffusion Experiments

Out diffusion experiments on four sections of DH-GAP04 core were carried out by Eichinger and Waber (2013). The out diffusion experiments performed by Eichinger and Waber (2013) were undertaken to demonstrate the out diffusion experimental process to the Nuclear Waste Management Organization of Canada. The report provides very detailed documentation on the out diffusion methodology. A brief summary of results is presented below followed by the results from the out diffusion experiments conducted in parallel at the University of Waterloo.

Chloride concentrations had reached equilibrium around 100 days into the out diffusion experiment for samples GAP04-1 and GAP04-2. Samples GAP04-3 and GAP04-4 equilibrated over a longer time period but had reached stable chloride concentrations at 200-250 days and 180-200 days respectively. Cl^- and Br^- were found to be the only ions that behaved conservatively during the experiments. Ca^{2+} and SO_4^{2-} are affected by rapid dissolution of gypsum causing the test solutions to quickly reach equilibrium with gypsum as well as calcite due to the common ion (Ca^{2+}). Precipitation

of calcite controls the Ca^{+2} concentrations during the experiments in all sections except the felsic gneiss (GAP04-4). In GAP04-1 and -3, calcite equilibrium was attained after only two weeks.

Final eluate solutions in the intermediate gneiss samples GAP04-1 to -3) were of Ca-Na-SO_4 type while the felsic gneiss (GAP04-4) was of Na-Ca-SO_4-HCO_3 type. Intermediate gneiss samples produced higher salinities (2347 - 2929 mg/L) in the final eluate solutions when compared to the felsic gneiss (403 mg/L). Final eluate solutions of the intermediate gneiss samples were at equilibrium with respect to gypsum while the felsic gneiss sample was undersaturated. All samples were undersaturated with respect to celesite ($SrSO_4$) as well as other secondary minerals such as mirabilite ($Na_2SO_4 \bullet 10H_2O$), brucite ($Mg(OH)_2$) or epsomite ($MgSO_4 \bullet 7H_2O$) (Eichinger and Waber, 2013). Chemistry of the final eluate solutions from GAP04-1 to -4 can be found in Appendix C Table C-9.

Due to the non-conservative nature of ions aside from Cl^- and Br^-, porewater concentrations were only determined for Cl^- and Br^-. Concentrations ranged from 960 to 2200 mg/kg_{H2O} and increased with depth in the borehole (Eichinger & Waber, 2013) (Table 4.10).

Table 4.10. Summary of calculated porewater Cl^- and Br^- concentrations in 4 sections of DH-GAP04 core (Eichinger and Waber, 2013).

Sample	Depth mbhl	Depth mbs	Lithology	Cl_{PW} mg/Kg_{H2O}	Error Cl_{PW} mg/Kg_{H2O}	Br_{PW} mg/Kg_{H2O}	Error Br_{PW} mg/Kg_{H2O}	Br*1000/Cl (mg/mg)
GAP04-1	501.5	473.4	IGN	980	200	-		
GAP04-2	651.9	572.8	IGN	1740	420	-		
GAP04-3	557.7	526.5	IGN	960	220	-		
GAP04-4	607.7	615.5	FGN	2200	480	12.8	2.8	5.8±1.8

University of Waterloo Out Diffusion Experiments

Two sets of out diffusion experiments were performed at the University of Waterloo: GAP04-A to -D and GAP04-E to -H. Out diffusion experiments on samples GAP A - GAP D were performed on core that had not been preserved at the borehole as a preliminary test of the method. Further discussion of the methodology and limitations of these experiments can be found in Appendix C. Major element chemistry for the eluate from GAP04-A - GAP D is included in Table 4.11 and trace elements in Appendix B. Due to experimental limitations, such as porewater evaporation, discussion of results from experiments GAP A - GAP D are limited to isotopic results, which can be considered representative.

Out diffusion experiments GAP04-E to -H were performed on core preserved at the DH-GAP04 drill site. Details on methodology, issues encountered and calculations can be found in Appendix C (Section C.3.2.1). Porewater concentrations of Cl^- were calculated for GAP04-E to -H following the methods in Section C.3.2.5. Due to the non-quantifiable dilution caused by leaking cells in the University of Waterloo experiments GAP04-E to -H, porewater Cl^- concentrations should be considered minimum values with an estimated error of 30%. Uncorrected chemistry results (i.e. not corrected to porewater concentrations) are presented for major elements in Table 4.11 and for trace elements in Appendix B. In general, ion ratios (which should be relatively unaffected by dilution) and Cl^- concentrations were similar to those observed in the crush and leach analyses on the same core at the end of the out diffusion experiments (Table 4.11).

Table 4.11. Major element chemistry of the final eluate solution from out diffusion experiments and crush and leach analyses on core previously used for GAP04-E to -H out diffusion experiments. The results from GAP04-A to -D are presented here but due to the limitations of these preliminary experiments on un-preserved core, the geochemical results from these experiments are not used in the results or discussion (see Appendix C). Results from the out diffusion experiments performed by Eichinger and Waber (2013) can be found in Appendix C. C.B.E. stands for charge balance error. Some results exceeded the maximum measurable concentration (>100 mg/L) for the method of analysis (see Section C.3.3).

Sample	Depth	Na	Mg	Ca	K	Sr	Cl	Br	SO4	Alkalinity	C.B.E.	Na/Cl	Br/Cl	Ca/SO4
	m	mg/L	mg/L	mg/L	mg/L	µg/L	mg/L	mg/L	mg/L	mg/L as CaCO3	%	meq/meq		
GAP04-A	209.83	87	0.9	<7	0.7	27	2.7	< 0.03	30			50		
GAP04-B	352.00	27	4	35	7	233	6.8	< 0.03	37			6		2.3
GAP04-C	570.32	29	14	746	9	4938	7.3	< 0.3	2800			6		0.6
GAP04-D	670.20	15	4	337	16	1754	1.5	< 0.1	1490			15		0.5
GAP04-E	377.65	47	10	242	20	1248	12.0	< 0.1	564	99	4.8	6		1.0
GAP04-F	448.07	52	6	84	9	668	16.5	0.24	167	116	6.7	5	0.006	1.2
GAP04-G	557.40	59	40	662	10	6720	2.6	< 0.1	1554	98	6.4	35		1.0
GAP04-H	681.21	30	7	46	16	105	4.6	<0.03	16	138		10		6.9
GAP04 E-CL	377.65	>100	9	139	70	548	44.6	< 0.1	460					0.7
GAP04 F-CL	448.07	72	2	5	25	44.2	43.6	0.6	15			3	0.006	0.9
GAP04 G-CL	557.40	95	43	>100	29	8940	6.8	< 0.3	3180			22		
GAP04 H-CL	681.21	>100	3	3	59	34	35.8	0.6	13				0.007	0.6

Based on the Ca^{2+} and SO_4^{2-} concentrations found in the eluate waters and the volume of test water compared to the porewater volume (See Appendix C), all porewaters were at equilibrium with respect to gypsum. The introduction of dilute test waters dissolved gypsum from the rock matrix. The final eluate waters from GAP04-C and GAP04-G were found to be saturated with respect to gypsum. All final eluate waters were undersaturated with other secondary minerals such as mirabilite, brucite, epsomite and calcite (where the alkalinity was measured). These findings are similar to those of Eichinger and Waber (2013). However, fewer of the University of Waterloo samples were saturated with gypsum, likely due to the larger volumes of test water used (see Appendix C).

It is assumed that porewaters were at equilibrium with respect to gypsum and that the majority of sulfate in the test waters was derived from the dissolution of gypsum. Under this assumption, it is possible to calculate the quantity of gypsum dissolved based on these assumptions (Table C-4). The exact nature of the $CaSO_4$ minerals within the core is unknown and hemi-hydrate ($CaSO_4 \bullet 1/2 H_2O$) or anhydrite ($CaSO_4$) may also exist with solubilities and temperature-solubility relationships that differ from gypsum.

Porewater concentrations of Cl^- were determined following the method outlined in Appendix C. Porewaters are significantly more saline than groundwaters from the GAP site. Minimum porewater Cl^- concentrations based on out diffusion experiments ranged from 436 to 4527 mg/kg_{H2O} in GAP04-A to -D and from 1020 to 5144 mg/ kg_{H2O} in GAP04-E to -H (Table 4.12). These results are comparable to porewater concentrations calculated by Eichinger and Waber (2013) which ranged from 960 to 2200 mg/ kg_{H2O}.

Table 4.12. Calculated porewater concentrations of Cl^- in GAP04-A to -H. These values represent minimum concentrations due issues encountered during the out diffusion experiments such as the cell leakage encountered in GAP04-E to -H (see Appendix C for a full description of how these concentrations were calculated).

Sample	Depth mbhl	Depth mbs	Lithology	Total C_{lss} mg/Kg_{H2O}	Cl_{TW} mg/Kg_{H2O}	Cl_{PW} mg/Kg_{H2O}	Error Cl_{PW} mg/Kg_{H2O}
A	209.83	197.18	MFGN		2.66	628	251
B	352	330.77	IGN		6.82	4527	1811
C	570.32	535.93	IGN		7.3	1122	449
D	670.2	629.78	IGN		1.54	436	174
E	377.55	354.78	FGN	0.15	20	2163	649
F	448.03	421.01	IGN	0.21	28.4	5144	1543
G	557.4	523.78	IGN	0.05	11.7	1020	306
H	681.21	640.13	IGN	0.06	8.3	1057	317

4.3.3.2 DH-GAP01, DH-GAP03 and DH-GAP04 Crush and Leach

Chemistry corrected to porewater concentrations (see Section C.3.1) for crush and leach experiments are presented in Table 4.13. Charge balance error was <10% for the majority of the DH-GAP01 and DH-GAP03 samples with the exception of DH-GAP01 179.6 m BHL and 188.98 m BHL. The error may be related to alkalinity, which was measured during analytical laboratory analyses after a delay rather than immediately following extraction of the crush and leach waters. Alkalinity was not measured for the DH-GAP04 crush and leach experiments and thus charge balance errors could not be calculated. Geochemical and some isotopic results from crush and leach analyses on the DH-GAP04 drill core were presented in Keir-Sage (2014).

DH-GAP01 and DH-GAP03 crush and leach porewaters were a Na-Ca-HCO_3-SO_4 type while DH-GAP04 porewaters (crush and leach and out diffusion) were Ca-Na-SO_4 type. Sulfate and calcium concentrations presented in Table 4.15 represent both sulfate and calcium from porewaters as well as from gypsum dissolved from the rock matrix during the crush and leach experiments. Almost all

Table 4.13. Porewater chemistry based on crush and leach experiments on DH-GAP01, DH-GAP03 and DH-GAP04. Correction to porewater values is based on Equations C.1 and C.2 (Section C.3.1) and has an estimated error of 25% due to the use of porosity from adjacent core sections). Saturation indices are calculated using PHREEEQC based on calculated porewater concentrations. NM = not measured. BD = below detection limit. Major geochemical results for DH-GAP04 first reported in Keir-Sage (2014).

Borehole	Length Along Core	K	Ca	Mg	Na	Cl	SO_4	Br	Sr	Gypsum	Celestite
	m	(mg/L)	(mg/L)	(mg/L)	(mg/L)	(mg/L)	(mg/L)	mg/L	mg/L	Saturation Indices	
DH-GAP01	64.96-65.06	5188	9889	3028	14039	1221	19045	11	136	0.8	0.7
	64.96-65.06	5604	9889	3034	13978	1209	18984	11	143	1.2	1.1
	90.65-90.75	10793	21586	13665	23153	1715	47002	34	404	1.0	1.1
	149.90-150.00	6684	7717	1203	16893	11242	4740	172	80	0.1	-0.2
	179.6-179.70	4646	16298	7431	14550	762	25852	8	100	1.1	0.6
	188.98-189.08	17126	7966	4952	12148	3983	12878	56	96	0.5	0.3
DH-GAP03	9.93-10.03	2405	9608	6431	11438	1242	7647	10	121	0.3	0.1
	41.50-41.60	10044	7672	2483	18271	13729	6461	225	64	0.1	-0.2
	80.80-80.90	4433	6087	1589	4901	1061	10770	11	64	0.6	0.3
	139.75-139.80	4368	14360	5348	17726	2004	16080	13	159	0.6	0.4
	236.24-236.34	10518	6128	1753	20797	15936	5737	228	70	-0.1	-0.3
	302.44-302.54	896	5079	2756	24498	1695	14564	14	53	0.2	0.0
DH-GAP04	11.11	525	5672	5777	7247	993	6512	263	25	0.5	-0.1
	120.19 total	1145	39601	7172	37083	1473	113233	206	266	2.4	1.9
	209.56	915	2614	1351	27232	684	12331	514	12	0.6	0.0
	289.91	22535	3384	1224	35926	14327	7099	526	16	0.4	-0.2
	399.84 total	55366	370026	7013	30636	13371	851245	BD	1473	BD	
	491.12 total	10737	156995	10737	23755	1424	373851	117	2023	3.8	3.8
	570.59	3888	152579	4159	12133	411	359299	BD	792	3.7	3.2
	640.28 total	52930	226841	28639	67107	10454	681469	BD	2994	BD	
	670.42	25833	200710	12075	19521	2816	524437	BD	641	4.4	4.2

porewaters analyzed by crush and leach in the three boreholes were supersaturated with respect to gypsum (Table 4.13) as a result of additional gypsum dissolution during the course of the crush and leach and out diffusion experiments. The in-situ porewaters are likely at equilibrium with respect to gypsum.

Calculated porewater concentrations of Cl^- are variable within each borehole but have similar ranges in all 3 boreholes, with higher concentrations generally being observed in the more felsic rocks and lower concentrations in the more mafic rocks (Figure 4.8)(Table 4.13). Porewater concentrations of various ions varied with depth in each of the GAP boreholes (Figures 4.9, 4.10 & 4.11).

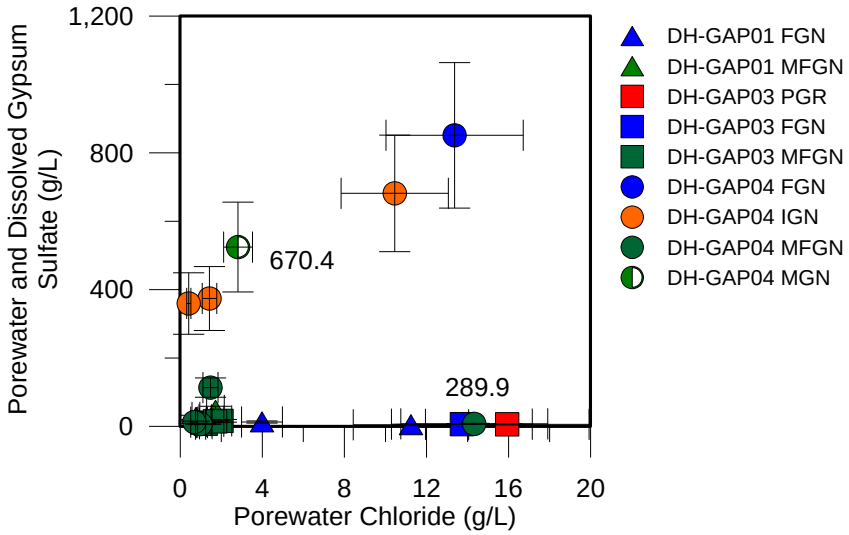

Figure 4.8. Porewater concentrations of SO_4^{2-} and Cl^- based on crush and leach experiments in DH-GAP01, DH-GAP03 and DH-GAP04. SO_4^2 concentrations are composed of porewater SO_4^{2-} and gypsum dissolved form the rock during the crush and leach experiment.

The results for porewater Cl^- concentrations calculated in DH-GAP04 using the two different porewater analysis methods (crush and leach and out diffusion) showed comparable trends with depth, although calculated chloride concentrations were generally higher for crush and leach results (Figure 4.12). Elevated chloride concentrations were observed around 300-450 m BHL and 600 - 660

m BHL in the crush and leach experiments as well as in all sets of out diffusion experiments including those performed by Eichinger and Waber (2013) (Figure 4.12) and as observed earlier are most likely related to rock type.

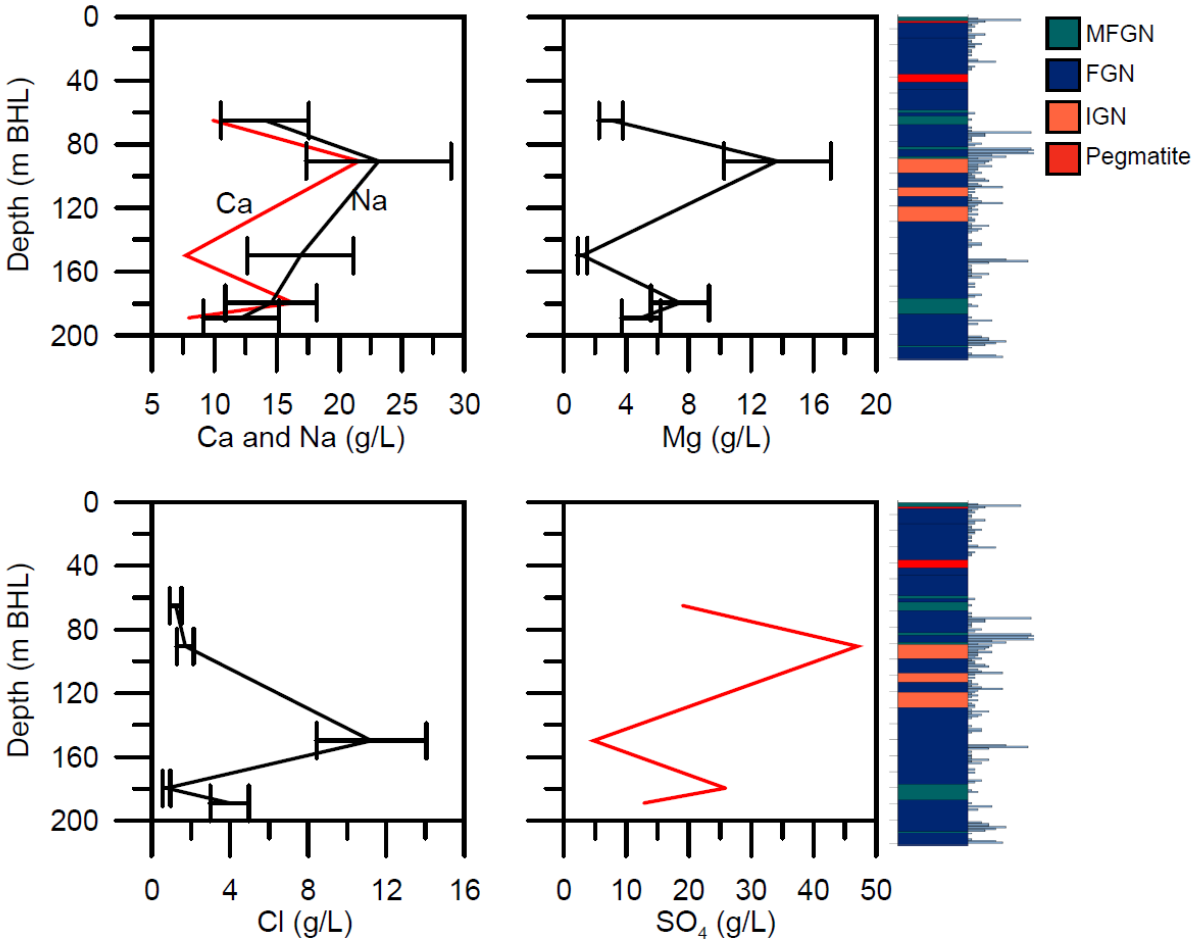

Figure 4.9. Changes in porewater ion concentrations with depth in DH-GAP01 based on crush and leach experiments. MFGN = mafic garnet bearing gneiss, FGH = felsic gneiss, IGN = intermediate gneiss. Fracture frequency is shown along the right side of the borehole log. Ca^{2+} and SO_4^{2-} concentrations are not assigned error bars as they represent both porewater concentrations as well as contributions from gypsum dissolved from the rock matrix during the crush and leach experiments.

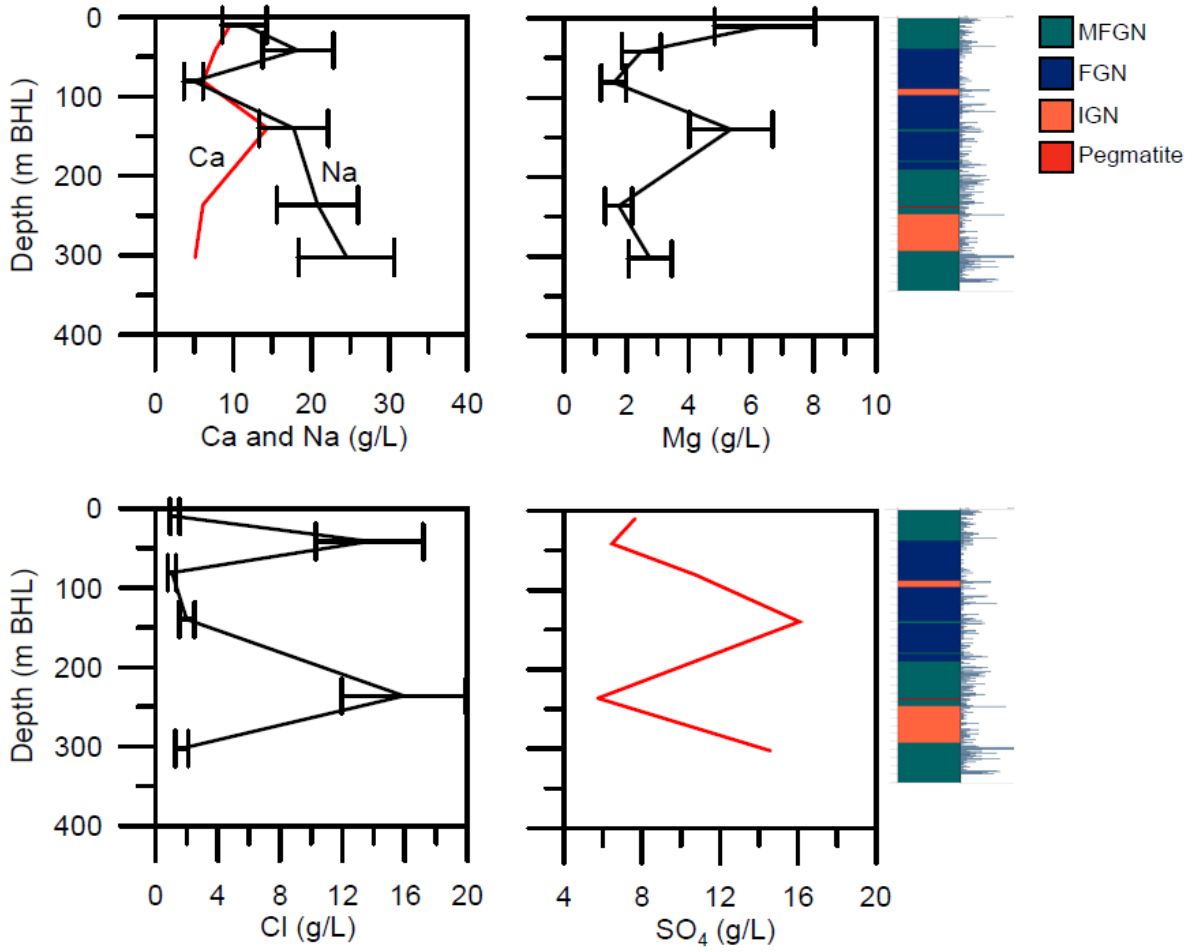

Figure 4.10. Changes in porewater ion concentrations with depth in DH-GAP03 based on crush and leach experiments. MFGN = mafic garnet bearing gneiss, FGH = felsic gneiss, IGN = intermediate gneiss. Fracture frequency is shown along the right side of the borehole log. Ca^{2+} and SO_4^{2-} concentrations are not assigned error bars as they represent both porewater concentrations as well as contributions from gypsum dissolved from the rock matrix during the crush and leach experiments.

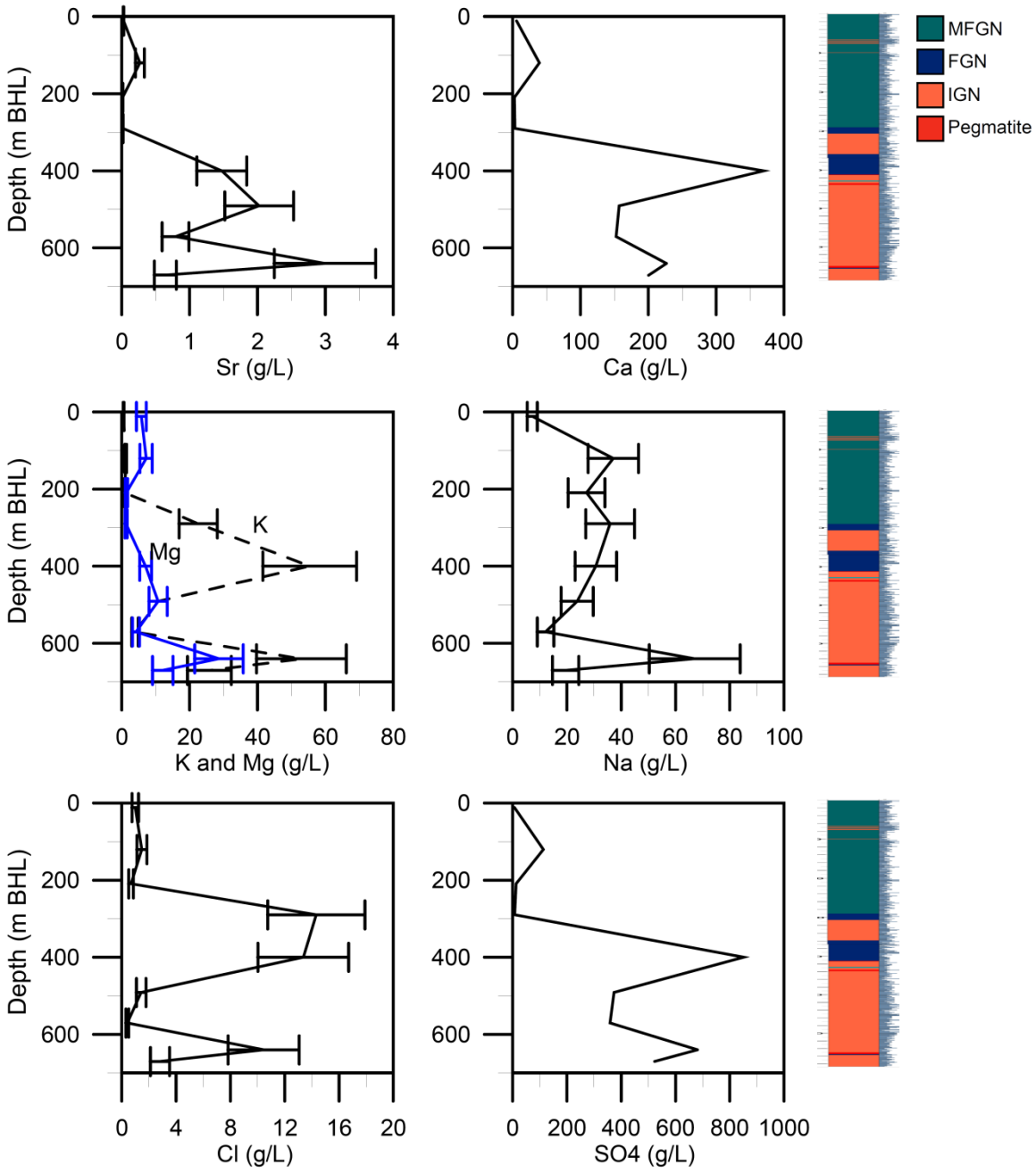

Figure 4.11. Changes in porewater ion concentrations with depth in DH-GAP04 based on crush and leach experiments. MFGN = mafic garnet bearing gneiss, FGH = felsic gneiss, IGN = intermediate gneiss. Fracture frequency is shown along the right side of the borehole log. Ca^{2+} and SO_4^{2-} concentrations are not assigned error bars as they represent both porewater concentrations as well as contributions from gypsum dissolved from the rock matrix during the crush and leach experiments. Adapted from Keir-Sage (2014).

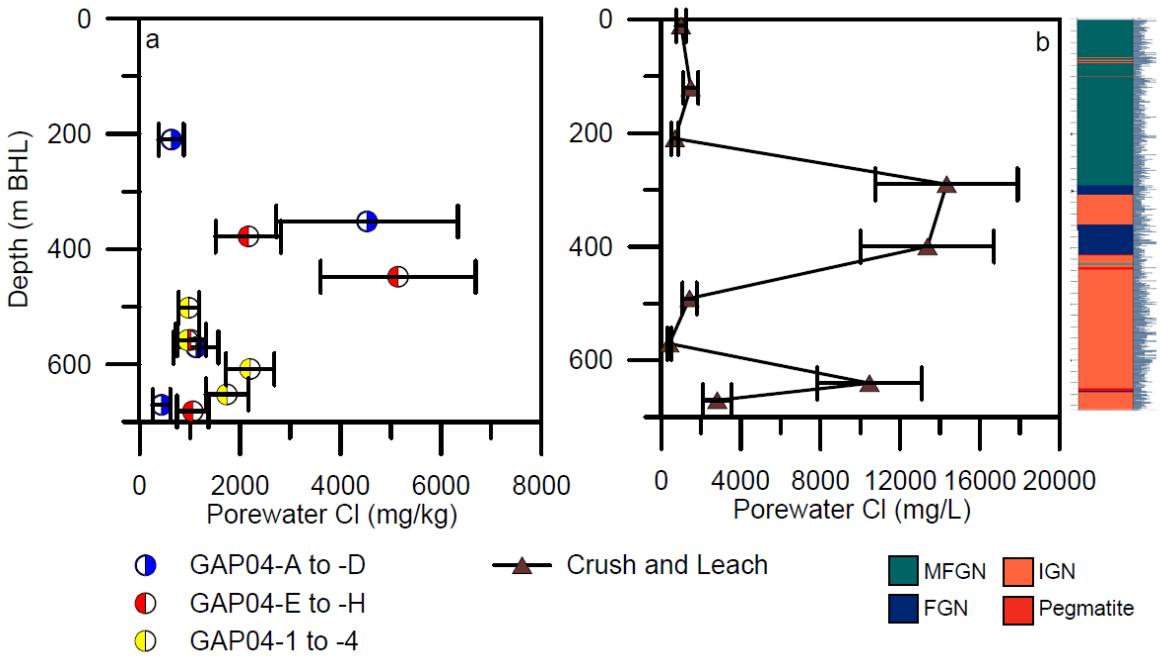

Figure 4.12. Chloride concentrations in porewaters in DH-GAP04 based on (a) out diffusion experiments at UW (GAP04-A to -H) and from Eichinger and Waber (2013) (GAP04-1 to -4) and (b) crush and leach experiments. MFGN = mafic garnet bearing gneiss, FGH = felsic gneiss, IGN = intermediate gneiss. Fracture frequency is shown along the right side of the borehole log.

4.3.3.3 Isotopic Results

Isotopic results for the out diffusion experiments can be found in Table 4.14 and for crush and leach (DH-GAP04) in Table 4.15. The isotopic composition of sulfate ($\delta^{34}S$ and $\delta^{18}O$) of porewaters from the crush and leach and out diffusion experiments fell within a similar range as the isotopic composition of the gypsum fracture mineral sulfate (Figure 4.13). Oxygen-18 of sulfate in porewaters ranged from 0.11 to 8.49 ‰. Sulfur-34 of sulfate in porewaters ranged from 1.66 to 6.69 ‰. Out diffusion experiment GAP04-A (209.83 m BHL) was depleted in both $\delta^{34}S$ (SO_4) and $\delta^{18}O$ (SO_4), possibly as a result of the oxidation of sulfides which were observed in this area of the core mainly as chalcopyrite (Pere, 2014).

Table 4.14. Isotopic results for out diffusion experiments on DH-GAP04 core and crush and leach experiments performed on GAP04 E to GAP04 H after completion of the out diffusion experiments. Chlorine-37 results from the Eichinger and Waber (2013) out diffusion experiments (GAP04-1 to -4) are also included for reference. It is likely, however that the $\delta^{37}Cl$ results from Eichinger and Waber (2013) should be discounted as they represent extremely depleted values for natural waters and such depleted $\delta^{37}Cl$ isotopic values are not observed in any other waters analyzed for this study.

Sample	Depth	$\delta^{34}S$		$\delta^{18}O$			
	m BHL	SO_4		SO_4		$^{87}Sr/^{86}Sr$	$\delta^{37}Cl$
		Result	Repeat	Result	Repeat		SMOC ± 0.1‰
		VCDT ± 0.3‰		VSMOW ± 0.5‰			
GAP04-1	501.5						-2.89
GAP04-2	651.9						-4.03
GAP04-3	557.7						-6.04
GAP04-4	607.7						-5.49
GAP04-A	209.83	2.40	1.81	0.11	-0.20	0.707500	
GAP04-B	352.00						
GAP04-C	570.32	5.47		6.37		0.702569	0.42
GAP04-D	670.20	6.69		8.06		0.710354	
GAP04-E	377.65					0.707770	0.52
GAP04-F	448.07					0.704524	-0.24
GAP04-G	557.40	6.62		4.80		0.702119	0.27
GAP04-H	681.21					0.705475	-0.42
GAP04 E-CL	377.65					0.712813	-0.29
GAP04 F-CL	448.07						
GAP04 G-CL	557.40	6.12	5.89	5.50	4.76	0.702272	0.05
GAP04 H-CL	681.21					0.714423	-0.44

$^{87}Sr/^{86}Sr$ isotopic ratios in porewaters ranged from 0.70212 to 0.72725. In general, less radiogenic strontium isotope ratios were observed in the out diffusion experiments (0.70212 - 0.70777) compared to the crush and leach experiments (0.70294 - 0.72725). It is likely that the milling process used in the crush and leach experiments allows additional strontium contributions from fresh surfaces on finely ground matrix minerals such as biotite and chlorite. This is similar to the observation made in Chapter 2, where fresh, glacially comminuted rock flour contributed more radiogenic strontium isotopic signatures to surface waters. More radiogenic $^{87}Sr/^{86}Sr$ ratios were observed in crush and leach experiments on the same core used for out diffusion experiments

GAP04-E to -H. The non-destructive out diffusion method yields $^{87}Sr/^{86}Sr$ results more representative of in-situ porewater conditions. Both out diffusion and crush and leach experiments are impacted by the additional dissolution of gypsum found within the rock matrix which has a less radiogenic $^{87}Sr/^{86}Sr$ isotopic signature (see Section 4.3.2).

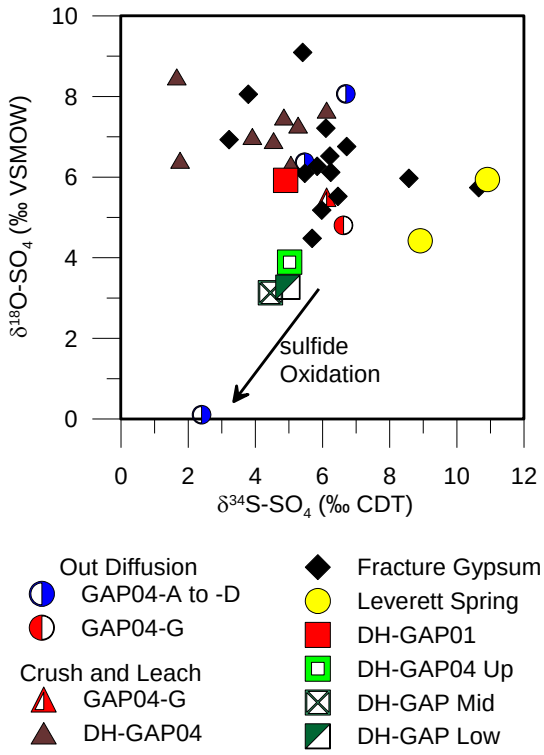

Figure 4.13. The isotopic composition ($\delta^{34}S$ and $\delta^{18}O$) of sulfate in porewaters, groundwaters and fracture filling gypsum.

The chlorine isotopic signature ($\delta^{37}Cl$) of porewaters ranged between -0.60 to +0.68 ‰ (Tables 4.14 & 4.15). The majority of crush and leach derived porewaters often have negative $\delta^{37}Cl$ isotopic compositions. However, when larger grain sizes are used for the crush and leach experiments (only performed on DH-GAP04 core), positive $\delta^{37}Cl$ values are observed. It is likely that the breakage of fluid inclusions is adding additional Cl^- with a negative $\delta^{37}Cl$ signature to the crush and leach waters. However, we also see negative $\delta^{37}Cl$ isotopic signatures in the GAP04 - F and GAP04 - H out diffusion

experiments. As out diffusion is a non-destructive method of porewater sampling, the destruction of fluid inclusions cannot adequately explain these negative $\delta^{37}Cl$ isotopic values.

Table 4.15. Isotopic results from crush and leach experiments performed on DH-GAP01, DH-GAP03 and DH-GAP04 core.

Borehole	Length Along Core	$^{87}Sr/86Sr$	$\delta^{34}S$ (SO_4)	$\delta^{18}O$ (SO_4)	$\delta^{37}Cl$	$\delta^{81}Br$
	m BHL		‰ CDT	‰ VSMOW	‰ SMOC	‰ SMOB
DH-GAP01	149.90-150.00	0.71347				
	188.98-189.08				-0.27	
DH-GAP03	41.50-41.60				-0.17	
	80.80-80.90	0.70935				
	139.75-139.80	0.70605				
	236.24-236.34				-0.07	
DH-GAP04	11.11	0.707706			-0.02	
	50.02	0.706656				
	120.19 1-6cm		1.66	8.49		
	120.19 <1cm	0.707194				
	120.19				-0.34	
	209.56					0.64
	289.76				-0.6	
	399.57	0.727254	4.54	6.91	0.35	
	399.84 1-6cm				0.68	
	399.84 <1cm		5.06	6.32		
	399.84		5.27	7.29	-0.51	
	430.17	0.717538	1.76	6.42		
	430.47				-0.29	
	491.12 1-6cm		3.91	7.01	0.6	0.67
	491.12 <1cm	0.703216				
	570.59	0.702941	6.12	7.66		
	639.98	0.704317			-0.27	
	640.28 Total	0.703865				
	640.28 <1cm				-0.13	
	640.28	0.703986				
	670.42	0.719780	4.85	7.49		

4.4. Discussion

Highly saline fluids, like those observed at depth in the Canadian and Fennoscandian shields (Frape et al, 2014), were not observed in the GAP boreholes (see Chapter 3): DH-GAP01 and DH-GAP04 were brackish (1 to 10 g/L) by the classification of Davis (1964). However, determining the source of salinity in the GAP boreholes, especially the high concentrations of sulfate, was important in terms of evaluating the impact of cold climate processes such as in-situ freeze-out on groundwater chemistry. As part of the discussion of the origin of salinity in the groundwater system, the extensive presence of gypsum below 300 m BHL in DH-GAP04 and porewaters with salinities much greater than those observed in groundwater found in fractures must also be evaluated. In situ freeze-out, water-rock interaction and hydrothermal processes are considered as potential processes for generation of salinity in the groundwater system.

4.4.1. Cold Climate Conditions and In-Situ Freeze-Out Background

The concentration of sulfate and other ions through in-situ freeze-out during permafrost formation has been discussed by other authors in relation to other cold-climate locations (e.g. Smellie et al., 2002; Alexeev and Alexeeva, 2002; Alexeev and Alexeeva, 2003; Shouakar-Stash et al., 2007). It is thus important to determine whether the high sulfate concentrations and the presence of gypsum at the GAP site is related to relatively recent cold climate conditions, permafrost formation and oxygenated glacial recharge or to local, site specific geology.

In Antarctic lakes, it was found that concentration through freezing resulted in the concentration of sulfate followed by precipitation of mirabilite ($Na_2SO_4 \bullet 10H_2O$) (Matsubaya et al., 1979). At Palmottu, Finland, it was proposed that Na-SO_4 waters associated with glacial recharge (depleted $\delta^{18}O$ isotopic signatures) could have been the result of SO_4^{2-} concentration through solute exclusion and/or the dissolution of mirabilite formed during previous glacial/permafrost cycles (Kaija

et al., 2000; Smellie et al., 2002). In the Palmottu case, one explanation suggest that the initial SO_4 was related to hydrothermal processes and was then concentrated through solute exclusion during permafrost formation (Kaija et al., 2000; Smellie et al., 2002).

The Siberian Platform has some of the deepest permafrost in the world, extending more than a kilometer beneath the surface in some places (Ershov & Kondratjeva, 1996; Williams & Warren, 1999; Vidstrand, 2003). High TDS (>300 g/L) brines are found in the Siberian Platform and attributed to a number of processes including, seawater evaporation, halite dissolution and water-rock interaction (Shouakar-Stash et al., 2007). Solute exclusion during permafrost formation has also been considered as a possible mechanism to generate salinity in the Siberian Platform from the pre-existing fluids existing in the rock (Alexeev & Alexeeva, 2002, 2003; Shouakar-Stash et al., 2007).

The extent of cryogenic alteration of waters is highly dependent on the starting TDS of the groundwaters. High TDS brines will have a highly depressed freezing point (<-23 °C) that may never be reached at the lowest natural temperatures found at depth in permafrost impacted environments (Alexeev & Alexeeva, 2003). Lower TDS waters will freeze at less negative temperatures and are thus more likely to undergo cryogenic concentration under natural subsurface temperatures in permafrost regions (max -8 to -13 °C at 100 to 200 m) (Stotler, 2008). Below these depths, the temperature may remain below zero but due to geothermal gradients, the temperatures begin to rise with depth.

In a large scale study of shield groundwaters, Stotler et al. (2012) found some evidence for in-situ freeze out at sites in the Canadian and Fennoscandian Shield. However, Stotler et al. (2012) found it was difficult to separate the evidence for in-situ freeze out from other cold climate processes such as intrusion of glacial meltwater or methane hydrate formation.

A number of geochemical and isotopic parameters can provide field evidence for cryogenic concentration. These include:

- Increasing TDS with depth, especially increases in sodium, magnesium and calcium sulfate and chloride salts. (Alexeev & Alexeeva, 2002, 2003).
- Fluid evolution in Na/Cl vs Br/Cl space that follows freezing pathways related to the initial fluid composition. E.g. Na-dominated fluids will fall on a near vertical slope while Ca-dominated fluids have a slightly positive slope (Stotler et al., 2012).
- Positive correlation between $\delta^{18}O$ depletion and the log Cl^- concentration (Zhang & Frape, 2003; Stotler et al., 2012).
- Depletion in $\delta^{18}O$ and $\delta^{2}H$, with isotopic values falling along a line with a slope less than that of the GMWL (4.3 to 7.4) (Souchez & Jouzel, 1984; Zhang & Frape, 2003).
- Precipitation of secondary minerals. On the Siberian Platform, calcite that had precipitated in caverns of the Zarnitsa kimberlite pipe was attributed to cryogenic concentration of groundwater (Alexeev & Alexeeva, 2003). Hexahydrite ($MgSO_4 \bullet 6H_2O$) was observed as a secondary mineral in the Osennyaya kimberlite pipe on the Siberian platform (Egorov et al., 1987). Freezing experiments on groundwaters from the Canadian and Fennoscandian shields showed that gypsum may precipitate during freezing of certain fluids (Zhang & Frape, 2003).

Several lines of evidence for in-situ freeze out are discussed previously in Chapter 3. In-situ freeze-out is further explored here using the geochemical and isotopic composition of porewaters and fracture infillings analyzed in this chapter.

4.4.2. Evidence for Freeze-Out in the GAP Study Area

4.4.2.1 Isotopic Evidence

The potential source of sulfate in an in-situ freeze out scenario at the GAP site is the oxidation of sulfide minerals present within the rock matrix and fracture infillings. Sulfate produced by the oxidation of sulfide will have a characteristic isotopic ($\delta^{34}S$ and $\delta^{18}O$) composition as discussed below. Sulfide oxidation may result in a small isotopic depletion of $\delta^{34}S$ in the order of 2 - 5.5 ‰ between the sulfide and sulfate (Toran & Harris, 1989). Negligible isotopic fractionation of sulfur isotopes between the sulfide and resulting sulfate is also reported at a significant number of field sites and in experimental results (Gavelin et al., 1960; Nakai & Jensen, 1964; Toran & Harris, 1989; Seal et al., 2000).

While the isotopic effects on $\delta^{34}S$ due to sulfide oxidation are small to negligible, the effect on $\delta^{18}O(SO_4)$ is very significant (van Everdingen & Krouse, 1985). The $\delta^{18}O$ (SO_4) of sulfate derived from sulfide oxidation will depend on the isotopic composition of the oxygen present as O_2 and H_2O. van Everdingen and Krouse (1985) developed an equation (4.3) to calculate the $\delta^{18}O$ of sulfate ($\delta^{18}O_s$) derived from sulfide oxidation:

$$\delta^{18}O_s = Y(\delta^{18}O_w + \varepsilon_w)+(1-Y)[0.875(\delta^{18}O_a + \varepsilon_a)+0.125(\delta^{18}O_w + \varepsilon_w)] \qquad [4.1]$$

Where $\delta^{18}Ow$ represents the $\delta^{18}O$ contents of water and $\delta^{18}Oa$ represents that of oxygen present. No dissolved oxygen was measured in the deep groundwaters. However, it is likely that the pyrite oxidation occurred in the shallow subsurface where evidence for oxidation was observed (Section 3.5.2; Harper et al. (2015a)). Oxidizing conditions in the subsurface under glacial conditions were also observed at the Laxemar Area in Sweden, and were similarly limited to the shallow

subsurface (Drake et al., 2009). Y represents the proportion of SO_4^{2-} derived using oxygen from H_2O versus O_2 described in equations 4.2 and 4.3:

(1) $FeS_2 + 14\ Fe^{3+} + 8\ H_2O = 15\ Fe^{2+} + 2\ SO_4^{2-} + 16\ H^+$ [4.2]

(2) $FeS_2 + 7/2\ O_2 + H_2O = Fe^{2+} + 2SO_4^{2-} + 2\ H+$ [4.3]

The enrichment factors between the $\delta^{18}O$ of sulfate and water and sulfate and oxygen are given by e_w and e_a respectively. Several unknowns are present in the Equation 4.1: Y, $\delta^{18}Ow$ and $\delta^{18}Oa$. If we assume $\delta^{18}Oa$ is +23.5 ‰ (atmospheric), $\delta^{18}Ow$ is similar to groundwater values (-24 ‰) and vary Y between 0.3 and 0.9 we arrive with $\delta^{18}O_s$ between 0 and -17 ‰. In groundwater, most of the oxygen should come from H_2O (higher values of Y) and thus $\delta^{18}O_s$ would most likely fall at the more isotopically depleted end (-17 ‰)of the given range.

Sulfides in the rock matrix at the GAP site were found to have a $\delta^{34}S$ between 2.26 - 3.73 ‰. Thus, sulfate derived from oxidation of sulfides under relatively modern cold-climate conditions should have a $\delta^{34}S$ (SO_4) between -3.2 and 3.7 ‰ and a $\delta^{18}O$ (SO_4) between 0 and -17 ‰. Groundwaters, porewaters and fracture infillings ($\delta^{18}O$ (SO_4) > 0 ‰) were not observed to have sulfate isotopic compositions that satisfied the ranges given above (Figure 4.13). Thus, an alternative source of sulfur is necessary to have precipitated the fracture and matrix gypsum responsible for high groundwater sulfate concentrations. A hydrothermal origin for sulfate is discussed in Section 4.4.3.

In-situ freezing may fractionate $\delta^{37}Cl$ as the heavy isotope is preferentially trapped into the ice. However, Zhang and Frape (2003) noted that this effect had little impact on the isotopic composition of dissolved chloride in the residual solution, as little chloride was incorporated into the ice. Thus freezing related fractionation was unable to affect the dissolved chloride pool.

Additionally, porewaters in low porosity crystalline rock, where diffusion is the dominant solute transport mechanism, may behave like a closed system where salts are not easily transported during freezing. Therefore, if freeze-out occurs in a closed system, it is unlikely that chloride isotopic fractionation will be observed. In DH-GAP04 depleted $\delta^{37}Cl$ isotopic values are observed at both shallow depths and below 600 m BHL (Figure 4.14). Variations in $\delta^{37}Cl$ may be related to rock type (Section 4.4.4) and do not appear to be related to the permafrost boundary at 400 m BHL.

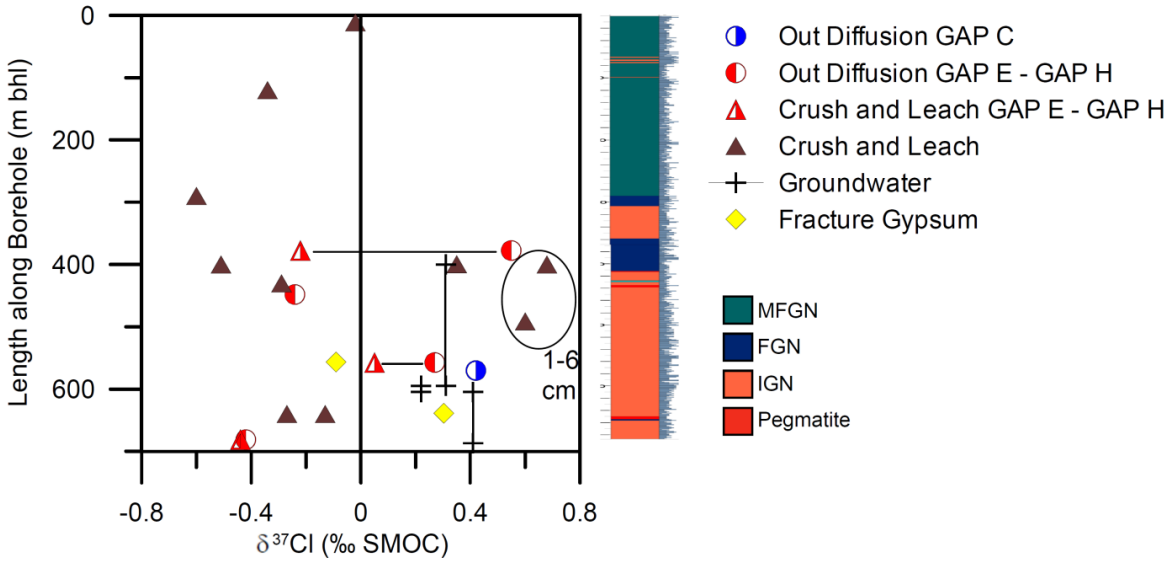

Figure 4.14. $\delta^{37}Cl$ isotopic composition of porewaters, groundwaters and fracture gypsum with depth in DH-GAP04. Horizontal lines indicate paired out diffusion - crush and leach samples. MFGN = mafic garnet bearing gneiss, FGH = felsic gneiss, IGN = intermediate gneiss. Fracture frequency is shown along the right side of the borehole log.

4.4.2.2 Depth Profiles in Boreholes

Increasing conductivity with depth, as is predicted by conventional ideas of in-situ freeze out (Alexeev & Alexeeva, 2002, 2003) is not observed in the DH-GAP04 porewaters. In the DH-GAP04 core, Cl^- concentrations increase abruptly at 300 m BHL, however, this increase coincides with the transition from mafic to felsic gneiss (Figures 4.11 & 4.12) and is not coincident with the permafrost

boundary (400 m BHL). A secondary increase in Cl^- concentrations is observed around 640 m BHL along with increases in the other major ions (Figures 4.11 & 4.12). It is not immediately clear what causes the increase in salinity around 640 m BHL though it coincides with the transition from more massive intermediate gneiss into increased layering with mafic gneiss. A large increase in SO_4^{2-} and Ca^{2+} concentrations was observed in crush and leach experiments around the permafrost boundary at 400 m BHL, however this is most likely due to the occurrence of abundant gypsum at that depth rather than to in-situ freeze out. The coincidence of abundant gypsum and the permafrost boundary underlines the necessity of understanding the origin of the gypsum and whether it is related to cold-climate processes.

4.4.2.3 Precipitation of Secondary Mineral Phases

Comparison of the chemistry of the DH-GAP01 and DH-GAP04 boreholes and groundwaters are complicated by the differences in elevation and geological environment (see Chapter 1). However, it seems likely that in-situ freeze-out would cause a similar impact on the porewaters, groundwaters and mineralizations of DH-GAP01 and DH-GAP04.

Gypsum dissolution plays a significant role in the groundwater chemistry of both DH-GAP01 and DH-GAP04 (see Chapter 3). Only one occurrence of gypsum has been noted in DH-GAP01, while gypsum is ubiquitous in the DH-GAP04 core below 300 m BHL. An important question is whether gypsum was previously present in DH-GAP01, DH-GAP03 and the upper 300 m BHL of DH-GAP04 and subsequently dissolved by shallow groundwater flow during permafrost free conditions or whether gypsum was never present or limited in occurrence. Several lines of evidence suggest that the latter is true in the boreholes/borehole sections described above:

(1) The matrix porosity in crystalline rock has poor transmissivity ($T<10^{-10}$ m^2/s) and is dominated by diffusive transport. Gypsum present in the rock matrix is unlikely to be flushed out even over

very long time periods as pore fluids will quickly reach equilibrium with gypsum. In DH-GAP04, gypsum is pervasive throughout the rock matrix below a depth of 300 m BHL (Figure 4.5). Crush and leach and out diffusion experiments show high sulfate concentrations as a result of dissolution of matrix gypsum (Table 4.11, Figures 4.8 & 4.11). In the upper 300 m BHL of core, where gypsum is observed less frequently in fractures, SO_4^{2-} in porewaters and from gypsum dissolution is significantly lower (Figure 4.11). In the DH-GAP01 and DH-GAP03 boreholes, the high SO_4^{2-} concentrations resulting from matrix gypsum dissolution are not observed (Figures 4.9 & 4.10), suggesting that gypsum is not extensively present in the rock matrix.

(2) Fractures observed in the upper 300 m BHL of the core do not indicate that gypsum was present and dissolved away. For example, fractures that have open porosity, lacking infillings or showing replacement mineralogy after gypsum were not observed.

Likely, the difference in gypsum occurrence between the boreholes is related to the differences in host rock geology rather than to gypsum being flushed from the fractures by groundwater flow. DH-GAP04 is drilled in a different lithological and structural environment than DH-GAP01 and DH-GAP03. DH-GAP04 was drilled into a shallowly plunging, open fold structure related to the F1 (oldest) fold system (Harper et al. 2015a, Chapter 1). For example, the noses of folds are often locations conducive to mineral precipitation due to stress conditions (Harris et al., 2012).

4.4.3. Gypsum: Hydrothermal Origins and Impact on Groundwater Chemistry

The following sections will explore alternative sources for sulfate and other ions which are related to old or long term processes. The morphology and occurrence of gypsum in the DH-GAP04 core suggests a hydrothermal origin. For example: the presence of embedded phyllosilicates (Table 4.7) and co-genetic calcite (Pere, 2014; Harper et al., 2015a). Consistent with a hydrothermal origin,

gypsum is extensive within microfractures and pore space in the rock matrix (Figure 4.5), is observed in SEM images described in Eichinger and Waber (2013) and is observed in whole rock XRD analysis (see Table 4.3). Fibrous crystal textures are also observed (Figure 4.6d) across fractures which indicates precipitation during fracture dilation in a structurally dynamic system. Most likely the gypsum was precipitated some time after peak metamorphism, which occurred during the Nagssugtoqidian Orogen (1.92 to 1.75 Ga).

Similar gypsum infillings have been observed at the Atikokan site in Ontario, Canada. The Atikokan site is located in the Eye-Dashwa lakes pluton of the Canadian Shield. The 2.5 Ga pluton is located in the Superior structural province and intrudes into gneisses. The pluton is composed of quartz-monzonite, hornblende-rich granodiorite and hornblende-poor biotite rich granite (Kamineni, 1983; Kerrich & Kamineni, 1988). The gneisses are characterized by amphibolite facies mineral assemblages, tectonic fabrics and mafic dykes (Kerrich & Kamineni, 1988). Gypsum (or possibly a precursor such as anhydrite), along with calcite and clays was determined to have precipitated at temperatures of <100 °C while higher temperature fracture fillings such as pegmatite, aplite, epidote and chlorite are also present (Kamineni et al., 1980; Stone & Kamineni, 1982; Kamineni, 1983). The higher temperature minerals were determined to have formed immediately after solidification of the pluton from residual magmatic fluids and by hydrothermal alteration (Kamineni & Dugal, 1982; Stone & Kamineni, 1982). The relationship between age and temperature of formation of fracture infillings in the Eye-Dashwa pluton suggests that fracturing and fracture filling occurred progressively as the pluton cooled. Similarities in site geology as well as in the REE (Figure 4.7b) and isotopic composition (Section 4.3.2.1.) of the fracture gypsum suggests that some parallels may be drawn between the GAP site and the intensively studied Atikokan site. Thus, the Atikokan site provides an analogous example of hydrothermal fracture gypsum to which the GAP gypsum samples can be compared.

4.4.3.1 Rare Earth Elements

Gypsum REE patterns resemble those of the intermediate and felsic gneisses with slightly lower absolute abundance (Figure 4.7a). Gypsum is found predominantly within sections of intermediate and felsic gneiss in DH-GAP04. This suggests the gypsum precipitated from a fluid that was at or close to equilibrium with the felsic/intermediate gneiss, likely under elevated temperature conditions during an older metamorphic or tectonic event, that would more effectively partition the REE into the fluid phase. Modern groundwater conditions (low temperatures, near neutral to slightly alkaline pH) are not conducive to leaching REE from the host rock (Michard, 1989). The regional tectonic history is described briefly in Chapter 1 (Section 1.3.3) and includes a number of tectonic and metamorphic events which could have produced the necessary elevated temperature conditions for a fluid to equilibrate with the rock mass. Temperature, pressure or pH changes in the fluid could induce precipitation of gypsum or another $CaSO_4$ phase such as anhydrite or hemihydrate.

REE patterns in the gypsum from the DH-GAP04 core are similar to gypsum found in felsic rocks of the Eye Dashwa Lakes pluton at Atikokan, Ontario, Canada. The Eye Dashwa Lakes pluton fracture filling gypsum was precipitated from a brine that was at equilibrium with the host rock (Mungall et al., 1987), potentially under higher temperature conditions before the pluton cooled (Kamineni, 1983). Studies of gypsum as a fracture mineral are rarely reported in the literature and, as previously discussed, the Eye Dashwa Lakes pluton site presents many similarities to the GAP site.

A LREE enriched pattern is expected for gypsum because LREE are preferentially incorporated into the structure of calcite and gypsum due to the smaller difference in ionic radius between Ca^{2+} and the $LREE^{3+.}$ than between Ca^{2+} and the $HREE^{3+}$ (Bau, 1991). A LREE enriched REE pattern is observed in both the DH-GAP04 and Atikokan gypsums. Eu^{2+} is excluded from the calcite crystal

lattice and this can create or strengthen a negative Eu anomaly (Bau, 1991). Negative Eu anomalies are observed in all gypsum samples from DH-GAP04 (Figures 4.4 & 4.7). However, the gypsums from the Atikokan site have only very small to no Eu anomaly, suggesting that gypsum does not behave in a similar fashion to calcite or that different redox conditions existed at the Atikokan site.

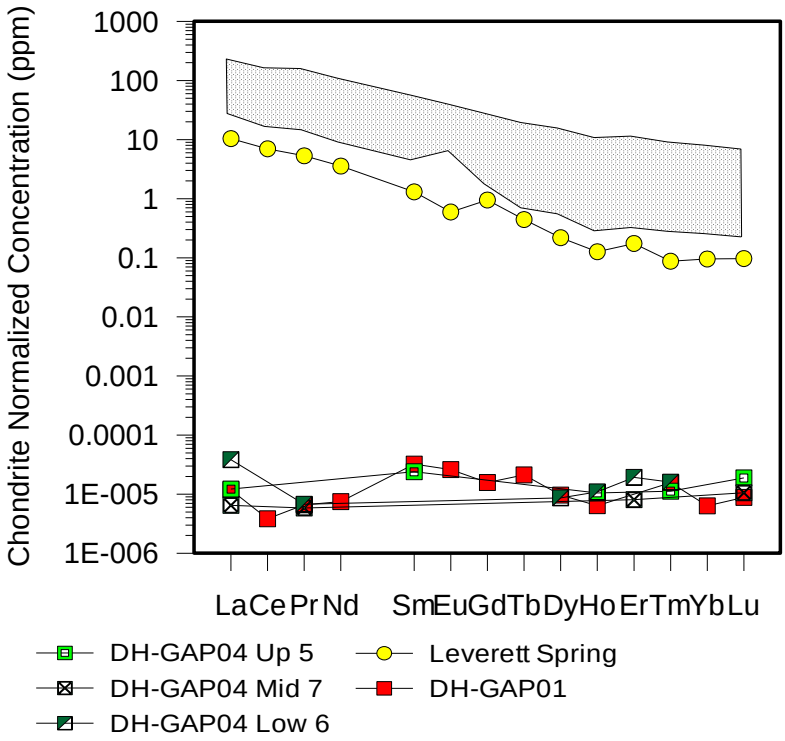

Figure 4.15. Groundwater REE profiles for boreholes and Leverett Spring compared to intermediate and felsic rock compositions (stippled area).

The Leverett Spring has been previously discussed in Chapter 3**.** The spring waters are unique from the borehole groundwaters geochemically and isotopically. From available information, it is difficult to draw conclusions on the origin of the Leverett Spring, however REE results provide an important line of evidence that suggests the spring may have a hydrothermal origin. While the borehole groundwaters found in DH-GAP01 and DH-GAP04 have very low concentrations of REEs that suggest low temperature conditions that are not conducive to leaching REEs from the rock

(Figure 4.15), the Leverett Spring has REE abundances similar to the gypsum and whole rock (Figures 4.7 & 4.15). The REE profile and abundance in Leverett spring suggests higher temperature water -rock interaction. The highconcentrations of REE in the Leverett spring are especially significant considering that the spring waters are dilute (EC 390 to 510 µS/cm). The only previous study of the Leverett Spring (Scholz & Baumann, 1997) also suggests the spring is hydrothermal in origin.

4.4.3.2 Strontium Background and Whole Rock Strontium Isotopic Composition

Strontium is a valuable tracer for examining the source of salinity and evaluating water-rock interaction due to the lack of fractionation during mineral precipitation and dissolution. Whole rock $^{87}Sr/^{86}Sr$ isotopic ratios represent a composite of the $^{87}Sr/^{86}Sr$ isotopic ratios of the various rock forming minerals. Briefly, ^{87}Rb decays to ^{87}Sr over time ($T_{1/2}$ = 4.88 x 10^{10} a). Older rocks have a lower initial $^{87}Sr/^{86}Sr$ ratio because there was less time for ^{87}Rb to decay to ^{87}Sr. For example, rocks formed in the Archean tend to have initial whole rock $^{87}Sr/^{86}Sr$ ratios close to 0.701 to 0.702 (McNutt et al., 1990). The decay of ^{87}Rb to ^{87}Sr imparts an $^{87}Sr/^{86}Sr$ isotopic signature that is proportional to the Rb/Sr ratio of the mineral phase (McNutt et al., 1984, 1990). Minerals with high Rb/Sr ratios (e.g. micas) will show a steep rate of increase in the $^{87}Sr/^{86}Sr$ ratio over time (Figure 4.16). A mineral with a low Rb/Sr ratio (e.g. plagioclase feldspar) will increase slowly with time and remain closer to the initial $^{87}Sr/^{86}Sr$ isotopic ratio of the rock at the time of formation. The whole rock $^{87}Sr/^{86}Sr$ ratio represents the strontium isotopic composition of the mineral phases present weighted by the concentration of Sr in the mineral. Sr^{2+} will substitute readily for Ca^{2+} while Rb^{+} substitutes for K^{+} in the crystal lattice.

Rock in the GAP study area consists of Archean gneiss that has been reworked in the Paleoproterozoic. Whole rock $^{87}Sr/^{86}Sr$ isotopic ratios in DH-GAP04 vary from 0.70151 to 0.72196.

Rock types containing mostly Rb-poor minerals such as quartz, plagioclase feldspar (predominantly albite) and pyroxene have $^{87}Sr/^{86}Sr$ whole rock signatures of less than 0.702, close to the original Archean whole rock $^{87}Sr/^{86}Sr$ isotopic ratio (e.g. 570.59 mbhl)(Figure 4.17)(Table 4.5). Sections of core with a greater abundance of micas (predominantly biotite and chlorite) have the greatest whole rock $^{87}Sr/^{86}Sr$ values.

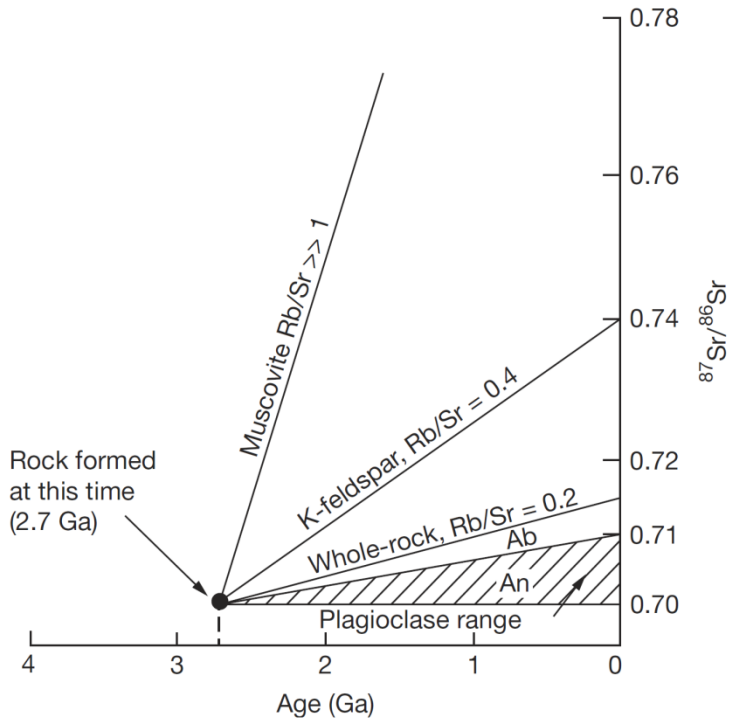

Figure 4.16. Evolution of the $^{87}Sr/^{86}Sr$ signature over time for a granitic rock and its major mineral phases. Minerals (such as micas) with high Rb/Sr ratios show a much faster rate of growth than low Rb/Sr minerals such as feldspars. From McNutt et al. (1990).

For example, the rock at 670.2 m BHL contains abundant biotite (Section 4.3.1.3)($^{87}Sr/^{86}Sr$ 1.10777) and has a whole rock $^{87}Sr/^{86}Sr$ signature of 0.72196(Figure 4.17). In DH-GAP04, whole rock $^{87}Sr/^{86}Sr$ isotopic ratios in the intermediate gneiss (<0.704) are dominated by the non-radiogenic feldspar isotopic signatures (< 0.705). The mafic sections of DH-GAP04 have more radiogenic whole

rock $^{87}Sr/^{86}Sr$ isotopic ratios (>0.709) due to lower proportions of non-radiogenic feldspars and increasing amounts of more radiogenic amphiboles and biotite (Table 4.5).

A section of altered wall rock at 570.07 m BHL had a more radiogenic $^{87}Sr/^{86}Sr$ ratio than the unaltered rock at 570.59 m BHL (0.70386 and 0.70174 respectively), indicating the alteration occurred sometime after the initial rock formation but likely on a time scale greater than 2 Ga. The altered wall rock at 570.07 m BHL may have initially had a similar $^{87}Sr/^{86}Sr$ isotopic ratio to the gypsum of the same fracture (0.70262 - 0.70277) and increased over time due to the presence of thin chlorite seams. The high Rb/Sr ratio of the chlorite would cause a faster rate of increase in the $^{87}Sr/^{86}Sr$ ratio of the chlorite, and thus also the bulk strontium isotope ratio of the altered wall rock, than in the gypsum, which has a very low Rb/Sr ratio.

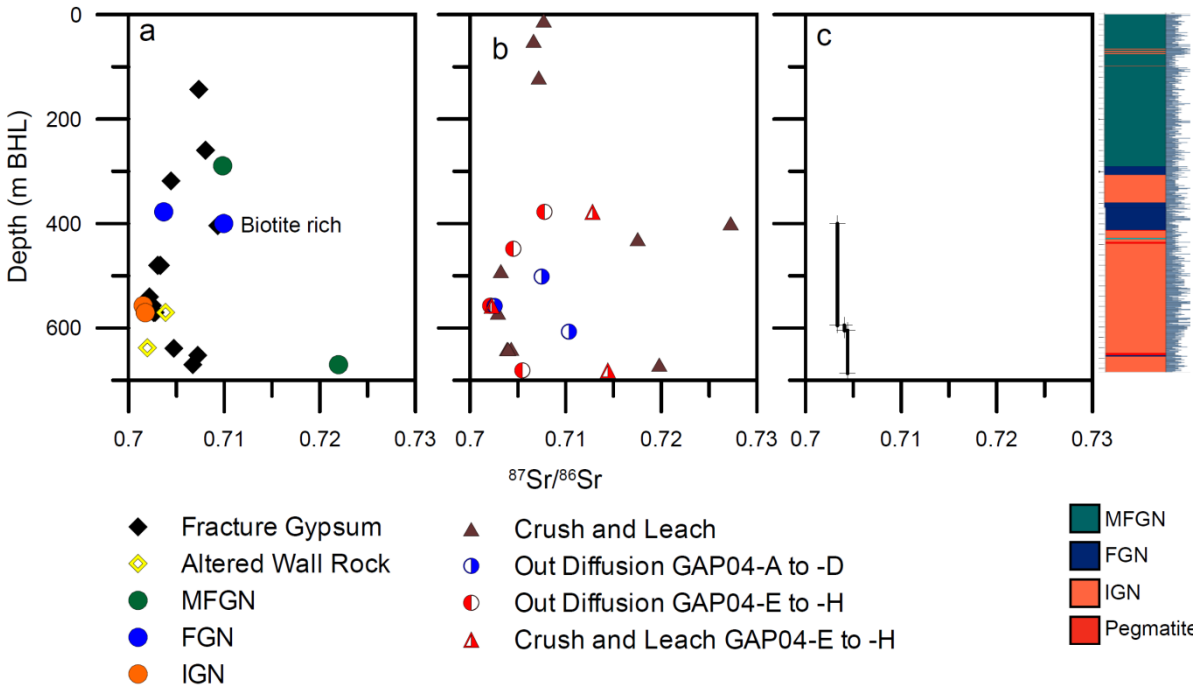

Figure 4.17. Strontium isotopic composition of DH-GAP04 for (a) whole rock, altered wall rock and gypsum, (b) porewaters and (c) groundwaters. MFGN = mafic garnet bearing gneiss, FGH = felsic gneiss, IGN = intermediate gneiss. Fracture frequency is shown along the right side of the borehole log.

Altered wall rock of a fracture at 638 m BHL also had a low $^{87}Sr/^{86}Sr$ isotopic ratio (0.70196), indicating again that the event that caused the alteration of the fracture wall was likely greater than 2 Ga.

4.4.3.3 Strontium Isotopic Composition of Gypsum

Further, information on the approximate age of gypsum may be inferred from the $^{87}Sr/^{86}Sr$ ratio. Gypsum is a Rb-poor mineral because Sr^{2+} substitutes readily for Ca^{2+} while Rb^{+} does not. Due to its low Rb/Sr ratio, gypsum reflects the $^{87}Sr/^{86}Sr$ isotopic signature at the time of mineral precipitation. Thus, the $^{87}Sr/^{86}Sr$ signature of gypsum may indicate the strontium isotopic signature of past fluids from which the fracture mineral precipitated. A gypsum precipitated from an old (Archean/Paleaoproterozoic) hydrothermal fluid at equilibrium with the rock will have a low/non-radiogenic $^{87}Sr/^{86}Sr$ isotopic signature on the order of 0.701-0.702 (Ruiz et al., 1984; Hattori & Cameron, 1986; McNutt et al., 1990). A gypsum precipitated from a more modern fluid would have a higher $^{87}Sr/^{86}Sr$ value that resembles modern day whole rock values, which range from 0.70151 to 0.72196 and may potentially also include a more radiogenic (0.72-0.76, see Chapter 2) surface water signature.

The $^{87}Sr/^{86}Sr$ of gypsum from the Eye-Dashwa Lakes pluton (0.704 - 0.707) (Peterman et al., 1990) also fell within a similar range to the DH-GAP04 gypsum (0.702 - 0.709). The $^{87}Sr/^{86}Sr$ isotopic composition of the Eye-Dashwa Lakes pluton is similar to that observed in the present day, deep, saline groundwaters (0.7057 - 0.707), which was derived from long term interaction between the water and plagioclase feldspar and epidote (Franklyn et al., 1991). Shallow groundwaters at the Eye Dashwa Lakes pluton had a modern, radiogenic component (Franklyn et al., 1991). It is quite probable that at the GAP site, the strontium in the gypsum and thus in the groundwater was also initially derived from water-rock interaction, potentially at higher temperatures, with plagioclase.

The $^{87}Sr/^{86}Sr$ isotopic composition of plagioclase in the DH-GAP04 core ranged from 0.70152 - 0.70860 which coincides well with the range of $^{87}Sr/^{86}Sr$ isotopic ratios in the gypsum in the GAP boreholes. The similarities between the GAP gypsum and the Eye Dashwa Lakes pluton provides additional support to an old origin to the gypsum rather than a modern, in-situ freeze-out origin.

In general, the gypsum in the mafic sections (0.70672 - 0.70803) are less radiogenic than the mafic whole rock $^{87}Sr/^{86}Sr$ isotopic ratio (0.70985 and 0.72196) (Figure 4.17), suggesting the gypsum was not precipitated from a modern fluid or impacted by infiltration of more radiogenic surface waters.

In the intermediate sections of DH-GAP04, a low, non-radiogenic strontium isotopic ratio is observed in both the gypsum and the whole rock (<0.704)(Figure 4.17). The more massive, intermediate gneiss section between 400 and 625 m BHL has the most homogoenous and least radiogenic $^{87}Sr/^{86}Sr$ isotopic ratio in both the fracture minerals and unaltered whole rock (0.70151 - 0.70332)(Figure 4.17). Generally in this case it is difficult to comment on the origin of the gypsum based on the strontium isotopic ratio alone.

4.4.3.4 Sulfur and Oxygen Isotopic Composition of Gypsum

The $\delta^{34}S$ isotopic composition of sulfate in hydrothermal systems has a broad range of values (see below), however it tends towards enriched values greater than +5 ‰. Hattori and Cameron (1986) and Fritz et al. (1994) determined a range of +8 to +14 for $\delta^{34}S$ (SO_4) for magmatic-hydrothermal sulfate formed in aqueous fluids. Marini et al. (2011) found that $\delta^{34}S$ (SO_4) isotopic values in modern hydrothermal systems fell predominantly between +13 to +23 ‰, however isotopic values down to -2 ‰ were noted. In the Eye-Dashwa Lakes pluton, Kamineni (1983) found the $\delta^{34}S$ (SO_4) of fracture gypsum ranged from +5.3 to +8.5 ‰, very similar to the range observed in the DH-GAP04 gypsum. Kamineni (1983) suggested that while the gypsum was precipitated at lower

temperatures (<100 °C), the sulfate in the parent fluid was a combination of hydrothermal sulfate and sulfate derived from the oxidation of pyrite in the host rock. The $\delta^{34}S$ (SO_4) of the GAP fracture gypsum (+3.22 to +10.65 ‰)(Figure 4.13) falls into the lower end of the range observed in dissolved sulfate and sulfate mineral phases of hydrothermal origin (Kamineni & Stone, 1983; Hattori & Cameron, 1986; Fritz et al., 1994; Marini et al., 2011).

As discussed in Section 4.4.2 the $\delta^{34}S$ (SO_4) of the gypsum (3.22 to 10.65 ‰) is too enriched for the sulfate to be solely derived from sulfides within the rock matrix. However, with the similarity of the lower range of $\delta^{34}S$ (SO_4) isotopic values of fracture filling gypsum to the $\delta^{34}S$ of sulfides (+2.26 to +3.73 ‰), it is plausible that, similar to the Atikokan site, some of the sulfate was acquired from local sulfides.

The $\delta^{18}O$ (SO_4) of the fracture gypsum from DH-GAP04 varies over a range of +4.48 to +9.09‰. $\delta^{18}O$ (SO_4) values of hydrothermal sulfates are generally reported to be near +10 ‰ (Fritz et al., 1994). Variations in $\delta^{18}O$ (SO_4) may be related to:

- Changes in the fractionation factor between $\delta^{18}O$ (H_2O) and $\delta^{18}O$ (SO_4) with temperature (Chiba & Sakai, 1985).
- Post-depositional changes caused by SO_4^{2-}-H_2O exchange under metamorphic conditions (Boschetti et al., 2011)
- Separate hydrothermal events with different $\delta^{18}O$ (SO_4).

At low temperatures, isotopic exchange of oxygen between H_2O and dissolved SO_4^{2-} is extremely slow (Seal et al., 2000), thus the variations in $\delta^{18}O$ (SO_4) are unlikely to be related to exchange under the low-temperature conditions that currently exist at the site. Additionally, the very low water content of the rock limits the reservoir of exchangeable $\delta^{18}O$.

4.4.3.5 Impact of Gypsum Dissolution and Sulfide Oxidation on Groundwater

The characterization of hydrothermal gypsum discussed in the previous section can be used to further examine the impact of gypsum dissolution and sulfide oxidation on groundwater chemistry. Intermediate groundwaters from DH-GAP01 have $\delta^{34}S$ and $\delta^{18}O$ (SO_4) consistent with sulfate derived from dissolution of gypsum from fractures and pore space, a non-fractionating process. Deep groundwaters from DH-GAP04 also have a $\delta^{34}S$ (SO_4) consistent with the fracture mineral sulfate isotopic signature, however the $\delta^{18}O$ (SO_4) of the deep groundwater is depleted relative to the range covered by fracture gypsum. Possible explanations for the depletion in $\delta^{18}O$ (SO_4) of the deep groundwaters were given in Chapter 3 (Section 3.5.2). Briefly: exchange between $\delta^{18}O$ (SO_4) and $\delta^{18}O$ (H_2O) is unlikely under modern, low temperature conditions. However, a secondary source of sulfate with a depleted $\delta^{18}O$ (SO_4) signature may explain the groundwater sulfate isotopic composition. Possible sources included (1) pyrite oxidation where the oxygen is derived from H_2O and any O_2 present and (2) fracture gypsum with a more depleted $\delta^{18}O$ (SO_4) signature that may be present elsewhere in the flow system. While (2) is impossible to rule out with the available data, the plausibility of (1) is explored further below.

It seems entirely plausible that the groundwater SO_4^{2-} is a mixture between SO_4^{2-} derived from oxidation of sulfides and, predominantly, from dissolution of fracture gypsum. Using the range of $\delta^{18}O$ (SO_4) values calculated in Section 4.4.2. for pyrite oxidation, the percentage of SO_4^{2-} in groundwater derived from pyrite oxidation can be calculated as 13 to 45% (Figure 4.18). Likely the percentage of $\delta^{18}O$ (SO_4) derived from pyrite oxidation is less than 20% as higher values of Y (Equation 4.1) are most likely in groundwater.

A large shift was observed in the $\delta^{18}O$ (SO_4) of DH-GAP04 Low between 2011 (5.47 ‰) to 2013 (3.27 ‰). This isotopic shift accompanies a large reduction in drilling water contamination from 99% to <5% drilling water in DH-GAP04 Low. Likely the depletion in $\delta^{18}O$ (SO_4) from 2011 to 2013 represents removal of drilling water containing SO_4^{2-} derived from fracture gypsum dissolved during drilling to more natural groundwater conditions where sulfate is a product of both gypsum dissolution and pyrite oxidation.

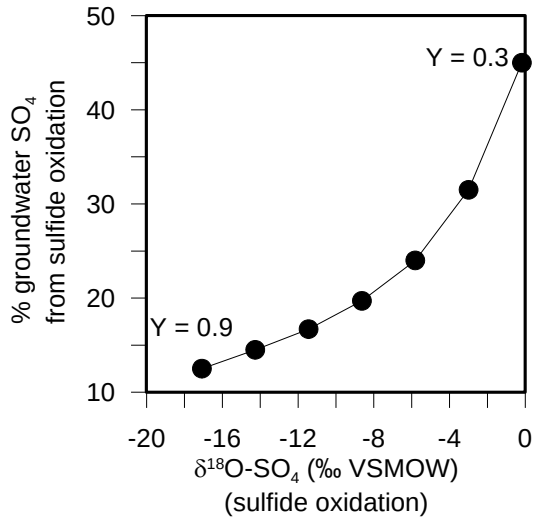

Figure 4.18. The range of potential isotopic values for $\delta^{18}O$ (SO_4) derived from oxidation of sulfides (x-axis) was calculated using equation 4.3 with Y ranging from of 0.3 to 0.9. The SO_4^{2-} in groundwater was considered a mixture of two end members: (1) SO_4^{2-} from sulfide oxidation and (2) SO_4^{2-} from gypsum dissolution (using average value of d18O (SO_4) of 6.4 ‰). The Y-axis represents the % of sulfate in groundwater derived from oxidation of sulfides that corresponds to a particular value of $\delta^{18}O$ (SO_4) for sulfate derived from sulfide oxidation.

Analysis of gypsum dissolved in ultrapure water revealed a trend of increasing Cl^- contents with depth, reaching a maximum of 1.5 x 10^{-2} mmol of Cl^- per mmol of gypsum dissolved (Table 4.9). Cl- content per mmol of gypsum dissolved was calculated using Equation 4.4 and by assuming that all SO_4^{2-} in the sample (mmol/mg sample dissolved) was derived from gypsum dissolution.

$$\frac{Cl^-_{(mmol)}}{gypsum_{(mmol)}} = \frac{Cl^-_{(\frac{mmol}{mg})}}{{SO_4}^{2-}_{(\frac{mmol}{mg})}} \qquad [4.4]$$

Using the maximum Cl^- concentration found in the fracture gypsum and the SO_4^{2-} concentration in the DH-GAP04 Low groundwaters, it can be extrapolated that a maximum of approximately 11 mg/L (6%) of the Cl^- in the DH-GAP04 groundwaters comes from dissolution of fracture gypsum.

4.4.4. Matrix Porewaters and Water Rock Interaction

Matrix porewaters analyzed in the GAP drill core had significantly higher salinities than measured in the groundwater found in fractures in DH-GAP01 and DH-GAP04 (Figure 4.11). High concentrations of $SO4^{2-}$ and Ca^{2+} in DH-GAP04 at the permafrost boundary (400 m BHL) (Figure 4.11) were especially significant as in-situ freeze out may create a high salinity cryopeg at the base of permafrost (van Everdingen, 1990; Gascoyne, 2000; Alexeev & Alexeeva, 2002). A cryopeg is an unfrozen layer of ground that exists within permafrost (i.e. where the ground temperature is below 0 °C) but is kept unfrozen by freezing point depression caused by high salinity. The source of salinity in the porewaters is explored below along with potential impact of porewater salinity on fracture groundwater chemistry.

As previously discussed, high concentrations of $SO4^{2-}$ and Ca^{2+} in matrix pore fluid experiments (crush and leach and out diffusion) were attributed to dissolution of gypsum found within the rock matrix. $^{87}Sr/^{86}Sr$ isotopic ratios in matrix porewaters were often similar to those of fracture gypsum found at similar depths (Figure 4.17).

Br/Cl meq ratios in porewaters from DH-GAP01, DH-GAP03 and DH-GAP04 are most likely related to rock type (Figure 4.19). It was noted that mafic gneisses tend to have lower Br/Cl ratios (<0.006) than felsic and intermediate gneisses in this study. While Br^- results in the DH-GAP04 crush and leach and out diffusion experiments were limited (poor or non-detect results), the available results are similar to Br/Cl ratios observed in crush and leach experiments on felsic gneiss in DH-GAP01 and DH-GAP03 (0.006-0.007). However, Br/Cl ratios measured in the eluate solutions of out

diffusion experiments performed on intermediate and felsic gneiss in the DH-GAP04 borehole by Eichinger and Waber (2013) were lower than those observed in other porewater experiments on the GAP boreholes involving the same gneissic rock types (Figure 4.19). Br/Cl ratios observed in porewaters at the GAP site (0.003-0.009) are similar to those observed in groundwaters at other shield sites by Stotler et al. (2010), which predominantly fell between 0.001 and 0.007.

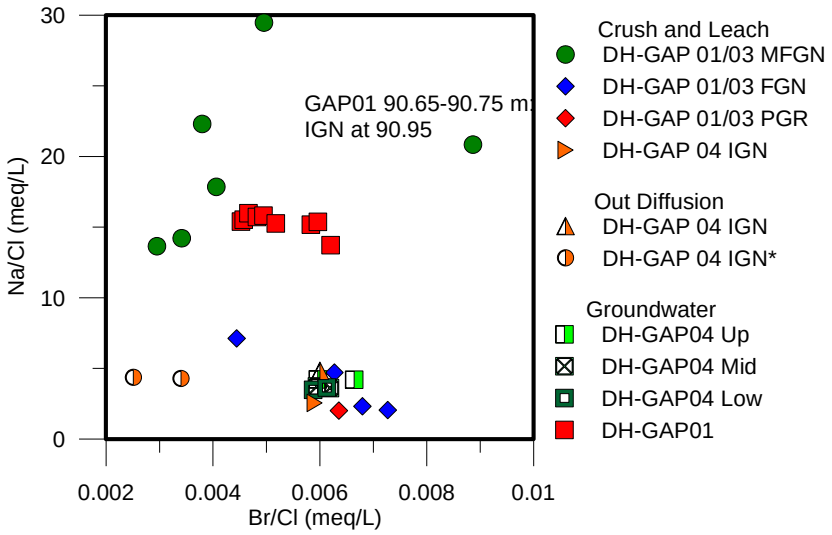

Figure 4.19. Br/Cl vs Na/Cl ratios in groundwaters and porewaters, categorized by lithology. MFGN = mafic garnet bearing gneiss, IGN = intermediate gneiss, FGN = felsic gneiss, PGR = pegmatite. Ion ratios from the final eluate of the out diffusion experiments conducted by Eichinger and Waber (2013) are also included as DH-GAP04 IGN*.

DH-GAP01, DH-GAP03 (Figure 4.19) and DH-GAP04 porewaters from out diffusion and crush and leach experiments also had a wide range of Na/Cl meq ratios, from 2 to 61. High Na/Cl ratios were observed in both out diffusion and crush and leach experiments (Appendix B). Na/Cl ratios in the DH-GAP01 and DH-GAP03 porewaters and the DH-GAP01 groundwaters are significantly higher than those observed in shield groundwaters. Stotler et al. (2010) document that Na/Cl ratios in groundwaters from the Canadian and Fennoscandian Shields tend to be less than 2.5, with a maximum Na/Cl ratio of 7.5. In matrix fluid experiments (crush and leach) on Äspö diorite and Ävrö

granite in at the Äspö Hard Rock Laboratory in Sweden, Br/Cl ratios covered a similar range to those observed in this study (0.002 to 0.01 meq ratio). However, Smellie et al. (2003) also found lower Na/Cl meq ratios, which ranged from 1.8 to 3 for experiments on size fractions <0.5 mm and from 6 to 8 in size fractions ranging from 1 to >3 mm (Smellie et al., 2003). High Na/Cl ratios in porewaters and groundwaters appear to be characteristic of the GAP site. Mirabilite ($NaSO4 \bullet 10H_2O$) is associated with cold climate conditions (Matsubaya et al., 1979; Bottomley et al., 1999; Smellie et al., 2002; Alexeev & Alexeeva, 2003); however mirabilite was not observed in any of the mineralogical analyses performed on the GAP drill core (Sections 4.3.1 and 4.3.2). The Na^+ may be derived from plagioclase feldspar, which was previously discussed in the context of the gypsum $^{87}Sr/^{86}Sr$ isotopic ratio in Section 4.4.3. Alteration of plagioclase was considered an important part of forming the Na-SO_4 groundwaters at Palmottu, Finland, which were associated with paleo hydrothermal activity (Smellie et al., 2002).

Stotler et al.(2012) describe the effect of solute exclusion on Ca dominated fluids as causing an increase in both the Na/Cl and Br/Cl ratio in the residual fluids as freezing progresses. Na-dominated fluids tend to show little or no change in the Na/Cl or Br/Cl ratio. The difference in fluid evolution between Na dominated and Ca dominated fluids is the result of the precipitation of calcite ($CaCO_3$), ikaite ($CaCO_3 \bullet 6H_2O$) and gypsum ($CaSO_4 \bullet 2H_2O$) during freezing (Zhang & Frape, 2003; Stotler et al., 2012). A Ca-Na water such as those observed at the GAP site is predicted to evolve along a trend somewhere between that predicted for Na vs Ca dominated fluids (Zhang & Frape, 2003; Stotler et al., 2012). Significant increases in Na/Cl ratios were not observed in any of the freezing experiments, suggesting that in-situ freeze out is an unlikely mechanism for producing the high Na/Cl ratios measured in porewaters and groundwaters in this study.

Groundwaters in the DH-GAP01 borehole show small variations in Br/Cl vs Na/Cl ratio, as well as many other chemical and isotopic parameters. The DH-GAP01 groundwaters have Br/Cl ratios that cover a similar range to porewaters from both mafic and felsic rocks (Figure 4.19). DH-GAP01 groundwaters high a higher Na/Cl ratio than DH-GAP04. In DH-GAP01 and DH-GAP03 higher porewater Na/Cl ratios were associated with mafic gneiss, however in DH-GAP04 high Na/Cl ratios up to 46 (meq) were also observed in intermediate gneiss samples (Appendix B, Table B-12). Thus, it is hard to draw any conclusions on Na/Cl ratios and rock type apart from that high Na/Cl ratios are observed in both groundwaters and porewaters relative to those observed at the majority of other shield locations (Stotler et al., 2012)(Section 3.5.4).

Groundwaters from the DH-GAP04 and DH-GAP01 boreholes have similar Br/Cl meq ratios (Figure 4.19). The values are similar to ratios observed for porewaters (crush and leach and out diffusion experiments) (Figure 4.19). It seems likely that the bulk of the Br^- and Cl^- present in the groundwater is derived from diffusive exchange with rock porewaters and water-rock interaction. The importance of matrix porewaters on Cl^- concentrations is supported by the minimal contribution of Cl^- from gypsum dissolution as discussed in Section 4.4.3.5.

Typically, $\delta^{37}Cl$ isotopic values in shield environments fall within ±1 ‰ of ocean chloride (0 ‰) (Stotler et al., 2010). $\delta^{37}Cl$ values observed in porewaters, groundwaters and fracture filings at the GAP site (-0.6 - +0.68 ‰) fall within the typical range. DH-GAP04 groundwaters were relatively enriched in $\delta^{37}Cl$, similar to matrix porewaters $\delta^{37}Cl$ isotopic values at similar depths to the upper (400 to 594 mbhl) and middle (594 to 604 mbhl) groundwater sampling intervals (Figure 4.14). The similarity between the porewater $\delta^{37}Cl$ values and the groundwater $\delta^{37}Cl$ isotopic signature suggests long term water-rock interaction similar to that observed at other crystalline rock sites (Sie & Frape, 2002; Stotler et al., 2010). The influence of porewaters on groundwater chloride is further

illustrated on a plot of $\delta^{37}Cl$ versus Cl^- concentration (Figure 4.20): DH-GAP04 groundwaters appear to fall between two end members: (1) low Cl^- concentrations and $\delta^{37}Cl$ isotopic values close to 0 ‰ that characterize the shallow groundwater of DH-GAP01 and surface waters and (2) the high Cl^- concentrations and enriched $\delta^{37}Cl$ isotopic values found in porewaters between 377 and 600 mbhl (Figure 4.20).

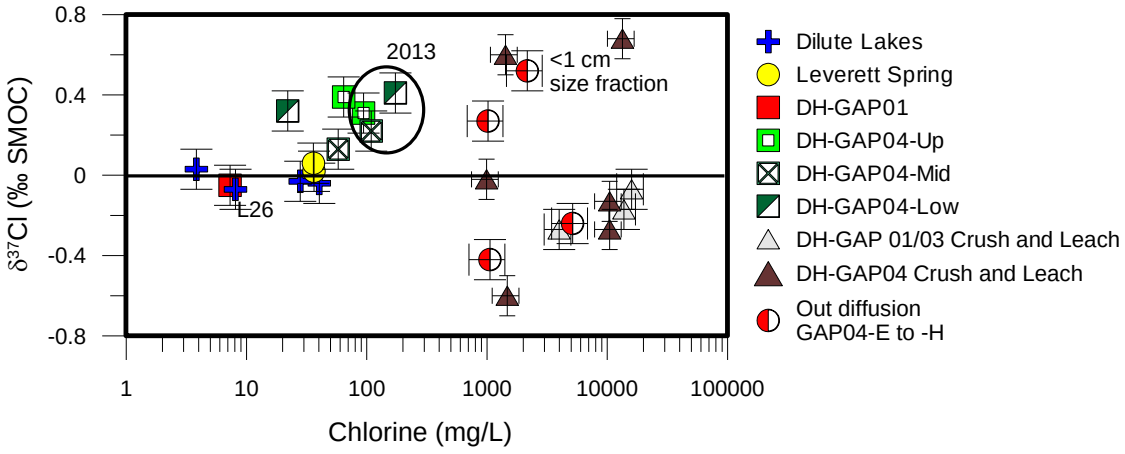

Figure 4.20. Isotopic composition and concentration of chloride in groundwater, surface waters and porewaters. Circled groundwater values represent the most recent groundwater samples (2013). Crush and leach experiments may introduce additional Cl^- from fluid inclusions.

A relationship between the $\delta^{37}Cl$ isotopic composition of porewaters and rock type is not readily apparent (Figure 4.14). Depleted chlorine-37 isotopic values occur in both mafic and intermediate sections of the DH-GAP04 core (Figure 4.14). $\delta^{37}Cl$ isotopic values are also not well correlated to porewater Cl^- concentrations (Figure 4.20). There may be a trend of increasing enrichment of $\delta^{37}Cl$ with increasing Cl^- concentration in porewaters wtih $\delta^{37}Cl < 0$ ‰, however it is not clear why this might be. The difference between $\delta^{37}Cl$ isotopic composition between out diffusion experiments and crush and leach experiments on the same sections of core suggest that $\delta^{37}Cl$ of crush and leach experiments are impacted by the introduction Cl^- with a depleted $\delta^{37}Cl$ signature from fluid inclusion breakage (Figure 4.14). Crush and leach experiments on different size fractions of core (see

Appendix C, Section C.3.1) (DH-GAP04 399.84 m) also showed enriched $\delta^{37}Cl$ values in the larger size fraction sample (1-6 cm pieces) (+0.68 ‰) compared to the milled fraction (-0.51 ‰)(Figure 4.14).

Two of the DH-GAP04 crush and leach samples were analyzed for $\delta^{81}Br$ (Table 4.17) with results of 0.64 and 0.67 ‰. Groundwaters also had enriched $\delta^{81}Br$ isotopic signatures (0.29 to 0.55 ‰). These positive values are typical of waters in shield environments which to date are reported in the literature as being enriched: +0.01 to +2.04 ‰ (Stotler et al., 2010). Enriched $\delta^{81}Br$ isotopic signatures are likely associated with long term water-rock interaction in shield environments (Stotler et al., 2010).

4.5. Summary and Conclusions

In Chapter 3 it was established that DH-GAP04 groundwater found in fractures below the permafrost boundary (~350 m depth) were intruded glacial meltwaters. Glacial meltwater is extremely dilute in nature and thus most of the solutes in the DH-GAP04 groundwater must be leached from the rock, derived from gypsum dissolution or diffused from porewaters. Comparison of the rock matrix, fracture mineral and porewater geochemical and isotopic composition to that of groundwater allows for further insight into the evolution of groundwater chemistry.

Borehole groundwaters from DH-GAP 01 and DH-GAP 04 have low concentrations of REE compared to the rock matrix and fracture gypsum, with a slight enrichment in the middle rare earth elements (Figure 4.15). Low temperature groundwaters with neutral pH will not readily leach REE from the rock matrix (Michard, 1989; Bau, 1991; Fulignati et al., 1999). The low REE concentrations of the borehole groundwaters reflect the modern, low temperature conditions encountered by the meltwater recharge (Figure 4.15).

Water-rock interaction involving Shield brines often imparts characteristic $^{87}Sr/^{86}Sr$ signatures related to the rock or its mineral components. (Frape et al., 1984; McNutt et al., 1984, 1990). DH-GAP04 groundwaters do not reflect the whole rock $^{87}Sr/^{86}Sr$ values but are likely equilibrating with a smaller selection of mineral phases (McNutt et al. 1984; McNutt et al., 1990). Figure 4.17 indicates that $^{87}Sr/^{86}Sr$ isotopic signature of the groundwater corresponds well to the strontium isotopic ratio of the gypsum found within the groundwater sampling sections of DH-GAP04 (Figure 4.17). The good correlation between Ca^{2+} and Sr^{2+} in the groundwaters and the importance of gypsum dissolution to the groundwater chemistry (See Chapter 2) suggests that the majority of groundwater Sr^{2+} comes from gypsum dissolution and this is reflected in the strontium isotopic signature. The gypsum $^{87}Sr/^{86}Sr$ isotopic signature may reflect a fluid that has a strontium isotopic signature resulting from interaction with plagiocalse feldspar (see Section 4.4.3.3.).

Permafrost formation has the potential to alter the geochemical and isotopic composition of groundwaters and porewaters through solute exclusion/in-situ freeze out. It was found that there was no evidence that in-situ freeze out had notably impacted the groundwaters or porewaters in the GAP research boreholes. Trends in ion concentrations with depth (Figures 4.9, 4.10 & 4.11) are not consistent with an in-situ freeze-out scenario for generation of salinity. In many cases, changes in matrix salt composition and concentration (e.g. Ca^{2+}, SO_4^{2-}, Na/Cl and Br/Cl meq ratios) correspond to changes in rock type and rock chemical changes. Cl^- in groundwater is derived from water-rock interaction, similar to other shield sites, and exchange with higher salinity porewaters with an enriched $\delta^{37}Cl$ isotopic signature as well as minor contributions (maximum 6 %) from dissolution of fracture minerals. Cl^- in groundwater was considered unlikely to be related to in-situ freeze-out. The isotopic composition of SO_4^{2-} of gypsum, which differs from what would be expected for SO_4^{2-} derived from pyrite oxidation, suggested that gypsum precipitation is not related

to modern, cold climate conditions. The low $^{87}Sr/^{86}Sr$ isotopic ratios of gypsum suggested that it was not precipitated from a modern fluid and thus were also supportive of an older origin for gypsum.

High sulfate concentrations in groundwaters are related to the presence of gypsum in fractures and the rock matrix. However, the $\delta^{34}S$ and $\delta^{18}O$ of SO_4^{2-} in groundwaters suggests that 13 - 20% of groundwater SO_4^{2-} may also be derived from pyrite oxidation during relatively modern groundwater circulation. The gypsum is attributed to a hydrothermal in origin and is pervasive in fractures and the rock matrix in DH-GAP04 below 300 m BHL. In other sections of the DH-GAP04 core and in DH-GAP01, DH-GAP03 gypsum is absent in both fractures and the rock matrix and relic open porosity from dissolution processes were not found. This seems to indicate that gypsum was not precipitated in these sections of rock. In the Canadian Shield at Atikokan, Kamineni (1983) found that gypsum filled fractures were highly impermeable and had remained stable over potentially very long time periods (Precambrian). The stability of the gypsum was attributed to equilibration of the porewaters with the gypsum and a lack of groundwater circulation through gypsum filled fractures. This stability was maintained through marine transgressions in the Paleozoic and beyond as well as glaciations. Similarly, it appears that gypsum filled fractures at the DH-GAP04 borehole have remained stable over a long time period (Section 4.4.3.) and are not related to modern groundwater circulation. Furthermore, the continued presence of gypsum at both the GAP site and the Atikokan study site (Kamineni, 1983) suggests that ice sheet induced meltwater circulation has not disturbed large sections of the rock matrix porosity and parts of the groundwater system sufficiently to dissolve gypsum and activate these sealed fractures.

5. Conclusions

Currently, geochemical and isotopic information concerning groundwater chemistry and movement adjacent to a continental scale ice sheet is very limited. It is anticipated that subglacial meltwater will infiltrate into the subsurface beneath the wet based portions of a glacier but evidence in a modern glacial system was lacking. This thesis provided a first look at groundwater geochemical and isotopic compositions immediately adjacent to a continental scale ice sheet. Surface water, groundwater and drill core studies were used to examine the impact that glaciation and permafrost have on surface and groundwater geochemical and isotopic composition.

Surface water studies in the Kangerlussuaq region had previously assumed that groundwater discharge into lakes was limited (Anderson et al., 2001). However, it had also been suggested that groundwater discharge of potentially significant volume or salinity will occur in lakes in the periglacial area in front of continental ice sheets (Boulton et al., 1996; Starinsky & Katz, 2003; Lemieux et al., 2008). An extensive survey of lakes in the Kangerlussuaq region found no geochemical evidence for significant groundwater discharge into lakes via taliks. Hydrogeologic and geochemical evidence at DH-GAP01 indicated that recharge conditions were present between the Talik Lake (L26) and the DH-GAP01 borehole at the present time. Recharge conditions between lakes and the groundwater system could also be an ongoing process and therefore help explain the lack of observable groundwater discharge into lakes. The presence of recharge conditions at DH-GAP01 was unanticipated due to the prediction that groundwater discharge would be occurring at the front of the ice sheet.

Isotopic evidence provided new insight into the impact of glaciation, permafrost and climatic conditions on the geochemical evolution of lakes in the Kangerlussuaq region. Previous work on

weathering in glacial environments (Blum & Erel, 1995, 1997; Anderson et al., 1997; Sharp et al., 2002) has shown that enhanced biotite weathering may be responsible for highly radiogenic $^{87}Sr/^{86}Sr$ isotopic signatures in natural waters associated with glacially comminuted sediment. Previously this theory had not been applied to surface waters in Greenland. It was found in this study that lakes in more recently deglaciated terrain, with plentiful fresh, glacial sediment, had more radiogenic $^{87}Sr/^{86}Sr$ isotopic signatures than lakes located further from the ice margin in terrains with more developed soil and vegetation cover. These findings support enhanced weathering of more radiogenic mineral phases such as biotite in glacial environments. Rapid melting of the ice sheet in the study area and increased runoff from the Greenland Ice Sheet could have possible implications for the impact of recently exposed glacial sediments on the marine $^{87}Sr/^{86}Sr$ record (Hodell et al., 1991; Anderson et al., 1997; Zachos et al., 1999.

Relative distance from the ice margin, time since deglaciation and proximity to the coast also affects sulfur sources and processes in lakes. In more recently deglaciated areas, sulfide oxidation is the main source of sulfate in lakes. With warmer temperatures and increased productivity in lakes further from the ice margin, bacterial sulfate reduction increases around the head of Søndre Strømfjord. Marine aerosols become an increasingly important source of sulfate closer to the coast.

Evaporation was found to be a key process in lake geochemical evolution and increases with distance from the coast. However, permafrost and active layer hydrology may impact the isotopic ($\delta^{18}O$, $\delta^{2}H$ and ^{3}H) composition of lakes, obscuring the positive relationship between isotopic enrichment and electrical conductivity/salinity during evaporation.

Borehole groundwaters were found to be isotopically ($\delta^{18}O/\delta^{2}H$) depleted relative to modern meteoric waters and were similar in isotopic composition to glacial meltwaters. The isotopic composition of groundwaters in the GAP study area suggests recharge of glacial meltwater to a

depth of at least 570 m. Recharging meltwaters are initially very dilute but evolve to brackish Ca-Na-SO_4 waters through water-rock interaction and dissolution of gypsum, found as a ubiquitous fracture and matrix filling below 300 m BHL in DH-GAP04. It was found that, based on the $\delta^{34}S$ and $\delta^{18}O$ (SO_4) isotopic composition of groundwaters, 13-20% of SO4 in the DH-GAP04 groundwaters may be derived from oxidation of sulfides during modern groundwater circulation. The lack of enrichment in the $\delta^{34}S$ isotopic composition supports microbiological evidence (Harper et al., 2015b) showing sulfate reducing bacteria were not active in borehole groundwaters. In-situ freeze out during permafrost formation was considered unlikely based the $\delta^{18}O$ isotopic composition, Cl^- concentration and ionic ratios of groundwaters. However, the continued presence of drilling fluid in the upper and middle sections of the DH-GAP04 borehole prevented definitive conclusions on the impact of in-situ freeze out on groundwater geochemical evolution at this time.

In-situ freeze-out was not found to impact matrix pore fluid chemistry and variations in pore fluid chemistry were often related to rock type. Porewaters had similar $\delta^{37}Cl$, $\delta^{81}Br$ isotopic compositions and Br/Cl ratios as found in other shield environments (Stotler et al., 2010, 2012). High Na/Cl ratios, in many cases much higher than previously documented in shield environments (Stotler et al., 2012), were found in borehole groundwaters and porewaters. One possible explanation for high Na/Cl ratios is interaction between groundwater and plagioclase, possibly under high temperature paleo-hydrothermal conditions. This was found to be the case at Palmottu, Finland where high Na/Cl ratios were also observed (Smellie et al., 2002).

Freezing experiments by Zhang and Frape (2003) showed that gypsum may precipitate from freezing impacted fluids. Thus it was considered important to determine the origin of gypsum, a highly soluble mineral phase, found extensively in the DH-GAP04 borehole. Fracture mineral investigations showed that gypsum was related to an older hydrothermal event based on gypsum

morphology, chemistry (REE) and isotopic composition ($\delta^{34}S$ and $\delta^{18}O$ of SO_4 and $^{87}Sr/^{86}Sr$). It appears that gypsum filled fractures at the DH-GAP04 borehole have remained hydrogeochemically stable over a long time period and are not impacted to any great extent by modern groundwater circulation. Furthermore, the continued presence of gypsum at both the GAP site and the Atikokan study site (Kamineni, 1983) suggests that ice sheet induced meltwater circulation has not disturbed large sections of the rock matrix porosity and parts of the groundwater system sufficiently to dissolve gypsum and activate these sealed fractures. This has implications for the extent to which glaciation may perturb the groundwater system in crystalline rock environments, especially where secondary minerals are present to seal fracture and matrix porosity.

This study contributes new data and scientific understanding in the follow areas:

- Glacial meltwater penetration beneath an ice sheet in a crystalline rock environments.
- The role of taliks in groundwater systems adjacent to an ice sheet.
- The lack of microbiologically enhanced sulfate reduction in cold climates and in a sulfate rich environment with implications to redox conditions in cold climate conditions.
- Gypsum mineralizations in crystalline rock environments and the implications for the stability of groundwater systems during continental scale glaciations.
- Groundwater salinity, chemical and isotopic composition and matrix porewater composition and stability under glacial and permafrost conditions.
- The role of enhanced biotite weathering on surface water $^{87}Sr/^{86}Sr$ isotopic signatures in recently deglaciated terrain in Greenland.

References

Aebly, F.A. & Fritz, S.C. (2009). Palaeohydrology of Kangerlussuaq (Søndre Strømfjord), West Greenland during the last ~ 8000 years. *The Holocene.* 19 (1). p. 91–104.

Alexeev, S. V. & Alexeeva, L.P. (2002). Ground ice in the sedimentary rocks and kimberlites of Yakutia, Russia. *Permafrost and Periglacial Processes*. 13 (1). p. 53–59.

Alexeev, S. V. & Alexeeva, L.P. (2003). Hydrogeochemistry of the permafrost zone in the central part of the Yakutian diamond-bearing province, Russia. *Hydrogeology Journal*. 11 (5). p. 574–581.

Alexeev, S.V., Alexeeva, L.P., Borisov, V.N., Shouakar-Stash, O., Frape, S.K., Chabaux, F. & Kononov, A.M. (2007). Isotopic composition (H, O, Cl, Sr) of ground brines of the Siberian Platform. *Russian Geology and Geophysics*. 48 (3). p. 225–236.

Allen, A.C.R., O'Brien, R.M.G. & Sheppard, S.M.F. (1976). The chemical and isotopic characteristics of some Northeast Greenland surface and pingo waters. *Arctic and Alpine Research*. 8 (3). p. 297–317.

Andersen, D.T., Pollard, W.H., McKay, C.P. & Heldmann, J. (2002). Cold springs in permafrost on Earth and Mars. *Journal of Geophysical Research*. 107 (E3). p. 1–7.

Anderson, N.J., Harriman, R., Ryves, D. & Patrick, S. (2001). Dominant factors controlling variability in the ionic composition of West Greenland lakes. *Arctic, Antarctic, and Alpine Research*. 33 (4). p. 418–425.

Anderson, N.J. & Brodersen, K.P. (2001). Determining the date of ice-melt for low Arctic lakes along Søndre Strømfjord, southern West Greenland. *Geology of Greenland Survey Bulletin*. 189. p. 54–58.

Anderson, N.J., Fritz, S.C., Gibson, C.E., Hasholt, B. & Leng, M.J. (2002). Lake-catchment interactions with climate in the low Arctic of southern West Greenland. *Geology of Greenland Survey Bulletin*. 191. p. 144–149.

Anderson, N.J. & Leng, M.J. (2004). Increased aridity during the early Holocene in West Greenland inferred from stable isotopes in laminated-lake sediments. *Quaternary Science Reviews*. 23 (7-8). p. 841–849.

Anderson, N.J., Brodersen, K.P., Ryves, D.B., McGowan, S., Johansson, L.S., Jeppesen, E. & Leng, M.J. (2008). Climate versus in-lake processes as controls on the development of community structure in a low-arctic lake (South-West Greenland). *Ecosystems*. 11 (2). p. 307–324.

Anderson, N.J., Liversidge, a. C., McGowan, S. & Jones, M.D. (2012). Lake and catchment response to Holocene environmental change: spatial variability along a climate gradient in southwest Greenland. *Journal of Paleolimnology*. 48 (1). p. 209–222.

Anderson, S.P., Drever, J.I. & Humphrey, N.F. (1997). Chemical weathering in glacial environments. *Geology*. 25 (5). p. 399–402.

Anisimov, O.A., Shiklomanov, N.I. & Nelson, F.E. (1997). Global warming and active layer thickness: results from transient general circulation models. *Global and Planetary Change*. 15. p. 61–77.

Anisimova, N.P. (1980). Hydrogeochemical investigations in permafrost studies. In: *Proceedings of the 3rd International Conference on Permafrost*. 1980, Edmonton, Alberta, p. 25–41.

van As, D., Hubbard, A.L., Hasholt, B., Mikkelsen, A.B., van den Broeke, M.R. & Fausto, R.S. (2012). Large surface meltwater discharge from the Kangerlussuaq sector of the Greenland ice sheet during the record-warm year 2010 explained by detailed energy balance observations. *The Cryosphere*. 6 (1). p. 199–209.

Balci, N., Turchyn, A.V., Lyons, T., Bruchert, V., Schrag, D.P. & Wall, J. (2006). Oxygen isotopic fractionation during bacterial sulfate reduction. In: *American Geophysical Union, Fall Meeting*. 2006, San Francisco, USA, Abstract.

Barker, J.F. & Fritz, P. (1981). Carbon isotope fractionation during microbial methane oxidation. *Nature*. 293. p. 289–291.

Bau, M. (1991). Rare-earth element mobility during hydrothermal and metamorphic fluid-rock interaction and the significance of the oxidation state of europium. *Chemical Geology*. 93 (3-4). p. 219–230.

Bekele, E.B., Rostron, B.J. & Person, M.A. (2003). Fluid pressure implications of erosional unloading, basin hydrodynamics and glaciation in the Alberta Basin, Western Canada. *Journal of Geochemical Exploration*. 78-79. p. 143–7.

Bennike, O. (2000). Palaeoecological studies of Holocene lake sediments from west Greenland. *Palaeogeography, Palaeoclimatology, Palaeoecology*. 155 (3-4). p. 285–304.

Bense, V.F. & Person, M.A. (2008). Transient hydrodynamics within intercratonic sedimentary basins during glacial cycles. *Journal of Geophysical Research*. 113. p. 1–17.

Beschel, R.E. (1963). Sulfur springs at Gypsum Hill. In: F. Muller (ed.). *Jacobesen-McGill Arctic Research Expedition 1959-1962: Preliminary Report 1961-1962*. McGill University, Montreal, Canada, p. 183–187.

Birks, H., Jones, V. & Rose, N. (2004). Recent environmental change and atmospheric contamination on Svalbard as recorded in lake sediments–synthesis and general conclusions. *Journal of Paleolimnology*. 31. p. 531–546.

Blomqvist, R., Ruskeeniemi, T., Kaija, J., Ahonen, L., Paananen, M., Smellie, J., Grundfelt, B., Pedersen, K., Bruno, J., Perez del Villar, L., Cera, E., Rasilainen, K., Pitkanen, P., Suksi, J., Casanova, J., Read, D. & Frape, S. (2000). *The Palmottu natural analogue project, Phase II: Transport of radionuclides in a natural flow system at Palmottu*. Luxembourg. pp.174

Blum, J. & Erel, Y. (1995). A silicate weathering mechanism linking increases in marine $^{87}Sr/^{86}Sr$ with global glaciation. *Nature*. 373 (2). p. 415–418.

Blum, J. & Erel, Y. (2003). Radiogenic isotopes in weathering and hydrology. In: J. I. Drever (ed.). *Treatise on Geochemistry, volume 5*. Amsterdam, Netherlands: Elsevier Ltd, p. 365–392.

Blum, J.D. & Erel, Y. (1997). Rb/Sr isotope systematics of a granitic soil chronosequence: The importance of biotite weathering. *Geochimica et Cosmochimica Acta*. 61 (15). p. 3193–3204.

Bocher, T.W. (1949). Climate, soil and lakes in continental west Greenland. *Medd. om Gronland*. 147 (2). p. 1–63.

Boschetti, T., Cortecci, G., Toscani, L. & Iacumin, P. (2011). Sulfur and oxygen isotope compositions of Upper Triassic sulfates from northern Apennines (Italy): Paleogeographic and hydrogeochemical implications. *Geologica Acta*. 9 (2). p. 129–147.

Bosson, E., Sassner, M., Sabel, U. & Gustafsson, L.-G. (2010). *Modelling of present and future hydrology and solute transport at Forsmark. SKB Report R-10-02*. Stockholm, Sweden. pp. 367.

Bosson, E., Lindborg, T., Berglund, S., Gustafsson, L.-G., Selroos, J.-O., Laudon, H., Claesson, L.L. & Destouni, G. (2013). Water balance and its intra-annual variability in a permafrost catchment: hydrological interactions between catchment, lake and talik. *Hydrology and Earth System Sciences Discussions*. 10 (7). p. 9271–9308.

Bottomley, D.J., Katz, A., Chan, L.H., Starinsky, A., Douglas, M., Clark, I.D. & Raven, K.G. (1999). The origin and evolution of Canadian Shield brines: evaporation or freezing of seawater? New lithium isotope and geochemical evidence from the Slave craton. *Chemical Geology*. 155 (3-4). p. 295–320.

Bouchard, F., Turner, K.W., MacDonald, L.A., Deakin, C., White, H., Farquharson, N., Medeiros, a. S., Wolfe, B.B., Hall, R.I., Pienitz, R. & Edwards, T.W.D. (2013). Vulnerability of shallow subarctic lakes to evaporate and desiccate when snowmelt runoff is low. *Geophysical Research Letters*. 40 (23). p. 6112–6117.

Boulton, G.S., Slot, T., Blessing, A., Glasbergen, P., Leijngen, T. & Van Gijssel, K. (1993). Deep circulation of groundwater in overpressured subglacial aquifers and its geological consequences. *Quaternary Science Review*. 12. p. 739–745.

Boulton, G.S., Caban, P.E. & Van Gijssel, K. (1995). Groundwater flow beneath ice sheets: part 1 - large scale patterns. *Quaternary Science Review*. 14. p. 545–562.

Boulton, G.S., Caban, P.E., van Gijssel, K., Leijnse, A., Punkari, M. & van Weert, F.H. a. (1996). The impact of glaciation on the groundwater regime of Northwest Europe. *Global and Planetary Change*. 12 (1-4). p. 397–413.

Breemer, C.W., Clark, P.U. & Haggerty, R. (2002). Modeling the subglacial hydrology of the late Pleistocene lake Michigan lobe, Laurentide ice sheet. *Geological Society of America Bulletin*. 114. p. 665–674.

Burn, C. & Michel, F. (1988). Evidence for recent temperature-induced water migration into permafrost from the tritium content of ground ice near Mayo, Yukon Territory, Canada. *Canadian Journal of Earth Sciences*. 25. p. 909–915.

Burn, C. (2002). Tundra lakes and permafrost, Richards Island, western Arctic coast, Canada. *Canadian Journal of Earth Sciences*. 39. p. 1281–1298.

Bursey, G.G. (1990). *Geochemical and isotopic investigations in a watershed of the eastern Arctic, Northwest Territories*. MSc Thesis. University of Waterloo.

Bursey, G.G., Edwards, T.W.D. & Frape, S.K. (1991). Hydrology and geochemistry studies, district of Keewatin, Northwest Territories, Canada. *Nordicana*. 54. p. 159–165.

Burton, H.R. & Barker, R.J. (1979). Sulfur chemistry and microbiological fractionation of sulfur isotopes in a saline Antarctic lake. *Geomicrobiology Journal*. 1 (4). p. 329–340.

Canfield, D.E. (2001a). Biogeochemistry of Sulfur Isotopes. *Reviews in Mineralogy and Geochemistry*. 43 (1). p. 607–636.

Canfield, D.E. (2001b). Isotope fractionation by natural populations of sulfate-reducing bacteria. *Geochimica et Cosmochimica Acta*. 65 (7). p. 1117–1124.

Cappelen, J. (ed) (2012). *Weather and climate data from Greenland 1958 - 2011 - Observational data with description. DMI Technical Report 12-15*. Copenhagen, Denmark.

Carey, S.K. & Woo, M.-K. (1998). Snowmelt hydrology of two subarctic slopes, Southern Yukon, Canada. *Nordic Hydrology*. 29. p. 331–346.

Carlson, A., Phillips, F.M., Elmore, D. & Bentley, H.W. (1990). Chlorine-36 tracing of salinity sources in the Dry Valleys of Victoria Land , Antarctica. *Geochimica et Cosmochimica Acta*. 54. p. 311–318.

Cartwright, K. & Harris, H.J.H. (1981). Hydrogeology of the Dry Valley Region, Antarctica. In: L. D. McGinnis (ed.). *Antarctic Research Series Volume 33: Dry Valley Drilling Project*. Washington D.C.: American Geophysical Union, p. 193–214.

Chiba, H. & Sakai, H. (1985). Oxygen isotope exchange rate between dissolved sulfate and water at hydrothermal temperatures. *Geochimica et Cosmochimica Acta*. 49. p. 993–1000.

Chizhov, A.B. (1980). The role of highly mineralized groundwater in the cooling of the lithosphere at depth. In: *Proceedings of the 3rd International Conference on Permafrost*. 1980, Edmonton, Alberta, p. 137–142.

Chizhov, A.B., Chizhova, N.I., Romanov, V.V., Morkovkina, K. & Boyarskiy, O.G. (1985). Tritium analysis in geocryological research. *International Geology Review*. 27. p. 1370–1377.

Claesson Liljedahl, L., Lehtinen, A., Harper, J., Näslund, J.-O., Selroos, J.-O., Pitkänen, P., Puigdomenech, I., Hobbs, M., Follin, S., Hirschorn, S., Jansson, P., Järvinen, H., Kennell, L., Marcos, N., Ruskeeniemi, T., Tullborg, E.-L. & Vidstrand, P. (2015). *Greenland Analogue Project Final Report. SKB Report TR-14-13*. Stockholm, Sweden. pp. 138.

Clark, I. & Fritz, P. (1997). *Environmental isotopes in hydrogeology*. J. Stein & A. W. Starkweather (eds.). New York: Lewis Publishers.

Clark, I., Douglas, M., Raven, K. & Bottomley, D. (2000). Recharge and preservation of Laurentide glacial melt water in the Canadian Shield. *Groundwater*. 38 (5). p. 735–742.

Cohen, D., Person, M.A., Wang, P., Gable, C., Hutchinson, D., Marksamer, A., Dungan, B., Kooi, H., Groen, K., Lizarralde, D. & Evans, R.L. (2009). Origin and extent of fresh Paleowaters beneath the Atlantic continental shelf. *Groundwater*. 48. p. 143–148.

Craig, H. (1963). The isotope geochemistry of water and carbon in geothermal areas. In: E. Tongiorgi (ed.). *Nuclear Geology on Geothermal Areas*. Pisa, Italy: Consiglio Nazionale delle Ricerche, Laboratorio di Geologia Nucleare, p. 17–53.

Cruickshank, J. & Colhoun, E. (1965). Observations on pingos and other landforms in Schuchertdal, northeast Greenland. *Geografiska Annaler. Series A, Physical Geography*. 47 (4). p. 224–236.

Cutler, P.M., MacAyeal, D.R., Mickelson, D.M., Parizek, B.R. & Colgan, P.M. (2000). A numerical investigation of ice-lobe–permafrost interaction around the southern Laurentide ice sheet. *Journal of Glaciology*. 46 (153). p. 311–325.

Dansgaard, W., Johnsen, S., Clausen, H.B., Dahl-Jensen, D., Gunderstrup, N.S., Hammer, C.U., Hvidberg, C.S., Steffensen, J.P., Sveinbjornsdottir, A.E., Jouzel, J. & Bond, G. (1993). Evidence for general instability of past climate from a 250-kyr ice-core record. *Nature*. 364. p. 218–220.

Davis, S.N. (1964). The chemistry of saline waters. In: Krieger, R.A. - Discussion. *Groundwater*. 2 (1). pp. 51.

DeFoor, W., Person, M., Larsen, H.C., Lizarralde, D., Cohen, D. & Dugan, B. (2011). Ice sheet-derived submarine groundwater discharge on Greenland's continental shelf. *Water Resources Research*. 47 (7). p. 1-14.

Desaulniers, D.E., Cherry, J.A. & Fritz, P. (1981). Origin, age and movement of pore water in argillaceous quaternary deposits at four sites in southwestern Ontario. *Journal of Hydrology*. 50. p. 231–257.

Dicken, A.P. (2000). *Radiogenic Isotopic Geology, 'the Rb-Sr-Method'.* New York: Cambridge University Press.

Douglas, M., Clark, I.D., Raven, K. & Bottomley, D. (2000). Groundwater mixing dynamics at a Canadian Shield mine. *Journal of Hydrology*. 235 (1-2). p. 88–103.

Drake, H., Tullborg, E. & MacKenzie, A. (2009). Detecting the near-surface redox front in crystalline bedrock using fracture mineral distribution, geochemistry and U-series disequilibrium. *Applied Geochemistry*. 24 (5). p. 1023–1039.

Drever, J. & Smith, C. (1978). Cyclic wetting and drying of the soil zone as an influence on the chemistry of ground water in arid terrains. *American Journal of Science*. 278. p. 1448–1454.

Eggenkamp, H.G.M. (1994). *The geochemistry of chlorine isotopes*. PhD Thesis. University of Utrecht, the Netherlands.

Eggenkamp, H.G.M., Kreulen, R. & Koster Van Groos, A.F. (1995). Chlorine stable isotope fractionation in evaporites. *Geochimica et Cosmochimica Acta*. 59 (24). p. 5169–5175.

Eggleston, C., Hochella, M.J. & Parks, G. (1989). Sample preparation and aging effects on the dissolution rate and surface composition of diopside. *Geochimica et Cosmochimica Acta*. 53. p. 797–804.

Egorov, K.N., Ushchapovskaya, Z.F., Shvyrev, G.G., Sizykh, U.I., Kadurin, V.A. & Nartova, N.V. (1987). Hexahydrite in the kimberlites of Yakutia. *Transactions of Russian Society of Mineralogy*. 6. p. 718–721 (in Russian).

Eichinger, F. & Waber, H.N. (2013). *Matrix Porewater in Crystalline Rocks : Extraction and Analysis. NWMO Report TR-2013-23*. Toronto, Canada. pp. 106.

Eisner, W., Törnqvist, T., Koster, E., Bennike, O. & van Leeuwen, J.F.N. (1995). Paleoecological studies of a Holocene lacustrine record from the Kangerlussuaq (Søndre Strømfjord) region of West Greenland. *Quaternary Research*. 43. p. 55–66.

Engstrom, D., Fritz, S., Almendinger, J. & Juggins, S. (2000). Chemical and biological lake evolution in recently deglaciated terrain. *Nature*. 408. p. 161–166.

Engström, J., Paananen, M. & Klint, K.E. (2012). *The Greenland Analogue Projet geomodel version 1 of the Kangerlussuaq area on Western Greenland. Posiva Working Report 2012-10*. Olkiluoto, Finland.

Engström, J. & Klint, K.E.S. (2014). Continental Collision Structures and Post-Orogenic Geological History of the Kangerlussuaq Area in the Southern Part of the Nagssugtoqidian Orogen, Central West Greenland. *Geosciences*. 4 (4). p. 316–334.

Epstein, S. & Mayeda, T.K. (1953). Variations of the ^{18}O content of waters from natural sources. *Geochimica et Cosmochimica Acta*. 4. p. 213–224.

Ershov, E.D. & Kondratjeva, K.A. (1996). *Geocryological map of USSR, scale 1:2 500 000*.

van Everdingen, R.O. & Krouse, H.R. (1985). Isotope composition of sulphates generated by bacterial and abiological oxidation. *Letters to Nature*. 315. p. 395–396.

van Everdingen, R.O. (1990). Ground-water hydrology. In: T. D. Prowse & C. S. L. Ommanney (eds.). *Northern Hydrology, Canadian Perspectives*. NHRI Science Report No 1.

Flowers, G., Marshall, S., Bjornsson, H. & Clark, G. (2005). Sensitivity of Vatnajokull ice cap hydrology and dynamics to climate warming over the next 2 centuries. *Journal of Geophysical Research*. 110. p. F0211.

Fotiev, S.M. (1980). Effect of long-term cryometamosphism. In: *Proceedings of the 3rd International Conference on Permafrost*. 1980, Edmonton, Alberta, p. 177–194.

Fourre, E., Jeanbaptiste, P., Dapoigny, a, Baumier, D., Petit, J. & Jouzel, J. (2006). Past and recent tritium levels in Arctic and Antarctic polar caps. *Earth and Planetary Science Letters*. 245 (1-2). p. 56–64.

Frank, T.D., Gui, Z. & Team, A.S.S. (2010). Cryogenic origin for brine in the subsurface of southern McMurdo Sound, Antarctica. *Geology*. 38 (7). p. 587–590.

Franklyn, M.T., McNutt, R.H., Kamineni, D.C., Gascoyne, M. & Frape, S.K. (1991). Groundwater $^{87}Sr/^{86}Sr$ values in the Eye-Dashwa Lakes pluton, Canada: Evidence for plagioclase-water reaction. *Chemical Geology*. 86. p. 111–122.

Frape, S.K., Fritz, P. & McNutt, R. (1984). Water-rock interaction and chemistry of groundwaters from the Canadian Shield. *Geochimica et Cosmochimica Acta*. 48. p. 1617–1627.

Frape, S.K., Stotler, R. & Harvey, F.E. (2013). The isotopic distribution of ^{37}Cl and ^{81}Br in highly evaporated alkaline lakes of the Sand Hills, Nebraska, U.S.A. In: *10th International Symposium on Applied Isotope Geochemistry*. 2013, Budapest, Hungary.

Frape, S.K., Blyth, A., Stotler, R.L., Ruskeeniemi, T., Blomqvist, R., McNutt, R.H. & Gascoyne, M. (2014). Deep fluids in the continents. In: J. I. Drever (ed.). *Treatise on Geochemistry, Volume 7*. Amsterdam, Netherlands: Elsevier Ltd.

Fredskild, B. (1977). The development of the Greenland lakes since the last glaciation. *Folia limnol. scand*.

Freifeld, B.M., Trautz, R.C., Kharaka, Y.K., Phelps, T.J., Myer, L.R. & Hovorka, S.D. (2005). The U-tube: A novel system for acquiring borehole fluid samples from a deep geologic CO_2 sequestration experiment. *Journal of Geophysical Research B. Solid Earth*. 110 (10). p. 1–10.

Fritz, P. & Frape, S. (1982). Saline groundwaters in the Canadian Shield—a first overview. *Chemical Geology*. 36. p. 179–190.

Fritz, P., Frape, S.K., Drimmie, R.J. & Appleyard, E.C. (1994). *Sulfate in brines in the crystalline rocks of the Canadian Shield*. 58 (1983). p. 57–65.

Fritz, S.C. (1996). Paleolimnological records of climatic change in North America. *Limnology and Oceanography*. 41 (5). p. 882–889.

Fritz, S.C. & Anderson, N.J. (2013). The relative influences of climate and catchment processes on Holocene lake development in glaciated regions. *Journal of Paleolimnology*. 49 (3). p. 349–362.

Fry, B., Ruf, W., Gest, H. & Hayes, J.M. (1988). Sulphur isotope effects associated with oxidation of sulphide by O_2 in aqueous solution. *Chemical Geology*. 73. p. 205–210.

Fulignati, P., Gioncada, A. & Sbrana, A. (1999). Rare-earth element (REE) behaviour in the alteration facies of the active magmatic-hydrothermal system of Vulcano (Aeolian Islands, Italy). *Journal of Volcanology and Geothermal Research*. 88 (4). p. 325–342.

Funder, S. & Hansen, L. (1996). The Greenland ice sheet - a model for its culmination and decay during and after the last glacial maximum. *Bulletin of the Geological Society of Denmark*. 42 (1989). p. 137–152.

Funder, S., Kjeldsen, K.K., Kjær, K.H. & Ó Cofaigh, C. (2011). The Greenland Ice Sheet During the Past 300,000 Years: A Review. In: J. Ehlers, P. I. Gibbard, & P. D. Hughes (eds.). *Quaternary Glaciations - Extent and Chronology. Vol. 15.* Amsterdam, Netherlands: Elsevier, p. 699–713.

Garde, A.A. & Hollis, J.A. (2010). A buried Palaeoproterozoic spreading ridge in the northern Nagssugtoqidian orogen, West Greenland. *Geological Society, London, Special Publications*. 338. p. 213–234.

Garrels, R. & Mackenzie, F. (1967). Origin of the chemical compositions of some springs and lakes. In: Stumm, W. (dds.) *Equilibrium concepts in natural water*. Washington, DC. ACS. p. 222–242.

Gascoyne, M. (2000). *A review of published literature on the effects of permafrost on the hydrogeochemistry of bedrock*. SKB Report R-01-56. Stockholm, Sweden. pp. 49.

Gavelin, S., Parwel, A. & Ryhage, R. (1960). Sulfur isotope fractionation in sulfide mineralization. *Economic Geology1*. 55. p. 510–530.

Glynn, P.D., Voss, C.I. & Provost, A.M. (1999). Deep penetration of oxygenated meltwaters from warm based ice sheets into the Fennoscandian shield. In: *Use of Hydrogeochemical Information in Testing Groundwater Flow Models, Technical Summary and Proceedings of a Workshop*. 1999, Borgholm, Sweden: Nuclear Energy Agency, Organization of Developed Countries, p. 201–241.

Gonfiantini, R. (1986). Environmental isotopes in lake studies. In: P. Fritz & J.-C. Fontes (eds.). *Handbook of Environmental Isotope Studies, Vol. 2, The Terrestrial Environment*. Amsterdam, Netherlands: Elsevier, pp. 113–168.

van Gool, J.A.., Connelly, J.N., Marker, M. & Mengel, F.C. (2002). The Nagssugtoqidian Orogen of West Greenland: tectonic evolution and regional correlations from a West Greenland perspective. *Canadian Journal of Earth Sciences*. 39 (5). p. 665–686.

Gooseff, M.N., Lyons, W.B., McKnight, D.M., Vaughn, B.H., Fountain, A.G. & Dowling, C. (2006). A Stable Isotopic Investigation of a Polar Desert Hydrologic System, McMurdo Dry Valleys, Antarctica. *Arctic Antarctic and Alpine Research*. 38 (1). p. 60–71.

Graly, J. A.., Humphrey, N.F., Landowski, C.M. & Harper, J.T. (2014). Chemical weathering under the Greenland Ice Sheet. *Geology*. 42(6) p. 551–554.

Grant, W.H. (1963). Weathering of Stone Mountain granite. In: B. Ingersol (ed.). *Clays and Clay Minerals*. Oxford: Pergamon, p. 65–73.

Grasby, S., Osadetz, K. & Render, F. (2000). Reversal of the regional-scale flow system of the Williston basin in response to Pleistocene glaciation. *Geology*. 28 (1986). p. 635–638.

Grasby, S.E., Allen, C.C., Longazo, T.G., Lisle, J.T., Griffin, D.W. & Beauchamp, B. (2003a). Supraglacial sulfur springs and associated biological activity in the Canadian high arctic-signs of life beneath the ice. *Astrobiology*. 3 (3). p. 583–96.

Grasby, S.E., Allen, C.C., Longazo, T.G., Lisle, J.T., Griffin, D.W. & Beauchamp, B. (2003b). Biogeochemical sulphur cycle in an extreme environment—lifebeneath a high arctic glacier, Nunavut, Canada. *Journal of Geochemical Exploration*. 78-79 (03). p. 71–74.

Green, W. & Canfield, D. (1984). Geochemistry of the Onyx River (Wright Valley, Antarctica) and its role in the chemical evolution of Lake Vanda. *Geochimica et cosmochimica acta*. 48 (198 1). p. 2457–2467.

Green, W.J., Angle, M.P. & Chave, K.E. (1988). The geochemistry of Antarctic streams and their role in the evolution of four lakes of the McMurdo Dry Valleys *. *Geochimica et Cosmochimica Acta*. 52. p. 1265–1274.

Green, W.J. & Lyons, W.B. (2008). The saline lakes of the McMurdo Dry Valleys, Antarctica. *Aquatic Geochemistry*. 15 (1-2). p. 321–348.

Gurney, S.D. (1998). Aspects of the genesis and geomorphology of pingos: perennial permafrost mounds. *Progress in Physical Geography*. 22 (3). p. 307–324.

Haliday, G., Kliim-Nielsen, L. & Smart, I.H.M. (1974). Studies on the flora of the North Blosseville Kyst and on the hot springs of Greenland. *Medd. om Gronland*. 199. p. 1–47.

Hall, K., Thorn, C.E., Matsuoka, N. & Prick, A. (2002). Weathering in cold regions: some thoughts and perspectives. *Progress in Physical Geography*. 26 (4). p. 577–603.

Hammer, C.U. (2006). Ice-core chronology. In: P. G. Knight (ed.). *Glacier science and environmental change*. Oxford, UK: Blackwell, p. 396403.

Hanlon, C. (2015). *A characterization of bromine and chlorine stable isotopes in the Sand Hills Region of Nebraska, USA*. MSc Thesis. University of Waterloo, Canada. pp. 102.

Harper, J., Hubbard, A., Ruskeeniemi, T., Claesson Liljedahl, L., Lehtinen, A., Booth, A., Brinkherhoff, D., Drake, H., Dow, C., Doyle, S., Engström, J., Fitzpatrik, A., Frape, S., Henkemans, E., Humphrey, N., Johnson, J., Jones, G., Joughin, I., Kilnt, K.E., Kukkonen, I., Kulessa, B., Londowski, C., Lindback, K., Makahnouk, M., Mejerbachtol, T., Pedersen, P.T., Pere, T., Petterson, R., Pimentel, S., Quincy, D., Tullborg, E.-L. & van As, D. (2011). *The Greenland Analogue Project yearly report 2010*. SKB Report R-11-23. Stockholm, Sweden. pp. 162.

Harper, J., Hubbard, A., Ruskeeniemi, T., Claesson Liljedahl, L., Lehtinen, A., Bougamont, M., Brown, J., Dirkson, A., Dow, C., Doyle, S., Drake, H., Engstrom, J., Fitzpatrick, A., Follin, S., Frape, S., Graly, J., Hansson, K., Harrington, J., Henkemans, E., Humphrey, N., Jansson, P., Johnson, J., Jones, G., Kinnbom, P., Klint, K.E., Liimatainen, J., Lindback, K., Meierbachtol, T., Pere, T., Pettersson, R., Tullborg, E.-L. & van As, D. (2015a). *GAP data, processes and conceptual understanding. SKB-Report-14-13 (In press)*. Stockholm, Sweden.

Harper, J., Ruskeeniemi, T., Henkemans, E. & Frape, S.K. (2015b). *Greenland Analogue Project Report 2011 (in prep.)*. Stockholm, Sweden.

Harris, H.J.H. & Cartwright, K. (1981). Hydrology of the Don Juan basin, Wright Valley, Antarctica. In: L. D. McGinnis (ed.). *Antarctic Research Series Volume 33: Dry Valley Drilling Project*. Washington D.C.: American Geophysical Union, p. 161–184.

Harris, K.J., Carey, a. E., Lyons, W.B., Welch, K. a. & Fountain, a. G. (2007). Solute and isotope geochemistry of subsurface ice melt seeps in Taylor Valley, Antarctica. *Geological Society of America Bulletin*. 119 (5-6). p. 548–555.

Harris, L.B., Yakymchuk, C. & Godin, L. (2012). Implications of centrifuge simulations of channel flow for opening out or destruction of folds. *Tectonophysics*. 526-529. p. 67–87.

Hasholt, B., Mikkelsen, A.B., Nielsen, M.H. & Larsen, M.A.D. (2012). Observations of runoff and sediment and dissolved loads from the Greenland ice sheet at Kangerlussuaq, West Greenland. *Zeitschrift für Geomorphologie*. supplement (2). p. 3–27.

Hattori, K. & Cameron, E.M. (1986). Archaean magmatic sulphate. *Nature*. 319 (6048). p. 45–47.

Hawkings, J.R., Wadham, J.L., Tranter, M., Lawson, E., Sole, A., Cowton, T., Tedstone, A.J., Bartholomew, I., Nienow, P., Chandler, D. & Telling, J. (2015). The effect of warming climate on nutrient and solute export from the Greenland Ice Sheet. *Geochemical Perspectives Letters*. 1. p. 94–104.

Herut, B., Starinsky, A., Katz, A. & Bein, A. (1990). The role of seawater freezing in the formation of subsurface brines. *Geochimica et Cosmochimica Acta*. 54. p. 13–21.

Hoaglund, J.R., Kolak, J.J., Long, D.T. & Larson, G.J. (2004). Analysis of modern and Pleistocene hydrologic exchange between Saginaw Bay (Lake Huron) and the Saginaw Lowlands area. *Geological Society of America Bulletin*. 116. p. 3–15.

Hodell, D., Mueller, P. & Garrido, J. (1991). Variations in the strontium isotopic composition of seawater during the Neogene. *Geology*. 19 (January). p. 24–27.

Holmer, M.. & Storkholm, P.. (2001). Sulphate reduction and sulphur cycling in lake sediments: a review. *Freshwater Biology*. 46. p. 431–451.

Hyndman, D.W. (1985). *Petrology of igneous and metamorphic rocks*. New York: McGraw-Hill Book Company.

Jensen, I.A.. (1889). Undersegelse af Gronlands Vestkyst fra 64-68 n.b. *Medd. om Gronland*. 8. p. 33–130.

Johansson, E., Berglund, S., Lindborg, T., Petrone, J., As, D. Van, Gustafsson, L., Näslund, J. & Laudon, H. (2014). Hydrological and meteorological investigations in a periglacial lake catchment near Kangerlussuaq , west Greenland – presentation of a new multi-parameter dataset. *Earth Systems Science Data*. 7. p. 713–756.

Johansson, E., Gustafsson, L.-G., Berglund, S., Lindborg, T., Selroos, J.-O., Claesson Liljedahl, L. & Destouni, G. (2015). Data evaluation and numerical modeling of hydrological interactions between active layer, lake and talik in a permafrost catchment, Western Greenland. *Journal of Hydrology*. 527. p. 688–703.

Jones, L.M. & Faure, G. (1978). A study of strontium isotopes in lakes and surficial deposits of the ice-free valleys, Southern Victoria Land, Antarctica. *Chemical Geology*. 22 (24). p. 107–120.

Kaija, J., Blomqvist, R., Suksi, J. & Rasilainen, K. (2000). *The Palmottu Natural Analogue Project Summary Report 1996-1999*. Espoo, Finland. pp. 93.

Kamineni, D. (1983). Sulfur-isotope geochemistry of fracture-filling gypsum in an Archean granite near Atikokan, Ontario, Canada. *Chemical Geology*. 39. p. 263–272.

Kamineni, D.C., Brown, P.A. & Stone, D. (1980). Fracture filling materials in the Atikokan area, northwestern Ontario. *Geological Survey of Canada Papers*. 80-1A. p. 369–374.

Kamineni, D.C. & Dugal, J.J.B. (1982). A study of rock alteration in the Eye-Dashwa Lakes pluton, Atikokan, northwestern Ontario, Canada. *Chemical Geology*. 36. p. 35–57.

Kamineni, D.C. & Stone, D. (1983). The ages of fractures in the Eye-Dashwa pluton, Atikokan, Canada. *Contributions to Mineralogy and Petrology*. 83 (3-4). p. 237–246.

Kaplan, I.R. & Rittenberg, S.C. (1963). Microbiological Fractionation of Sulphur Isotopes. *Journal of General Microbiology*. 34. p. 195–212.

Kaufmann, R., Long, A., Bentley, H. & Davis, S. (1984). Natural chlorine isotope variations. *Nature*. 309.

Keir-Sage, J. (2014). *Pore fluid study of Greenland bedrock from the Kangerlussuaq area*. Undergraduate Thesis. University of Waterloo. pp. 54.

Keller, K., Blum, J. & Kling, G. (2007). Geochemistry of soils and streams on surfaces of varying ages in arctic Alaska. *Arctic, Antarctic, and Alpine Research*. 39 (1). p. 84–98.

Kern Hansen, C. (1990). Data basis for permafrost studies in Greenland. In: *Polartech '90: International Conference on Development and Commerical Utilization of Technologies in Polar Regions*. 1990, Copenhagen, Denmark: Danish Polar Center, pp. 635–644.

Kerrich, R. & Kamineni, D.C. (1988). Characteristics and chronology of fracture - fluid infiltration in the Archean, Eye Dashwa Lakes pluton, Superior Province: evidence from H, C, O-isotopes and fluid inclusions. *Contributions to Mineralogy and Petrology*. 99 (4). p. 430–445.

Keys, J.R. & Williams, K. (1981). Origin of crystalline, cold desert salts in the McMurdo region, Antarctica. *Geochimica et Cosmochimica Acta*. 45. p. 2299–2309.

King-Clayton, L., Chapman, N., Ericsson, L.O. & Kautsky, F. (1997). Glaciation and hydrogeology. In: *Impact of climate change & glaciations on rock stresses, groundwater flow and hydrochemistry - past, present and future.* 1997, SKB Report R 97 13. Stockholm, Sweden: SKB.

Klint, K.E.S., Engström, J., Parmenter, A., Ruskeeniemi, T., Claesson Liljedahl, L. & Lehtinen, A. (2013). Lineament mapping and geological history of the Kangerlussuaq region, southern West Greenland. *Geological Survey Of Denmark And Greenland Bulletin*. 28. p. 57–60.

Kokelj, S. V., Smith, C. a. S. & Burn, C.R. (2002). Physical and chemical characteristics of the active layer and permafrost, Herschel Island, western Arctic Coast, Canada. *Permafrost and Periglacial Processes*. 13 (2). p. 171–185.

Kokelj, S.V., Zijdlik, B. & Thompson, M.S. (2009). The impacts of thawing permafrost on the chemistry of lakes across the subarctic boreal-tundra transition, Mackenzie Delta Region Canada. *Permafrost and Periglacial Processes*. 20. p. 185–199.

Kristiansen, S.M., Yde, J.C., Bárcena, T.G., Jakobsen, B.H., Olsen, J. & Knudsen, N.T. (2013). Geochemistry of groundwater in front of a warm-based glacier in Southeast Greenland. *Geografiska Annaler: Series A, Physical Geography*. 95 (2). p. 97–108.

Laaksoharju, M., Tullborg, E., Wikberg, P., Wallin, B. & Smellie, J. (1999). Hydrogeochemical conditions and evolution at the Äspö HRL, Sweden. *Applied Geochemistry*. 14. p. 835–859.

Laaksoharju, M. & Rehn, I. (1999). Aspo project: Hydrogeology and hydrogeochemistry used to indicate present flow dynamics. In: *Use of Hydrogeochemical Information in Testing Groundwater Flow Models, Technical Summary and Proceedings of a Workshop*. 1999, Borgholm, Sweden: Nuclear Energy Agency, Organization of Developed Countries, p. 65–78.

Lambert, F., Delmonte, B., Petit, J., Bigler, M., Kaufmann, P.R., Hutterli, M.A., Stocker, T.F., Ruth, U., Steffensen, J.P. & Maggi, V. (2008). Dust-climate couplings over the past 800,000 years from the EPICA Dome C ice core. *Nature*. 452. p. 616–619.

Lambie, K.E. (2008). *The design of an out-diffusion experiment and the use of geochemical analyses for the purpose of matrix pore fluid extraction and characterization: a case study for radioactive waste disposal*. MSc Thesis. University of Waterloo. pp. 86.

Lamoureux, S., Gilbert, R. & Lewis, T. (2002). Lacustrine sedimentary environments in High Arctic proglacial Bear Lake, Devon Island, Nunavut, Canada. *Arctic, Antarctic, and Alpine Research*. 34 (2). p. 130–141.

Landström, O. & Tullborg, E.-L. (1990). *The influence of fracture mineral/groundwater interaction on the mobility of U, Th, REE and other trace elements.* SKB Technical Report 90-37. Stockholm, Sweden. pp. 71.

Lawrence, C.R. & Neff, J.C. (2009). The contemporary physical and chemical flux of aeolian dust: A synthesis of direct measurements of dust deposition. *Chemical Geology*. 267 (1-2). p. 46–63.

Lemieux, J.-M., Sudicky, E.A., Peltier, W.R. & Tarasov, L. (2008a). Dynamics of groundwater recharge and seepage over the Canadian landscape during the Wisconsinian glaciation. *Journal of Geophysical Research*. 113.

Lemieux, J.-M., Sudicky, E.A., Peltier, W.R. & Tarasov, L. (2008b). Simulating the impact of glaciations on continental groundwater flow systems: 2. Model application to the Wisconsinian glaciation over the Canadian landscape. *Journal of Geophysical Research*. 113.

Leng, M.J. & Anderson, N.J. (2003). Isotopic variation in modern lake waters from western Greenland. *The Holocene*. 13 (4). p. 605–611.

Leng, M.J., Wagner, B., Anderson, N.J., Bennike, O., Woodley, E. & Kemp, S.J. (2012). Deglaciation and catchment ontogeny in coastal south-west Greenland: implications for terrestrial and aquatic carbon cycling. *Journal of Quaternary Science*. 27 (6). p. 575–584.

Lyons, W., Welch, K. & Sharma, P. (1998). Chlorine-36 in the waters of the McMurdo Dry Valley lakes, southern Victoria Land, Antarctica: revisited. *Geochimica et Cosmochimica Acta*. 62 (2). p. 185–191.

Lyons, W., Welch, K., Carey, A., Doran, P., Wall, D., Virginia, R., Fountain, A., Csatho, B. & Tremper, C. (2005a). Groundwater seeps in Taylor Valley Antarctica: an example of a subsurface melt event. *Annals Of Glaciology*. 40. p. 200–206.

Lyons, W.B., Nezat, C. a, Benson, L. V, Bullen, T.D., Graham, E.Y., Kidd, J., Welch, K. a & Thomas, J.M. (2002). Strontium isotopic signatures of the streams and lakes of Taylor Valley, Southern Victoria Land, Antarctica: Chemical weathering in a polar climate. *Aquatic Geochemistry*. 8 (2). p. 75–95.

Lyons, W.B., Welch, K. a., Snyder, G., Olesik, J., Graham, E.Y., Marion, G.M. & Poreda, R.J. (2005b). Halogen geochemistry of the McMurdo dry valleys lakes, Antarctica: Clues to the origin of solutes and lake evolution. *Geochimica et Cosmochimica Acta*. 69 (2). p. 305–323.

Ma, L., Castro, M. & Hall, C. (2004). A late Pleistocene-Holocene noble gas paleotemperatures record in southern Michigan. *Geophysical Research Letters*. 31. p.p. 1-4.

Mackay, J.R. (1997). A full-scale field experiment (1978-1995) on the growth of permafrost by means of lake drainage, western Arctic coast: a discussion of the method and some results. *Canadian Journal of Earth Sciences*. 34. p. 17–33.

Magenheim, A., Spivack, A., Michael, P.. & Gieskes, J.M. (1995). Chlorine stable isotope composition of the oceanic crust: Implications for Earth's distribution of chlorine. *Earth and Planetary Science Letters*. 131. p. 427–432.

Makahnouk, M. (n.d.). *A review and comparison of fracture calcite investigations conducted at the Stripa Mine Site, Central Sweden: Evaluating fluid origin and past thermal and chemical conditions in a complex geological setting*. PhD Thesis (In progress), University of Waterloo.

Marini, L., Moretti, R. & Accornero, M. (2011). Sulfur Isotopes in Magmatic-Hydrothermal Systems, Melts, and Magmas. *Reviews in Mineralogy and Geochemistry*. 73. p. 423–492.

Marksamer, A.J., Person, M., Day-Lewis, F. & Lane, J. (2007). Integrating geophysical, hydrochemical and hydrologic data to understand the freshwater resources on Nantucket Island, Massachusetts. In: D. W. Hynmann, F. Day-Lewis, & K. Singha (eds.). *Data integration in subsurface hydrology*. AGU Water Resources Monograph, p. 17.

Martini, A., Walter, L., Budai, J., Ku, T., Kaiser, C. & Schoell, M. (1998). Genetic and temporal relations between formation waters and biogenic methane: Upper Devonian Antrim Shale, Michigan Basin, USA. *Geochimica et Cosmochimica Acta*. 62 (10). p. 1699–1720.

Matsubaya, O., Sakai, H., Toril, T., Burton, H. & Kerry, K. (1979). Antarctic saline lakes-stable isotopic ratios , chemical compositions and evolution. *Geochimica et Cosmochimica Acta*. 43. p. 7–25.

Mazurek, M. (2000). Geological and hydraulic properties of water-conducting features in crystalline rocks. In: I. Stober & K. Bucher (eds.). *Hydrogeology of Crystalline Rocks*. Boston, USA: Kluwer Academic Publishers, p. 275.

McGowan, S., Ryves, D.B. & Anderson, N.J. (2003). Holocene records of effective precipitation in West Greenland. *The Holocene*. 13 (2). p. 239–249.

McIntosh, J.C. & Walter, L.M. (2005). Volumetrically significant recharge of Pleistocene glacial meltwaters into epicratonic basins: Constraints imposed by solute mass balances. *Chemical Geology*. 222 (3-4). p. 292–309.

McIntosh, J.C. & Walter, L.M. (2006). Paleowaters in Silurian-Devonian carbonate aquifers: Geochemical evolution of groundwater in the Great Lakes region since the Late Pleistocene. *Geochimica et Cosmochimica Acta*. 70 (10). p. 2454–2479.

McIntosh, J.C., Garven, G. & Hanor, J.S. (2011). Impacts of Pleistocene glaciation on large-scale groundwater flow and salinity in the Michigan Basin. *Geofluids*. 11 (1). p. 18–33.

McLeod, M., Bockheim, J.G. & Balks, M.R. (2008). Glacial geomorphology, soil development and permafrost features in central-upper Wright Valley, Antarctica. *Geoderma*. 144 (1-2). p. 93–103.

McNutt, R.H., Frape, S.K. & Fritz, P. (1984). Strontium isotope composition of some brines from the Precambrian Shield of Canada. *Isotope Geoscience*. 2. p. 205–215.

McNutt, R.H., Frape, S.K., Fritz, P., Jones, M.G. & Macdonald, I.A.N.M. (1990). The $^{87}Sr/^{86}Sr$ values of Canadian Shield brines and fracture minerals with applications to groundwater mixing, fracture history, and geochronology. *Geochimica et Cosmochimica Acta*. 54. p. 205–215.

Michalski, G., Böhlke, J.K. & Thiemens, M. (2004). Long term atmospheric deposition as the source of nitrate and other salts in the Atacama Desert, Chile: New evidence from mass-independent oxygen isotopic compositions. *Geochimica et Cosmochimica Acta*. 68 (20). p. 4023–4038.

Michard, A. (1989). Rare earth element systematics in hydrothermal fluids. *Geochimica et Cosmochimica Acta*. 53 (3). p. 745–750.

Mikkelsen, A.B. (2014). *Freshwater discharge and sediment transport to Kangerlussuaq Fjord, West Greenland - processes, modelling and implications*. PhD Thesis. University of Copenhagen, Denmark.

Morgan, J.W. & Wandless, G.A. (1980). Rare earth element distribution in some hydrothermal minerals : evidence for crystallographic control. *Geochimica et Cosmochimica Acta*. 44. p. 973–980.

Morrison, J., Fallick, T., Donelly, T., Leossen, M., St. Jean, G. & Drimmie, R.J. (1996). $\delta^{34}S$ measurements of standards from several laboratories by continuous flow isotope ratio mass spectrometry (CF-IRMS). *Micromass UK Ltd. Technical Report*.

Morrison, J. (1997). Inorganic oxygen isotope analysis by EA-pyrolysis-IRMS. In: *Presented at 4th Canadian Continuous Flow – IRMS Conference*. 1997, Waterloo, Ontario.

Morrison, J.T., Brockwell, T., Merren, T., Fourel, F. & Phillips, A.M. (2001). On-line high precision stable hydrogen isotopic analyses on nanoliter water samples. *Analytical chemistry*. 73. p. 3570–3575.

Moser, H. (1977). Internal report of the Institute for Radiohydrometrie. *GSF Munich*. 169. p. 70–71.

Muller, F. (1959). Bobachtungen uber pingos. Detailuntersuchungen in Ostgroenland und in der kanadischen Arktis. *Medd. om Gronland*. 153 (3). pp. 127 (Also as Nat. Res. Counc. Can. Tech. Transl. 1).

Mungall, J.E., Frape, S.K., Gigson, I.A.N.L. & Kamineni, D.C. (1987). Rare-earth abundances in host granitic rocks and fracture-filling gypsum associated with saline groundwaters from a deep borehole, Atikokan, Ontario. *Canadian Mineralogist*. 25. p. 539–543.

Nakai, N. & Jensen, M.L. (1964). The kinetic isotope effect in the bacterial reduction and oxidation of sulfur. *Geochimica et Cosmochimica Acta*. 28 (2). p. 1893–1912.

Négrel, P. & Casanova, J. (2005). Comparison of the Sr isotopic signatures in brines of the Canadian and Fennoscandian shields. *Applied Geochemistry*. 20 (4). p. 749–766.

Nesbitt, H. & Young, G. (1996). Petrogenesis of sediments in the absence of chemical weathering: effects of abrasion and sorting on bulk composition and mineralogy. *Sedimentology*. 43 (2). p. 341–358.

Normani, S.D. & Sykes, J.F. (2012). Paleohydrogeologic simulations of Laurentide ice-sheet history on groundwater at the eastern flank of the Michigan Basin. *Geofluids*. 12 (1). p. 97–122.

Olsen, J., Anderson, N.J. & Leng, M.J. (2013). Limnological controls on stable isotope records of late-Holocene palaeoenvironment change in SW Greenland: a paired lake study. *Quaternary Science Reviews*. 66. p. 85–95.

Osterkamp, T. & Romanovsky, V. (1999). Evidence for warming and thawing of discontinuous permafrost in Alaska. *Permafrost and Periglacial Processes*. 10. p. 17–37.

Ouellet, M., Dickman, M. & Page, P. (1989). Physico-chemical characteristics and origin of hypersaline meromictic Lake Garrow in the Canadian High Arctic. *Hydrobiologia*. 172. p. 215–234.

Pedersen, A. (1926). De varme kilder i Scoresby Sund. *Medd. om Gronland*. 68 (4). p. 253–257.

Pere, T. (2014). *Geological logging of the Greenland Analogue Project drill cores DH-GAP01, 03 and 04. Posiva Working Report 2013-59*. Olkiluoto, Finland.

Person, M., Dungan, B., Swenson, J.B., Urbano, L., Sttot, C., Taylor, J. & Willett, M. (2003). Pleistocene hydrogeology of the Atlantic continental shelf, New England. *Geological Society of America Bulletin*. 115. p. 1324–1343.

Person, M., Bense, V., Cohen, D. & Banerjee, A. (2012). Models of ice-sheet hydrogeologic interactions: a review. *Geofluids*. 12 (1). p. 58–78.

Peterman, Z.E., Futa, K. & Kamineni, C. (1990). Rb-Sr systematics in drill cor esamples of the Eye-Dashwa Lakes Pluton at the whole rock and mineral scale. In: Z. E. Peterman & D. C. Kamineni (eds.). *Isotopic Studies of the Eye-Dashwa Lakes Pluton and the Long-Term Integrity of Whole-Rock and Mineral Systems*. Pinawa, Manitoba: AECL, pp. 11–24.

Piotrowski, J.A. (1997). Subglacial groundwater flow during the last glaciation in northwestern Germany. *Sedimentary Geology*. 111. p. 217–224.

Piotrowski, J.A. (2006). Groundwater under ice sheets and glaciers. In: P. G. Knight (ed.). *Glacier Science and Environmental Change*. Oxford, UK: Blackwell Publishing, pp. 50–60.

Pitkanen, P., Luukkonen, A., Ruotsalainen, P., Leino-Forsman, H. & Vuorinen, U. (2001). Similar to the Olkiluoto site in terms of hydrochemical conditions. *Geochemical modelling of groundwater evolution and residence time at the Hiistholmen site.* Posiva Report 2001-01. Eurajoki, Finland. pp. 175.

Pitkanen, P., Partamies, S. & Luukkonen, A. (2004). *Hydrogeochemical Interpretation of Baseline Groundwater Conditions at the Olkiluoto Site.* Posiva Report 2003-07. Eurajoki, Finland. pp. 159.

Pollanen, J., Heikkinen, P. & Lehtinen, A. (2012). *Difference flow measurements in Greenland, Drillhole DH-GAP04 in July 2011. Posiva Working Report 2012-13*. Olkiluoto, Finland.

Pöllänen, J., Heikkinen, P. & Lehtinen, A. (2012). *Difference flow measurements in Greenland, Drillhole DH-GAP04 in July 2011.* Posiva Report 2012-13. Olkiluoto, Finland. pp. 37.

Pollard, W., Omelon, C., Andersen, D. & Mckay, C. (1999). Perennial spring occurrence in the Expedition Fjord area of western Axel Heiberg Island, Canadian high arctic. *Canadian Journal of Earth Sciences*. 36 (1). p. 105–120.

Quinton, W. & Marsh, P. (1999). A Conceptual Framework for Runo Generation in a Permafrost Environment. *Hydrological Processes*. 13. p. 2563–2581.

Quinton, W.L., Gray, D.M. & March, P. (2000). Subsurface drainage from hummock-covered hillslopes in the Arctic tundra. *Journal of Hydrology*. 237. p. 113–125.

Raidla, V., Kirsimäe, K., Vaikmäe, R., Jõeleht, A., Karro, E., Marandi, A. & Savitskaja, L. (2009). Geochemical evolution of groundwater in the Cambrian–Vendian aquifer system of the Baltic Basin. *Chemical Geology*. 258 (3-4). p. 219–231.

Rasilainen, K., Suksi, J., Ruskeeniemi, T., Pitkänen, P. & Poteri, A. (2003). Release of uranium from rock matrix--a record of glacial meltwater intrusions? *Journal of contaminant hydrology*. 61 (1-4). p. 235–46.

Reeh, N., Oerter, H. & Thomsen, H.H. (2002). Comparison between Greenland ice-margin and ice-core oxygen-18 records. *Annals Of Glaciology*. 35 (1). p. 136–144.

Rees, C.E. (1984). *The isotopic analysis of sulphur*. McMaster University Isotopic Nuclear and Geochemical Studies Group, Contribution No. 139, Hamilton, Ontario.

Remenda, V., Cherry, J. & Edwards, T. (1994). Isotopic composition of old ground water from Lake Agassiz: Implications for late Pleistocene climate. *Science*. 266. p. 1975–1978.

Rinterknecht, V., Gorokhovich, Y., Schaefer, J. & Caffee, M. (2009). Preliminary ^{10}Be chronology for the last deglaciation of the western margin of the Greenland Ice Sheet. *Journal of Quaternary Science*. 24 (3). p. 270–278.

Romanov, V.V., Morkovkina, K., Chizhov, A.B. & Chizhova, N.I. (1986). Use of tritium studies of underrgound ice [in Russian]. *Soviet Academy of Sciences, Moscow, Data from Glacioogical Studies*. 55. p. 98–100.

Rouhianen, P. (1993). *TVO Flowmeter, Posiva Report YJT-93-01*. Helsinki, Finland. p. 55.

Ruiz, J., Jones, L.M. & Kelly, W.C. (1984). Rubidium-strontium dating of ore deposits hosted by rubidium-rich rocks, using calcite and other common Sr-bearing minerals. *Geology*. 12. p. 259–262.

Schnetzler, C.. & Philpotts, J. a (1970). Partition coefficients of rare-earth elements between igneous matrix material and rock-forming mineral phenocrysts—II. *Geochimica et Cosmochimica Acta*. 34 (3). p. 331–340.

Scholz, H. & Baumann, M. (1997). An ‘ open system pingo ’ near Kangerlussuaq (Søndre Strømfjord), West Greenland. *Geologiy of Greenland Survey Bulletin*. 176. p. 104–108.

Schütz, L. & Sebert, M. (1987). Mineral aerosols and source identification. *Journal of Aerosol Science*. 18 (I). p. 1–10.

Seal, R.R., Alpers, C.N. & Rye, R.O. (2000). Stable Isotope Systematics of Sulfate Minerals. *Reviews in Mineralogy and Geochemistry*. 40. p. 541–602.

Sharp, M., Creaser, R.A. & Skidmore, M. (2002). Strontium isotope composition of runoff from a glaciated carbonate terrain. *Geochimica et Cosmochimica Acta*. 66 (4). p. 595–614.

Shouakar-Stash, O., Frape, S.K. & Drimmie, R.J. (2005a). Determination of bromine stable isotopes using continuous-flow isotope ratio mass spectrometry. *Analytical chemistry*. 77 (13). p. 4027–33.

Shouakar-Stash, O., Drimmie, R.J. & Frape, S.K. (2005b). Determination of inorganic chlorine stable isotopes by continuous flow isotope ratio mass spectrometry. *Rapid Communications in Mass Spectrometry*. 19. p. 121–127.

Shouakar-Stash, O., Alexeev, S.V., Frape, S.K., Alexeeva, L.P. & Drimmie, R.J. (2007). Geochemistry and stable isotopic signatures, including chlorine and bromine isotopes, of the deep groundwaters of the Siberian Platform, Russia. *Applied Geochemistry*. 22 (3). p. 589–605.

Shvartsev, S.L. (1998). Brines in the Siberian Platform: Geochemical and isotopic evidence for water–rock interaction. In: G. B. Arehart & J. R. Hulston (eds.). *Water-Rock Interaction*. 1998, Balkema: Proc. 9th Int. Symp. Water–Rock Interaction, p. 357–360.

Sie, P.M.J. & Frape, S.K. (2002). Evaluation of the groundwaters from the Stripa mine using stable chlorine isotopes. *Chemical Geology*. 182 (2-4). p. 565–582.

Siegel, D. & Mandle, R. (1984). Isotopic evidence for glacial meltwater recharge to the Cambrian-Ordovician aquifer, north-central United States. *Quaternary Research*. 335. p. 328–335.

Siegel, D.I. (1991). Evidence for dilution of deep, confined ground water by vertical recharge of isotopically heavy Pleistocene water. *Geology*. 19 (5). p. 433.

SKB (2010). *The Greenland Analogue Project yearly report 2009.* SKB Report R-10-59. Stockholm, Sweden. pp. 153.

Smellie, J.A.T. & Frape, S.K. (1997). Hydrochemical aspects of glaciation. In: L. King-Clayton, N. Chapman, L. O. Ericsson, & F. Kautsky (eds.). *Glaciation and Hydrogeology*. Stockholm, Sweden: SKI Report 13, Swedish Nuclear Power Inspectorate, pp. 45–51.

Smellie, J.A.T., Blomqvist, R., Frape, S.K., Pitkänen, P., Ruskeeniemi, T., Suksi, J., Casanova, J. & Kaija, J. (2002). Palaeohydrogeological implications for long-term hydrochemical stability at Palmottu. *European Comission*. pp. 7.

Smellie, J.A.T., Waber, N.H. & Frape, S.K. (2003). *Matrix fluid chemistry experiment, SKB Technical Report TR-03-18*. Stockholm, Sweden. pp. 379.

Souchez, R.A. & Jouzel, J. (1984). On the isotopic composition in dD and d18O of water and ice during freezing. *Journal of Glaciology*. 30 (106). p. 369–372.

Starinsky, A. & Katz, A. (2003). The formation of natural cryogenic brines. *Geochimica et Cosmochimica Acta*. 67 (8). p. 1475–1484.

Stober, I. & Bucher, K. (2006). Hydraulic properties of the crystalline basement. *Hydrogeology Journal*. 15 (2). p. 213–224.

Stone, D. & Kamineni, D.C. (1982). Fractures and fracture infillings of the Eye–Dashwa Lakes pluton, Atikokan, Ontario. *Canadian Journal of Earth Sciences*. 19 (4). p. 789–803.

Stotler, R.L. (2008). *Evolution of Canadian Shield Groundwaters and Gases: Influence of Deep Permafrost*. PhD Thesis. University of Waterloo, Waterloo, Ontario. pp. 283.

Stotler, R.L., Frape, S.K., Ruskeeniemi, T., Ahonen, L., Onstott, T.C. & Hobbs, M.Y. (2009). Hydrogeochemistry of groundwaters in and below the base of thick permafrost at Lupin, Nunavut, Canada. *Journal of Hydrology*. 373 (1-2). p. 80–95.

Stotler, R.L., Frape, S.K. & Shouakar-Stash, O. (2010). An isotopic survey of $\delta^{81}Br$ and $\delta^{37}Cl$ of dissolved halides in the Canadian and Fennoscandian Shields. *Chemical Geology*. 274 (1-2). p. 38–55.

Stotler, R.L., Frape, S.K., Freifeld, B.M., Holden, B., Onstott, T.C., Ruskeeniemi, T. & Chan, E. (2011). Hydrogeology, chemical and microbial activity measurement through deep permafrost. *Ground water*. 49 (3). p. 348–64.

Stotler, R.L., Frape, S.K., Ruskeeniemi, T., Pitkänen, P. & Blowes, D.W. (2012). The interglacial–glacial cycle and geochemical evolution of Canadian and Fennoscandian Shield groundwaters. *Geochimica et Cosmochimica Acta*. 76. p. 45–67.

Strebel, O., Böttcher, J. & Fritz, P. (1990). Use of isotope fractionation of sulfate-sulfur and sulfate-oxygen to assess bacterial desulfurication in a sandy aquifer. *Journal of Hydrology*. 121 (1-4). p. 155–172.

Takamatsu, N., Kat, N., Matsumot, G. & Torii, T. (1998). The origin of salts in water bodies of the McMurdo Dry Valleys. *Antarctic Science*. 10 (4). p. 439–448.

Van Tatenhove, F.G.M. & Olesen, O. (1994). Ground temperature and related permafrost characteristics in West Greenland. *Permafrost and Periglacial Processes*. 5 (April). p. 199–215.

Van Tatenhove, F.G.M. (1996). Changes in morphology at the margin of the Greenland ice sheet (Leverett Glacier), in the period 1943–1992: a quantitative analysis. *Earth Surface Processes and Landforms*. 21 (9). p. 797–816.

Taylor, A. & Blum, J.D. (1995). Relation between soil age and silicate weathering rates determined from the chemical evolution of a glacial chronosequence. *Geology*. 23 (11). p. 979–982.

Taylor, C.B. (1977). Tritium enrichment of environmental waters by electrolysis: development of cathodes exhibiting high isotopic separation and precise measurements of tritium enrichment factors. In: *Proceedings of the International Conference of Low-Radioactivity Measurements and Applications*. 1977, Bratislava: Slovenski Pedagogicke Nakladatelstvo, p. 131–140.

Tedesco, M., Fettweis, X., Mote, T., Wahr, J., Alexander, P., Box, J.E. & Wouters, B. (2013). Evidence and analysis of 2012 Greenland records from spaceborne observations, a regional climate model and reanalysis data. *The Cryosphere*. 7 (2). p. 615–630.

Terwilliger, J.P. & Dizio, S.F. (1970). Salt rejection phenomena in the freezing of saline solutions. *Chemical Engineering Science*. 25. p. 1331–1349.

Thiede, J., Jessen, C., Knutz, P., Kuijpers, A., Mikkelsen, N., Nørgaard-Pedersen, N. & Spielhagen, R.F. (2010). Millions of years of Greenland ice sheet history recorded in Ocean sediments. *Polarforschung*. 80 (3). p. 141–159.

Toran, L. & Harris, R.F. (1989). Interpretation of sulfur and oxygen isotopes in biological and abiological sulfide oxidation. *Geochimica et Cosmochimica Acta*. 53 (9). p. 2341–2348.

Torii, T. & Ossaka, J. (1965). Antarcticite: A New Mineral, Calcium Chloride Hexahydrate, Discovered in Antarctica. *Science (New York, N.Y.)*. 149 (3687). p. 975–977.

Truesdell, A.H. & Hulston, J.R. (1980). Isotopic evidence of environments of geothermal systems. In: P. Fritz & J. Fontes (eds.). *Handbook of Environmental Isotope Geochemistry Vol. 1, the Terrestrial Environment*. Amsterdam, Netherlands: Elsevier, p. 179–226.

Turner, K.W., Wolfe, B.B. & Edwards, T.W.D. (2010). Characterizing the role of hydrological processes on lake water balances in the Old Crow Flats, Yukon Territory, Canada, using water isotope tracers. *Journal of Hydrology*. 386 (1-4). p. 103–117.

Vaikmae, R., Vallner, L., Loosli, H.H., Blaser, P.C. & Juillard-Tardent, M. (2001). Palaeogroundwater of glacial origin in the Cambrian-Vendian aquifer of northern Estonia. *Geological Society, London, Special Publications*. 189 (1). p. 17–27.

Vidstrand, P. (2003). *Surface and subsurface conditions in permafrost areas - a literature review. SKB Report TR-03-06*. Stockholm, Sweden. pp. 72.

Vidstrand, P., Wallroth, T. & Ericsson, L.O. (2008). Coupled HM effects in a crystalline rock mass due to glaciation: indicative results from groundwater flow regimes and stresses from an FEM study. *Bulletin of Engineering Geology and the Environment*. 67 (2). p. 187–197.

Waber, H.N. & Smellie, J. a. T. (2008). Characterisation of pore water in crystalline rocks. *Applied Geochemistry*. 23 (7). p. 1834–1861.

Waller, R. & Tuckwell, G. (2005). Glacier-permafrost interactions and glaciotectonic landform generation at the margin of the Leverett Glacier, West Greenland. In: C. Harris & J. B. Murton (eds.). *Cryosphere Systems: Glaciers and Permafrost*. [Online]. London: the geological society of London, pp. 39–50.

Williams, P.J. & Warren, I.M.T. (1999). *The English version of the geocryological map of Russia and the neighbouring republics*.

Williams, W.D. (1991). Comments on the so-called salt lakes of Greenland. *Hydrobiologia*. 210. p. 67–74.

Wilson, R.W., Klint, K.E.S., Van Gool, J. a M., McCaffrey, K.J.W., Holdsworth, R.E. & Chalmers, J. a (2006). Faults and fractures in central West Greenland: onshore expression of continental break-up and sea-floor spreading in the Labrador–Baffin Bay Sea. *Geological Survey Of Denmark And Greenland Bulletin*. 11. p. 185–204.

Witherow, R. a., Lyons, W.B. & Henderson, G.M. (2010). Lithium isotopic composition of the McMurdo Dry Valleys aquatic systems. *Chemical Geology*. 275 (3-4). p. 139–147.

Wolfe, B.B., Light, E.M., Macrae, M.L., Hall, R.I., Eichel, K., Jasechko, S., White, J., Fishback, L. & Edwards, T.W.D. (2011). Divergent hydrological responses to 20th century climate change in shallow tundra ponds, western Hudson Bay Lowlands. *Geophysical Research Letters*. 38 (23). p. n/a..

Woo, M. & Steer, P. (1983). Slope hydrology as influenced by thawing of the active layer, Resolute, NWT. *Canadian Journal of Earth Sciences*. 20 (6). p. 978–986.

Wood, W.W., Sanford, W.E. & Frape, S.K. (2005). Chemical openness and potential for misinterpretation of the solute environment of coastal sabkhat. *Chemical Geology*. 215 (1-4). p. 361–372.

Worsley, P. & Gurney, S.D. (1996). Geomorphology and hydrogeological significance of the Holocene pingos in the Karup Valley area, Traill Island, northern east Greenland. *Journal of Quaternary Science*. 11 (3). p. 249–262.

Yoshikawa, B.K., Nakamura, T. & Igarashi, Y. (1996). *Growth and Collapse History of Pingos, Kuganguaq, Disko Island, Greenland*. 64 (3). p. 109–113.

Zachos, J., Opdyke, B., Quinn, T., Jones, C.E. & Halliday, A.. (1999). Early cenozoic glaciation, antarctic weathering, and seawater 87Sr/86Sr: is there a link? *Chemical Geology*. 161. p. 165–180.

Zhang, M. & Frape, S. (2003). *Permafrost: evolution of Shield groundwater compositions during freezing*. OPG Report 06819-REP-01200-10098-R00. Toronto, Canada. pp. 57.

Zhang, M., Frape, S.K., Love, A.J., Herczeg, A.L., Lehmann, B.E., Beyerle, U. & Purtschert, R. (2007). Chlorine stable isotope studies of old groundwater, southwestern Great Artesian Basin, Australia. *Applied Geochemistry*. 22 (3). p. 557–574.

A. Appendix A. Analytical Data Quality Assessment

A.1. Geochemical Analyses

Four different laboratories were used for various geochemical analyses. The various methodologies followed by these labs are outlined in Chapter 1 (Labtium Oy and TVO) and Chapter 4 (York Durham Regional Environmental Laboratory and ACTLABS Inc.).

(1) Labtium Oy

Analyses package: major and trace elements, alkalinity.

Labtium Oy was the main laboratory used for the GAP water samples including surface waters, ground waters and crush and leach waters from experiments on DH-GAP01 and DH-GAP03 core. For the vast majority of samples anlayzed at Labtium Oy, charge balance errors (C.B.E.) were < 10%. Glacial meltwater samples are the exception, with the majority of meltwater samples having charge balance errors above 10%. Only meltwater chemistry with charge balance errors <10% were considered in this study. Duplicate analyses were also run for quality assurance and duplicate results showed good agreement.

(2) TVO

Analyses Package: Major elements.

The TVO laboratory in Finland was used exclusively for samples acquired during the summer field campaign in 2009. Technical issues encountered with field alkalinity measurements and alkalinity was not measured at TVO. Due to the lack of alkalinity results, C.B.E. could not be calculated. The DH-GAP01 borehole chemistry results from TVO were not used in this study as they

were the first samples following completion of the DH-GAP01 borehole and the samples were still heavily impacted by drilling water. A small number of lake samples were analyzed at TVO and results were consistent with samples from the same lakes (different sample date) analyzed at Labitum Oy. Lake L12 is provided as an example below (Table A-1).

Table A-1. Comparison of major ion chemistry results for Lake L12 from Labtium Oy and TVO. The three TVO samples were taken on the same date at the same depth (4m) at different locations around the lake. The small increases in concentration between Labtium Oy and TVO may be due to a slight increase in conductivity in the lake between 2008 and 2009.

Sample	Date	Lab	Ca mg/l	Mg mg/l	K mg/l	Na mg/l	Cl mg/l	SO4 mg/l	EC (field) uS/cm
L12 1	2008-06-29	Labtium Oy	39.6	5.84	7.69	4.92	3.8	71	297
L12 2 4m	2009-06-27	TVO	44.5	6.74	7.94	6.47	4.2	79.8	313
L12 3 4m	2009-06-27	TVO	44.9	6.84	8.13	6.6	4.2	80.1	313
L12 4 4m	2009-06-27	TVO	44.4	6.86	7.99	6.5	4.2	80	313

(3) York-Durham Regional Environmental Laboratory

Analysis package: major elements.

The York-Durham Regional Environmental Laboratory was used exclusively to analyze the results of crush and leach experiments performed on DH-GAP04 drill core. Alkalinity was not measured and thus C.B.E. could not be calculated. No cross laboratory comparisons are available.

(4) ACTLABS (Ancaster)

Analysis package: major and trace elements.

Actlabs Inc (Ancaster) provided commercial laboratory analyses of solid rock and fracture mineral samples as well as analysis of water samples from out diffusion experiments on DH-GAP04

core and dissolved fracture mineral samples (see Chapter 4). Duplicate samples were run for quality assurance and provided consistent results.

A.2. Isotopic Analyses

Isotopic analyses were conducted at the University of Waterloo Environmental Isotope Laboratory (EIL). Several steps were taken to assure data quality including: duplication of samples and duplicate analysis on the same sample.

$\delta^{18}O$ and $\delta^{2}H$

In 2013, 12 samples previously analyzed for $\delta^{18}O$ were re-run at the University of Waterloo EIL for quality control purposes. The difference between the original and 2013 results was <1 ‰ in all but one sample (L21 Supraglacial) (Table A-2). The re-run samples were decanted into 100 mL vials from the same sample bottles originally tested and assigned new, randomized sample numbers.

Table A-2. Comparison of original $d^{18}O$ isotopic results from 2009 to 2011 with sample re-runs in 2013. The difference between the original value and the 2013 value is also given.

Sample Name	δ18O original	δ18O original rpt	δ2H original	δ18O 2013	Difference
Lake 0010W 06/07/2009	-9.00	-9.3	-102.75	-8.93	-0.07
L21 Supraglacial 30/06/2008	-30.03		-227.1	-28.45	-1.58
Lake 3 27/06/2008	-12.63		-118.69	-12.04	-0.59
DH-GAP01 07/09/2009	-20.46		-157.99	-19.72	-0.74
L25 Drill Water Lake	-13.11		-120.85	-13.41	0.30
Pingo 05/09/2010	-18.46		-152.39	-18.46	0.00
Lake 0025W 06/09/2010	-10.58	-10.55	-106.91	-10.08	-0.50
DH-GAP01 11/05/2010	-21.59	-21.65	-165.13	-20.96	-0.63
Ice Dammed Lake 07/07/2011	-28.20		-217.04	-27.95	-0.25
Pingo 11/09/2011	-18.73		-153.66	-18.75	0.02
DH-GAP04-Mid 09/09/2011	-15.75		-138.44	-16.33	0.58
Braya So 10/09/2011	-8.92		-94.82	-8.37	-0.55

$\delta^{34}S$ and $\delta^{18}O$ (SO_4)

Sample repeats were used to ensure quality $\delta^{34}S$ and $\delta^{18}O$ (SO_4). Repeats are included in Appendix Datatables. Repeat results showed variations of <1‰. Comparison of isotope results from the same sampling location over multiple years also show good consistency (example in Table A-3)

Table A-3. $\delta^{34}S$ and $\delta^{18}O$ (SO_4) isotope results for Lake L22 (Braya Sø): comparison of results between sample dates and results and repeats.

Short Name	Sample Name	Sample Date	$\delta^{34}S$ (SO_4) ‰ CDT	$\delta^{34}S$ rpt	$\delta^{18}O$ (SO_4) ‰ VSMOW	$\delta^{18}O$ rpt
L22 2	Braya Sø (2)	2011-09-10	22.91		4.64	
L22 3 (21m)	Braya Sø (3) (21m)	2012-09-02	23.47		5.99	5.81
L22 4	Braya Sø (4)	2012-09-01	23.60	23.21	6.18	

$\delta^{37}Cl$ and $\delta^{81}Br$ and $^{87}Sr/^{86}Sr$

$\delta^{37}Cl$ and $\delta^{81}Br$ and $^{87}Sr/^{86}S$ isotope results had small standard deviations: 2s values were at the 5th decimal place for $^{87}Sr/^{86}Sr$ results and in the second decimal place for $\delta^{37}Cl$ and $\delta^{81}Br$ results. These values are shown in Appendix B. $^{87}Sr/^{86}Sr$ results showed good consistency for multiple samples of gypsum from the same fracture (Table 4.8).

B. Appendix B. Chemistry Data Tables

Full geochemical and isotopic datasets are presented in this appendix. Blank entries indicate that sample was not analyzed for that parameter.

B.1. List of Tables:

B.2. Geochemical Results

Table B-1. Ponds 209

Table B-2. Dilute Lakes 212

Table B-3. Saline Lakes 218

Table B-4. Meltwater and Thaw Lakes 224

Table B-5. Descriptions of miscellaneous samples: spring runoff, ice dammed lakes springs andmeltwaters. 230

Table B-6. spring runoff, ice dammed lakes springs andmeltwaters. 231

Table B-7. DH-GAP01 237

Table B-8. DH-GAP04 242

Table B-9. Leverett Spring 247

Table B-10. Out diffusion and associated crush and leach experiments. 249

Table B-11. Crush and leach for DH-GAP01 and DH-GAP03 256

Table B-12. Crush and leach for DH-GAP04. 259

Table B-13. Whole rock chemistry. 261

Table B-14. Fracture Gypsum chemistry. 264

B.3. Isotopic Results

Table B-15. Ponds 269

Table B-16. Dilute Lakes 270

Table B-17. Saline Lakes 271

Table B-18. Melt water and thaw lakes. 272

Table B-19. Spring runoff, ice dammed lake springs, meltwaters and ice samples. 273

Table B-20. DH-GAP01 275

Table B-21. DH-GAP04 276
Table B-22. Leverett Spring 277

B.2. Chemistry Results

Table B-1. Major and trace element chemistry for surface water bodies classified as "ponds" (see Chapter 2).

Lake Type	Name	Sample Date	Ca	Mg	K	Na	Cl	SO4	Alk	EC	pH	CBE
			mg/l	mg/l	mg/l	mg/l	mg/l	mg/l	mmol/l	µS/cm		%
Ponds	L3	2008-06-27	64.4	27.6	9.1	9.2	11.1	189.0	1.7	578	8.0	1.9
	L7	2008-06-28	32.2	13.7	5.9	8.3	10.4	34.4	2.1	310	8.1	2.5
	L8	2008-06-28	32.4	19.5	1.7	3.5	2.4	132.0	0.8	344	7.7	-2.1
	L16	2008-07-01	21.3	17.1	11.1	8.0	10.5	28.4	2.0	282	9.2	4.3
	L44	2012-05-12	3.5	1.1	1.8	0.9	1.4	6.1	0.2	39	6.1	0.8
	L11	2008-06-29	210.0	85.8	31.0	17.6	19.4	816.0	1.1	1610	7.7	1.2
	L18	2008-07-01	130.0	135.0	44.8	77.7	102.0	725.0	3.0	1850	8.9	2.7
	L20 1	2008-07-01	20.4	8.8	2.6	2.9	2.4	116.0	<0.02	362	3.5	**-12.5**
	L20 2	2010-09-05	182.0	74.0	28.5	17.2	14.0	949.0	<0.02	1750	3.4	-9.5

lake type	Name	Ag	Al	As	B	Ba	Be	Bi	Br	Cd	Co	Cr
		µg/l	µg/l	µg/l	µg/l	µg/l	µg/l	µg/l	µg/l	µg/l	µg/l	µg/l
Ponds	L3	<0.01	2.0	0.1	18	8.4	<0.1	<0.02	79	<0.02	0.1	0.3
	L7	0.01	29	0.1	9.0	14	<0.1	<0.02	54	<0.02	0.3	0.2
	L8	<0.01	18	0.1	6.6	15	<0.1	<0.02	36	<0.02	0.3	0.5
	L16	<0.01	31	0.2	21	3.4	<0.1	<0.02	109	<0.02	0.5	0.7
	L44	<0.01	141	<0.05	2.2	7.6	<0.1	0.0	8.1	<0.02	0.5	0.9
	L11	0.01	111	0.7	31	33	<0.1	<0.02	174	0.2	4.0	1.3
	L18	0.01	74	0.3	5.7	24	<0.1	<0.02	420	<0.02	0.9	0.9
	L20 1	<0.01	1190	<0.05	5.7	8.7	<0.1	<0.02	21	0.3	9.8	0.4
	L20 2	<0.002	12600	0.2	<0.02	24	0.6	<0.01	123	2.5	117.0	1.6

Table B-1 continued.

lake type	Name	Cu	I	Li	Mn	Mo	Ni	P	Pb	Rb	Sb	Se
		µg/l	µg/l	µg/l	µg/l	µg/l	µg/l	µg/l	µg/l	µg/l	µg/l	µg/l
Ponds	L3	1.4		6.3	2.5	0.1	5.4	<10	<0.05	7.5	<0.02	<0.5
	L7	2.2		3.2	2.2	0.1	9.9	<10	<0.05	10.6	<0.02	<0.5
	L8	1.4		5.3	8.8	0.0	10.5	12.3	<0.05	5.3	<0.02	<0.5
	L16	6.3		2.4	3.3	0.7	12.9	13.5	<0.05	6.2	<0.02	<0.5
	L44	9.8	<2	0.6	13	0.2	4.3	13.2	<0.05	3.4	<0.02	<0.5
	L11	18		16	59	1.6	87.8	11.2	0.1	17.1	0.03	<0.5
	L18	12		3.3	5.5	1.2	16.6	20.3	<0.05	12.2	0.02	0.5
	L20 1	8.7		5.2	382	<0.02	40.9	<10	<0.05	8.2	<0.02	<0.5
	L20 2	29	8.35		3810	0.0	487.0	<10	0.3	59.5	<0.01	<0.5

lake type	Name	Sr	Th	Tl	U	V	Zn	Fe	S	Si	Ce	Dy
		µg/l	µg/l	µg/l	µg/l	µg/l	µg/l	mg/l	mg/l	mg/l	µg/l	µg/l
Ponds	L3	100	0.01	<0.01	0.1	0.5	1.4	<0.03	64.5	0.96	0.028	0.003
	L7	58	0.01	<0.01	0.2	0.2	1.6	0.04	13.0	0.06	0.062	0.005
	L8	62	0.02	<0.01	0.0	0.2	1.8	0.13	41.8	0.28	0.099	0.007
	L16	51	0.08	<0.01	0.1	0.5	1.8	0.62	11.1	0.22	0.466	0.016
	L44	11	0.11	0.01	0.0	0.2	2.7	0.13	2.3	1.07	2.034	0.042
	L11	331	0.03	0.04	3.5	1.0	10.4	0.12	255	0.68	1.245	0.029
	L18	540	0.04	0.01	3.2	0.8	5.1	0.07	226	0.11	0.358	0.011
	L20 1	26	0.01	0.01	0.1	0.1	77.8	0.86	39.6	<0.06	11.2	0.347
	L20 2	217	0.22	<0.001	0.5	<0.02	864	12.2	279	2.7	150	4.2

Table B-1 continued.

lake type	Name	Er	Eu	Gd	Ho	La	Lu	Nd	Pr	Sm	Tb	Tm
		µg/l	µg/l	µg/l	µg/l	µg/l	µg/l	µg/l	µg/l	µg/l	µg/l	µg/l
Ponds	L3	0.002	0.0010	0.004	0.0007	0.027	0.0003	0.027	0.007	0.005	0.0005	<0.0002
	L7	0.003	0.0022	0.009	0.0008	0.066	0.0004	0.054	0.014	0.009	0.0009	0.0003
	L8	0.005	0.0024	0.013	0.0018	0.058	0.0007	0.067	0.017	0.012	0.0015	0.0006
	L16	0.009	0.0066	0.037	0.0032	0.299	0.0010	0.281	0.074	0.043	0.0043	0.0010
	L44	0.006	0.0197	0.082	0.0051	1.2017	0.0022	0.848	0.2331	0.095	0.0099	0.0016
	L11	0.017	0.0123	0.059	0.0056	0.901	0.0020	0.454	0.141	0.055	0.0074	0.0020
	L18	0.007	0.0053	0.027	0.0026	0.259	0.0009	0.232	0.060	0.032	0.0042	0.0009
	L20 1	0.202	0.1115	0.580	0.0719	6.67	0.0253	4.026	1.17	0.513	0.0758	0.0252
	L20 2	2.42	1.23	7.57	0.8451	98.3	0.2606	46.5	14.4	5.45	0.8595	0.2994

lake type	Name	Yb	F	NO3
		µg/l	mg/l	mg/l
Ponds	L3	0.001	0.4	<0.2
	L7	0.002	0.3	<0.2
	L8	0.005	0.3	<0.2
	L16	0.008	<0.1	<0.2
	L44	0.030	<0.1	0.6
	L11	0.011	<1	<0.2
	L18	0.005	<1	<0.2
	L20 1	0.161	0.1	<0.2
	L20 2	1.73		<2

Table B-2. Major and trace element chemistry for dilute lakes (lakes with EC < 800 µS/cm).

Lake Type	Name	Sample Date	Ca mg/l	Mg mg/l	K mg/l	Na mg/l	Cl mg/l	SO4 mg/l	Alk mmol/l	EC µS/cm	pH	CBE %
Dilute Lakes	L1	2008-06-27	27	19	11	19	31	2.5	3.0	381	8.4	1.4
	L2	2008-06-27	2	2.6	2.5	1.3	2.8	0.1	6.0	44	6.9	-86.4
	L4	2008-06-27	5	4.3	10	2.7	4.8	3.1	0.6	91	7.7	8.4
	L5	2008-06-27	19	10	2.4	3.2	3.1	46	0.9	202	7.9	2.1
	L10	2008-06-29	17	29	19	24	33	0.1	3.7	418	9.1	2.5
	L10 2	2009-07-06	21	37	19	29	40	0.2		490	8.9	
	L15	2008-06-30	5	3.6	1.2	1.8	1.7	1.4	0.6	74	8.0	1.5
	L19	2008-07-01	3	2.2	1.8	1.3	1.9	0.8	0.4	50	8.4	-0.2
	L25-1	2009-07-02	11	7.9	2.2	5.0	5.0	5.5		131	8.6	
	L25-2	2011-06-25	12	7.9	3.7	5.2	5.9	3.8	0.5	160	7.6	38.8
	L26-1 (8m)	2009-07-02	15	10	4.9	6.8	8.1	3.5		175	8.2	
	L26-2 (26m)	2010-05-11	18	11	6.4	6.7	10	3.5	1.9	232	7.7	1.0
	L28	2009-07-06	11	10	3.8	7.2	7.8	0.3		171	9.3	
	L31	2010-09-02	23	32	28	53	62	7.8	4.4	600	9.6	3.8
	L33	2010-09-04	7	2.8	1.7	2.6	2.9	2.4	0.6	66	7.6	1.9
	L34	2010-09-06	7	3.7	2.5	2.8	3.5	2.3	0.7	77	7.6	0.0
	L42	2011-09-12	27	29	10	25	33	2.6	3.5	440	9.2	6.8
	L41	2011-09-12	26	36	18	29	40	<1	4.5	550	8.6	3.4
	L40	2011-09-12	12	34	17	24	29	<1	4.2	450	9.6	-0.5
	L43	2011-09-12	12	7.4	3.0	6.9	9.0	3.4	1.1	150	7.7	4.5
	L46	2012-09-03	23	15	11	21	28	1.7	2.4	236	8.9	5.5

Table B-2 continued.

Lake Type	Name	Ag µg/l	Al µg/l	As µg/l	B µg/l	Ba µg/l	Be µg/l	Bi µg/l	Br µg/l	Cd µg/l	Co µg/l	Cr µg/l
Dilute Lakes	L1	0.01	12.1	0.1	21.0	7.9	<0.1	<0.02	156	<0.02	0.1	<0.2
	L2	0.02	123.0	0.1	7.5	2.4	<0.1	<0.02	20.7	<0.02	0.2	0.9
	L4	0.01	129.0	0.2	30.3	3.5	<0.1	<0.02	41.4	<0.02	0.1	1.3
	L5	0.01	28.4	0.2	8.0	7.0	<0.1	<0.02	34.7	<0.02	0.2	0.5
	L10	<0.01	1.3	<0.05	21.9	6.2	<0.1	<0.02	56.4	<0.02	0.0	<0.2
	L10 2								<10			
	L15	<0.01	15.9	<0.05	2.3	7.1	<0.1	<0.02	15.9	<0.02	0.2	0.2
	L19	<0.01	34.1	<0.05	4.5	2.1	<0.1	<0.02	14.4	<0.02	0.2	0.3
	L25-1								<10			
	L25-2	<0.01	9.1	<0.05	4.4	11.6	<0.1	<0.02	36.1	<0.02	0.1	<0.2
	L26-1 (8m)								50			
	L26-2 (26m)	<0.01	<1	0.1	10.4	13.0	<0.1	<0.02	40.2	0.17	0.4	<0.2
	L28								<10			
	L31	<0.002	45.2	<0.02	0.0	13.3	<0.05	<0.01	283	0.02	0.1	1.6
	L33	<0.002	17.3	0.1	<0.02	7.4	<0.05	<0.01	21.1	0.02	0.0	1.1
	L34	<0.002	5.1	<0.02	<0.02	6.3	<0.05	<0.01	15.9	0.01	<0.005	1.0
	L42	<0.01	10.5	0.1	7.4	9.5	<0.1	<0.02	204	<0.02	0.1	<0.2
	L41	<0.01	12.3	0.1	21.8	9.3	<0.1	<0.02	141	<0.02	0.1	<0.2
	L40	<0.01	5.3	<0.05	16.7	3.8	<0.1	<0.02	75.2	<0.02	0.1	<0.2
	L43	<0.01	4.3	0.1	8.4	8.2	<0.1	<0.02	84.1	<0.02	0.2	<0.2
	L46	<0.01	17.7	<0.05	20.4	12.0	<0.1	0.02	103	<0.02	0.1	0.3

Table B-2 continued

Lake Type	Name	Cu µg/l	I µg/l	Li µg/l	Mn µg/l	Mo µg/l	Ni µg/l	P µg/l	Pb µg/l	Rb µg/l	Sb µg/l	Se µg/l
Dilute Lakes	L1	1.96		1.44	2.02	0.08	1.98	<10	<0.05	4.04	<0.02	<0.5
	L2	7.39		0.81	2.58	0.11	4.91	38.4	<0.05	6.23	<0.02	<0.5
	L4	12.8		0.61	0.94	0.40	9.47	29.9	<0.05	3.80	<0.02	<0.5
	L5	4.37		2.81	11.1	0.03	9.37	11.5	<0.05	6.01	<0.02	<0.5
	L10	0.50		10.0	0.42	<0.02	1.31	<10	<0.05	10.8	<0.02	<0.5
	L10 2											
	L15	1.61		0.76	10.9	0.02	2.94	<10	<0.05	5.60	<0.02	<0.5
	L19	2.82		0.92	3.21	0.05	3.23	<10	<0.05	6.06	<0.02	<0.5
	L25-1											
	L25-2	0.82	2.51	1.26	3.25	0.98	1.83	28.1	<0.05	4.81	<0.02	<0.5
	L26-1 (8m)											
	L26-2 (26m)	1.27	<2	2.51	<0.001	1.01	1.72	<10	<0.05	11.8	<0.02	<0.5
	L28											
	L31	0.06	12.0		4.16	0.18	1.85	<10	0.02	10.6	0.02	<0.5
	L33	3.76	4.05		0.11	0.16	3.61	<10	0.01	3.15	<0.01	<0.5
	L34	0.57	3.94		0.42	0.04	1.01	<10	0.02	3.51	<0.01	<0.5
	L42	0.60	5.52	4.66	4.76	0.96	4.27	<10	0.05	2.97	0.26	<0.5
	L41	0.18	2.99	9.03	7.72	0.12	2.46	<10	0.13	8.78	0.54	<0.5
	L40	0.34	2.30	7.96	4.35	0.03	1.06	<10	<0.05	7.78	0.41	<0.5
	L43	2.00	6.02	0.90	4.02	0.11	2.30	<10	0.08	2.61	0.27	<0.5
	L46	0.76	5.80	7.05	7.42	0.02	1.93	10.3	0.15	6.63	0.47	<0.5

Table B-2 continued...

Lake Type	Name	Sr µg/l	Th µg/l	Tl µg/l	U µg/l	V µg/l	Zn µg/l	Fe mg/l	S mg/l	Si mg/l	Ce µg/l	Dy µg/l
Dilute Lakes	L1	94.4	0.03	<0.01	0.20	<0.05	1.51	0.09	1.31	0.08	0.165	0.0071
	L2	4.07	0.26	<0.01	0.04	0.49	6.39	0.24	0.39	0.60	0.877	0.0221
	L4	11.5	0.30	<0.01	0.12	0.79	5.47	0.40	1.66	1.72	1.14	0.0360
	L5	35.3	0.04	<0.01	0.05	0.25	1.55	0.14	16.4	0.19	0.146	0.0083
	L10	46.2	<0.01	<0.01	0.01	<0.05	4.07	0.06	0.54	0.26	0.016	0.0014
	L10 2							0.032	<1.25	0.25		
	L15	14.9	0.02	<0.01	<0.01	0.13	1.55	0.79	0.69	0.11	0.203	0.0056
	L19	6.75	0.06	<0.01	0.01	0.24	5.45	0.51	0.57	0.06	0.528	0.0123
	L25-1							0.171	1.8	0.09		
	L25-2	37.1	0.01	<0.01	0.01	<0.05	3.96	0.20	1.53	0.10	0.1396	0.0077
	L26-1 (8m)							0.01	1.5	0.43		
	L26-2 (26m)	63.4	<0.01	<0.01	0.01	0.05	4.39	0.03	1.27	0.93	0.003	<0.0006
	L28							0.073	<1.25	0.18		
	L31	258	0.03	<0.001	0.21	0.32	5.23	0.05	3.80	1.38	0.2647	0.0111
	L33	40.5	0.02	<0.001	0.03	0.07	0.74	<0.03	0.90	0.12	0.1866	0.0075
	L34	22.8	<0.002	<0.001	<0.001	<0.02	0.45	<0.03	0.88	<0.06	0.0157	0.0007
	L42	80.9	0.04	0.03	0.55	1.03	1.25	0.13	2.65	1.98	0.5044	0.0179
	L41	93.3	0.02	0.03	0.11	0.06	3.02	0.29	0.87	0.20	0.1996	0.0074
	L40	47.9	0.02	0.03	0.02	0.14	2.03	0.12	0.74	1.01	0.1257	0.0043
	L43	39.7	0.08	0.03	0.17	0.10	1.73	0.07	1.46	0.32	0.7998	0.0266
	L46	95.9	0.02	0.03	0.02	0.14	0.41	0.04	1.12	0.55	0.041	0.0022

Table B-2 continued.

Lake Type	Name	Er µg/l	Eu µg/l	Gd µg/l	Ho µg/l	La µg/l	Lu µg/l	Nd µg/l	Pr µg/l	Sm µg/l	Tb µg/l	Tm µg/l
Dilute Lakes	L1	0.004	0.0023	0.014	0.0013	0.119	0.0005	0.103	0.028	0.015	0.0018	0.0004
	L2	0.013	0.0092	0.053	0.0042	0.548	0.0012	0.461	0.128	0.063	0.0061	0.0013
	L4	0.019	0.0164	0.082	0.0066	0.806	0.0021	0.682	0.192	0.097	0.0092	0.0020
	L5	0.006	0.0024	0.015	0.0018	0.106	0.0007	0.096	0.026	0.015	0.0018	0.0007
	L10	0.001	<0.0008	0.003	0.0005	0.012	<0.0003	0.015	0.004	0.003	0.0004	<0.0002
	L10 2											
	L15	0.004	0.0026	0.012	0.0011	0.115	0.0005	0.096	0.027	0.016	0.0014	0.0003
	L19	0.007	0.0051	0.027	0.0023	0.287	0.0006	0.234	0.066	0.031	0.0036	0.0009
	L25-1											
	L25-2	0.0034	0.0045	0.0178	0.002	0.0667	0.0008	0.0659	0.0189	0.0128	0.0017	0.0007
	L26-1 (8m)											
	L26-2 (26m)	<0.001	0.003	<0.001	<0.0005	0.0044	<0.0003	0.0041	0.0009	<0.001	<0.0004	<0.0002
	L28											
	L31	0.006	0.0081	0.0187	0.0014	0.1260	0.0008	0.1414	0.0352	0.0242	0.0019	0.0006
	L33	0.005	0.0055	0.0232	0.0011	0.2783	0.0003	0.1831	0.0504	0.0224	0.0023	0.0008
	L34	0.002	0.0040	0.0070	<0.0005	0.0117	0.0003	0.0139	0.0025	0.0041	<0.0004	<0.0002
	L42	0.012	0.0091	0.041	0.0035	0.3431	0.0012	0.304	0.080	0.046	0.0042	0.0015
	L41	0.004	0.0059	0.015	0.0014	0.1200	0.0007	0.122	0.030	0.019	0.0015	0.0007
	L40	0.003	0.0026	0.009	0.0011	0.0647	<0.0003	0.075	0.018	0.010	0.0012	0.0004
	L43	0.017	0.0120	0.064	0.0057	0.6104	0.0016	0.515	0.133	0.074	0.0071	0.0021
	L46	<0.001	0.0015	0.003	<0.0005	0.0338	<0.0003	<0.001	0.008	0.004	<0.0004	<0.0002

Table B-2 continued.

Lake Type	Name	Yb µg/l	Y µg/l	F mg/l	NO3 mg/l
Dilute Lakes	L1	0.003		0.6	<0.2
	L2	0.009		<0.1	<0.2
	L4	0.014		0.2	<0.2
	L5	0.005		0.1	<0.2
	L10	<0.001		0.7	<0.2
	L10 2			1.0	
	L15	0.003		<0.1	<0.2
	L19	0.004		<0.1	<0.2
	L25-1			0.1	
	L25-2	0.0036		0.1	<0.2
	L26-1 (8m)			0.3	
	L26-2 (26m)	<0.001	0.0031	0.3	0.5
	L28			0.4	
	L31	0.0050			<2
	L33	0.0045			1.1
	L34	0.0035			<0.2
	L42	0.012	0.101	<1	<2
	L41	0.005	0.040	<1	<2
	L40	0.003	0.021	<1	<2
	L43	0.012	0.149	0.2	<0.2
	L46	<0.001	0.010		<0.2

Table B-3. Major and trace element chemistry for saline lakes (lakes with EC > 800 µS/cm).

Lake Type	Name	Sample Date	Ca mg/l	Mg mg/l	K mg/l	Na mg/l	Cl mg/l	SO4 mg/l	Alk mmol/l	EC µS/cm	pH	CBE %
Saline Lakes	L29-1	2009-07-06	13.5	78.5	46.2	99.6	144	0.2		1073	9.2	
	L29-2	2010-09-04	14.7	84.6	87.6	105	152	<1	8.59	1250	9.2	6.5
	L17 1	2008-07-01	22.5	85.0	35.3	74.2	121	24	8.2	902	9.0	1.2
	L17 2	2010-09-05	22.0	118	59.8	99.4	155	30	10.6	1360	9.1	3.8
	L45	2012-08-28	108	150	80.2	340	722	384	6.56	3470	8.3	-0.3
	L21 1	2008-06-01	15.8	203	182	545	797	180	21	4030	8.8	-0.7
	L21 2	2010-09-02	15.8	193	195	467	639	180	18.9	3790	9.0	1.9
	L21 3	2011-09-10	16.1	198	171	490	684	149	19.2	3880	9.0	1.8
	L22 1	2008-06-01	21.5	166	134	430	581	103	18	3340	8.5	1.3
	L22 2	2011-09-10	19.9	149	128	362	493	91	15.6	3000	8.9	1.8
	L22 3 (21m)	2012-09-02	23.3	185	159	430	628	104	18.5	3510		1.4
	L32	2010-09-04	21.1	155	181	343	372	18	18.8	3110	8.9	6.4
	L39	2011-09-10	14.8	233	190	588	782	190	22.3	4500	9.0	2.4

Table B-3 continued.

Lake Type	Name	Ag µg/l	Al µg/l	As µg/l	B µg/l	Ba µg/l	Be µg/l	Bi µg/l	Br µg/l	Cd µg/l	Co µg/l	Cr µg/l
Saline Lakes	L29-1								<10			
	L29-2	0.010	13.4	<0.02	<0.02	7.43	<0.05	<0.01	79.4	0.02	0.14	3.09
	L17 1	<0.01	5.3	0.09	6.06	12.2	0.1	<0.02	277	<0.02	0.12	<0.2
	L17 2	<0.002	16.6	<0.02	<0.02	10.7	0.08	<0.01	356	<0.003	0.19	3.01
	L45	<0.01	11.2	<0.05	248	32.6	<0.1	0.19	1960	<0.02	0.09	<0.2
	L21 1	<0.04	14.8	<0.4	139	52.2	<1	<0.2	980	<0.03	0.31	<2
	L21 2	<0.002	6.4	<0.02	0.09	37.1	<0.05	<0.01	817	0.02	0.13	5.25
	L21 3	0.01	6.8	1.04	136	43.4	0.42	0.04	900	0.03	0.27	<0.2
	L22 1	<0.04	<10	<0.4	95.6	51.1	<1	<0.2	848	<0.03	0.15	3.87
	L22 2	0.02	5.9	0.68	82.3	46.0	0.38	0.04	759	<0.02	0.16	<0.2
	L22 3 (21m)	0.01	6.3	<0.05	132	52.0	<0.1	0.10	859	<0.02	0.15	<0.2
	L32	0.010	12.0	<0.02	<0.02	45.4	0.05	0.01	667	0.04	0.4	6.43
	L39	0.03	7.2	0.41	145	38.4	0.47	0.04	944	0.02	0.28	<0.2

Table B-3 continued.

Lake Type	Name	Cu µg/l	I µg/l	Li µg/l	Mn µg/l	Mo µg/l	Ni µg/l	P µg/l	Pb µg/l	Rb µg/l	Sb µg/l	Se µg/l
Saline Lakes	L29-1											
	L29-2	<0.05	9.92		9.42	0.07	1.76	17.6	0.08	20.0	0.01	<0.5
	L17 1	0.82		3.41	2.77	0.03	1.77	<10	<0.05	10.5	<0.02	<0.5
	L17 2	<0.05	17.0		11.7	0.05	1.81	10.6	0.02	13.3	0.01	<0.5
	L45	<0.1	62.6	31.4	8.46	1.56	4.56	41.6	2.97	11.4	0.14	1.44
	L21 1	<1		26.8	6.19	1.33	2.64	<200	<0.1	49.3	<0.2	<10
	L21 2	5.03	14.4		1.61	1.27	1.57	<10	0.09	39.1	0.01	<0.5
	L21 3	<0.1	13.1	28.2	1.02	2.28	5.11	<10	0.42	42.3	0.14	1.55
	L22 1	<1		24.7	40.7	<0.4	2.33	<200	<0.1	41.8	<0.2	<10
	L22 2	<0.1	31.0	25.2	3.49	0.50	4.70	<10	0.40	36.0	0.51	1.98
	L22 3 (21m)	<0.1	31.4	47.5	104	<0.02	2.43	62.5	2.97	41.0	0.02	<0.5
	L32	<0.05	43.1		4.86	1.33	6.18	24.1	0.09	53.0	0.02	<0.5
	L39	<0.1	19.3	30.7	0.99	2.62	5.11	<10	0.36	45.3	0.46	0.67

Table B-3 continued.

Lake Type	Name	Sr µg/l	Th µg/l	Tl µg/l	U µg/l	V µg/l	Zn µg/l	Fe mg/l	S mg/l	Si mg/l	Ce µg/l	Dy µg/l
Saline Lakes	L29-1							0.049	<1.25	1.1		
	L29-2	69.7	0.01	<0.001	0.15	<0.02	<0.1	0.14	0.69	1.47	0.0972	0.0061
	L17 1	72.1	0.02	<0.01	0.22	0.28	2.30	0.03	9.75	0.22	0.090	0.0082
	L17 2	76.9	0.02	<0.001	0.33	<0.02	0.91	0.04	12.1	0.99	0.2509	0.0118
	L45	883	0.05	0.42	12.1	<0.05	3.65	0.04	128	0.29	0.145	0.0117
	L21 1	574	0.07	<0.02	3.53	<0.4	5.37	<0.03	57.2	1.15	0.494	0.0165
	L21 2	501	0.05	<0.001	2.92	<0.02	4.52	<0.03	56.7	0.69	0.3486	0.0178
	L21 3	495	0.12	0.56	3.23	<0.05	4.36	<0.03	59.1	0.85	0.6324	0.0206
	L22 1	424	0.10	<0.02	1.60	1.04	3.38	<0.03	34.1	1.96	0.891	0.0240
	L22 2	356	0.06	0.47	1.37	<0.05	4.20	<0.03	30.5	0.31	0.4811	0.0239
	L22 3 (21m)	432	0.09	0.54	1.56	<0.05	3.07	<0.03	39.2	1.73	0.487	0.0188
	L32	238	0.08	<0.001	6.47	<0.02	2.44	<0.03	7.18	0.41	0.2013	0.0320
	L39	337	0.06	0.55	3.52	<0.05	3.64	<0.03	74.1	0.65	0.6553	0.0196

Table B-3 continued.

Lake Type	Name	Er µg/l	Eu µg/l	Gd µg/l	Ho µg/l	La µg/l	Lu µg/l	Nd µg/l	Pr µg/l	Sm µg/l	Tb µg/l	Tm µg/l
Saline Lakes	L29-1											
	L29-2	0.002	0.0024	0.0188	0.0012	0.0456	<0.0003	0.0378	0.0119	0.0059	0.0004	0.0006
	L17 1	0.005	0.0031	0.015	0.0017	0.074	0.0007	0.091	0.023	0.013	0.0017	0.0005
	L17 2	0.006	0.0070	0.0234	0.0022	0.1674	0.0014	0.1356	0.0394	0.0229	0.0018	0.0009
	L45	0.007	0.0079	0.017	0.003	0.1619	0.0007	0.005	0.022	0.024	0.0027	0.0009
	L21 1	0.011	0.0080	0.029	0.0063	0.167	0.0015	0.197	0.051	0.031	0.0034	0.0014
	L21 2	0.010	0.0164	0.0245	0.0032	0.1141	0.0021	0.1247	0.0322	0.0280	0.0043	0.0013
	L21 3	0.011	0.0215	0.028	0.0057	0.1960	0.0021	0.231	0.062	0.039	0.0040	0.0020
	L22 1	0.015	0.0126	0.046	0.0059	0.433	0.0020	0.388	0.105	0.053	0.0055	0.0015
	L22 2	0.024	0.0255	0.041	0.0065	0.2041	0.0036	0.256	0.069	0.035	0.0059	0.0035
	L22 3 (21m)	0.009	0.0127	0.030	0.0037	0.2203	0.0019	0.110	0.057	0.035	0.0036	0.0014
	L32	0.016	0.0178	0.0436	0.0054	0.0929	0.0031	0.1237	0.0278	0.0333	0.0047	0.0039
	L39	0.016	0.0163	0.030	0.0033	0.2271	0.0026	0.250	0.064	0.036	0.0035	0.0012

Table B-3 continued.

Lake Type	Name	Yb µg/l	Y µg/l	F mg/l	NO3 mg/l
Saline Lakes	L29-1			2.5	
	L29-2	0.0073			<2
	L17 1	0.004		1.0	<0.2
	L17 2	0.0077			<2
	L45	0.008	0.064		<0.2
	L21 1	0.009		2.3	<2
	L21 2	0.0130			<2
	L21 3	0.043	0.169	4.9	<2
	L22 1	0.013		2.3	<2
	L22 2	0.031	0.192	3.1	<2
	L22 3 (21m)	0.011	0.093		2.03
	L32	0.0168			<2
	L39	0.033	0.177	4.4	<2

Table B-4. Major and trace element chemistry of meltwater and thaw lakes.

Lake Type	Name	Sample Date	Ca	Mg	K	Na	Cl	SO4	Alk	EC	pH	CBE
			mg/l	mg/l	mg/l	mg/l	mg/l	mg/l	mmol/l	µS/cm		%
Thaw Lakes	L12 1	2008-06-29	39.6	5.8	7.7	4.9	3.8	71	1.3	297	7.8	0.0
	L12 2	2009-06-27	44.5	6.7	7.9	6.5	4.2	79.8		313	8.2	
	L12 3	2009-06-27	44.9	6.8	8.1	6.6	4.2	80.1		313	8.3	
	L12 4	2009-06-27	44.4	6.9	8.0	6.5	4.2	80		313	8.3	
	L13	2008-06-29	7.19	0.9	1.7	1.1	0.9	12	0.3	61	7.5	-4.0
	L14	2008-06-29	45.5	7.3	8.5	5.2	2.7	77	1.6	327	8.4	0.6
	L23	2009-06-28	35.8	5.7	7.3	5.1	2.8	67.3		259	8.2	
	L24	2009-06-28	35.2	5.5	6.3	4.6	3	58.2		246	8.3	
Melt-water Lakes	L6	2008-06-28	25.5	9.3	3.4	3.1	3.0	44	1.2	223	7.7	1.3
	L36	2011-06-19	5.86	3.3	0.4	1.8	1.8	3.3	0.43	62	6.8	9.2
	L36	2011-06-19	5.82	3.3	0.4	1.8	1.8	3.2	0.44	59	6.8	8.1
	L37	2011-06-22	8.36	1.5	2.0	0.7	0.6	14	0.37	71	7.1	-4.0

Table B-4 continued.

Lake Type	Name	Ag µg/l	Al µg/l	As µg/l	B µg/l	Ba µg/l	Be µg/l	Bi µg/l	Br µg/l	Cd µg/l	Co µg/l	Cr µg/l
Thaw Lakes	L12 1	<0.01	20.0	<0.05	9.15	25.9	<0.1	<0.02	26.5	<0.02	<0.02	<0.2
	L12 2								30			
	L12 3								30			
	L12 4								30			
	L13	<0.01	24.2	<0.05	2.49	4.94	<0.1	<0.02	6.41	<0.02	0.03	<0.2
	L14	<0.01	5.26	<0.05	4.71	17.1	<0.1	<0.02	7.80	<0.02	<0.02	<0.2
	L23								50			
	L24								40			
Melt-water Lakes	L6	0.01	63.8	0.24	6.02	13.0	<0.1	<0.02	40.0	<0.02	0.18	0.64
	L36	<0.01	114	0.05	3.64	8.27	<0.1	<0.02	25.2	<0.02	0.54	1.00
	L36	<0.01	113	0.06	2.82	7.96	<0.1	<0.02	34.2	<0.02	0.49	0.87
	L37	0.01	247	<0.05	2.02	15.4	<0.1	<0.02	5.54	<0.02	0.23	0.41

Table B-4 continued.

Lake Type	Name	Cu µg/l	I µg/l	Li µg/l	Mn µg/l	Mo µg/l	Ni µg/l	P µg/l	Pb µg/l	Rb µg/l	Sb µg/l	Se µg/l
Thaw Lakes	L12 1	1.49		0.54	0.52	4.89	0.46	<10	<0.05	4.13	<0.02	<0.5
	L12 2											
	L12 3											
	L12 4											
	L13	2.31		0.79	3.41	1.53	0.87	<10	<0.05	1.33	<0.02	<0.5
	L14	1.23		2.42	1.39	4.75	0.85	<10	<0.05	3.19	<0.02	<0.5
	L23											
	L24											
Melt-water Lakes	L6	11.6		1.62	6.65	0.28	10.6	10.5	0.08	6.12	<0.02	<0.5
	L36	6.31	2.41	1.09	3.21	0.62	7.55	40.7	0.05	1.33	3.83	<0.5
	L36	6.20	3.07	0.84	3.18	0.20	7.48	39.6	<0.05	1.32	3.77	<0.5
	L37	7.53	<2	0.67	6.00	0.42	4.33	26.5	0.11	3.12	<0.02	<0.5

Table B-4 continued.

Lake Type	Name	Sr µg/l	Th µg/l	Tl µg/l	U µg/l	V µg/l	Zn µg/l	Fe mg/l	S mg/l	Si mg/l	Ce µg/l	Dy µg/l
Thaw Lakes	L12 1	130	<0.01	0.01	0.31	0.06	0.65	<0.03	24.7	0.16	0.098	0.0019
	L12 2							0.006	27	0.27		
	L12 3							0.009	27	0.26		
	L12 4							0.028	27	0.39		
	L13	25.7	<0.01	<0.01	0.01	0.11	0.82	<0.03	4.27	0.82	0.077	0.0013
	L14	137	<0.01	<0.01	0.28	0.08	0.53	<0.03	28.0	2.52	0.018	<0.0006
	L23							0.007	22	0.77		
	L24							0.006	19	0.91		
Melt-water Lakes	L6	52.2	0.10	0.01	0.37	0.41	1.66	0.43	15.6	0.36	1.03	0.0250
	L36	17.5	0.09	<0.01	0.02	0.37	2.66	0.85	1.58	0.84	0.7175	0.0241
	L36	17.1	0.08	0.01	0.02	0.37	2.66	0.85	1.55	0.84	0.7877	0.0242
	L37	25.2	0.03	<0.01	0.04	0.48	4.03	0.26	4.56	2.63	0.9704	0.0186

Table B-4 continued.

Lake Type	Name	Er µg/l	Eu µg/l	Gd µg/l	Ho µg/l	La µg/l	Lu µg/l	Nd µg/l	Pr µg/l	Sm µg/l	Tb µg/l	Tm µg/l
Thaw Lakes	L12 1	0.001	0.0015	0.006	<0.0005	0.120	<0.0003	0.059	0.017	0.005	0.0005	<0.0002
	L12 2											
	L12 3											
	L12 4											
	L13	<0.001	0.0011	0.003	<0.0005	0.051	<0.0003	0.034	0.010	0.004	<0.0004	<0.0002
	L14	<0.001	<0.0008	0.001	<0.0005	0.015	<0.0003	0.009	0.003	0.002	<0.0004	<0.0002
	L23											
	L24											
Melt-water Lakes	L6	0.014	0.0105	0.057	0.0047	0.681	0.0015	0.487	0.139	0.066	0.0064	0.0015
	L36	0.0283	0.0129	0.0459	0.0073	0.3832	0.0034	0.3829	0.1055	0.0476	0.0065	0.0045
	L36	0.0163	0.0148	0.0583	0.0052	0.4441	0.0029	0.4104	0.1084	0.0666	0.0055	0.0024
	L37	0.0137	0.0128	0.0408	0.003	0.613	0.0013	0.4984	0.1317	0.0622	0.0054	0.0015

Table B-4 continued.

Lake Type	Name	Yb µg/l	F mg/l	NO3 mg/l
Thaw Lakes	L12 1	<0.001	0.2	<0.2
	L12 2		0.2	
	L12 3		0.2	
	L12 4		0.2	
	L13	<0.001	<0.1	<0.2
	L14	<0.001	0.1	<0.2
	L23		0.2	
	L24		0.2	
Melt-water Lakes	L6	0.010	<0.1	<0.2
	L36	0.0117	<0.1	<0.2
	L36	0.0148	<0.1	<0.2
	L37	0.0053	<0.1	0.7

Table B-5. Descriptions of spring runoff samples, ice dammed lake springs and meltwater samples.

	Name	Long Name	Description
Spring Runoff	**Run-1**	Spring Runoff 1	Samples of spring runoff from 2012 collected from runoff streams in 2012.
	Run-2	Spring Runoff 2	
IDL Springs	SP-2	IDL Spring 2	Waters collected from springs that emerged from the lake bed after the ice-dammed lake drained in 2011.
	SP-3	IDL Spring 3	
Meltwater and Meltwater River Samples	MW 1	MW1	Subglacial meltwater from Leverett Glacier (collected at small outflow).
	MW 2	MW2	Supraglacial meltwater from Leverett Glacier
	MW 3	MW3	Subglacial meltwater sample collected at Isunnguata Sermia near drill site
	MW 4	MW4	Supraglacial meltwater from Isunnguata Sermia
	MW5-2	Leverett River	Sample from large meltwater river in front of Leverett Glacier
	MW8 (012)	GL11-IT-012	Samples from large meltwater river at Isunnguata Sermia Terminus. Collected by Sub Project B (Claire Landowski)
	MW8 (013)	GL11-IT-013	
	C River-1	Caribou Outflow	Samples of meltwater collected at same site as MW2.
	C River-2	Caribou Outflow(2)	
	MW9	S4 Surface Stream	Sample collected from supraglacial stream by Sub Project A.
	MW10	Kan-L Pond	Sample collected from supraglacial lake by Sub Project A.
	MW24	Point 660	Sample of glacial meltwater outflow at Point 660.
	Q River	Qinquata Kuusua	Sample of large meltwater river near Kangerlussuaq (Qinquata Kuusua).
	MW12	GL12-2-1	Samples of subglacial meltwater taken at ice bed on Isunnguata Sermia. Sub Project B used hot water drilling to penetrate to the glacier bed. Samples were treated with various degrees of filtering. Fine filtering contributed significantly to reduced charge balance errors.
	MW13	GL12-2-1, 0.1 µm filtering	
	MW14	GL12-2-2	
	MW15	GL12-2-2, 0.1 µm filtering	
	MW16	GL12-2-3	
	MW17	GL12-2-4, sample 1	
	MW18	GL12-2-4, sample 2	
	MW19	GL12-2-4, samp 2, 0.1µm filtering	
	MW20	GL12-PGS1	
	MW21	GL12-PGS2	
	MW22	GL12-TM	
	MW23	GL12-TM, 0.1 µm filtering	

Table B-6. Major and trace element chemistry of spring runoff, ice dammed lake springs and meltwater samples.

	Name	Sample Date	Ca mg/l	Mg mg/l	K mg/l	Na mg/l	Cl mg/l	SO4 mg/l	Alk mmol/l	EC µS/cm	pH	CBE %
Spring Runoff	Run-1	2012-05-06	3.3	2.2	4.2	1.5	2.1	5.8	0.2	57	6.1	10.3
	Run-2	2012-05-06	2.0	2.1	5.6	1.2	1.5	1.2	0.4	47	6.2	6.1
IDL springs	SP-2	2011-07-05	7.1	3.2	1.8	1.3	1.7	11.6	0.3	77	6.6	3.5
	SP-3	2011-07-01	13.4	5.6	2.9	1.4	0.8	26.0	0.7	140	7.3	-2.5
Meltwater and Meltwater River Samples	MW 1	2008-06-29	0.3	<0.1	0.1	<0.2	0.1	<0.1	0.1	2	7.6	-60.9
	MW 2	2008-06-29	<0.1	<0.1	<0.01	<0.2	0.0	<0.1	0.0	1	7.4	-100.0
	MW 3	2008-06-30	0.8	0.1	0.3	0.3	0.0	0.4	0.1	6	8.0	-21.4
	MW 4	2008-06-30	0.2	<0.1	0.1	<0.2	0.0	<0.1	0.1	2	8.6	-66.0
	MW5-2	2011-09-07	2.4	0.5	1.1	1.7	0.2	2.8	0.3	28		-11.0
	MW8 (012)	2011-06-14	4.5	0.4	1.4	1.7	0.3	8.9	0.4	58	7.4	-22.7
	MW8 (013)	2011-06-17	2.9	0.3	1.4	1.4	0.2	4.1	0.4	37	7.9	-25.3
	C River-1	2011-09-07	1.3	0.3	0.5	0.3	0.4	1.2	0.1	14	6.4	-7.6
	C River-2	2011-09-07	1.3	0.3	0.5	0.3	0.4	1.2	0.1	14	6.4	-15.3
	MW9	2012-07-20	<0.1	<0.1	0.0	<0.2	<0.4	<0.1	0.1	2	5.4	-99.1
	MW10	2012-07-20	<0.1	<0.1	0.4	0.6	1.2	0.6	0.1	9	6.2	-58.9
	MW24	2012	3.5	1.1	1.8	0.9	1.4	6.1	0.2	39	6.1	0.8
	Q River	2011-09-09	2.7	0.4	1.1	1.3	<0.2	3.0	0.2	27	7.0	-8.5
	MW12	summer-2012	3.5	0.2	27.3	2.2	0.2	1.7	0.3	36	7.5	45.9
	MW13	summer-2012	3.2	0.2	0.8	1.4	0.2	1.7	0.3	-	-	-17.9
	MW14	summer-2012	0.6	<0.1	3.9	1.6	6.3	0.3	0.1	34	6.3	-20.6
	MW15	summer-2012	0.5	<0.1	7.1	2.3	6.3	0.3	0.1	-	-	1.1
	MW16	summer-2012	0.5	<0.1	9.0	1.3	28.0	0.3	0.1	121	6.4	-49.8
	MW17	summer-2012	1.2	<0.1	0.5	0.6	<0.2	0.7	0.1	11	6.6	-23.1
	MW18	summer-2012	3.7	0.2	11.5	1.4	4.5	3.0	0.4	51.4	7.2	1.8
	MW19	summer-2012	3.9	0.2	9.5	1.4	4.5	3.0	0.4	-	-	-2.2
	MW20	summer-2012	0.4	<0.1	0.4	0.5	<0.2	0.2	0.2	5	6.3	-53.2
	MW21	summer-2012	0.4	<0.1	0.9	0.9	<0.2	0.2	0.2	4	6.2	-36.2
	MW22	summer-2012	3.1	0.3	3.4	2.9	0.3	5.9	0.5	43	7.7	-21.3
	MW23	summer-2012	3.5	0.4	5.1	3.9	0.3	5.9	0.5	-	-	-9.2

Table B-6 continued.

	Name	Sample Date	Ag µg/l	Al µg/l	As µg/l	B µg/l	Ba µg/l	Be µg/l	Bi µg/l	Br µg/l	Cd µg/l	Co µg/l
Spring Runoff IDL springs	**Run-1**	2012-05-06	<0.01	68.6	<0.05	4.68	6.38	<0.1	0.06	14.6	<0.02	0.35
	Run-2	2012-05-06	<0.01	85.0	<0.05	9.87	2.06	<0.1	0.04	12.2	<0.02	0.31
	SP-2	2011-07-05	0.01	121	0.06	5.14	11.8	<0.1	<0.02	15.6	<0.02	1.36
	SP-3	2011-07-01	0.01	58.5	<0.05	8.27	16.4	<0.1	<0.02	15.7	<0.02	0.27
Meltwater and Meltwater River Samples	MW 1	2008-06-29	<0.01	24.8	<0.05	<0.5	0.82	<0.1	<0.02	1.50	<0.02	0.10
	MW 2	2008-06-29	<0.01	5.93	<0.05	<0.5	0.51	<0.1	<0.02	0.67	<0.02	<0.02
	MW 3	2008-06-30	<0.01	43.2	<0.05	<0.5	1.41	<0.1	<0.02	1.37	<0.02	0.12
	MW 4	2008-06-30	<0.01	46.7	<0.05	<0.5	0.83	<0.1	<0.02	0.66	<0.02	0.03
	MW5-2	2011-09-07	<0.01	276	0.05	1.74	4.59	<0.1	<0.02	<5	<0.02	0.13
	MW8 (012)	2011-06-14	<0.01	25.8	0.07	1.05	2.25	<0.1	<0.02	6.44	0.02	<0.02
	MW8 (013)	2011-06-17	<0.01	37.1	0.05	0.8	1.98	<0.1	<0.02	<5	0.02	0.02
	C River-1	2011-09-07	<0.01	98.0	<0.05	0.95	3.64	<0.1	<0.02	<5	0.02	0.26
	C River-2	2011-09-07	<0.01	90.9	<0.05	<0.5	3.64	<0.1	<0.02	<5	0.02	0.23
	MW9	2012-07-20	<0.01	2.08	<0.05	<0.5	0.10	<0.1	<0.02	<5	<0.02	<0.02
	MW10	2012-07-20	<0.01	5.18	<0.05	<0.5	0.15	<0.1	<0.02	<5	0.07	<0.02
	MW24	2012	<0.01	141	<0.05	2.15	7.63	<0.1	0.04	8.06	<0.02	0.52
	Q River	2011-09-09	0.01	151	<0.05	1.40	3.47	<0.1	<0.02	<5	<0.02	0.11
	MW12	summer-2012	0.01	132	<0.05	2.33	8.04	<0.1	<0.02	7.75	<0.02	0.20
	MW13	summer-2012	<0.01	52.4	<0.05	1.79	1.90	<0.1	<0.02	<3	0.02	0.08
	MW14	summer-2012	<0.01	4.05	<0.05	0.82	1.21	<0.1	<0.02	5.97	0.16	0.12
	MW15	summer-2012	0.01	36.9	<0.05	<0.5	2.51	<0.1	<0.02	3.32	0.15	0.11
	MW16	summer-2012	<0.01	18.0	<0.05	0.54	1.44	<0.1	<0.02	<3	0.08	2.04
	MW17	summer-2012	0.01	14.9	<0.05	0.63	1.76	<0.1	<0.02	<3	0.18	0.07
	MW18	summer-2012	0.01	36.5	<0.05	1.32	2.03	<0.1	<0.02	4.09	0.02	0.03
	MW19	summer-2012	<0.01	64.5	<0.05	1.45	2.60	<0.1	<0.02	4.33	0.03	0.07
	MW20	summer-2012	<0.01	1.76	<0.05	<0.5	1.36	<0.1	<0.02	<3	<0.02	0.11
	MW21	summer-2012	0.01	75.2	<0.05	<0.5	2.67	<0.1	<0.02	<3	<0.02	0.18
	MW22	summer-2012	<0.01	79.1	0.06	1.28	2.04	<0.1	<0.02	5.89	0.02	0.06
	MW23	summer-2012	0.02	39.2	0.06	1.88	3.49	<0.1	<0.02	8.65	0.05	0.17

Table B-6 continued.

	Name	Sample Date	Cr µg/l	Cu µg/l	I µg/l	Li µg/l	Mn µg/l	Mo µg/l	Ni µg/l	P µg/l	Pb µg/l	Rb µg/l
Spring Runoff IDL springs	**Run-1**	2012-05-06	0.95	7.06	<2	0.67	6.79	0.13	6.11	31.6	<0.05	7.80
	Run-2	2012-05-06	0.87	7.21	<2	1.09	2.10	0.13	5.62	46.7	0.05	5.06
	SP-2	2011-07-05	0.80	43.7	2.18	0.65	17.3	0.29	10.7	14.6	<0.05	0.75
	SP-3	2011-07-01	0.37	9.94	<2	0.54	35.4	1.39	5.37	20.9	<0.05	1.03
Meltwater and Meltwater River Samples	MW 1	2008-06-29	<0.2	0.66		0.14	3.95	0.02	0.24	<10	<0.05	0.33
	MW 2	2008-06-29	<0.2	0.11		<0.1	0.38	<0.02	<0.05	<10	<0.05	0.03
	MW 3	2008-06-30	<0.2	1.76		0.12	8.30	0.02	0.81	<10	<0.05	0.42
	MW 4	2008-06-30	<0.2	0.32		<0.1	0.72	<0.02	0.10	<10	<0.05	0.10
	MW5-2	2011-09-07	0.26	1.04	<2	0.60	4.52	0.76	0.38	<10	0.09	0.68
	MW8 (012)	2011-06-14	<0.2	0.44	<2	0.55	0.38	0.83	0.32	<10	<0.05	0.57
	MW8 (013)	2011-06-17	<0.2	0.32	<2	0.61	1.15	0.64	0.16	<10	<0.05	0.55
	C River-1	2011-09-07	<0.2	1.87	<2	0.32	13.8	0.08	1.06	<10	0.05	0.49
	C River-2	2011-09-07	<0.2	1.69	<2	0.19	12.7	0.06	0.93	<10	0.05	0.47
	MW9	2012-07-20	0.29	0.13	<2	<0.1	0.07	<0.02	0.07	<10	<0.05	<0.01
	MW10	2012-07-20	0.50	2.46	<2	<0.1	0.49	<0.02	0.68	<10	0.20	0.29
	MW24	2012	0.86	9.82	<2	0.64	13.0	0.15	4.26	13.2	<0.05	3.40
	Q River	2011-09-09	0.24	0.72	<2	0.58	3.81	0.53	0.67	<10	<0.05	0.79
	MW12	summer-2012	1.16	2.94	<2	1.28	4.06	1.88	1.11	102	0.05	1.57
	MW13	summer-2012	1.34	1.69	<2	0.51	1.80	1.54	0.28	<10	0.08	0.28
	MW14	summer-2012	6.09	7.13	<2	0.30	2.11	0.27	1.17	<10	0.27	0.60
	MW15	summer-2012	1.35	4.45	<2	0.32	1.89	0.16	0.57	17.7	0.21	0.63
	MW16	summer-2012	0.84	3.17	<2	0.34	1.19	0.12	0.23	14.2	0.09	0.56
	MW17	summer-2012	0.42	1.61	<2	0.17	0.88	0.58	0.17	<10	0.10	0.24
	MW18	summer-2012	0.46	2.04	<2	0.92	0.14	2.46	0.14	37.6	0.08	0.95
	MW19	summer-2012	0.63	2.46	<2	0.83	0.82	2.44	0.28	27.6	0.12	0.98
	MW20	summer-2012	0.26	1.56	<2	0.14	6.47	0.10	0.31	<10	<0.05	0.19
	MW21	summer-2012	0.30	2.20	<2	0.24	7.11	0.08	0.6	<10	0.06	0.37
	MW22	summer-2012	0.32	4.67	<2	1.15	2.36	1.32	1.20	<10	0.11	0.97
	MW23	summer-2012	0.78	8.56	<2	1.43	4.89	0.71	1.85	<10	0.25	1.59

Table B-6 continued.

	Name	Sample Date	Sb µg/l	Se µg/l	Sr µg/l	Th µg/l	Tl µg/l	U µg/l	V µg/l	Zn µg/l	Fe mg/l	S mg/l
Spring Runoff IDL springs	**Run-1**	2012-05-06	0.84	<0.5	11.8	0.08	0.01	0.02	0.12	3.57	0.1	2.11
	Run-2	2012-05-06	0.52	<0.5	4.99	0.19	<0.01	0.02	0.18	4.29	0.16	0.73
	SP-2	2011-07-05	1.00	<0.5	22.0	0.39	0.01	0.19	0.87	1.67	0.15	4.10
	SP-3	2011-07-01	1.51	<0.5	43.2	0.04	0.01	0.06	0.59	1.24	0.10	8.78
Meltwater and Meltwater River Samples	MW 1	2008-06-29	<0.02	<0.5	1.34	0.01	<0.01	<0.01	0.35	3.64	0.03	<0.1
	MW 2	2008-06-29	<0.02	<0.5	0.47	<0.01	<0.01	<0.01	<0.05	1.45	<0.03	<0.1
	MW 3	2008-06-30	<0.02	<0.5	4.08	<0.01	<0.01	<0.01	0.26	10.9	0.08	0.16
	MW 4	2008-06-30	<0.02	<0.5	1.07	<0.01	<0.01	<0.01	0.15	1.07	0.05	<0.1
	MW5-2	2011-09-07	1.05	<0.5	10.6	0.04	0.01	0.07	2.06	1.31	0.20	1.05
	MW8 (012)	2011-06-14	<0.02	<0.5	15.6	<0.01	0.03	0.01	1.87	0.55	<0.03	2.26
	MW8 (013)	2011-06-17	<0.02	<0.5	10.6	<0.01	0.03	<0.01	2.26	0.87	0.04	1.17
	C River-1	2011-09-07	2.33	<0.5	7.81	0.01	0.02	0.01	0.32	4.40	0.11	0.44
	C River-2	2011-09-07	2.31	<0.5	7.51	0.01	0.02	0.01	0.32	4.38	0.12	0.45
	MW9	2012-07-20	<0.02	<0.5	0.38	<0.01	<0.01	<0.01	<0.05	1.03	<0.03	<0.1
	MW10	2012-07-20	0.03	<0.5	0.40	<0.01	<0.01	<0.01	<0.05	90.6	<0.03	<0.1
	MW24	2012	<0.02	<0.5	11.3	0.11	0.01	0.04	0.18	2.66	0.13	2.26
	Q River	2011-09-09	<0.02	<0.5	9.65	0.03	0.01	0.02	1.27	0.76	0.16	1.14
	MW12	summer-2012	0.19	<0.5	15.7	0.01	0.01	0.03	2.10	1.81	0.09	0.56
	MW13	summer-2012	0.10	<0.5	9.87	<0.01	<0.01	0.03	1.37	4.34	<0.03	0.63
	MW14	summer-2012	0.26	<0.5	2.39	<0.01	<0.01	<0.01	<0.05	50.5	<0.03	0.31
	MW15	summer-2012	0.16	<0.5	2.69	0.01	<0.01	<0.01	0.09	29.2	0.05	0.21
	MW16	summer-2012	0.09	<0.5	2.07	<0.01	<0.01	<0.01	<0.05	43.0	<0.03	0.16
	MW17	summer-2012	0.06	<0.5	4.18	<0.01	<0.01	0.01	1.41	112	<0.03	0.35
	MW18	summer-2012	0.14	<0.5	13.4	<0.01	<0.01	0.09	5.39	9.54	<0.03	1.14
	MW19	summer-2012	0.15	<0.5	13.2	0.01	<0.01	0.09	5.19	16.0	0.03	1.19
	MW20	summer-2012	0.06	<0.5	2.22	<0.01	<0.01	<0.01	0.08	6.28	<0.03	0.19
	MW21	summer-2012	0.08	<0.5	2.27	<0.01	<0.01	<0.01	0.30	7.61	0.09	0.10
	MW22	summer-2012	0.15	<0.5	13.0	<0.01	<0.01	0.01	4.03	2.60	<0.03	1.91
	MW23	summer-2012	0.41	<0.5	15.1	<0.01	0.01	0.04	3.78	8.95	<0.03	1.92

Table B-6 continued.

	Name	Sample Date	Si mg/l	Ce µg/l	Dy µg/l	Er µg/l	Eu µg/l	Gd µg/l	Ho µg/l	La µg/l	Lu µg/l
Spring Runoff IDL springs	Run-1	2012-05-06	1.090	0.651	0.018	0.001	0.006	0.037	0.001	0.403	0.001
	Run-2	2012-05-06	1.510	1.233	0.026	0.013	0.011	0.064	0.003	0.687	0.003
	SP-2	2011-07-05	3.700	7.323	0.116	0.056	0.067	0.369	0.020	4.515	0.008
	SP-3	2011-07-01	2.850	1.246	0.026	0.013	0.015	0.068	0.005	0.711	0.001
Melt-water and Melt-water River Samples	MW 1	2008-06-29	0.140	0.165	0.002	0.001	0.001	0.007	<0.0005	0.079	<0.0003
	MW 2	2008-06-29	<0.06	0.014	<0.0006	<0.001	<0.0008	<0.001	<0.0005	0.005	<0.0003
	MW 3	2008-06-30	0.320	0.183	0.003	0.002	0.001	0.008	0.001	0.097	<0.0003
	MW 4	2008-06-30	0.130	0.065	0.001	<0.001	<0.0008	0.003	<0.0005	0.035	<0.0003
	MW5-2	2011-09-07	1.310	0.511	0.011	0.005	0.007	0.026	0.002	0.264	0.001
	MW8 (012)	2011-06-14	0.980	0.033	<0.0006	<0.001	<0.0008	0.002	<0.0005	0.020	<0.0003
	MW8 (013)	2011-06-17	0.940	0.054	<0.0006	<0.001	0.001	0.002	<0.0005	0.029	<0.0003
	C River-1	2011-09-07	0.480	0.553	0.008	0.005	0.006	0.024	0.001	0.282	0.000
	C River-2	2011-09-07	0.470	0.589	0.009	0.004	0.006	0.023	0.001	0.296	0.000
	MW9	2012-07-20	<0.06	0.011	<0.0006	0.001	0.001	0.003	0.001	0.007	0.000
	MW10	2012-07-20	<0.06	0.009	0.002	<0.001	<0.0008	<0.001	<0.0005	0.006	0.000
	MW24	2012	1.070	2.034	0.042	0.006	0.020	0.082	0.005	1.202	0.002
	Q River	2011-09-09	1.110	0.296	0.007	0.003	0.004	0.017	0.001	0.151	0.000
	MW12	summer-2012	0.940	0.781	0.030	0.018	0.011	0.063	0.007	0.351	0.002
	MW13	summer-2012	0.830	0.541	0.029	0.011	0.006	0.050	0.006	0.226	0.001
	MW14	summer-2012	0.070	0.521	0.033	0.020	0.007	0.055	0.009	0.214	0.002
	MW15	summer-2012	0.130	0.630	0.035	0.013	0.005	0.055	0.007	0.266	0.002
	MW16	summer-2012	0.120	0.550	0.036	0.023	0.007	0.050	0.007	0.243	0.003
	MW17	summer-2012	0.660	0.558	0.030	0.016	0.009	0.050	0.005	0.246	0.002
	MW18	summer-2012	2.160	0.500	0.035	0.010	0.011	0.048	0.006	0.239	0.003
	MW19	summer-2012	2.210	0.628	0.037	0.014	0.007	0.054	0.007	0.267	0.003
	MW20	summer-2012	0.130	0.555	0.022	0.025	0.008	0.048	0.009	0.248	0.001
	MW21	summer-2012	0.210	0.760	0.037	0.013	0.009	0.053	0.008	0.335	0.003
	MW22	summer-2012	1.220	0.590	0.040	0.017	0.008	0.047	0.008	0.257	0.002
	MW23	summer-2012	1.160	0.587	0.032	0.018	0.007	0.042	0.010	0.252	0.004

Table B-6 continued.

	Name	Sample Date	Nd µg/l	Pr µg/l	Sm µg/l	Tb µg/l	Tm µg/l	Yb µg/l	Y µg/l	F mg/l	NO3 mg/l
Spring Runoff IDL springs	**Run-1**	2012-05-06	0.308	0.081	0.047	0.005	0.001	0.013	0.087	<0.1	2.2
	Run-2	2012-05-06	0.474	0.140	0.057	0.009	0.002	0.040	0.133	0.1	0.8
	SP-2	2011-07-05	3.816	1.032	0.446	0.037	0.007	0.050		<0.1	5.4
	SP-3	2011-07-01	0.551	0.144	0.061	0.006	0.002	0.009		0.1	3.6
Meltwater and Meltwater River Samples	MW 1	2008-06-29	0.062	0.018	0.009	0.001	<0.0002	<0.001		<0.1	<0.2
	MW 2	2008-06-29	0.003	0.001	0.001	<0.0004	<0.0002	<0.001		<0.1	<0.2
	MW 3	2008-06-30	0.066	0.020	0.009	0.001	<0.0002	<0.001		<0.1	<0.2
	MW 4	2008-06-30	0.023	0.007	0.004	0.000	<0.0002	<0.001		<0.1	<0.2
	MW5-2	2011-09-07	0.186	0.056	0.027	0.003	0.001	0.005	0.052	<0.1	<0.2
	MW8 (012)	2011-06-14	0.009	0.003	0.002	<0.0004	<0.0002	<0.001	0.003	<0.1	<0.2
	MW8 (013)	2011-06-17	0.013	0.006	0.003	<0.0004	0.000	<0.001	0.004	<0.1	<0.2
	C River-1	2011-09-07	0.211	0.060	0.025	0.002	0.001	0.003	0.040	<0.1	<0.2
	C River-2	2011-09-07	0.232	0.068	0.032	0.002	0.001	0.005	0.038	<0.1	<0.2
	MW9	2012-07-20	<0.001	0.001	0.003	0.001	0.000	0.004	0.003		<0.2
	MW10	2012-07-20	0.099	0.001	0.001	0.001	<0.0002	0.003	0.002		0.3
	MW24	2012	0.848	0.233	0.095	0.010	0.002	0.030	0.186	<0.1	0.6
	Q River	2011-09-09	0.119	0.035	0.016	0.002	0.001	0.004	0.031	<0.1	<0.2
	MW12	summer-2012	0.314	0.086	0.053	0.006	0.005	0.025	0.256	<0.1	<0.2
	MW13	summer-2012	0.202	0.063	0.041	0.006	0.003	0.019	0.231	<0.1	<0.2
	MW14	summer-2012	0.199	0.058	0.036	0.005	0.003	0.032	0.233	<0.1	<0.2
	MW15	summer-2012	0.277	0.066	0.036	0.009	0.003	0.031	0.214	<0.1	<0.2
	MW16	summer-2012	0.221	0.069	0.045	0.008	0.002	0.036	0.230	<0.1	<0.2
	MW17	summer-2012	0.201	0.061	0.046	0.006	0.003	0.021	0.225	<0.1	<0.2
	MW18	summer-2012	0.232	0.059	0.028	0.007	0.002	0.015	0.231	<0.1	<0.2
	MW19	summer-2012	0.241	0.074	0.032	0.008	0.002	0.023	0.230	<0.1	<0.2
	MW20	summer-2012	0.235	0.059	0.038	0.008	0.002	0.037	0.238	<0.1	<0.2
	MW21	summer-2012	0.253	0.073	0.057	0.008	0.002	0.026	0.233	<0.1	<0.2
	MW22	summer-2012	0.218	0.065	0.055	0.008	0.003	0.031	0.239	<0.1	<0.2
	MW23	summer-2012	0.219	0.065	0.044	0.008	0.002	0.022	0.232	-	<0.2

Table B-7. Major and trace element chemistry for groundwater samples from the DH-GAP01 borehole.

Short Name	Sample Date	Ca mg/l	Mg mg/l	K mg/l	Na mg/l	Cl mg/l	SO4 mg/l	Alk mmol/l	EC µS/cm	pH	CBE	NaFE µg/l
GAP01 1	2009-06-30	34.2	6.9	6.0	41.1	8.9	123		456			
GAP01 2	2009-07-01	54.6	6.6	5.7	65.1	9.0	229		752			
GAP01 3	2009-07-08	47.4	5.2	5.2	46.2	9.5	168		576			
GAP01 4	2009-09-03	52.2	4.8	5.2	47.5	9.1	192		640			110
GAP01 5	2009-09-07	82.5	4.0	4.5	68.9	9.4	327		710			35
GAP01 6	2010-05-11	85.3	3.6	2.5	68.7	6.9	322	0.5	789	7.9	1.6	3.4
GAP01 6(2)	2010-05-11	85.6	3.6	2.7	69.4	7.8	346		793	8.0	1.5	
GAP01 7	2010-05-11	87.9	3.6	2.6	68.9	7.0	355	0.5	803	8.0	2	3.8
GAP01 7(2)	2010-05-11							0.5	NA			
GAP01 8(1)	2010-09-01	89.1	3.6	2.9	71.8	7.0	344	0.5	764	7.4	0.5	
GAP01 8(2)	2010-09-01	88.3	3.6	2.7	71.9	7.2	343		777	7.5	3.6	
GAP01 9(1)	2010-09-03	93.7	3.9	2.9	72.9	7.2	364	0.5	817	7.5	0.2	
GAP01 9(2)	2010-09-03							0.5				
GAP01 10	2010-09-04	84.8	4.4	3.0	72.1	7.2	348	0.5	800	7.5	0.8	
GAP01 11	2010-09-05	86.0	5.2	3.3	75.7	7.3	393	0.5	834	7.7	4.6	
GAP01 14	2011-09-09	95.8	3.6	2.2	76.2	7.7	347	0.5	830	8.3	2.9	3.603

Table B-7 continued.

Short Name	Sample Date	Ag µg/l	Al µg/l	As µg/l	B µg/l	Ba µg/l	Be µg/l	Bi µg/l	Br µg/l	Cd µg/l	Co µg/l	Cr µg/l	Cu µg/l	I µg/l
GAP01 1	2009-06-30								300					
GAP01 2	2009-07-01								300					
GAP01 3	2009-07-08								300					
GAP01 4	2009-09-03				0.04				100					
GAP01 5	2009-09-07				0.05				200					
GAP01 6	2010-05-11	<0.01	14.0	1.29	95.8	11.8	<0.1	<0.02	92.6	0.06	0.44	<0.2	<0.1	4.37
GAP01 6(2)	2010-05-11	<0.01	13.3	1.32	92.9	12.0	<0.1	<0.02	109	0.06	0.59	<0.2	<0.1	4.48
GAP01 7	2010-05-11	<0.01	12.4	1.26	91.4	11.7	<0.1	<0.02	92.0	0.05	0.54	<0.2	<0.1	4.90
GAP01 7(2)	2010-05-11													
GAP01 8(1)	2010-09-01	<0.002	21.2	1.09	0.06	9.96	<0.05	<0.01	78.0	0.04	0.09	0.32	<0.05	16.0
GAP01 8(2)	2010-09-01	<0.002	10.2	1.05	0.06	9.52	<0.05	<0.01	73.4	0.05	0.09	0.40	<0.05	13.2
GAP01 9(1)	2010-09-03	<0.002	14.3	1.12	0.06	10.7	<0.05	<0.01	77.7	0.04	<0.005	0.28	<0.05	15.5
GAP01 9(2)	2010-09-03													
GAP01 10	2010-09-04	<0.002	17.3	1.03	0.06	9.77	<0.05	<0.01	73.8	0.05	<0.005	0.28	<0.05	16.5
GAP01 11	2010-09-05	<0.002	11.3	1.08	0.04	10.3	<0.05	<0.01	76.7	0.10	0.07	0.35	<0.05	15.3
GAP01 14	2011-09-09	<0.01	14.0	0.48	81.1	10.9	0.12	<0.02	89.8	0.03	0.12	<0.2	<0.1	10.4

Table B-7 continued.

Short Name	Sample Date	Li µg/l	Mn µg/l	Mo µg/l	Ni µg/l	P µg/l	Pb µg/l	Rb µg/l	Sb µg/l	Se µg/l	Sr µg/l	Th µg/l	Tl µg/l	U µg/l
GAP01 1	2009-06-30													
GAP01 2	2009-07-01													
GAP01 3	2009-07-08													
GAP01 4	2009-09-03	19									1050			4.9
GAP01 5	2009-09-07	18									1900			1.1
GAP01 6	2010-05-11	10.9	0.02	43.8	3.40	10.3	0.08	3.41	0.87	<0.5	2980	<0.01	<0.01	0.27
GAP01 6(2)	2010-05-11	10.6	0.02	44.0	3.28	<10	<0.05	3.35	0.87	<0.5	2960	0.01	<0.01	0.27
GAP01 7	2010-05-11	10.3	0.02	39.2	1.46	<10	<0.05	3.33	0.37	<0.5	2990	<0.01	<0.01	0.25
GAP01 7(2)	2010-05-11													
GAP01 8(1)	2010-09-01		22.5	26.6	3.59	<10	0.02	2.66	0.64	<0.5	2600	<0.002	<0.001	0.35
GAP01 8(2)	2010-09-01		21.3	25.6	3.88	<10	0.02	2.53	0.60	<0.5	2450	<0.002	<0.001	0.34
GAP01 9(1)	2010-09-03		20.5	26.7	0.54	<10	0.04	2.77	0.24	<0.5	2640	<0.002	<0.001	0.25
GAP01 9(2)	2010-09-03													
GAP01 10	2010-09-04		18.7	28.6	0.74	<10	0.02	2.63	0.21	<0.5	2560	<0.002	<0.001	0.41
GAP01 11	2010-09-05		25.5	32.2	3.20	<10	0.01	2.81	0.22	<0.5	2690	<0.002	<0.001	0.31
GAP01 14	2011-09-09	9.75	19.2	21.4	1.39	<10	<0.05	2.95	0.32	<0.5	2670	0.02	0.06	0.39

Table B-7 continued.

Short Name	Sample Date	V µg/l	Zn µg/l	Fe mg/l	S mg/l	Si mg/l	Ce µg/l	Dy µg/l	Er µg/l	Eu µg/l	Gd µg/l	Ho µg/l	La µg/l	Lu µg/l
GAP01 1	2009-06-30			0.256	40									
GAP01 2	2009-07-01			0.006	77									
GAP01 3	2009-07-08			0.003	55									
GAP01 4	2009-09-03			0.006	65									
GAP01 5	2009-09-07			0.004	110									
GAP01 6	2010-05-11	0.11	1.94	0.06	109	3.43	0.004	<0.0006	<0.001	0.0019	<0.001	<0.0005	0.0032	<0.0003
GAP01 6(2)	2010-05-11	0.12	1.71	0.06	110	3.43	0.003	<0.0006	<0.001	0.0016	<0.001	<0.0005	0.0015	<0.0003
GAP01 7	2010-05-11	0.09	1.05	0.05	112	3.46	0.001	0.0007	<0.001	0.0027	<0.001	<0.0005	0.001	<0.0003
GAP01 7(2)	2010-05-11													
GAP01 8(1)	2010-09-01	<0.02	1.62	<0.03	113	3.63	0.0035	0.0029	<0.001	0.0019	0.0041	0.0005	0.0040	0.0003
GAP01 8(2)	2010-09-01	<0.02	1.40	<0.03	113	3.63	0.0036	<0.0006	<0.001	0.0037	0.0029	<0.0005	0.0043	<0.0003
GAP01 9(1)	2010-09-03	<0.02	1.10	0.03	118	3.62	0.0040	0.0009	0.002	0.0029	0.0030	<0.0005	0.0027	0.0004
GAP01 9(2)	2010-09-03													
GAP01 10	2010-09-04	<0.02	0.44	<0.03	112	3.52	0.0025	0.0022	0.001	0.0042	0.0026	<0.0005	0.0030	<0.0003
GAP01 11	2010-09-05	<0.02	2.17	<0.03	116	3.44	0.0021	0.0006	<0.001	0.0019	0.0032	<0.0005	0.0017	<0.0003
GAP01 14	2011-09-09	0.05	1.62	0.03	123	3.99	<0.0006	<0.0006	0.002	0.0029	0.005	0.0006	0.0006	<0.0003

Table B-7 continued.

Short Name	Sample Date	Nd µg/l	Pr µg/l	Sm µg/l	Tb µg/l	Tm µg/l	Yb µg/l	Sc µg/l	Y µg/l	F mg/l	NO3 mg/l	TDS mg/L	DIC	DOC
GAP01 1	2009-06-30									0.5		228		
GAP01 2	2009-07-01									0.6		376	9.5	3.8
GAP01 3	2009-07-08									0.7		288	9.8	8.2
GAP01 4	2009-09-03									0.8		317	9.7	7.6
GAP01 5	2009-09-07									0.8		505	4.3	2.2
GAP01 6	2010-05-11	0.0022	<0.0005	<0.001	0.0006	<0.0002	<0.001	0.978	0.0099	<1	<0.2			
GAP01 6(2)	2010-05-11	0.0014	<0.0005	<0.001	0.0004	<0.0002	<0.001	0.858	0.0101	<1	<0.2			
GAP01 7	2010-05-11	0.0017	<0.0005	<0.001	<0.0004	<0.0002	<0.001	0.827	0.0089	<1	<0.2			
GAP01 7(2)	2010-05-11													
GAP01 8(1)	2010-09-01	0.0048	0.0008	0.0063	0.0010	0.0005	0.0014			<1	<2		0.859	2.46
GAP01 8(2)	2010-09-01	0.0031	0.0006	0.0038	0.0004	0.0002	<0.001			0.4	<2		0.807	2.45
GAP01 9(1)	2010-09-03	0.0048	0.0006	0.0031	0.0013	<0.0002	0.0024			<1	<0.2		1.02	2.26
GAP01 9(2)	2010-09-03												1.03	2.25
GAP01 10	2010-09-04	0.0020	0.0006	0.0029	<0.0004	<0.0002	0.0023			<1	<2		1.09	2.39
GAP01 11	2010-09-05	0.0029	0.0008	0.0037	0.0007	<0.0002	0.0023			<1	<2		1.11	3.90
GAP01 14	2011-09-09	<0.001	0.002	<0.001	0.0006	0.0004	0.030		0.033	<1	<2	576		

Table B-8. Major and trace element chemistry of GAP04 upper (U), middle (M) and lower (L) sampling sections. Returned flushing water (FW) chemistry is also included.

Short Name	Sample Date	Ca	Mg	K	Na	Cl	SO4	Alk	EC	pH	CBE	NaFE
		mg/l	mg/l	mg/l	mg/l	mg/l	mg/l	mmol/l	µS/cm			µg/l
GAP04-U-1	2011-09-10	237	19.4	4.01	190	64	885	0.44	1890	7.7	2.5	148
GAP04-U-2	2013-09-02	339	23.3	3.83	229	90	1250	0.37	250	7.4	0.0	118
GAP04-U-3	2013-09-08	371	22.8	3.41	252	95	1350	0.37	261	7.6	0.4	88
GAP04-U-4	2013-09-12	364	24.7	3.76	248	95	1330	0.34	261	7.6	0.6	88
GAP04-U-5	2013-09-18	365	22.8	4.34	257	94	1330	0.36	260	7.7	1.1	88
GAP04-U-6	2013-09-22	368	23.1	3.64	257	94	1310	0.32	258	7.2	2.1	86
GAP04-M-1	2011-07-10	128	19.0	5.07	123	56	552	0.61	1230	8.3	-0.9	
GAP04-M-2	2011-09-09	150	23.2	5.91	144	58	705	0.43	1470	8.2	-3.0	153
GAP04-M-3	2013-09-02	192	23.4	5.16	162	76	933	0.53	197	6.9	8.3	121
GAP04-M-4	2013-09-08	324	29.3	6.02	246	103	1260	0.33	251	7.6	0.0	74
GAP04-M-5	2013-09-12	321	28	5.14	249	102	1240	0.33	253	7.7	0.5	74
GAP04-M-6	2013-09-18	326	28.1	5.68	249	103	1260	0.32	254	7.7	0.2	74
GAP04-M-7	2013-09-23	325	27.8	5.62	255	109	1230	0.35	251	7.4	1.2	75
GAP04-L-1	2011-09-08	124	13.6	3.63	60	22	392	1.18	940	8.0	0.2	226
GAP04-L-2	2013-09-02	407	16.9	3.35	82	28	832	1.23	160	7.6	13.5	209
GAP04-L-3	2013-09-08	463	58.8	4.31	407	176	1950	0.42	372	7.6	0.2	4.3
GAP04-L-4	2013-09-12	449	57.8	5.13	389	177	1950	0.44	376	7.6	2.0	3.6
GAP04-L-5	2013-09-18	457	59	3.33	398	176	1910	0.38	371	7.5	0.1	7.3
GAP04-L-6	2013-09-24	459	58.6	5.9	409	173	1880	0.4	367	7.4	1.4	9.6
FW04-99	2011-06-19	6.57	3.32	0.43	2.0	1.7	3.2	0.46	66	7.2	9.6	
FW04-300	2011-06-22	8.00	1.39	3.40	2.2	0.7	13	0.46	78	8.6	-4.1	
FW04-441	2011-06-24	20.7	6.42	9.62	14.7	10	73	0.37	350	8.9	5.7	
FW04-558	2011-06-26	208	14.0	7.99	38.0	-	-	-	-	-	Only Cations	
FW04-603	2011-06-27	21.7	3.69	4.73	32.4	8.0	57	1.53	300	8.6	-0.3	
FW04-687-1	2011-06-28	37.6	9.26	12.0	47.2	21	153	1.31	540	8.8	-1.0	
FW04-687-2	2011-07-01	13.1	8.15	3.78	5.6	6.2	4.6	1.38	170	7.9	0.4	

Table B-8 continued.

Short Name	Sample Date	Ag µg/l	Al µg/l	As µg/l	B µg/l	Ba µg/l	Be µg/l	Bi µg/l	Br µg/l	Cd µg/l	Co µg/l	Cr µg/l	Cu µg/l	I µg/l
GAP04-U-1	2011-09-10	0.01	49.6	0.31	92.1	49.9	0.20	<0.02	757	0.08	0.02	<0.2	<0.1	31.0
GAP04-U-2	2013-09-02	0.03	8.12	6.47	0.13	34.5	<0.1	0.23	1130	0.02	0.75	0.51	2.71	32.7
GAP04-U-3	2013-09-08	0.01	34.6	3.2	0.13	28	<0.1	0.06	1120	0.03	0.74	0.31	3.1	33.3
GAP04-U-4	2013-09-12	0.02	44.4	2.56	0.13	30.5	<0.1	0.05	1290	0.03	0.8	0.28	3.49	40.4
GAP04-U-5	2013-09-18	0.01	52.5	1.93	0.14	34.1	<0.1	0.08	1410	0.03	0.93	0.31	3.96	39.2
GAP04-U-6	2013-09-22	<0.01	43.9	1.49	0.12	28.5	<0.1	0.04	1260	0.02	0.79	<0.2	3.32	47.0
GAP04-M-1	2011-07-10	0.01	7.5	0.07	67.3	66.8	<0.1	<0.02	613	0.09	0.82	<0.2	3.48	16.5
GAP04-M-2	2011-09-09	0.01	21.0	0.19	55.7	48.9	0.19	<0.02	629	0.17	<0.02	<0.2	1.87	16.0
GAP04-M-3	2013-09-02	0.01	4.1	4.54	0.11	46.6	<0.1	0.13	1080	0.05	0.39	<0.2	1.92	24.1
GAP04-M-4	2013-09-08	0.01	10.6	3	0.1	44.8	<0.1	0.07	1400	0.04	0.72	0.21	3.3	43.2
GAP04-M-5	2013-09-12	0.01	11.2	1.84	0.11	39.6	<0.1	0.07	1360	<0.02	0.66	<0.2	2.76	44.1
GAP04-M-6	2013-09-18	0.01	16.1	1.74	0.12	44.4	<0.1	0.05	1380	0.03	0.74	<0.2	3.37	48.0
GAP04-M-7	2013-09-23	0.01	16.6	1.44	0.11	41.6	<0.1	0.05	1520	0.03	0.73	<0.2	3.31	50.4
GAP04-L-1	2011-09-08	0.01	41.8	0.10	30.6	42.2	0.24	<0.02	263	0.09	0.07	<0.2	1.27	8.36
GAP04-L-2	2013-09-02	0.01	4.5	3.51	<0.05	37.6	<0.1	0.09	303	0.04	0.84	0.49	2.97	12.4
GAP04-L-3	2013-09-08	0.01	5.49	2.55	0.13	16.8	<0.1	<0.02	2030	<0.02	0.97	<0.2	4.56	134
GAP04-L-4	2013-09-12	0.01	5.87	1.97	0.13	15.6	<0.1	<0.02	2350	<0.02	1.11	0.21	4.74	139
GAP04-L-5	2013-09-18	0.01	4.72	1.20	0.13	10.2	<0.1	<0.02	2330	<0.02	0.7	<0.2	3.13	161
GAP04-L-6	2013-09-24	0.01	11.5	1.67	0.13	16.9	<0.1	<0.02	2390	<0.02	1.22	<0.2	5.67	158
FW04-99	2011-06-19	0.05	244	0.15	8.78	3.82	<0.1	0.03	23.6	0.02	0.73	1.06	13.5	2.04
FW04-300	2011-06-22	0.04	331	0.06	6.06	6.00	<0.1	<0.02	6.62	0.03	0.09	<0.2	2.96	<2
FW04-441	2011-06-24	0.14	464	0.07	10.5	9.33	<0.1	<0.02	52.8	1.07	0.08	<0.2	11.8	<2
FW04-558	2011-06-26	<0.01	157	0.13	15.5	15.6	<0.1	<0.02	49.2	0.02	0.11	0.21	<0.1	2.96
FW04-603	2011-06-27	0.01	252	0.28	45.2	3.29	<0.1	<0.02	46.4	<0.02	0.06	<0.2	<0.1	2.53
FW04-687-1	2011-06-28	0.05	286	0.15	32.1	17.6	<0.1	<0.02	257	0.36	0.13	<0.2	0.17	7.25
FW04-687-2	2011-07-01	<0.01	30.6	0.05	6.72	9.43	<0.1	<0.02	37.3	0.02	0.92	0.25	10.3	2.22

Table B-8. continued.

Short Name	Sample Date	Li µg/l	Mn µg/l	Mo µg/l	Ni µg/l	P µg/l	Pb µg/l	Rb µg/l	Sb µg/l	Se µg/l	Sr µg/l	Th µg/l	Tl µg/l	U µg/l
GAP04-U-1	2011-09-10	17.4	81.1	42.6	4.93	<10	0.07	4.53	0.30	2.29	4060	0.01	0.16	0.37
GAP04-U-2	2013-09-02	30.7	379	37.2	9.22	172	<0.05	4.25	1.50	3.92	5540	0.59	0.04	0.04
GAP04-U-3	2013-09-08	29.8	92	30.6	6.39	142	<0.05	3.52	0.84	2.97	6270	0.05	0.04	0.06
GAP04-U-4	2013-09-12	32.6	101	31.8	6.98	146	<0.05	3.97	0.45	2.8	6210	0.04	0.04	0.07
GAP04-U-5	2013-09-18	36.5	116	35.4	7.96	298	0.05	4.47	0.54	2.91	6410	0.26	0.06	0.07
GAP04-U-6	2013-09-22	30.5	97.7	29.3	6.69	120	<0.05	3.78	0.20	2.69	6490	0.12	0.04	0.07
GAP04-M-1	2011-07-10	15.7	369	58.2	29.1	47.0	0.07	5.35	3.29	0.56	2470	0.01	0.01	1.08
GAP04-M-2	2011-09-09	18.5	63.6	105	6.69	<10	0.05	4.95	0.22	1.25	2520	0.02	0.14	0.30
GAP04-M-3	2013-09-02	28	299	102	5.07	214	<0.05	5.1	1.85	2.8	3330	0.14	0.04	0.01
GAP04-M-4	2013-09-08	39.4	84.1	45.2	7.53	68.5	<0.05	5.31	1	3.08	5820	0.03	0.05	0.09
GAP04-M-5	2013-09-12	34.5	76.9	38.4	6.31	42.4	<0.05	4.63	0.33	2.28	5920	0.59	0.05	0.10
GAP04-M-6	2013-09-18	38.6	88.6	42.6	7.41	4320	<0.05	5.16	0.38	2.33	5950	0.17	0.04	0.11
GAP04-M-7	2013-09-23	37.2	85.7	42.8	6.98	53.1	<0.05	4.97	0.28	2.47	6120	0.13	0.05	0.10
GAP04-L-1	2011-09-08	8.15	122	52.1	6.98	15.9	0.13	3.90	2.24	<0.5	1150	0.02	0.07	0.67
GAP04-L-2	2013-09-02	12.9	448	61.3	10.7	395	0.07	3.32	2.37	2.24	2970	0.14	0.04	0.06
GAP04-L-3	2013-09-08	74.3	544	9.36	8.23	26.8	<0.05	5.00	0.75	3.31	8300	0.04	0.04	0.02
GAP04-L-4	2013-09-12	85.3	645	8.52	9.58	33.2	0.05	5.92	0.62	3.72	7920	0.5	0.05	0.04
GAP04-L-5	2013-09-18	55.6	394	6.41	5.79	759	<0.05	3.98	0.25	2.3	8070	0.09	0.03	0.03
GAP04-L-6	2013-09-24	92.4	637	11.6	10.4	46.7	0.07	6.82	0.74	4.39	8170	0.2	0.05	0.06
FW04-99	2011-06-19	6.15	23.5	9.76	8.95	118	0.28	1.22	8.05	<0.5	18.9	0.08	<0.01	0.02
FW04-300	2011-06-22	4.02	4.96	24.1	1.32	35.0	0.07	5.84	0.03	<0.5	30.7	0.08	0.01	0.03
FW04-441	2011-06-24	16.7	4.21	832	1.76	35.9	0.07	10.4	0.04	<0.5	89.9	<0.01	0.01	0.02
FW04-558	2011-06-26	26.9	34.1	7.86	5.88	53.0	0.05	4.45	1.00	<0.5	1520	<0.01	0.01	0.01
FW04-603	2011-06-27	45.9	4.97	10.1	2.00	74.4	0.05	3.65	0.38	<0.5	314	0.01	<0.01	<0.01
FW04-687-1	2011-06-28	29.7	10.9	254	2.44	46.0	0.06	9.36	2.01	<0.5	490	0.01	0.02	0.01
FW04-687-2	2011-07-01	1.42	42.5	9.89	4.53	<10	<0.05	5.08	3.20	<0.5	44.0	<0.01	<0.01	0.02

Table B-8 continued.

Short Name	Sample Date	V µg/l	Zn µg/l	Fe mg/l	S mg/l	Si mg/l	Ce µg/l	Dy µg/l	Er µg/l	Eu µg/l	Gd µg/l	Ho µg/l	La µg/l	Lu µg/l
GAP04-U-1	2011-09-10	0.16	5.46	<0.03	282	2.38	0.0073	<0.0006	0.026	0.0166	0.002	0.0018	0.0064	0.0006
GAP04-U-2	2013-09-02	0.43	3.3	0.11	449	2.21	<0.0006	<0.0006	<0.001	0.0021	0.003	<0.0005	0.0034	0.0008
GAP04-U-3	2013-09-08	0.42	3.78	<0.05	498	2.53	<0.0006	<0.0006	0.004	<0.0008	0.002	<0.0005	0.0025	<0.0003
GAP04-U-4	2013-09-12	0.48	6.82	<0.05	493	2.51	<0.0006	0.0032	<0.001	<0.0008	<0.001	<0.0005	0.0081	0.0003
GAP04-U-5	2013-09-18	0.57	5.49	<0.05	505	2.55	<0.0006	<0.0006	<0.001	<0.0008	<0.001	0.0008	0.0041	0.0006
GAP04-U-6	2013-09-22	0.49	3.69	<0.05	505	2.57	<0.0006	<0.0006	0.003	0.0011	0.004	<0.0005	0.0041	<0.0003
GAP04-M-1	2011-07-10	<0.05	3.78	0.05	172	1.86	0.1925	0.0013	0.0015	0.0155	0.0129	0.0012	0.1272	0.0005
GAP04-M-2	2011-09-09	0.30	4.54	<0.03	208	2.75	0.0042	<0.0006	0.001	0.0132	0.003	0.0019	0.0044	0.0003
GAP04-M-3	2013-09-02	0.41	3	0.2	275	2.15	<0.0006	<0.0006	<0.001	0.0017	<0.001	<0.0005	0.0012	0.0005
GAP04-M-4	2013-09-08	0.63	4.39	<0.05	461	3.04	<0.0006	<0.0006	0.003	0.0023	<0.001	<0.0005	<0.0003	0.0005
GAP04-M-5	2013-09-12	0.60	3.65	<0.05	459	3.07	<0.0006	<0.0006	<0.001	0.0023	<0.001	<0.0005	0.0004	<0.0003
GAP04-M-6	2013-09-18	0.70	4.38	<0.05	466	3.07	<0.0006	<0.0006	<0.001	0.0017	0.006	<0.0005	0.0022	<0.0003
GAP04-M-7	2013-09-23	0.71	3.9	<0.05	465	3.1	<0.0006	<0.0006	0.002	<0.0008	<0.001	<0.0005	0.0022	0.0004
GAP04-L-1	2011-09-08	<0.05	5.82	0.05	127	1.30	0.0407	0.0011	0.325	0.0136	0.006	0.0014	0.0252	<0.0003
GAP04-L-2	2013-09-02	0.51	3.36	0.43	391	2.04	<0.0006	<0.0006	0.002	<0.0008	0.001	0.0005	0.0049	<0.0003
GAP04-L-3	2013-09-08	0.46	4.11	0.13	727	4.02	<0.0006	<0.0006	<0.001	<0.0008	<0.001	<0.0005	0.0074	<0.0003
GAP04-L-4	2013-09-12	0.57	5.58	0.09	718	3.91	<0.0006	<0.0006	0.001	<0.0008	<0.001	<0.0005	0.0034	<0.0003
GAP04-L-5	2013-09-18	0.39	2.66	0.12	726	3.88	<0.0006	<0.0006	<0.001	<0.0008	<0.001	<0.0005	0.0067	0.0005
GAP04-L-6	2013-09-24	0.63	5.01	0.1	737	3.88	<0.0006	0.0026	0.004	<0.0008	<0.001	0.0009	0.0131	<0.0003
FW04-99	2011-06-19	0.86	131	2.07	1.59	1.31	1.5225	0.0318	0.0149	0.0151	0.0677	0.0076	0.8447	0.0022
FW04-300	2011-06-22	0.26	6.74	0.14	4.20	2.67	0.3308	0.0066	0.0055	0.0041	0.0171	0.0025	0.166	0.0007
FW04-441	2011-06-24	1.49	4.59	0.03	11.6	2.28	0.0684	0.0026	0.0016	0.0027	0.0138	0.0015	0.0326	<0.0003
FW04-558	2011-06-26	0.12	7.06	0.07	177	2.82	0.0915	0.0015	0.0051	0.0049	0.0117	0.0027	0.0437	0.0011
FW04-603	2011-06-27	0.09	4.18	<0.03	19.6	6.67	0.0831	0.0026	0.0048	0.0016	0.0122	0.0008	0.0424	0.0009
FW04-687-1	2011-06-28	0.18	1.69	0.03	48.1	3.32	0.0894	0.0007	0.0018	0.0043	0.0158	0.001	0.0447	0.0003
FW04-687-2	2011-07-01	<0.05	3.32	0.05	1.90	0.35	0.0271	0.0044	0.0011	0.0026	0.0063	0.0015	0.0145	0.0007

Table B-8 continued.

Short Name	Sample Date	Nd µg/l	Pr µg/l	Sm µg/l	Tb µg/l	Tm µg/l	Yb µg/l	Sc µg/l	Y µg/l	F mg/l	Br mg/L	NO3 mg/l	TDS mg/L	DOC mg/L
GAP04-U-1	2011-09-10	0.010	0.002	0.004	0.0011	0.0007	0.024		0.052	<1	<1	<2	1440	
GAP04-U-2	2013-09-02	<0.001	0.001	0.004	0.0016	0.0004	<0.001	0.691	0.029	<1	1.41	<2		
GAP04-U-3	2013-09-08	<0.001	0.001	<0.001	<0.0004	<0.0002	<0.001	0.504	0.035	<1	1.49	<2		8.1
GAP04-U-4	2013-09-12	0.003	0.002	<0.001	<0.0004	0.0002	<0.001	0.695	0.040	<1	1.47	<2		7.9
GAP04-U-5	2013-09-18	<0.001	<0.0005	0.005	<0.0004	0.0004	<0.001	0.675	0.043	<1	1.48	<2		6.6
GAP04-U-6	2013-09-22	<0.001	0.002	0.004	<0.0004	<0.0002	<0.001	0.475	0.037	<1	1.45	<2		6.3
GAP04-M-1	2011-07-10	0.0514	0.0179	<0.001	0.0011	<0.0002	<0.001			<0.1	0.5	<0.2	928	
GAP04-M-2	2011-09-09	0.008	0.003	0.004	0.0012	0.0005	0.018		0.038	<1	<1	<2	1120	
GAP04-M-3	2013-09-02	0.004	<0.0005	0.002	0.0004	<0.0002	<0.001	0.492	0.019	<1	1.29	<2		
GAP04-M-4	2013-09-08	<0.001	0.001	<0.001	<0.0004	<0.0002	<0.001	0.756	0.033	<1	1.57	<2		5.9
GAP04-M-5	2013-09-12	<0.001	0.001	0.007	<0.0004	<0.0002	<0.001	0.753	0.035	<1	1.57	<2		5.5
GAP04-M-6	2013-09-18	<0.001	0.001	<0.001	<0.0004	<0.0002	<0.001	0.636	0.038	<1	1.57	<2		4.7
GAP04-M-7	2013-09-23	<0.001	0.001	<0.001	<0.0004	<0.0002	<0.001	0.163	0.032	<1	1.55	<2		4.8
GAP04-L-1	2011-09-08	0.024	0.007	0.001	0.0005	0.0008	0.022		0.031	<1	0.2	<0.2	693	
GAP04-L-2	2013-09-02	0.004	0.002	0.003	<0.0004	<0.0002	<0.001	0.0627	0.021	<1	<1	<2		
GAP04-L-3	2013-09-08	<0.001	<0.0005	0.001	0.0006	<0.0002	<0.001	1.66	0.046	<1	2.29	<2		1.4
GAP04-L-4	2013-09-12	0.002	0.001	0.002	<0.0004	0.0004	<0.001	1.3	0.053	<1	2.28	<2		1.3
GAP04-L-5	2013-09-18	<0.001	<0.0005	0.003	<0.0004	<0.0002	<0.001	0.91	0.037	<1	2.26	<2		1.3
GAP04-L-6	2013-09-24	<0.001	0.001	<0.001	<0.0004	0.0005	<0.001	1	0.055	<1	2.25	<2		1.5
FW04-99	2011-06-19	0.6379	0.1859	0.0777	0.0077	0.0025	0.0093			1.0	<0.1	<0.2	51	
FW04-300	2011-06-22	0.1436	0.0375	0.0174	0.0022	0.0011	0.0028			<0.1	<0.1	0.7	63	
FW04-441	2011-06-24	0.0386	0.0073	0.0064	0.0006	<0.0002	<0.001			0.4	<0.1	<0.2	163	
FW04-558	2011-06-26	0.0621	0.0123	0.0102	<0.0004	0.0007	0.0047			-	-	-		
FW04-603	2011-06-27	0.0402	0.0093	<0.001	<0.0004	0.0004	0.003			0.3	<0.1	<0.2	235	
FW04-687-1	2011-06-28	0.0374	0.0106	0.0083	0.0005	0.0003	0.0047			0.4	0.2	<0.2	369	
FW04-687-2	2011-07-01	0.0164	0.0054	0.0011	<0.0004	0.0002	0.0034			0.1	<0.1	<0.2	127	

Table B-9. Major and trace element chemistry of the Leverett Spring.

Short Name	Sample Date	Ca mg/l	Mg mg/l	K mg/l	Na mg/l	Cl mg/l	SO4 mg/l	Alk mmol/l	EC (lab) mS/cm	pH (lab)	CBE
Spring 1	2008-06-29	38.3	16.8	4.25	14.1	36	65	1.7	411	7.0	0.3
Spring 2	2009-06-27	42.4	18.7	4.37	16.1	38	70			7.2	2.2
Spring 3	2009-06-27	42.0	18.7	4.45	16.3	38	70.1			7.2	2.1
Spring 5	2010-05-10	38.8	16.9	4.55	13.3	36	66	1.71	415	7.1	0.6
Spring 6	2010-09-05	39.5	17.2	5.23	14.0	34	68	1.69	412	6.8	1.1
Spring 9	2011-09-11	40.8	17.9	4.70	15.5	36	68	1.80	440	6.8	0.2

Short Name	Sample Date	Ag µg/l	Al µg/l	As µg/l	B µg/l	Ba µg/l	Be µg/l	Bi µg/l	Br µg/l	Cd µg/l	Co µg/l	Cr µg/l	Cu µg/l	I µg/l
Spring 1	2008-06-29	<0.01	13.2	<0.05	49.3	45.7	<0.1	<0.02	944	<0.02	0.30	0.51	0.14	
Spring 2	2009-06-27								1000					
Spring 3	2009-06-27								1000					
Spring 5	2010-05-10	<0.01	23.2	0.10	60.7	53.7	<0.1	<0.02	930	<0.02	0.72	0.74	0.16	101
Spring 6	2010-09-05	<0.002	10.5	<0.02	<0.02	44.3	<0.05	<0.01	938	0.06	0.29	0.88	<0.05	169
Spring 9	2011-09-11	0.01	7.11	0.06	49.4	50.7	<0.1	<0.02	1040	<0.02	0.31	0.27	<0.1	163

Short Name	Sample Date	Li µg/l	Mn µg/l	Mo µg/l	Ni µg/l	P µg/l	Pb µg/l	Rb µg/l	Sb µg/l	Se µg/l	Sr µg/l	Th µg/l	Tl µg/l	U µg/l
Spring 1	2008-06-29	0.27	321	0.21	0.60	<10	<0.05	6.62	<0.02	<0.5	114	0.55	<0.01	0.03
Spring 2	2009-06-27													
Spring 3	2009-06-27													
Spring 5	2010-05-10	0.33	310	0.58	0.73	<10	<0.05	7.98	<0.02	<0.5	129	0.72	<0.01	0.03
Spring 6	2010-09-05		335	0.19	0.79	<10	0.04	6.82	<0.01	<0.5	123	0.35	<0.001	0.03
Spring 9	2011-09-11	0.35	314	0.22	0.66	<10	0.05	7.09	0.02	1.21	118	0.49	0.02	0.03

Table B-9 continued.

Short Name	Sample Date	V µg/l	Zn µg/l	Fe mg/l	S mg/l	Si mg/l	Ce µg/l	Dy µg/l	Er µg/l	Eu µg/l	Gd µg/l	Ho µg/l	La µg/l	Lu µg/l
Spring 1	2008-06-29	0.97	1.10	12.8	22.6	4.56	5.98	0.0715	0.037	0.0314	0.212	0.0123	3.22	0.0039
Spring 2	2009-06-27			9.52	23	9.95								
Spring 3	2009-06-27			8.84	23	9.86								
Spring 5	2010-05-10	1.57	3.04	14.8	21.9	4.66	6.352	0.0656	0.035	0.0435	0.247	0.0099	3.53	0.0033
Spring 6	2010-09-05	0.21	3.93	4.34	22.9	4.45	2.49	0.0507	0.026	0.0298	0.1362	0.0088	1.19	0.0028
Spring 9	2011-09-11	0.47	2.20	6.29	23.9	4.66	5.1435	0.0762	0.035	0.0525	0.213	0.0132	2.5743	0.0042

Short Name	Sample Date	Nd µg/l	Pr µg/l	Sm µg/l	Tb µg/l	Tm µg/l	Yb µg/l	Sc µg/l	Y µg/l	F mg/l	NO3 mg/l	EC (FLD)	pH (FLD)	TDS mg/L
Spring 1	2008-06-29	2.18	0.624	0.252	0.0222	0.0035	0.022			0.1	<0.2	445	7.20	
Spring 2	2009-06-27									<0.1		451	7.19	210
Spring 3	2009-06-27									<0.1		458	7.17	209
Spring 5	2010-05-10	2.28	0.6433	0.254	0.0209	0.0028	0.021	1.40	0.2595	0.1	<0.2	508.00	6.96	
Spring 6	2010-09-05	1.08	0.2740	0.1391	0.0107	0.0029	0.0211				<2	390	7.31	
Spring 9	2011-09-11	2.212	0.589	0.293	0.0194	0.0039	0.027		0.333	<1	<2			314

Table B-10. Raw major and trace element chemistry for out diffusion experiments on the DH-GAP04 core and associated crush and leach experiments.

Sample	Depth	Na	Mg	Ca	K	Sr	Cl	Br	SO4	Alkalinity	C.B.E.	Na/Cl	Br/Cl	Ca/SO4
	m	mg/L	mg/L	mg/L	mg/L	µg/L	mg/L	mg/L	mg/L	mg/L as CaCO3	%		meq/meq	
GAP04-A	209.83	87	0.9	<7	0.7	27	2.7	< 0.03	30			50		
GAP04-B	352.00	27	4	35	7	233	6.8	< 0.03	37			6		2.3
GAP04-C	570.32	29	14	746	9	4938	7.3	< 0.3	2800			6		0.6
GAP04-D	670.20	15	4	337	16	1754	1.5	< 0.1	1490			15		0.5
GAP04-E	377.65	47	10	242	20	1248	12.0	< 0.1	564	99	4.8	6		1.0
GAP04-F	448.07	52	6	84	9	668	16.5	0.24	167	116	6.7	5	0.006	1.2
GAP04-G	557.40	59	40	662	10	6720	2.6	< 0.1	1554	98	6.4	35		1.0
GAP04-H	681.21	30	7	46	16	1058	4.6	< 0.03	16	138	17.3	10		6.9
GAP04 E-CL	377.65	>100	9	139	70	548	44.6	< 0.1	460					0.7
GAP04 F-CL	448.07	72	2	5	25	44.2	43.6	0.6	15			3	0.006	0.9
GAP04 G-CL	557.40	95	43	>100	29	8940	6.8	< 0.3	3180			22		
GAP04 H-CL	681.21	>100	3	3	59	34	35.8	0.6	13				0.007	0.6

Table B-10 continued.

Sample	Depth	Li	Be	Al	Si	Sc	Ti	V	Cr	Mn	Fe
	m	µg/L	µg/L	µg/L	µg/L	µg/L	µg/L	µg/L	µg/L	µg/L	µg/L
GAP04-A	209.83	< 10	< 1	67	13333	< 10	3	593	< 5	3	< 100
GAP04-B	352.00	4	< 0.1	4	3529	2	1	2	< 0.5	165	< 10
GAP04-C	570.32	< 10	< 1	< 20	7077	< 10	2	3	< 5	995	< 100
GAP04-D	670.20	< 10	< 1	< 20	< 2000	< 10	< 1	3	< 5	218	< 100
GAP04-E	377.65	20	< 1	380	6000	< 10	34	4.4	< 5	480	480
GAP04-F	448.07	20	< 1	60	5400	< 10	10	3.6	< 5	498	< 100
GAP04-G	557.40	< 10	< 1	100	6000	< 10	30	<1	< 5	1700	< 100
GAP04-H	681.21	20	< 1	60	5400	< 10	8	30	< 5	304	< 100
GAP04 E-CL	377.65	84	< 0.1	404	9400	2	3.2	18.8	< 0.5	2.8	< 10
GAP04 F-CL	448.07	46	< 0.1	2880	17000	8	92.2	138	18	17.8	1100
GAP04 G-CL	557.40	48	< 0.2	100	7200	4	2.8	6	< 1	24.8	< 20
GAP04 H-CL	681.21	58	< 0.1	5860	27000	8	372	500	15	58	4120

Table B-10 continued.

Sample	Depth	Co	Ni	Cu	Zn	Ga	Ge	As	Se	Rb	Y
	m	µg/L	µg/L	µg/L	µg/L	µg/L	µg/L	µg/L	µg/L	µg/L	µg/L
GAP04-A	209.83	0.10	< 3	130	183	0.17	<0.01	< 0.3	3.3	0.9	0.2
GAP04-B	352.00	< 0.005	1	28	77	0.12	0.02	0.1	0.4	7.2	0.0
GAP04-C	570.32	< 0.05	< 3	125	849	<0.01	<0.01	< 0.3	< 0.2	13.3	0.3
GAP04-D	670.20	< 0.05	< 3	102	163	<0.01	<0.01	< 0.3	< 0.2	94.0	0.2
GAP04-E	377.65	0.38	< 3	76	124	0.20	<0.01	< 0.3	< 0.2	33.8	0.2
GAP04-F	448.07	0.88	< 3	72	92	<0.01	<0.01	< 0.3	< 0.2	6.4	0.1
GAP04-G	557.40	< 0.05	34	74	98	0.20	<0.01	< 0.3	4.0	6.8	0.4
GAP04-H	681.21	< 0.05	< 3	166	388	<0.01	<0.01	< 0.3	< 0.2	18.6	0.3
GAP04 E-CL	377.65	< 0.005	0.8	2.8	3.2	4.42	0.26	0.54	0.4	16.0	0.0
GAP04 F-CL	448.07	0.648	2.4	4.4	105.2	11.80	0.16	1.6	1	3.2	0.2
GAP04 G-CL	557.40	< 0.01	1.6	6.4	28.4	1.88	0.16	0.32	1	7.3	0.1
GAP04 H-CL	681.21	2.32	3	6.8	15.4	16.16	0.20	1.5	0.6	14.3	0.7

Table B-10 continued.

Sample	Depth	Zr	Nb	Mo	Ag	Cd	In	Sb	Te	Cs	Ba
	m	µg/L	µg/L	µg/L	µg/L	µg/L	µg/L	µg/L	µg/L	µg/L	µg/L
GAP04-A	209.83	0.83	< 0.05	1.67	< 2	0.17	< 0.01	< 0.1	< 1	0.02	138.3
GAP04-B	352.00	0.02	0.16	0.98	< 0.2	0.02	< 0.001	0.14	< 0.1	0.01	142.9
GAP04-C	570.32	0.46	< 0.05	1.54	< 2	< 0.1	< 0.01	< 0.1	< 1	0.03	67.7
GAP04-D	670.20	0.15	< 0.05	1.54	< 2	< 0.1	< 0.01	< 0.1	< 1	0.89	50.8
GAP04-E	377.65	0.2	< 0.05	2	< 2	< 0.1	< 0.01	< 0.1	< 1	0.02	42.0
GAP04-F	448.07	< 0.1	< 0.05	4	< 2	< 0.1	< 0.01	< 0.1	< 1	< 0.01	24.0
GAP04-G	557.40	< 0.1	< 0.05	2	< 2	< 0.1	< 0.01	< 0.1	< 1	< 0.01	44.0
GAP04-H	681.21	0.2	< 0.05	40	< 2	0.2	< 0.01	< 0.1	< 1	0.04	238.0
GAP04 E-CL	377.65	0.2	0.024	7.4	< 0.2	0.02	< 0.001	0.28	< 0.1	0.004	34.2
GAP04 F-CL	448.07	0.34	0.042	1.8	4.8	0.06	< 0.001	0.22	< 0.1	0.012	37.0
GAP04 G-CL	557.40	0.08	< 0.01	7.2	6	0.04	< 0.002	0.2	< 0.2	0.004	78.0
GAP04 H-CL	681.21	0.38	0.136	1.8	0.4	0.02	0.002	1.38	< 0.1	0.034	68.8

Table B10 continued.

Sample	Depth	La	Ce	Pr	Nd	Sm	Eu	Gd	Tb	Dy	Ho
	m	µg/L	µg/L	µg/L	µg/L	µg/L	µg/L	µg/L	µg/L	µg/L	µg/L
GAP04-A	209.83	0.05	0.07	< 0.01	0.05	< 0.001	0.02	0.02	< 0.001	< 0.001	0.53
GAP04-B	352.00	0.00	0.01	< 0.001	0.00	< 0.001	0.01	0.00	< 0.001	< 0.001	< 0.001
GAP04-C	570.32	0.95	0.75	0.08	0.28	0.05	0.02	0.06	< 0.001	0.02	< 0.001
GAP04-D	670.20	0.82	0.89	0.12	0.54	0.05	0.02	0.05	< 0.001	0.02	< 0.001
GAP04-E	377.65	0.6	0.72	0.06	0.32	0.04	0.02	0.06	< 0.001	0.02	< 0.001
GAP04-F	448.07	0.32	0.38	0.04	0.12	0.02	0.02	0.02	< 0.001	0.02	< 0.001
GAP04-G	557.40	4.34	7.22	0.82	3.06	0.38	0.08	0.36	0.02	0.06	0.06
GAP04-H	681.21	0.32	0.58	0.06	0.28	0.04	0.02	0.06	< 0.001	0.04	< 0.001
GAP04 E-CL	377.65	0.004	0.006	< 0.001	0.004	< 0.001	0.002	< 0.001	< 0.001	< 0.001	< 0.001
GAP04 F-CL	448.07	0.556	1.066	0.12	0.472	0.078	0.024	0.076	0.008	0.034	0.006
GAP04 G-CL	557.40	0.044	0.044	0.004	0.024	0.004	0.004	0.004	< 0.001	< 0.001	< 0.001
GAP04 H-CL	681.21	4.44	8.94	0.952	3.5	0.534	0.106	0.454	0.044	0.162	0.024

Table B-10 continued.

Sample	Depth	Er	Tm	Yb	Lu	Hf	Ta	W	Hg	Tl	Pb
	m	µg/L	µg/L	µg/L	µg/L	µg/L	µg/L	µg/L	µg/L	µg/L	µg/L
GAP04-A	209.83	< 0.01	< 0.01	< 0.01	< 0.01	0.02	< 0.01	1.00	< 2	0.02	11.7
GAP04-B	352.00	< 0.001	< 0.001	< 0.001	< 0.001	< 0.001	0.07	0.73	< 0.2	0.00	1.2
GAP04-C	570.32	0.02	< 0.01	< 0.01	< 0.01	0.02	< 0.01	0.31	< 2	0.02	10.8
GAP04-D	670.20	0.02	< 0.01	< 0.01	< 0.01	0.02	< 0.01	1.23	< 2	0.20	9.2
GAP04-E	377.65	0.02	< 0.01	< 0.01	< 0.01	0.02	< 0.01	< 0.2	< 2	0.06	6.0
GAP04-F	448.07	< 0.01	< 0.01	< 0.01	< 0.01	< 0.001	< 0.01	< 0.2	< 2	0.04	6.0
GAP04-G	557.40	0.04	< 0.01	< 0.01	< 0.01	< 0.001	< 0.01	0.4	< 2	< 0.01	6.0
GAP04-H	681.21	0.02	< 0.01	< 0.01	0.02	0.02	< 0.01	1.6	< 2	0.02	14.0
GAP04 E-CL	377.65	< 0.001	< 0.001	< 0.001	< 0.001	0.004	0.008	0.4	< 0.2	0.022	< 0.01
GAP04 F-CL	448.07	0.02	< 0.001	0.012	< 0.001	0.006	< 0.001	0.52	< 0.2	0.01	1.1
GAP04 G-CL	557.40	< 0.002	< 0.002	< 0.002	< 0.002	< 0.001	< 0.002	0.68	4.4	0.012	< 0.02
GAP04 H-CL	681.21	0.068	0.006	0.038	0.006	0.016	0.006	0.6	< 0.2	0.028	1.4

Table B-10 continued.

Sample	Depth	Bi	Th	U	F	NO2 (as N)	NO3 (as N)	PO4 (as P)
	m	µg/L	µg/L	µg/L	mg/L	mg/L	mg/L	mg/L
GAP04-A	209.83	< 3	< 0.01	< 0.01	< 0.01	< 0.01	< 0.01	< 0.02
GAP04-B	352.00	< 0.3	< 0.001	0.79	0.44	< 0.01	< 0.01	< 0.02
GAP04-C	570.32	< 3	0.02	0.66	< 0.1	< 0.1	0.55	< 0.2
GAP04-D	670.20	< 3	0.02	< 0.01	< 0.05	< 0.05	< 0.05	< 0.1
GAP04-E	377.65	< 3	0.02	0.18	< 0.05	< 0.05	< 0.05	< 0.1
GAP04-F	448.07	< 3	< 0.01	5.6	0.24	< 0.01	< 0.01	< 0.02
GAP04-G	557.40	< 3	0.02	0.24	< 0.05	< 0.05	< 0.05	< 0.1
GAP04-H	681.21	< 3	0.02	0.64	0.06	0.06	0.2	< 0.02
GAP04 E-CL	377.65	< 0.3	< 0.001	< 0.001	1.72	< 0.05	0.3	< 0.1
GAP04 F-CL	448.07	< 0.3	0.032	0.29	1.6	< 0.01	0.22	0.66
GAP04 G-CL	557.40	< 0.6	0.028	0.114	< 0.1	< 0.1	< 0.1	< 0.2
GAP04 H-CL	681.21	< 0.3	0.294	0.01	4.14	< 0.01	0.2	2.12

Table B-11. Raw major and trace element chemistry for crush and leach experiments on DH-GAP01 and DH-GAP03 drill core.

Borehole	Depth	Ag	Al	As	Ba	Be	Bi	Br	Cd	Co	Cr	Cs	Cu	I	K
	m core length	µg/l	µg/l	µg/l	µg/l	µg/l	µg/l	µg/l	µg/l	µg/l	µg/l	µg/l	µg/l	µg/l	mg/l
DH-GAP01	64.96	0.59	43.7	0.77	1.03	<0.05	<0.01	17.4	0.01	0.08	1.00	<0.005	1.53	<2	8.50
	64.96	0.64	47.2	0.82	1.13	<0.05	<0.01	18.1	0.01	0.06	0.95	<0.005	1.68	<2	9.18
	90.65	<0.002	47.6	0.12	10.4	<0.05	<0.01	39.3	0.01	0.21	0.68	<0.005	2.14	<2	12.4
	149.9	0.01	3090	3.28	68.1	<0.05	<0.01	283	0.02	0.76	7.79	0.03	11.3	3.15	11.0
	179.6	0.01	4720	0.35	6.28	<0.05	<0.01	13.6	0.04	11.0	10.6	0.02	57.9	<2	7.44
	179.6	-	-	-	-	-	-	-	-	-	-	-	-	-	-
	188.98	0.02	6590	0.58	115	0.10	0.01	84.7	0.05	5.16	24.2	0.04	31.6	<2	25.8
DH-GAP03	9.93	0.14	637	0.42	3.41	<0.05	0.01	14.6	0.01	0.43	3.33	<0.005	2.51	<2	3.68
	41.5	0.01	1090	0.58	16.6	<0.05	0.01	445	0.01	0.56	2.92	0.02	6.55	<2	19.9
	80.8	<0.002	58.2	0.19	10.7	<0.05	<0.01	34.0	0.03	0.08	0.75	<0.005	1.22	<2	14.2
	139.75	0.02	45.1	0.26	1.10	<0.05	<0.01	17.8	0.02	0.10	0.77	<0.005	1.03	<2	5.84
	236.24	0.07	1470	0.76	30.4	<0.05	0.02	286	0.58	0.53	3.52	0.07	9.34	2.66	13.2
	302.44	0.07	407	1.46	1.48	<0.05	0.01	19.4	0.29	0.81	2.95	0.01	5.06	<2	1.20

Table B-11 continued.

	Depth m core length	Mn µg/l	Mo µg/l	Ni µg/l	P µg/l	Pb µg/l	Rb µg/l	Sb µg/l	Se µg/l	Sn µg/l	Sr µg/l	Th µg/l	Tl µg/l	U µg/l
DH-GAP01	64.96	1.74	4.66	3.20	<10	<0.005	2.70	0.55	2.22	<0.05	222	<0.002	0.01	0.85
	64.96	5.97	8.57	3.44	<10	0.01	2.86	0.58	2.31	<0.05	235	<0.002	0.01	0.92
	90.65	8.78	5.85	2.20	<10	0.03	3.55	0.35	1.51	<0.05	464	<0.002	0.01	0.27
	149.9	37.7	0.95	3.08	21.5	9.69	9.56	0.22	<0.5	<0.05	131	0.01	0.04	0.31
	179.6	228	5.82	22	293	4.83	3.44	0.07	1.85	<0.05	160	0.49	0.02	0.68
	179.6	-	-	-	-	-	-	-	-	-	-	-	-	-
	188.98	265	0.17	22.1	172	9.01	15.1	0.08	<0.5	0.11	144	0.18	0.07	0.19
DH-GAP03	9.93	22.4	1.91	6.48	<10	0.49	1.47	0.07	0.83	<0.05	185	0.01	<0.001	0.33
	41.5	15.3	3.78	2.49	63.8	2.31	9.89	0.50	<0.5	0.05	126	0.01	0.02	1.25
	80.8	8.69	21.0	5.42	<10	0.01	6.64	0.42	1.23	<0.05	206	<0.002	0.01	0.44
	139.75	2.66	8.11	2.28	11.1	<0.005	2.33	0.64	<0.5	<0.05	213	<0.002	<0.001	0.79
	236.24	6.52	6.22	3.06	<10	4.70	10.4	0.45	<0.5	0.07	87.7	0.22	0.03	15.8
	302.44	25.1	2.58	7.46	94.6	1.54	0.58	5.50	<0.5	<0.05	70.5	0.04	<0.001	0.19

Table B-11 continued.

Borehole	Depth	V	Zn	B	Ca	Fe	Li	Mg	Na	S	Si	Cl	SO4	Alk	CBE
	m core length	µg/l	µg/l	mg/l	mg/l	mg/l	mg/l	mg/l	mg/l	mg/l	mg/l	mg/l	mg/l	mmol/l	%
DH-GAP01	64.96	24.8	0.21	0.02	16.2	<0.03	0.018	4.96	23.0	30.6	7.09	2.0	31	1.38	8.2
	64.96	26.4	0.36	0.02	16.2	<0.03	0.017	4.97	22.9	30.6	7.09	2.0	31	-	8.6
	90.65	5.09	0.90	0.03	24.8	<0.03	0.022	15.7	26.6	20.3	5.17	2.0	54	2.62	3.2
	149.9	6.84	10.2	0.02	12.7	2.29	0.038	1.98	27.8	3.12	11.1	18.5	7.8	1.41	4.9
	179.6	46.9	127	0.02	26.1	15.2	0.014	11.9	23.3	15.8	19.0	1.2	41	1.69	15.3
	179.6	-	-	-	-	-	-	-	-	-	-	-	-	1.64	
	188.98	29.1	49.0	0.02	12.0	12.3	0.029	7.46	18.3	13.6	12.4	6.0	19	1.29	18.3
DH-GAP03	9.93	25.2	4.69	0.08	14.7	1.60	0.010	9.84	17.5	11.9	11.5	1.9	12	1.76	8.3
	41.5	3.40	6.21	0.08	15.2	1.25	0.035	4.92	36.2	6.19	4.87	27	13	1.99	4.1
	80.8	1.95	0.83	0.02	19.5	<0.03	0.016	5.09	15.7	13.5	5.43	3.4	35	1.57	1.6
	139.75	13.4	0.51	0.05	19.2	<0.03	0.005	7.15	23.7	9.56	6.84	2.7	22	2.09	2.8
	236.24	6.08	18.1	0.04	7.69	1.23	0.050	2.20	26.1	2.63	7.13	20	7.2	1.45	2.5
	302.44	33.6	4.55	0.05	6.80	1.69	0.007	3.69	32.8	6.99	11.1	2.3	20	1.66	0.1

Table B-12. Raw geochemical results for crush and leach experiments on DH-GAP04 core. Results first reported in Keir-Sage (2014).

Sample	Depth m	EC uS/cm	Sr mg/L	Ca mg/L	K mg/L	Mg mg/L	Na mg/L	F mg/L	Cl mg/L	SO4 mg/L
11.11	11.11	186	0.0479	10.8	1	11	13.8	<0.01	1.89	12.4
120.19 1-6cm	120.19	322	0.201	25.4	0.7	2.9	37.6	0.02	0.62	105
120.19 <1cm	120.19	120	0.104	13.6	0.4	1.5	7	<0.01	0.58	28.6
120.19	120.19	117	0.0436	12.9	0.4	5	4	0.04	0.73	14.8
209.56	209.56	324	0.0285	6	2.1	3.1	62.5	0.02	1.57	28.3
289.76	289.91	329	0.0224	4.7	31.3	1.7	49.9	0.63	19.9	9.86
399.84 1-6cm	399.84	1028	0.817	289	4.5	0.9	6.5	0.03	3.15	589
399.84 <1cm	399.84	1013	0.496	253	4.5	0.4	1.8	0.03	1.33	518
399.84	399.84	1538	1.88	260	111	13.9	58.1	0.94	24.5	738
491.12 1-6cm	491.12	949	1.88	181	4.7	10	28.7	0.02	1.02	418
491.12 <1cm	491.12	399	0.984	70.3	3.2	2.9	3.5	0.02	0.62	157
491.12	491.12	289	0.773	30.9	11.4	6.4	10.5	0.22	0.92	97
570.59	570.59	2260	3.22	620	15.8	16.9	49.3	0.04	1.67	1460
640.28 1-6cm	640.28	482	0.838	81.8	4.8	4.6	12.7	0.02	0.8	185
640.28 <1cm	640.28	426	0.69	76.3	4.4	3	3.8	0.03	0.76	170
640.28	640.28	869	1.64	81.9	46.8	22.7	54.5	0.69	9.5	366
670.42	670.42	2540	1.98	620	79.8	37.3	60.3	0.15	8.7	1620

Table B-12 continued. Hardness is a calculated parameter.

Sample	Calculated Hardness as CaCO3 mg/L	NH3 + NH4 as N mg/L	NO3 + NO2 as N mg/L	NO2 as N mg/L	NO3 as N mg/L	PO4 as P mg/L	Na/Cl meq/meq	Ca/SO4 meq/meq
11.11	72.4	0.04	0.17	0.04	0.13	<0.005	11.3	2.1
120.19 1-6cm	75.4	0.031	<0.008	<0.008	<0.002	0.068	93.5	0.6
120.19 <1cm	39.9	0.029	<0.008	<0.008	<0.002	<0.005	18.6	1.1
120.19	52.7	0.036	<0.008	<0.008	<0.002	<0.005	8.4	2.1
209.56	27.6	<0.005	0.041	0.041	<0.002	<0.005	61.4	0.5
289.91	18.9	0.032	0.134	<0.008	0.134	0.049	3.9	1.1
399.84 1-6cm	725	0.027	<0.008	<0.008	<0.002	<0.005	3.2	1.2
399.84 <1cm	634	0.028	<0.008	<0.008	<0.002	<0.005	2.1	1.2
399.84	712	0.033	<0.008	<0.008	<0.002	<0.005	3.7	0.8
491.12 1-6cm	493	0.026	<0.008	<0.008	<0.002	<0.005	43.4	1.0
491.12 <1cm	187	0.027	<0.008	<0.008	<0.002	<0.005	8.7	1.1
491.12	104	0.032	<0.008	<0.008	<0.002	0.012	17.6	0.8
570.59	1610	0.053	0.31	<0.008	0.31	<0.005	45.5	1.0
640.28 1-6cm	223	0.032	<0.008	<0.008	<0.002	<0.005	24.5	1.1
640.28 <1cm	203	0.028	<0.008	<0.008	<0.002	<0.005	7.7	1.1
640.28	298	<0.005	<0.008	<0.008	<0.002	<0.005	8.8	0.5
670.42	1700	0.017	<0.008	<0.008	<0.002	<0.005	10.7	0.9

Table B-13 Major and trace element composition of whole rock samples from DH-GAP04.

Borehole length	SiO2	Al2O3	Fe2O3(T)	MnO	MgO	CaO	Na2O	K2O	TiO2	P2O5	LOI	Total
mbgs	%	%	%	%	%	%	%	%	%	%	%	%
50.3	48.9	15.5	12.7	0.2	10.3	11.9	1.03	0.02	0.47	0.02	-0.31	100.6
50.3	48.8	15.2	12.6	0.2	10.3	11.8	1.03	0.02	0.47	0.02	-0.12	100.2
209.56	49.3	14.6	11.5	0.2	8.2	14.4	1.29	0.07	0.57	0.05	0.33	100.6
289.76	68.8	14.7	3.8	0.0	1.1	3.9	4.12	1.4	0.38	0.12	0.86	99.2
399.84	69.4	15.7	2.8	0.0	0.9	2.9	5.01	1.91	0.27	0.11	0.61	99.7
570.59	56.9	20.7	5.7	0.1	1.9	6.9	6.01	1.01	0.77	0.27	0.4	100.7
570.59	56.7	20.3	5.6	0.1	1.9	7.0	5.97	0.98	0.74	0.26	0.62	100.2
640.28	59.8	17.5	5.7	0.1	2.4	6.9	5.21	1.12	0.64	0.38	1.27	100.9
670.2	55.2	12.9	10.0	0.2	7.7	6.4	3.12	2.39	0.55	0.19	1.36	99.8
670.32	53.5	11.9	9.5	0.2	9.1	9.9	3.07	0.91	0.43	0.14	1.36	99.9

Table B-13 continued.

Borehole Length	Rock Type	Sc	Be	V	Cr	Co	Ni	Cu	Zn	Ga	Ge	As
Mbgs		ppm	ppm	ppm	ppm	ppm	ppm	ppm	ppm	ppm	ppm	ppm
50.3	MFGN	62	< 1	315	270	51	150	30	80	13	2.1	< 5
50.3	MFGN	61	< 1	315	270	51	140	30	80	12	2.2	< 5
209.56	MFGN	66	< 1	365	380	45	130	250	110	14	2.1	< 5
289.76	MFGN	7	< 1	51	80	9	< 20	30	40	17	1.3	< 5
399.84	FGN	2	1	34	90	6	< 20	< 10	40	19	1.1	< 5
570.59	IGN	10	1	106	40	12	< 20	< 10	60	23	1	< 5
570.59	IGN	10	1	101	40	12	< 20	< 10	50	23	1.1	< 5
640.28	IGN	14	1	104	70	14	< 20	40	70	23	1.5	< 5
670.2	MGN	27	1	135	310	37	270	< 10	150	18	1.9	< 5
670.32	IGN	31	1	132	460	34	230	< 10	130	19	2.2	< 5

Borehole Length	Rb	Sr	Y	Zr	Nb	Mo	Ag	In	Sn	Sb	Cs	Ba
Mbgs	ppm	ppm	ppm	ppm	ppm	ppm	ppm	ppm	ppm	ppm	ppm	ppm
50.3	< 1	72	11.6	10	< 0.2	< 2	< 0.5	< 0.1	< 1	< 0.2	< 0.1	< 3
50.3	< 1	70	11.6	10	< 0.2	< 2	< 0.5	< 0.1	< 1	< 0.2	< 0.1	< 3
209.56	< 1	99	13.8	21	< 0.2	< 2	< 0.5	< 0.1	< 1	< 0.2	< 0.1	19
289.76	22	330	5.8	125	2.5	< 2	1.3	< 0.1	< 1	< 0.2	< 0.1	698
399.84	53	637	1.6	88	< 0.2	< 2	0.9	< 0.1	< 1	< 0.2	0.4	519
570.59	7	1379	9.6	196	2	< 2	1.9	< 0.1	2	< 0.2	< 0.1	297
570.59	7	1357	9.6	186	2.2	< 2	1.7	< 0.1	2	< 0.2	< 0.1	298
640.28	6	1038	13.9	250	2	4	2.4	< 0.1	2	< 0.2	< 0.1	463
670.2	138	520	14	98	2.2	< 2	1	< 0.1	2	< 0.2	6.4	1060
670.32	20	351	21	52	2.4	< 2	0.6	< 0.1	3	< 0.2	0.7	283

Table B-13 continued.

Borehole Length	La	Ce	Pr	Nd	Sm	Eu	Gd	Tb	Dy	Ho	Er	Tm
Mbgs	ppm	ppm	ppm	ppm	ppm	ppm	ppm	ppm	ppm	ppm	ppm	ppm
50.3	0.38	1.63	0.33	1.9	0.87	0.326	1.26	0.27	1.97	0.45	1.4	0.233
50.3	0.41	1.65	0.31	1.95	0.84	0.316	1.27	0.25	1.8	0.43	1.37	0.229
209.56	3.47	7.73	1.05	5.12	1.37	0.503	1.82	0.35	2.31	0.5	1.59	0.277
289.76	27.2	48.3	4.96	16.6	2.75	0.788	1.83	0.25	1.28	0.23	0.63	0.086
399.84	18.3	32.6	3.49	12.3	1.85	0.694	0.97	0.1	0.39	0.06	0.15	0.018
570.59	39.7	80.8	9.62	38.2	5.91	1.5	3.64	0.47	2.1	0.37	1.03	0.138
570.59	41.8	84.3	10	38.4	6.25	1.48	3.69	0.46	2.13	0.36	1	0.144
640.28	73.7	145	16.6	61.1	9.59	1.84	5.57	0.64	2.95	0.54	1.52	0.195
670.2	21.3	51.6	6.73	27.6	5.7	0.725	4.41	0.61	3.15	0.54	1.43	0.217
670.32	21.6	56.3	8.09	35.6	7.93	1.26	6.01	0.86	4.41	0.78	2.2	0.297

Borehole Length	Yb	Lu	Hf	Ta	W	Tl	Pb	Bi	Th	U
Mbgs	ppm	ppm	ppm	ppm	ppm	ppm	ppm	ppm	ppm	ppm
50.3	1.57	0.239	0.4	< 0.01	< 0.5	< 0.05	< 5	< 0.1	< 0.05	0.01
50.3	1.55	0.228	0.4	< 0.01	< 0.5	< 0.05	< 5	< 0.1	< 0.05	< 0.01
209.56	1.82	0.259	0.7	< 0.01	< 0.5	< 0.05	< 5	< 0.1	0.22	0.01
289.76	0.5	0.079	3.2	0.13	< 0.5	< 0.05	6	< 0.1	7.8	0.3
399.84	0.12	0.024	2.1	< 0.01	< 0.5	0.19	7	< 0.1	0.49	0.21
570.59	0.8	0.112	4.6	0.22	< 0.5	< 0.05	< 5	< 0.1	0.71	0.16
570.59	0.79	0.11	4.4	0.22	< 0.5	< 0.05	5	< 0.1	0.78	0.17
640.28	1.08	0.16	5.9	0.18	< 0.5	< 0.05	6	< 0.1	5.85	0.24
670.2	1.25	0.189	2.4	0.15	< 0.5	0.52	6	< 0.1	2.39	0.35
670.32	1.79	0.268	1.6	0.18	< 0.5	0.12	< 5	< 0.1	0.37	0.08

Table B-14. Major and trace element chemistry for fracture filling gypsum.

Borehole Length	SiO2	Al2O3	Fe2O3(T)	MnO	MgO	CaO	Na2O	K2O	TiO2	P2O5	Total
Mbgs	%	%	%	%	%	%	%	%	%	%	%
259.6	4.1	< 0.01	0.9	0.1	1.6	35.8	0.01	< 0.01	< 0.001	< 0.01	42.5
318.21	0.3	0.1	0.1	0.1	0.0	39.3	0.02	< 0.01	0.005	< 0.01	39.9
403.81	9.4	3.0	2.2	0.0	0.9	28.0	0.47	1.14	0.285	0.25	45.7
540.27	1.1	0.3	0.2	0.1	0.1	35.8	0.03	0.01	0.009	< 0.01	37.6
638.85	0.1	0.1	0.2	0.0	0.1	37.7	0.01	< 0.01	0.004	< 0.01	38.1
638.85	0.1	0.1	0.2	0.0	0.1	38.3	0.01	< 0.01	0.004	< 0.01	38.8
670.57	1.1	0.3	0.4	0.0	0.4	36.9	0.03	0.08	0.033	0.02	39.3
670.57	1.1	0.3	0.4	0.0	0.4	37.4	0.03	0.09	0.036	0.01	39.8
67.95	6.2	0.8	1.6	0.7	1.6	47.8	0.05	0.02	0.007	0.02	58.8
259.6	40.7	0.1	9.0	0.3	15.0	9.5	0.12	0.02	0.006	< 0.01	74.8
345.42	2.0	0.7	0.6	0.0	0.3	32.9	0.09	0.07	0.011	0.02	36.7
403.81	38.7	13.1	14.6	0.2	7.3	7.5	1.11	5.51	1.673	0.36	90.1

Table B-14 continued.

Borehole Length	Sc	Be	V	Cr	Co	Ni	Cu	Zn	Ga	Ge	As	Rb
mbgs	ppm	ppm	ppm	ppm	ppm	ppm	ppm	ppm	ppm	ppm	ppm	ppm
259.6	< 1	< 1	6	< 20	< 1	< 20	< 10	< 30	< 1	< 0.5	< 5	< 1
318.21	< 1	< 1	8	< 20	< 1	< 20	< 10	< 30	< 1	< 0.5	< 5	< 1
403.81	2	< 1	41	40	3	< 20	< 10	50	6	< 0.5	< 5	41
540.27	< 1	< 1	7	< 20	< 1	< 20	< 10	< 30	< 1	< 0.5	< 5	< 1
638.85	< 1	< 1	6	< 20	< 1	< 20	< 10	< 30	< 1	< 0.5	< 5	< 1
638.85	< 1	< 1	7	30	< 1	< 20	< 10	< 30	< 1	< 0.5	< 5	< 1
670.57	< 1	< 1	11	< 20	< 1	< 20	< 10	< 30	< 1	< 0.5	< 5	4
670.57	< 1	< 1	10	< 20	< 1	< 20	< 10	< 30	< 1	< 0.5	< 5	5
E1	3	< 1	10	30	< 1	120	< 10	< 30	2	< 1	< 5	< 2
E2	< 1	< 1	< 5	20	< 1	< 20	< 10	< 30	1	< 1	< 5	< 2
E3	< 1	< 1	7	30	< 1	< 20	< 10	< 30	2	< 1	< 5	< 2
E4	23	1	266	160	41	90	< 10	260	30	1	< 5	225

Table B-14 continued.

Borehole Length	Sr	Y	Zr	Nb	Mo	Ag	In	Sn	Sb	Cs	Ba	La
mbgs	ppm	ppm	ppm	ppm	ppm	ppm	ppm	ppm	ppm	ppm	ppm	ppm
259.6	397	< 0.5	3	< 0.2	< 2	< 0.5	< 0.1	< 1	< 0.2	< 0.1	143	0.14
318.21	345	< 0.5	3	< 0.2	< 2	< 0.5	< 0.1	< 1	< 0.2	< 0.1	68	21.2
403.81	182	4.9	100	0.5	< 2	1.2	< 0.1	< 1	< 0.2	0.5	268	48.1
540.27	305	1.3	10	< 0.2	< 2	0.7	< 0.1	< 1	< 0.2	< 0.1	7	30.7
638.85	246	< 0.5	3	< 0.2	< 2	< 0.5	< 0.1	< 1	< 0.2	< 0.1	23	3.2
638.85	245	< 0.5	3	< 0.2	3	< 0.5	< 0.1	< 1	< 0.2	< 0.1	22	3.15
670.57	576	< 0.5	12	< 0.2	< 2	< 0.5	< 0.1	< 1	< 0.2	0.2	146	5.5
670.57	562	< 0.5	6	< 0.2	< 2	< 0.5	< 0.1	< 1	< 0.2	0.2	146	6.08
E1	142	12	10	< 1	< 2	6.1	< 0.2	< 1	< 0.5	< 0.5	9	57.2
E2	131	3	33	< 1	< 2	0.9	< 0.2	< 1	< 0.5	< 0.5	23	3
E3	282	5	4	< 1	< 2	0.5	< 0.2	< 1	< 0.5	< 0.5	23	3.3
E4	979	8	264	5	< 2	0.9	< 0.2	3	< 0.5	2.8	1015	78

Table B-14 continued.

Borehole Length	Ce	Pr	Nd	Sm	Eu	Gd	Tb	Dy	Ho	Er	Tm	Yb
mbgs	ppm	ppm	ppm	ppm	ppm	ppm	ppm	ppm	ppm	ppm	ppm	ppm
259.6	0.37	0.05	0.22	0.07	0.01	0.05	< 0.01	0.02	< 0.01	< 0.01	< 0.005	< 0.01
318.21	35.5	3.43	11.2	1.22	0.136	0.51	0.04	0.14	0.02	0.04	< 0.005	0.02
403.81	94.7	11	41.9	6.2	1.11	3.59	0.34	1.26	0.18	0.42	0.048	0.26
540.27	41.7	3.95	12.6	1.26	0.218	0.65	0.07	0.19	0.03	0.08	0.009	0.05
638.85	5.79	0.64	2.08	0.32	0.045	0.13	0.01	0.04	< 0.01	0.02	< 0.005	0.03
638.85	5.59	0.61	1.95	0.26	0.041	0.14	0.01	0.04	< 0.01	< 0.01	< 0.005	< 0.01
670.57	8.56	0.81	2.73	0.3	0.054	0.17	0.02	0.07	0.01	0.03	< 0.005	0.03
670.57	9.36	0.88	3.09	0.28	0.069	0.17	0.02	0.08	0.01	0.04	0.006	0.04
E1	67.1	6.44	24.1	3.2	0.76	3	0.3	1	0.1	0.3	< 0.05	0.2
E2	5.9	0.72	2.7	0.6	0.09	0.5	< 0.1	0.3	< 0.1	0.1	< 0.05	0.2
E3	6.2	0.65	2.1	0.4	0.1	0.3	< 0.1	0.1	< 0.1	< 0.1	< 0.05	< 0.1
E4	156	17.6	64.4	9.3	1.92	6	0.5	2.3	0.4	0.9	0.12	0.6

Table B-14 continued.

Borehole Length	Lu	Hf	Ta	W	Tl	Pb	Bi	Th	U	Comments
mbgs	ppm	ppm	ppm	ppm	ppm	ppm	ppm	ppm	ppm	
259.6	< 0.002	< 0.1	< 0.01	< 0.5	< 0.05	< 5	< 0.1	< 0.05	< 0.01	some chlorite impurities
318.21	0.004	< 0.1	< 0.01	< 0.5	< 0.05	< 5	< 0.1	< 0.05	< 0.01	mix gyp + calcite (acid test)
403.81	0.037	2.4	0.04	< 0.5	0.13	< 5	< 0.1	0.83	0.38	some biotite impurities
540.27	0.008	0.2	< 0.01	< 0.5	< 0.05	< 5	< 0.1	< 0.05	0.01	minimal clay and silicate imp
638.85	0.004	< 0.1	< 0.01	< 0.5	< 0.05	< 5	< 0.1	< 0.05	< 0.01	duplicate
638.85	< 0.002	< 0.1	< 0.01	4.2	< 0.05	< 5	< 0.1	< 0.05	< 0.01	minor calcite impurities
670.57	0.005	0.3	< 0.01	< 0.5	< 0.05	< 5	< 0.1	< 0.05	0.02	some chlorite impurities
670.57	0.006	< 0.1	< 0.01	< 0.5	< 0.05	< 5	< 0.1	< 0.05	< 0.01	duplicate
E1	< 0.04	< 0.2	< 0.1	< 1	< 0.1	< 5	< 0.4	< 0.1	< 0.1	gypsum/calcite
E2	< 0.04	0.7	< 0.1	< 1	< 0.1	< 5	< 0.4	0.2	< 0.1	chlorite (+ trace gyp)
E3	< 0.04	< 0.2	< 0.1	< 1	< 0.1	< 5	< 0.4	< 0.1	< 0.1	gypsum + trace clays
E4	0.1	6.3	0.2	< 1	1	5	< 0.4	2.3	0.7	biotite (+ trace gyp)

B.3. Isotopic Datasets

Table B-15.Isotopic results for lakes classified as "ponds".

Lake Type	Name	Sample Date	$\delta^{18}O$	$\delta^{18}O$ Rpt	$\delta^{2}H$	$\delta^{2}H$ Rpt	^{3}H	± 1σ	$\delta^{34}S$	$\delta^{34}S$ Rpt	$\delta^{18}O$	$\delta^{18}O$ Rpt	$\delta^{37}Cl$	$\delta^{37}Cl$ Std	$^{87/86}Sr$
			‰ VSMOW				TU		(SO4) ‰ CDT		(SO4) ‰ VSMOW		‰ SMOC		
Ponds	L3	2008-06-27	-12.6		-119	-119	10.4	1.0							
	L7	2008-06-28	-7.9		-95	-94	10.1	1.0							
	L8	2008-06-28	-16.2		-134	-135	10.2	1.0							
	L16	2008-07-01	-11.2		-110	-110									
	L36	2011-06-19	-18.1		-146	-146	9.4	0.77							
	L44	2012-05-12	-14.9	-14.8	-128	-129	9.4	0.8							0.75062
	L11	2008-06-29	-5.8		-86	-86	12.0	1.1							0.73466
	L18	2008-07-01	-5.2		-85	-84	9.6	1.1	1.1		3.4	4.0	-0.41	0.03	0.74592
	L20 1	2008-07-01	-11.3		-112	-112	8.1	1.0	0.4	0.1	-3.9	-3.2			0.74623
	L20 2	2010-09-05	-10.6	-10.6	-107	-107	10.0	0.9	-0.7	-1.0	-3.0	-2.6			

Table B-16. Isotopic results for dilute lakes (<800 µS/cm).

Lake Type	Name	Sample Date	$\delta^{18}O$		$\delta^{2}H$		^{3}H	± 1σ	$\delta^{34}S$		$\delta^{18}O$	$\delta^{37}Cl$	$\delta^{37}Cl$ Std	$\delta^{81}Br$	$\delta^{81}Br$ Std	$^{87/86}Sr$
			‰ VSMOW				TU		(SO4) ‰ CDT		(SO4) ‰ VSMOW	‰ SMOC		‰ SMOB		
Dilute Lakes	L1	2008-06-27	-11.0		-111	-110	10.6	1.0								0.75534
	L2	2008-06-27	-10.5		-111	-111	10.9	1.0								
	L4	2008-06-27	-8.5		-100	-100	10.7	1.0								
	L5	2008-06-27	-15.0	-15.1	-129	-129	10.3	1.0								
	L9	2008-06-29	-12.3		-115	-115	9.8	1.2								
	L10	2008-06-29	-10.8		-108	-108	7.9	1.0								
	L10 2	2009-07-06	-9.0	-9.3	-103		8.9	1.0								
	L15	2008-06-30	-14.8	-14.8	-132	-132	8.4	1.1								0.75363
	L19	2008-07-01	-15.1		-128	-128	9.4	1.1								
	L25-1	2009-07-02	-13.1		-121		10.1	1.0								
	L25-2	2011-06-25	-11.9		-117	-116	8.7	0.7								
	L26-1 (8m)	2009-07-02	-12.2		-118	-109	11.6	1.1								0.73854
	L26-2 (26m)	2010-05-11	-12.9		-118	-118	10.1	0.8								0.73847
	L26-3 (5m)	2011-04-16	-11.9		-116	-116	9.4	0.8				-0.07	0.08			
	L26-4 (25m)	2011-04-16	-11.8		-118	-117	10.5	0.9								0.73849
	L27	2009-07-06	-10.3		-108		9.2	1.0								
	L28	2009-07-06	-9.4		-104		8.3	0.9								
	L31	2010-09-02	-8.4	-8.5	-95	-95	8.7	1								
	L33	2010-09-04	-12.7	-12.6	-112	-111	12	1								0.71874
	L34	2010-09-06	-12.2	-12.2	-115	-115	12.9	1								
	L35	2010-09-04	-10.4	-10.3	-104	-105	10	0.9								
	L42	2011-09-12	-6.8	-6.8	-92	-92	8.7	0.8								0.75055
	L41	2011-09-12	-7.5		-95	-95	9.3	0.8				-0.04	0.1	1.68	0.09	0.74873
	L40	2011-09-12	-8.5		-97	-97	8.5	0.8								0.75108
	L43	2011-09-12	-12.5		-115	-115	8	0.7	12.5	12.6	-1.0					0.74385
	L46	2012-09-03	-10.2	-10.1	-95	-95	7.4	0.7				-0.03	0.02			

Table B-17. Isotopic results for saline lakes (>800 µS/cm).

Lake Type	Name	Sample Date	$\delta^{18}O$	$\delta^{18}O$ Rpt	$\delta^{2}H$	$\delta^{2}H$ Rpt	^{3}H	± 1σ	$\delta^{34}S$	$\delta^{34}S$ Rpt	$\delta^{18}O$	$\delta^{18}O$ Rpt	$\delta^{37}Cl$	$\delta^{37}Cl$ Std	$\delta^{81}Br$	$\delta^{81}Br$ Std	$^{87/86}Sr$
			‰ VSMOW				TU		(SO4) ‰ CDT		(SO4) ‰ VSMOW		‰ SMOC		‰ SMOB		
Saline Lakes	L29-1	2009-07-06	-8.2		-99		9.0	0.9									0.74066
	L29-2	2010-09-04	-6.5	-6.5	-96	-96	10.0	0.9					-0.29	0.07	0.96	0.03	
	L47	2012-09-01	-8.5	-8.5	-95	-94	9.9	0.8									
	L17 1	2008-07-01	-11.4		-113	-113	10.5	1.1									0.75102
	L17 2	2010-09-05	-8.0	-7.7	-100	-100	9.8	0.9									
	L45	2012-08-28	-9.0	-9.1	-101	-101	9.2	0.8	14.1		5.4						0.7267
	L21 1	2008-06-01	-10.1		-101	-102	14.7	1.4	23.4		5.3	5.8	-0.19	0.03			0.72982
	L21 2	2010-09-02	-8.2	-8.2	-93	-93	12.1	1.0									
	L21 3	2011-09-10	-8.3	-8.2	-94	-93	12.9	1.1									
	L22 1	2008-06-01	-9.6	-9.3	-95	-95	15.4	1.4									
	L22 2	2011-09-10	-8.9		-95	-95	11.5	1.0	22.9		4.6		-0.02	0.06	0.78	0.03	0.72947
	L22 3 (21m)	2012-09-02	-8.8	-8.9	-94	-94	10.6	0.9	23.5		6.0	5.8					
	L22 4	2012-09-01	-9.1	-9.0	-98	-98	10.2	0.9	23.6	23.2	6.2						
	L32	2010-09-04	-9.9	-9.7	-104	-105	8.3	0.7									0.75397
	L32-2	2013-09-16	-9.7	-9.8	-103	-103	8.0	0.8					-0.23	0.05	-0.06	0.08	
	L39	2011-09-10	-7.7		-93	-93	11.4	1	20.2		8.0						
	L39 2	2012-09-01	-8.0	-7.8	-95	-95	10.4	0.9									

Table B-18. Isotopic results for meltwater lakes and thaw lakes.

Lake Type	Name	Sample Date	δ18O	δ18O Rpt	δ2H	δ2H Rpt	3H	± 1σ	δ34S	δ34S Rpt	δ18O	δ18O Rpt	δ37Cl	δ37Cl Std	$^{87/86}$Sr
			‰ VSMOW				TU		(SO4) ‰ CDT		(SO4) ‰ VSMOW		‰ SMOC		
Melt-water Lakes	L38	2011-07-07	-28.2		-217	-217	1.0	0.4							
	L37	2011-06-22	-25.4		-201	-201	3.7	0.5							
	L6	2008-06-28	-15.1		-129	-128	10.5	1.0							0.75144
Thaw Lakes	L12 1	2008-06-29	-13.6	-128.5	-128		7.4	0.9	3.8	4.1	-11.0	-10.6	0.03	0.07	0.75333
	L12 2	2009-06-27	-12.9		-127	-128	6.3								
	L12 3	2009-06-27	-13.1		-128	-127	5.6								
	L12 4	2009-06-27	-12.9	-13.2	-127	-127	7.1								
	L13	2008-06-29	-15.3	-15.4	-136	-135	8.9	0.9							
	L14	2008-06-29	-14.2		-130	-130	10.5	1.0							0.75735
	L23	2009-06-28	-13.6		-127		8.4	0.9							
	L24	2009-06-28	-14.0		-129		7.8	0.8							

Table B-19. Isotopic results from spring runoff samples, samples from the ice dammed lake springs, precipitation and meltwaters.

	Short Name	Name	Sample Date	$\delta^{18}O$	$\delta^{18}O$ Rpt	$\delta^{2}H$	$\delta^{2}H$ Rpt	^{3}H	± 1σ	$^{87/86}Sr$
				‰ VSMOW				TU		
Spring Runoff	Run-1	Spring Runoff 1	2012-05-06	-18.7	-18.7	-144	-144	9.9	0.7	
	Run-2	Spring Runoff 2	2012-05-06	-19.1	-19.0	-147	-147	9.2	0.8	
IDL springs	SP-2	IDL Spring 2	2011-07-05	-21.8		-165	-165	7.6	0.7	
	SP-3	IDL Spring 3	2011-07-01	-24.4		-186	-186	4.8	0.5	
Precipitation	Snow	July 1st Snowfall	2009-07-01	-20.2		-156		13.8	1.3	
Meltwaters (small outflows)	MW 1	MW 1	2008-06-29	-28.3		-214	-214	<0.8	0.8	
	MW 2	MW 2	2008-06-29	-30.5	-30.6	-232	-232	<0.8	0.8	
	MW 3	MW 3	2008-06-30	-29.0		-219	-219	0.9	0.7	
	MW 4	MW 4	2008-06-30	-30.0		-227	-228	0.9	0.9	
	C River-1	Caribou Outflow	2011-09-07	-27.7		-212	-213	1.3	0.4	
	C River-2	Caribou Outflow(2)	2011-09-07							
	MW6	Outflow Issunguata Sermia 1	2011-07-16	-29.9		-223	-224	<0.8	0.3	
	MW7	Outflow Issunguata Sermia 2	2011-07-16	-29.5	-29.5	-225	-225	<0.8	0.3	
	MW24	Point 660	2012							0.74936
	MW9	Russel Outflow Winter	2011-04-16	-27.0		-205	-205			
Large Meltwater Rivers	MW5-1	Leverett River	2010-09-04	-23.6	-23.3	-180	-180	1.3	0.3	
	MW5-2	Leverett River	2011-09-07	-23.4	-23.4	-181	-181	2.8	0.5	0.73683
	MW8 (012)	GL11-IT-012	2011-06-14							
	MW8 (018)	GL11-IT-018	2011-06-18	-24.7		-183	-183	3.1	0.5	
	MW8 (019)	GL11-IT-019	2011-06-18	-24.3		-181	-181	2.3	0.4	
	Q River	Qinquata Kuusua	2011-09-09	-25.4		-188	-188	4.6	0.5	0.75111
Supraglacial (Interior Ice)	MW9	S4 Surface Stream	2012-07-20	-27.5	-27.7	-212	-211	<0.8	0.4	
	MW10	Kan-L Pond	2012-07-20	-27.1	-27.0	-204	-204	<0.8	0.3	
	MW11	Kan-(bo?)	2012-07-20	-26.6	-26.6	-203	-203	<0.8	0.4	
Glacial Ice	Ice-P	Pleistocene Ice	2011-07-23	-34.8		-267	-267	<0.8	0.3	
	Ice-H	Holocene Ice	2011-07-23	-27.3		-211	-211	<0.8	0.3	

Table B-19 continued.

	Short Name	Name	Sample Date	$\delta^{18}O$	$\delta^{18}O$ Rpt	$\delta^{2}H$	$\delta^{2}H$ Rpt	^{3}H	± 1σ	^{8786}Sr
				‰ VSMOW				TU		
Subglacial Samples from Ice Drilling	MW12	GL12-2-1	summer-2012	-26.6	-26.6	-201	-201	<0.8	0.4	
	MW14	GL12-2-2	summer-2012	-25.8	-25.8	-195	-195	1.1	0.4	
	MW16	GL12-2-3	summer-2012	-26.1	-26.1	-202	-203	0.8	0.5	
	MW17	GL12-2-4, s1	summer-2012	-26.6	-26.6	-200	-200	<0.8	0.3	
	MW18	GL12-2-4, s2	summer-2012	-29.0	-29.0	-220	-220	<0.8	0.4	
	MW20	GL12-PGS1	summer-2012	-27.8	-27.9	-215	-216	1.1	0.5	
	MW21	GL12-PGS2	summer-2012	-28.0	-28.0	-217	-216	1.3	0.7	
	MW22	GL12-TM	summer-2012	-23.5	-23.6	-179	-179	4.8	0.5	
	R Ice	Russell Icing (ice)	2010-05-11	-26.0		-201	-201	2.9	0.4	
	R-Ice 2	Mini Blood Falls	2011-04-16	-27.5		-211	-211			

Table B-20. Isotopic results from the DH-GAP01 borehole.

Short Name	Sample Date	$\delta^{18}O$	$\delta^{18}O$ Rpt	$\delta^{2}H$	$\delta^{2}H$ Rpt	^{3}H	± 1σ	$\delta^{34}S$	$\delta^{34}S$ Rpt	$\delta^{18}O$	$\delta^{18}O$ Rpt	$\delta^{37}Cl$	$\delta^{37}Cl$ Std	$\delta^{81}Br$	$\delta^{81}Br$ Std	$^{87}Sr/^{86}Sr$
		‰ VSMOW				TU		(SO4) ‰ CDT		(SO4) ‰ VSMOW		‰ SMOC		‰ SMOB		
GAP01 2	2009-07-01	-16.4		-137	-141	5.7	0.7									
GAP01 3	2009-07-08	-16.1		-139	-139	5.5	0.8									
GAP01 4	2009-09-03	-17.5		-143	-142	5.4	0.8									
GAP01 5	2009-09-07	-20.5		-158	-158	1.5	0.8									
GAP01 6	2010-05-11	-21.6	-21.65	-165	-166	<0.8	0.3									
GAP01 7	2010-05-11	-21.5		-165	-165	<0.8	0.3									
GAP01 8(1)	2010-09-01	-21.0		-165	-166	<0.8	0.3									
GAP01 9(1)	2010-09-03	-21.0		-165	-165	<0.8	0.3									
GAP01 10	2010-09-04	-21.4		-165	-165	<0.8	0.3									0.70753
GAP01 11	2010-09-05	-20.9		-164	-164	<0.8	0.3									
GAP01 12	2010-09-04											-0.05	0.15			
GAP01 13	2010-09-04							4.9		5.92	6.00					
GAP01 14	2011-09-09	-21.6	-21.5	-167	-167	<0.8	0.3							0.29	0.03	

Table B-21. Isotopic results from the DH-GAP04 borehole upper (U), middle (M) and lower (L) sampling sections and from flushed drilling fluid.

Short Name	Sample Date	$\delta^{18}O$	$\delta^{18}O$ Rpt	$\delta^{2}H$	$\delta^{2}H$ Rpt	^{3}H	± 1σ	$\delta^{34}S$	$\delta^{34}S$ Rpt	$\delta^{18}O$	$\delta^{18}O$ Rpt	$\delta^{37}Cl$	$\delta^{37}Cl$ Std	$\delta^{81}Br$	$\delta^{81}Br$ Std	$^{87/86}Sr$
		‰ VSMOW				TU		(SO4) ‰ CDT		(SO4) ‰ VSMOW		‰ SMOC		‰ SMOB		
GAP04-U-1	2011-09-10	-16.7		-143	-143	4.5	0.5	4.51		3.56		0.39	0.07			0.70334
GAP04-U-2	2013-09-02	-16.9	-16.8	-145	-145	4	0.5									
GAP04-U-3	2013-09-08															
GAP04-U-4	2013-09-12	-19.6	-19.7	-158	-158	3.8	0.5									
GAP04-U-5	2013-09-18	-19.7	-19.5	-157	-157	3	0.5									
GAP04-U-6	2013-09-22	-19.7	-19.7	-159	-159	2.9	0.4	5.02		3.89		0.31	0.07	0.44	0.05	
GAP04-M-1	2011-07-10	-16.3		-138	-138	5.8	0.6									
GAP04-M-2	2011-09-09	-15.8		-138	-138	5.1	0.6	4.95		3.39		0.13	0.04			0.70407
GAP04-M-3	2013-09-02	-16.4	-16.2	-139	-139	5.7	0.6									
GAP04-M-4	2013-09-08															
GAP04-M-5	2013-09-12	-19.2	-19.1	-157	-157	2.3	0.5									
GAP04-M-6	2013-09-18	-19.7	-19.7	-159	-158	2.2	0.4									
GAP04-M-7	2013-09-23	-19.7	-19.7	-160	-160	2.5	0.4	4.45		3.13		0.22	0.07			
GAP04-L-1	2011-09-08	-12.6	-12.7	-122	-122	6.9	0.7	5.46	5.73	5.47		0.32	0.14			0.7044
GAP04-L-2	2013-09-02	-13.2	-13.3	-120	-120	6	0.6									
GAP04-L-3	2013-09-08															
GAP04-L-4	2013-09-12	-23.6	-23.6	-179	-179	<0.8	0.3									
GAP04-L-5	2013-09-18	-23.4	-23.6	-178	-178	<0.8	0.4									
GAP04-L-6	2013-09-24	-23.2	-23.3	-176	-177	1.0	0.4	4.97		3.27		0.41	0.04	0.55	0.05	
FW04-99	2011-06-19	-18.0		-147	-147	7.6	0.7									
FW04-300	2011-06-22	-26.4		-203	-203	4.1	0.5									
FW04-441	2011-06-24	-12.2		-118	-118	8.2	0.8									
FW04-558	2011-06-26															
FW04-603	2011-06-27	-12.7		-117	-117	9	0.78									
FW04-687-1	2011-06-28	-13.3	-13.2	-119	-119											
FW04-687-2	2011-07-01	-12.6		-115	-115	7.2	0.6									

Table B-22. Isotopic results from the Leverett Spring.

Short Name	Sample Date	$\delta^{18}O$	$\delta^{18}O$ Rpt	$\delta^{2}H$	$\delta^{2}H$ Rpt	^{3}H	± 1σ	$\delta^{34}S$	$\delta^{34}S$ Rpt	$\delta^{18}O$	$\delta^{18}O$ Rpt	$\delta^{37}Cl$	$\delta^{37}Cl$ Std	$\delta^{81}Br$	$\delta^{81}Br$ Std	$^{87/86}Sr$
		‰ VSMOW				TU		(SO4) ‰ CDT		(SO4) ‰ VSMOW		‰ SMOC		‰ SMOB		
Spring 1	2008-06-29	-18.69		-152.38	-152.06	1.2	0.6	8.91		4.42	4.66	0.02	0.09			0.74283
Spring 2	2009-06-27	-18.02		-152.67		<0.8	0.6									0.73249
Spring 3	2009-06-27	-17.99		-152.05		<0.8	0.7									
Spring 4	2009-09-05	-19.03		-152.89	-153.31	<0.8	0.6									
Spring 5	2010-05-10	-18.48	-18.49	-150.42	-150.56	<0.8	0.3	10.91	11.17	5.94	5.55					
Spring 6	2010-09-05	-18.46	-18.45	-152.39	-152.29	<0.8	0.3									
Spring 7	2010-09-05											0.06	0.06			
Spring 8	2011-04-14	-18.34		-152.63	-153.05	<0.8	0.3									
Spring 9	2011-09-11	-18.73		-153.66	-153.89	<0.8	0.3									

C. Appendix C. Drill Core Investigation Methods

C.1. *Whole Rock Analyses*

Samples for whole rock analyses were ground using a ball mill that was cleaned thoroughly and run with silica sand between samples. Samples were ground to a fine powder (approximately <0.2 mm). Whole rock powders were analyzed for chemical composition by commercial analyses through ActLabs Inc. (Ancaster, Ontario) using lithium metaborate/lithium tetraborate fusion and analyzed on a combination simultaneous/sequential Thermo Jarrell-Ash ENVIRO II ICP or a Varian Vista 735 ICP. Additional trace elements were analyzed using lithium metaborate/tetraborate fusion on a Perkin Elmer Sciex ICP/MS.

A subsample of the whole rock samples described above were separated and analyzed for the $^{87}Sr/^{86}Sr$ ratio of the bulk rock. Additionally, two samples of altered wall rock along fractures at 557.4 mbhl and 638.0 mbhl in the DH-GAP04 borehole were removed using a dremel tool and ground in an agate mortar. Powders were washed using ultra pure water and acetic acid to remove any calcite or gypsum then centrifuged to separate the washing fluids. Samples were digested using hydrofluoric acid in a mixture of 1 mL each of HF, HNO_3 and ultra pure water. Samples were allowed to evaporate. Dissolved whole rock samples were analyzed for $^{87}Sr/^{86}Sr$ using the methods outlined in Chapter 1.

Five of the samples analyzed for whole rock $^{87}Sr/^{86}Sr$ isotopic ratios were also selected to analyze the strontium isotopic ratio of separate mineral components. Quartz was excluded as it contains negligible strontium concentrations. Samples of intact core were separated into grain size <0.5 mm using a SELFRAG system (www.selfrag.com), which utilizes short, high voltage electric pulses to shear rock along grain boundaries due to the difference in dielectric constants. Minerals

were then hand separated under a binocular microscope using tweezers. Silicate mineral separates were washed using acetic acid followed by ultrapure water to remove carbonates and gypsum and then digested using hydrofluoric acid in a mixture of 1 mL each HF, HNO_3 and ultra pure water. Sample material was then analyzed for $^{87}Sr/^{86}Sr$ on a thermal ionization mass spectrometer (TIMS) using the method outlined in (Chapter 1).

Samples of sulfide minerals, mainly pyrite and chalcopyrite, were separated from the crushed DH-GAP04 core using a magnet and hand separation. These samples were analyzed for $\delta^{34}S$ at the University of Waterloo Environmental Isotope Laboratory using the following methods: sulfide samples are combusted to convert the solid sample to SO_2 gas which is analyzed through an elemental analyzer (Costech CNSO 4010 UK) coupled to an Isochrom continuous flow isotope ratio mass spectrometer (CFIRMS) (GVInstruments/Micromass UK).

C.1.1. X-Ray Diffraction Analysis

Rock samples for XRD analyses were powdered in an agate mortar. Diffraction data was collected on a Bruker D8 diffractometer using a sample holder that contained a silicon wafer cut parallel to the 511 Miller index. This type of holder allows for small aliquots of powder to be used. Diffraction data was collected between 10 and 70 °C for 2-theta angles using a step increment of 0.025 degrees with 1.25 second counts for each step. Diffraction data was indexed using the Joint Committee on Powder Diffraction Standards (JCPDS) database in identify the mineral phases in each sample.

C.2. *Fracture Mineral Analyses*

Samples for fracture mineral analyses in this study were mostly limited to gypsum in the DH-GAP04 borehole, with the exception of a single gypsum sample from DH-GAP01. Parallel studies on fracture infilling minerals were also performed on calcite (Makahnouk at al. (unpublished)) and by

Eva-Lena Tullborg and Heinrich Drak on redox related mineralogy (Harper et al., 2015). Fracture gypsum was studied in order to understand if gypsum precipitated by in-situ freeze out. Fracture gypsum samples were selected to cover a range of borehole depths as well as a variety of gypsum morphologies. Gypsum was removed by hand using dental tools using a binocular microscope. Samples were ground to a fine powder in an agate mortar. Solid samples were analyzed for major and trace element chemistry as well as isotopic composition ($\delta^{34}S$, $\delta^{18}O$, $^{87}Sr/^{86}Sr$). Fracture mineral samples were analyzed for chemical composition by commercial analyses through ActLabs Inc. (Ancaster, Ontario) using the methodology outlined in Section C.1 above. Isotopic analyses were performed at the University of Waterloo Environmental Isotope Lab. Isotope analysis methods followed those outlined in Chapter 1 with the following additional sample preparation:

For $\delta^{34}S$ and $\delta^{18}O$ analyses: powdered gypsum samples were dissolved in ultra-pure water before SO_4^{2-} is extracted using $BaCl_2$ and converted to $BaSO_4$. For $^{87}Sr/^{86}Sr$ analysis of fracture mineral samples, the solid sample was dissolved in ultrapure water before analysis following the methods outlined in Chapter 1.

C.2.1. Gypsum Dissolution Samples

A subset of six of the gypsum fracture mineral samples were dissolved in ultrapure water. The resulting solution was analyzed for chemical composition by commercial analyses at ActLabs Inc (Ancaster, Ontario) using ICP-OES and ICP-MP. Two of the dissolved samples, those which contained the highest Cl^- concentrations, were also analyzed for $\delta^{37}Cl$ using the methods described in Chapter 1.

C.2.2. X-Ray Diffraction Methods

Six fracture mineral samples were selected from DH-GAP04 to be analyzed by X-ray Diffraction at the Finnish Geological Survey. Rock samples for XRD analyses were powdered in an agate mortar. Spectra were measured on a Bruker D8 Discover A25 Diffractometer over a range of 2θ 2-70° CuKα.

C.3. *Porewaters*

Matrix fluids were extracted from samples of the drilled core from the GAP boreholes using crush and leach and out diffusion methods. The crush and leach and out diffusion techniques are discussed in Smellie et al., 2003; Waber and Smellie, 2008; Eichinger and Waber, 2013 and Frape et al., 2014. A brief description of matrix porewaters and the rationale for examining these fluids is outlined below based on the aforementioned references. Matrix porewater consists of water contained within the interconnected pore space of the rock matrix that exists along grain boundaries (intergranular pore space) and within mineral grains (intragranular pore space). Water movement in this pore space is dominated by diffusion. Matrix porewaters and groundwaters in water-conducting fractures interact with one another with the greatest interaction occurring in pore space located closest to the water-conducting fractures. Given a long enough time period with a stable groundwater compositions the matrix porewaters will reach chemical equilibrium with the fracture groundwaters, thus preserving a record of past groundwater compositions (Smellie et al., 2003; Waber and Smellie, 2008; Eichinger and Waber, 2013). For example, matrix porewaters may preserve a seawater geochemical signature that represents past subsurface infiltration of seawater. Two methods were used to examine porewater and readily dissolvable salts in the rock matrix: crush and leach and out diffusion. In both cases the porewaters are diluted and actual porewater concentrations must be calculated. The accuracy of these calculations is very dependent on knowledge of the connected porosity or porosity of the rock (Eichinger and Waber, 2013).

C.3.1. Crush and Leach Methods

Crush and leach experiments were performed on sections of core from DH-GAP01, DH-CAP03 and DH-GAP04 (Table C-1). Crush and leach experiments on DH-GAP04 drill core were part of an Undergraduate Thesis and results were first reported in Keir-Sage (2014). Samples for crush and leach were paired with petrophysical measurements performed by the Geophysical Laboratory at the Finnish Geological Survey on adjacent lengths of core. The samples used for crush and leach are described in Table C-1. Petrophysical results and methodologies are report in the GAP final data report (Harper et al., 2015). The sections of core were pulverized (sieve size 200, <0.074 mm) using a Fritsch Laboratory ball mill, which was thoroughly cleaned between samples as described earlier in Section C.1. Three sections of DH-GAP04 core were selected for sequential crush and leach experiments on progressively smaller particle sizes (1-6 cm, <1cm, <0.0.74 mm). Salts may also be released from fluid inclusions during the crushing process. The effect of fluid inclusions on the crush and leach experiments was examined using the sequential crush and leach experiments described above, where the larger size fractions represent samples that are less likely to be impacted by crushed fluid inclusions(Waber and Smellie, 2008). Pulverized rock was mixed with nano-pure water in a 1L nalgene container in a ratio of approximately 1 mL water to 1 g rock. Samples were then placed on a shaker for 24 hours. After shaking the samples were allowed to settle before the water was extracted using vacuum filtration. The salts found in the crush and leach extracts represent the readily available salts that can be weathered or leached from the rock into the groundwater regime by water-rock interaction. (Smellie et al., 2003; Frape et al., 2004; Waber and Smellie, 2008; Stotler et al., 2009). Fluids from ruptured fluid inclusions may also be represented in the crush and leach extracts (Waber and Smellie, 2008). As such, these results are useful for determining which waters in the study area

Table C-1: Summary of crush and leach samples. MFGN = mafic garnet bearing gneiss. FGN = felsic gneiss. IGN = intermediate gneiss. AR = altered wall rock. MGN = mafic gneiss, non-garnet bearing. Distance to fracture represents the distance from the sample to a water conducting fracture as measured by the Posiva Flowlog system *(Pöllänen et al., 2012)*.

Out Diffusion	Depth Intervals	Start length	End length m	Av. Bore-hole length	Av. Depth m	Sample length	Lithology	Dist to frac	φ (n)	Bulk Density
	m BHL	m BHL	BHL	m BHL	bgs	m		m	%	kg/m3
DH-GAP01	64.96-65.06	64.96	65.06	65.01	56	0.1	MFGN		0.5	3052
	90.65-90.75	90.65	90.75	90.7	79	0.1	MFGN		0.35	3042
	149.90-150.00	149.9	150	149.95	130	0.1	FGN		0.44	2664
	179.6-179.70	179.6	179.7	179.65	156	0.1	MFGN		0.5	3111
	188.98-189.08	188.98	189.08	189.03	164	0.1	FGN		0.42	2775
DH-GAP03	9.93-10.03	9.93	10.03	9.98	9	0.1	MFGN		0.45	2941
	41.50-41.60	41.5	41.6	41.55	36	0.1	FGN		0.53	2675
	80.80-80.90	80.8	80.9	80.85	70	0.1	FGN		0.86	2675
	139.75-139.80	139.75	139.8	139.775	121	0.05	MFGN		0.4	2981
	236.24-236.34	236.24	236.34	236.29	205	0.1	PGR		0.34	2691
	302.44-302.54	302.44	302.54	302.49	262	0.1	MFGN		0.39	2903
DH-GAP04	11.11	11.11	11.26	11.185	10	0.15	MFGN	404	0.58	3300
	50.02	50.02	50.18	50.1	43	0.16	MFGN	366	0.37	3238
	120.19 total	120.19	120.34	120.265	104	0.15	MFGN	300	0.43	3281
	209.56	209.56	209.71	209.635	182	0.15	MFGN	206	0.76	3311
	289.76	289.76	289.91	289.835	251	0.15	MFGN/IGN	126	0.29	2715
	399.57	399.57	399.72	399.645	346	0.15	FGN	16	0.58	2676
	399.84 total	399.84	399.99	399.915	346	0.15	FGN	16	0.58	2676
	430.17	430.17	430.32	430.245	373	0.15	IGN	14	0.37	2685
	430.47	430.47	430.62	430.545	373	0.15	IGN	15	0.37	2685
	491.12 total	491.12	491.27	491.195	425	0.15	IGN	57	0.49	2726
	570.59	570.59	570.74	570.665	494	0.15	IGN	14	1.14	2736
	639.98	639.98	640.13	640.055	554	0.15	IGN	2	0.29	2741
	640.28 total	640.28	640.43	640.355	555	0.15	IGN	2	0.29	2741
	670.42	670.42	670.53	670.475	581	0.11	MGN	<1	0.92	2901

have chemistry and isotope signatures that are primarily the result of interaction between recharging groundwaters and the host rock. Processes such as in-situ freeze out or the past infiltration of waters that differ from modern groundwaters may also be preserved in matrix porewater geochemical and isotopic compositions (e.g. Smellie et al., 2003; Waber and Smellie, 2008).

Measured concentrations in the crush and leach waters must be corrected to porewater concentrations to account for the differences in water volume between the test water and the porewater. Porosities and bulk densities used for crush and leach calculations are based on petrophysical results on pieces of core adjacent to crush and leach samples(Harper et al., 2015). It should be kept in mind that porosities can vary over short distances. Due to the unquantifiable uncertainties from to the use of adjacent porosities, porewater concentrations are assigned an error of ±25%.

Waber and Smellie (2008) outline the procedure for correcting measured concentrations to porewater concentrations:

$$C_R^i = C_L^i \frac{V_{TW}}{M_R} \qquad [C.1]$$

$$C_{PW}^i = C_R^i \rho \frac{1}{n} \qquad [C.2]$$

Equation 4.1 calculates the concentration of element i per unit rock mass (C_R) (mg/g). C_L^i is the concentration measured by Lab (mg/L). V_{TW} is the volume of water added (L) for the experiment while M_R is the mass of rock being leached (g).

Equation 4.2 calculates the concentration of element i found in the porewater (C_{PW}) C_{PW} does not take into consideration the dissolution of soluble mineral phases or leakage from broken fluid inclusions, which may significantly impact the chemistry in some cases. ρ represents the bulk density of the intact piece of core in g/cm^3 and n is porosity expressed as a ratio, not as a %. Equation 4.2 yields porewater concentrations in mg/cm^3.

C.3.2. Out Diffusion Methods

Out diffusion experiments involve placing a section of rock core into a cell which is then filled with a known test water (usually ultrapure water). The dissolved constituents of the porewater will then diffuse from the core until the porewater and testwater have equilibrated (Lambie, 2008; Waber and Smellie, 2008; Eichinger and Waber, 2013). Equilibration is determined by taking small volume sub samples and analyzing them for Cl^- until a stable concentration is reached. Upon equilibration, the eluate is removed and analyzed for chemical and isotopic composition which can then be translated into porewater concentrations. A detailed of the out diffusion methodology can be found in Eichinger and Waber (2013) and methods specific to this are discussed in more detail below.

Two sets of out diffusion experiments were run on DH-GAP04 core. The first set (GAP04-A to -D) the core was not preserved at the borehole site and thus was not fully saturated before the experiment was initiated. As such, this experiment was not a true out diffusion experiment and likely involved the dissolution of soluble salts left after evaporation of porewater as well as diffusion from any remaining porewaters. The second set (GAP04-E to -H) of core was wrapped and sealed on site and preserved hydration of pore fluids. GAP04-E to -H followed more traditional out diffusion methodology. The sections of core used for the out diffusion experiments are summarized in Table C-2. The out diffusion studies conducted at the University of Waterloo were in parallel to a study by Eichinger and Waber (2013) on DH-GAP04 core. Data from the Eichinger and Waber (2013) study will be integrated into the dataset acquired from the eight core sections discussed above.

After completion of the out diffusion experiments on GAP04-E to -H, the cores were crushed and leached following the methods outlined for other crush and leach experiments in Section C.3.1.

Table C-2. Summary of samples used in out diffusion experiments from the DH-GAP04 core. MFGN = mafic garnet bearing gneiss. FGN = felsic gneiss. IGN = intermediate gneiss. AR = altered wall rock. MGN = mafic gneiss, non-garnet bearing. Distance to fracture represents the distance from the sample to a water conducting fracture as measured by the Posiva Flowlog system *(Pöllänen et al., 2012)*.

Out Diffusion	Start length	End length	Av. Bore-hole length	Av. Depth	Sample length	Initial Wt. Core	Diameter	Volume	Lithology	Distance to Fracture
	m BHL	m BHL	mbgs	mbgs	m	(g)	mm	m3		m
GAP04-A	209.83	209.97	209.90	197.24	0.14	931.73	48.67	0.00026	MFGN	206
GAP04-B	352.00	352.15	352.08	330.84	0.15	865.00	49.75	0.00030	IGN	64
GAP04-C	570.32	570.46	570.39	535.99	0.14	793.99	48.26	0.00026	IGN	14
GAP04-D	670.20	670.31	670.25	629.83	0.11	656.80	48.64	0.00020	MGN	<1
GAP04-E	377.65	377.8	377.725	354.95	0.15	844.54	48.62	0.00028	FGN	38
GAP04-F	448.07	448.18	448.12	421.10	0.11	831.46	48.68	0.00020	IGN	32
GAP04-G	557.40	557.56	557.48	523.86	0.16	900.40	48.55	0.00030	IGN	6
GAP04-H	681.21	681.37	681.29	640.20	0.16	868.14	48.58	0.00030	IGN	<1

C.3.2.1 Experiments GAP04-E to -H

Samples acquired for out diffusion must preserve the in-situ saturated state of the rock core. To achieve the requirement of saturated rock, core material is wiped off quickly upon extraction and then packed immediately packaged following the methods described in Eichinger and Waber (2013) for the DH-GAP04 core. However, it was noted on unpacking that core and packaging appeared dry. Two samples (GAP04-E 377.55 and GAP04-H 681.21 m bhl) still had strong vacuum seals on the core packaging, indicating that it was unlikely evaporation and water loss had occurred from the core after packaging. The core may have been allowed to dry slightly before packing or another processes, such as mineral hydration, may be responsible for drying the core. The two other core samples (GAP04-F 448.03 and GAP04-G 557.40 m bhl) were noted to have poor vacuum seal and some oxidation was observed on the core exterior indicating these samples may have experienced evaporation after packaging. Issues with improperly preserved core (or another drying effect) were also noted by Eichinger and Waber (2013). At the completion of the out diffusion experiment, the re-saturated core sections (GAP04 E-H) had gained between 0.16 and 1.12 g of additional water.

Samples were unwrapped and uneven ends quickly cut to yield even core lengths (Table C-1) using a rock saw and ultrapure water. Dimensions of core sections (average length and diameter) were measured using callipers (± 0.01 mm). Lengths varied by less than 1 mm while diameters varied by less than 0.25 mm for a given section of core. Samples were then quickly wiped off to remove any excess water from cutting and weighed immediately. The out diffusion cells were prepared with known volumes of ultrapure water (Table C-1) and set in a warm shaker bath at 40 °C and 20 RPM to increase the diffusion rate. The matrix pore water and the water in the cells were then allowed to equilibrate with each other until constant Cl^- concentrations were reached in the cell. 11 sub-samples of 1 mL were removed over the testing period in order to monitor the Cl^- concentration.

After 275 days (GAP E-H), the cells were removed from the shaker bath and allowed to cool to room temperature. The cells were weighed and alkalinity (Hach digital titrator) and pH were measured immediately. It was discovered that the loss of water in the cells was less than the known volume removed for the sub samples, indicating that the cells were likely leaking slowly over the course of the experiment. As well, the wet weights of the sealed core samples (GAP04-E to -H) were greater than the weight of the core before the experiment suggesting the cores may not have been completely saturated before the experiment was initiated. This is supported by the dry appearance of the cores after unwrapping.

In order to determine the dry mass of the rock, the samples were broken up into smaller pieces and dried in an oven at 40 °C to prevent the loss of crystalline water from gypsum which would cause an overestimate of the water loss. After an initial drop in mass over the first 20 days, the core samples began to show fluctuations in weight without further loss compared to the weight at 20 days. One sample (GAP04-E) was removed to be dried under vacuum in a desiccator for

comparison. It is likely that oxidation occurring on the surface of the core samples is causing a spurious increase in mass. The sample (GAP04-E) showed a smooth drying curve once the sample was placed in the desiccator under vacuum.

C.3.2.2 Water Content Determinations

Gravimetric water content was determined using the dry and saturated core weights of GAP04-E to -H. The details of those calculations are described below.

Table C-3. Parameters used to calculated gravimetric water content in samples GAP04-E to -H. Gyp water represents difference in weight caused by the dissolution of gypsum and its replacement by test water.

Sample	Depth (length along core) (m)	Initial weight m_{Ti} (g)	Final Weight m_{Tf} (g)	Gyp water m_{wgyp} (g)	Difference in wet weights (g)	Total Initial m_T (g)	weight lost drying %	Mass pore-water m_{PW} (g)	gravimetric water content u %
E	377.55	844.54	844.7	0.136	0.16	844.84	0.26	2.21	0.26
F	448.03	831.46	832.12	0.041	0.66	832.16	0.16	1.34	0.16
G	557.4	900.4	900.57	0.351	0.17	900.92	0.28	2.53	0.28
H	681.21	868.14	869.26	0.002	1.12	869.26	0.21	1.80	0.21

Gravimetric water content (u) is calculated as:

$$u = \frac{m_{pw}}{m_T} \times 100 \qquad [C.3]$$

u = gravimetric water content (in %)

$\mathbf{m_{pw}}$ = mass of porewater

$\mathbf{m_T}$ = total saturated mass of core

The total saturated mass of the core under ideal circumstances is the initial wet weight of the core after unwrapping. However, it appears evaporation may have impacted the DH-GAP04 core. Core that was not fully saturated was also noted by Eichinger and Waber (2013). As well, the

dissolution of gypsum within the core and its replacement by test water must be accounted for. For the DH-GAP04 core, the total mass saturated mass of core is determined as:

$$m_T = m_{Ti} + (m_{Ti} - m_{Tf}) + m_{wgyp} \qquad [C.4]$$

Where $\mathbf{m_{Ti}}$ is the initial weight of the core before the experiment and after unwrapping. $\mathbf{m_{Tf}}$ is the final saturated mass of the core after the experiment and the difference between m_{Ti} and m_{Tf} is attributed to resaturation of pore space from which porewater had evaporated. $\mathbf{m_{wgyp}}$ is the difference in weight between the gypsum and the water that replaces it (Table C-4). The water is lighter than the gypsum and thus the difference between the initial and final weights of the core underestimates the amount of evaporation.

Gypsum solubilities ranging from 0.013 to 0.017 mol/L were used to calculate the mass of dissolved gypsum (Eichinger and Waber, 2013). It is assumed that porewaters are at equilibrium with respect to gypsum and that all additional SO_4^{2-} in the eluate is derived from gypsum dissolution. The concentration of SO_4^{2-} measured in the eluate that corresponds to a porewater saturated with gypsum is determined by the ratio of the porewater volume $\mathbf{(V_{PW})}$ to the test water volume $\mathbf{(V_{TW})}$ by:

$$SO4_{TW} = \frac{V_{PW}}{V_{TW}} \times SO4_{PW} \qquad [C.5]$$

$\mathbf{V_{pw}}$ is calculated using the petrophysics porosity in samples GAP04-A to -D and using water contents for GAP04-E to -H. $\mathbf{V_{pw}}$ calculated using porosities are likely an overestimate. SO_4^{2-} concentrations in testwaters based on gypsum saturated porewaters are in the range of 1.9×10^{-5} to 1.9×10^{-4} mol/L while measured values ranged from 1.7×10^{-4} to 2.9×10^{-2} mol/L (Table C-2).

Table C-4: Mass of gypsum dissolved from core samples. Porosities are from petrophysical measurements on adjacent core. Maximum and minimum values of gypsum dissolved are based on gypsum solubilities of 0.013 and 0.017 mol/L respectively.

S	Depth	Gravi-metric WC	Porosity (P)	V_{pw} (WC)	V_{pw} (P)	VTw:Vpw (WC)	VTw:Vpw (P)	SO_4 in eluate	Gypsum dissolved (m_{gyp})	
	(m)	%	%	mm3	mm3			mg/L	g - max	g -min
A	209.83		0.76		1989		252	30.2	0.023	0.021
B	352		0.23		682		713	37.4	0.031	0.031
C	570.32		1.14		3021		164	2800	2.485	2.483
D	670.2		0.92		1827		301	1490	1.465	1.464
E	377.65	0.26	0.43	2208	1274	108	187	564	0.236	0.235
F	448.07	0.16	0.36	1338	745	182	327	167.2	0.070	0.069
G	557.40	0.28	0.8	2524	2356	88	95	1554	0.616	0.614
H	681.21	0.21	0.4	1793	1195	128	192	15.86	0.003	0.001

The mass of gypsum dissolved in grams **(m_{gyp})** can then be converted to a volume (cm^3) by multiplying by 0.43 g/cm3. The volume of gypsum dissolved in cm3 is equivalent to the mass of water that replaces the dissolved gypsum **(m_{rw})** in grams. The mass difference between the dissolved gypsum and the water that replaces it can then be calculated by:

$$m_{wgyp} = m_{gyp} - m_{rw} \qquad [C.6]$$

C.3.2.3 Experiments GAP04-A to -D

Four experiments (GAP04-Ato -D) were run in a similar fashion to the out diffusion experiments (GAP04-E to -H). GAP04-Ato -D were run prior to the out diffusion experiments as a test run on non-preserved core. Conductivities were measured instead of analyzing Cl^- in subsamples. Conductivities had not yet stabilized in experiments GAP04-C and -D after 2328 hours, however the experiments were terminated at this time in order to initiate experiments GAP04-E to -H. Due to using unsealed core, heavily impacted by evaporation, and terminating some of the experiments before they had stabilized, limited information can be drawn from experiments A-D. However, isotopic results and ionic ratios may still be useful.

Additionally, gravimetric water contents were not experimentally determined. Instead, water connected porosity values (Table C-4) from petrophysical experiments conducted on adjacent sections of core at the Geological Survey of Finland (Harper et al., 2015).

C.3.2.4 Time Series Data

Time series sub samples are used to determine whether the test water has equilibrated with the porewater within the out diffusion cells. Small volumes of sample are removed to limited the effect on the ratio of test water to the rock volume as well as to avoid bringing the water level below the top of the core in the cell. In GAP04-A to -D the subsamples were analyzed for electrical conductivity (Table C-5). Subsamples from GAP04-E to -H were analyzed for Cl^- (Table C-6). Cl^- is more accurate means of determining whether steady state has been reached as conductivity may continue to rise due to gypsum dissolution after Cl^- has equilibrated.

The impact of leakage into the out diffusion cells in GAP04-E to -H is evident by the reduction in Cl- concentration in the last subsample and the final eluate (Table C-6). In order to estimate a minimum porewater Cl- concentration the maximum measured Cl- concentration was used as the final Cl- concentration (Table C-7). As Cl^- concentrations were not measured in all subsamples it was necessary to interpolate Cl^- concentrations in the unmeasured subsamples in order to account for the loss of Cl^- from the testwater in the subsamples (Table C-7). Overall the total mass of Cl^- removed from the subsamples is low relative to that in the final eluate.

Table C-5. Time series data for experiments A-D. EC (µS/cm) was monitored instead of Cl^-.

		A		B		C		D	
Date	hrs	Vss	EC	Vss	EC	Vss	EC	Vss	EC
2013-07-03 12:00	0:00								
2013-07-03 20:00	8:00	1	66	1	44	1	462	1	184
2013-07-04 8:00	20:00	1.01	65.6	1	45.3	1	499	1	261
2013-07-05 12:00	48:00	0.99	83.9	1	57.3	0.98	654	1	366
2013-07-08 12:00	120:00	1	121	1	71	1.1	941	1	499
2013-07-12 12:00	216:00	0.99	145	1	83	1	1110	1	567
2013-07-19 12:00	384:00	10	190	10	110	10	1388	10	746
2013-08-13 12:00	984:00	10	228	10	167	10	1726	10	930
2013-10-08 12:00	2328:00	10	296	10	235	10	2120	10	1182

Table C-6. Time series data for experiments E-H. Cl concentrations in mg/L. A subset of samples was analyzed for Cl^- concentrations and the remaining values were interpolated in between. The low concentrations in the final eluate versus the last time series is due to dilution from leakage from cells.

	Time	E		F		G		H	
Date	hrs	Vss	Cl	Vss	Cl	Vss	Cl	Vss	Cl
2013-12-23 12:30	0:00								
2013-12-23 20:15	7:45	1		1		1		1	
2013-12-24 11:30	23:00	0.9	6.8	1	8.6	1	1	1	3.4
2013-12-25 12:00	47:30	1		1		1		1	
2013-12-27 12:00	95:30	1	14.4	1.1	21.2	1	1.1	1.2	6.6
2013-12-31 12:00	191:30	0.9		1.2		1		1	
2014-01-09 12:00	407:30	1		1		1		1	
2014-01-24 12:00	767:30	1	21	1	28.8	1	8.9	1	7.5
2014-02-21 12:00	1439:30	1		1		1		1	
2014-03-26 12:00	2231:30	1		1		1		1	
2014-05-15 12:00	3431:30	1	20	1	28.4	1	11.7	1	8.3
2014-09-25 12:00	6623:30	final	12.02	final	16.54	final	2.56	final	4.64

Table C-7. GAP04-E to -H, Cl time series values used in porewater Cl^- calculations (Equation C.5). Red values are calculated using a simple linear interpolation (y = mx + b) until a maximum value is reached. Maximum measured concentrations are then carried forward through the rest of the time series. These assumptions, which likely do not fully account for the unknown degree of dilution due to cell leakage, allow for an estimate of the minimum porewater Cl concentration.

	Time	E		F		G		H	
Date	hrs	Vss	Cl	Vss	Cl	Vss	Cl	Vss	Cl
2013-12-23 12:30	0:00								
2013-12-23 20:15	7:45	1	2.3	1	2.9	1	0.3	1	1.1
2013-12-24 11:30	23:00	0.9	6.8	1	8.6	1	1	1	3.4
2013-12-25 12:00	47:30	1	9.4	1	12.9	1	1.0	1	4.5
2013-12-27 12:00	95:30	1	14.4	1.1	21.2	1	1.1	1.2	6.6
2013-12-31 12:00	191:30	0.9	15.3	1.2	22.3	1	2.2	1	6.7
2014-01-09 12:00	407:30	1	17.5	1	24.7	1	4.7	1	7.0
2014-01-24 12:00	767:30	1	21	1	28.8	1	8.9	1	7.5
2014-02-21 12:00	1439:30	1	21	1	28.8	1	9.6	1	7.7
2014-03-26 12:00	2231:30	1	21	1	28.8	1	10.4	1	7.9
2014-05-15 12:00	3431:30	1	21	1	28.8	1	11.7	1	8.3
2014-09-25 12:00	6623:30	final	21	final	28.8	final	11.7	final	8.3

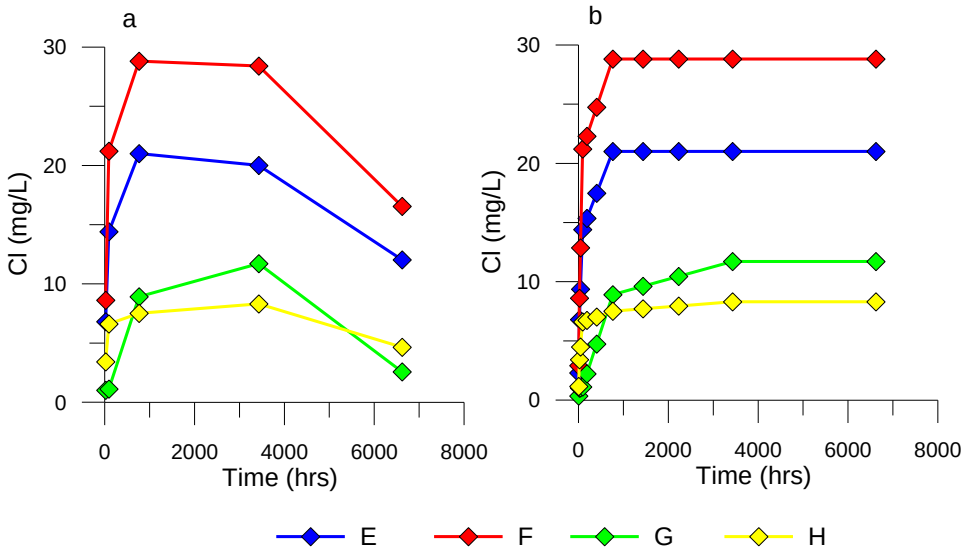

Figure C-1. Time series profiles for (a) measured Cl^- concentrations in sub samples and (b) the calculated Cl^- concentrations used in calculations.

C.3.2.5 Porewater Calculations

Concentrations measured in the final eluate must be corrected to porewater concentrations due to the difference in volume between the testwater and porewater. The following equation is used to determine the porewater concentration of an ion:

$$C_{pw} = \frac{(m_{pw}+m_{tw}-\sum_i^n m_{ss})\times C_{tw}+\sum_i^n m_{ss}\times C_i}{m_{pw}} \qquad [C.7]$$

C_{pw} = concentration of ion in porewater (by weight)

m_{tw} = mass testwater

m_{ss} = mass in subsample

C_i = concentration in subsample

C_{tw} = concentration in testwater at the end of the experiment

Time series data used for m_{ss} and C_i can be found in Table C-7.

Many elements, especially SO_4^{2-}, Ca^{2+} and Sr^{2+} do not behave in a conservative fashion. Eichinger and Waber (2013) found that only Cl^- and Br^- behaved conservatively during the out diffusion experiments. In the University of Waterloo experiments, Br- concentrations were not measured in the subsamples and Br- concentrations were non-detect in the final eluate waters of most of the out diffusion experiments. Thus porewater concentrations were only calculated for Cl^- using Equation C.7 above. Cl^- concentrations were not available for subsamples from GAP04-A to -D causing a small underestimate of the porewater Cl^- concentration. Porewater Cl^- concentrations for GAP04-E to -H are also likely underestimated due to dilution from the leaking cells that cannot be accounted for. The Cl^- concentrations in Table C-6 should be considered minimum values. Due to

the non-quantifiable nature of some of the issues encountered during the experiments, error for porewater Cl^- concentrations in GAP04-A to -D is considered to be 40% and 30% in GAP04-E to -H.

Table. C-8. Calculated porewater concentrations of Cl^- in GAP04-A to -H. This table is also included in Chapter 4 as Table 4.12.

Sample	Depth mbhl	Depth mbs	Lithology	Total C_{lss} mg/Kg_{H2O}	Cl_{TW} mg/Kg_{H2O}	Cl_{PW} mg/Kg_{H2O}	Error Cl_{PW} mg/Kg_{H2O}
A	209.83	197.18	MFGN		2.66	628	251
B	352	330.77	IGN		6.82	4527	1811
C	570.32	535.93	IGN		7.3	1122	449
D	670.2	629.78	IGN		1.54	436	174
E	377.55	354.78	FGN	0.15	20	2163	649
F	448.03	421.01	IGN	0.21	28.4	5144	1543
G	557.4	523.78	IGN	0.05	11.7	1020	306
H	681.21	640.13	IGN	0.06	8.3	1057	317

C.3.3. Matrix Porewater Geochemical and Isotopic Analyses

Chemistry of the out diffusion and crush and leach waters were analyzed at Labtium Oy (Finland), the York Durham Laboratory and Actlabs (Table 4.1). Samples analyzed by commercial analyses at Actlabs Inc. (Ancaster) for out diffusion samples and for the crush and leach analyses on core previously used for out diffusion (GAP04-E to -H) were analyzed under a high resolution ICP-MS package (code 6 HR-ICP/MS) which resulted in two samples from the crush and leach experiments exceeding the maximum allowable concentration (>100 mg/L). Isotopic analyses were performed at the University of Waterloo Environmental Isotope Laboratory following the methods described in (Chapter 1).

Table C-9. Chemistry and major ion ratios of the final eluate solutions from the University of Bern out diffusion experiments (GAP04-1 to -4) (Eichinger and Waber, 2013).

Sample	Depth mbhl	Depth mbs	Lithology	Na mg/L	K mg/L	Ca mg/L	Mg mg/L	Sr mg/L	F mg/L	Cl mg/L	Br mg/L	NO3 mg/L	SO4 mg/L	alkalinity meq/L	CBE %	pH
GAP04-1	501.5	473.4	IGN	218.1	12.2	524.8	61	7.7	0.18	18.4	<0.16	<0.16	2008	1.72	-3.22	7.4
GAP04-2	651.9	572.8	IGN	62.6	20.8	539.3	28.5	5.3	0.34	22.5	<0.16	<0.16	1581	1.46	-3.7	7.1
GAP04-3	557.7	526.5	IGN	97.4	15.7	559.2	33	7.9	<0.16	15.8	<0.16	<0.16	1750	1.35	-3.78	7.2
GAP04-4	607.7	615.5	FGN	58.3	3.3	48.2	5.2	1.2	0.07	20.5	0.12	<0.16	139.8	2.07	-0.76	7.6

Table C-9. continued.

Sample	Depth mbhl	Depth mbs	Lithology	Cl/SO4 mol/mol	Br/Cl mol/mol	Na/Cl mol/mol	Na/K mol/mol	Ca/SO4 mol/mol	Mg/SO4 mol/mol	Ca/Sr mol/mol
GAP04-1	501.5	473.4	IGN	0.025		18.32	30.34	0.63	0.12	149.5
GAP04-2	651.9	572.8	IGN	0.039	0.0034	4.29	5.12	0.81	0.07	222.2
GAP04-3	557.7	526.5	IGN	0.025		9.49	10.54	0.77	0.07	155.5
GAP04-4	607.7	615.5	FGN	0.398	0.00251	4.37	30.36	0.83	0.15	87

D. Appendix D. X-Ray Diffraction Patterns

D.1 Whole Rock X-Ray Diffraction Patterns

X-ray diffraction patterns for whole rock samples analyzed at the University of Waterloo. From Section 4.2.1.1: Rock samples for XRD analyses were powdered in an agate mortar. Diffraction data was collected on a Bruker D8 diffractometer using a sample holder that contained a silicon wafer cut parallel to the 511 Miller index. This type of holder allows for small aliquots of powder to be used. Diffraction data was collected between 10 and 70 °C for 2-theta angles using a step increment of 0.025 degrees with 1.25 second counts for each step. Diffraction data was indexed using the Joint Committee on Powder Diffraction Standards (JCPDS) database in identify the mineral phases in each sample.

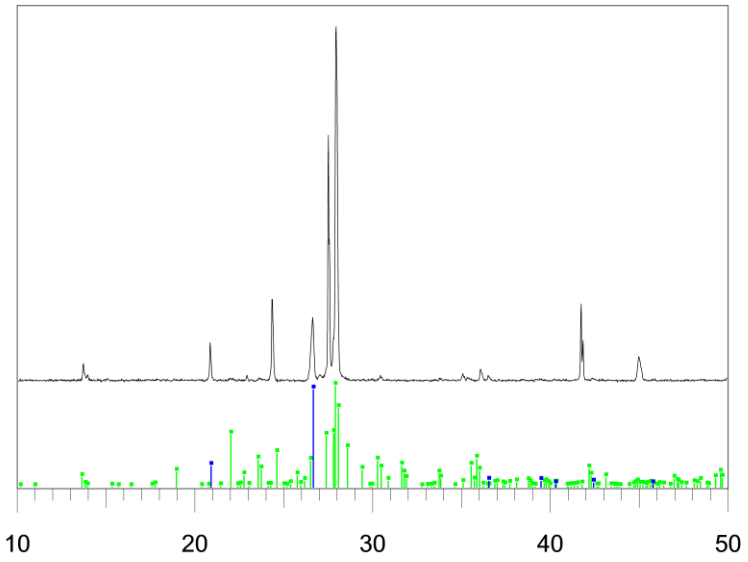

Figure D-1. DH-GAP04 289.76 m - Mafic gneiss transitioning to intermediate rock type. Green: anorthite, Blue: quartz.

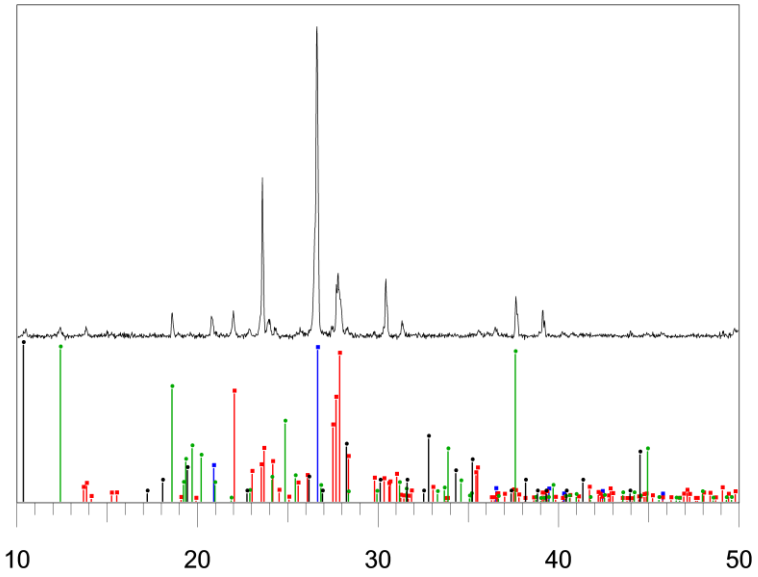

Figure D-2. DH-GAP04 377.65 m. Felsic gneiss. Blue: quartz, Red: albite, black: ferroactinolite, dark green: chlorite.

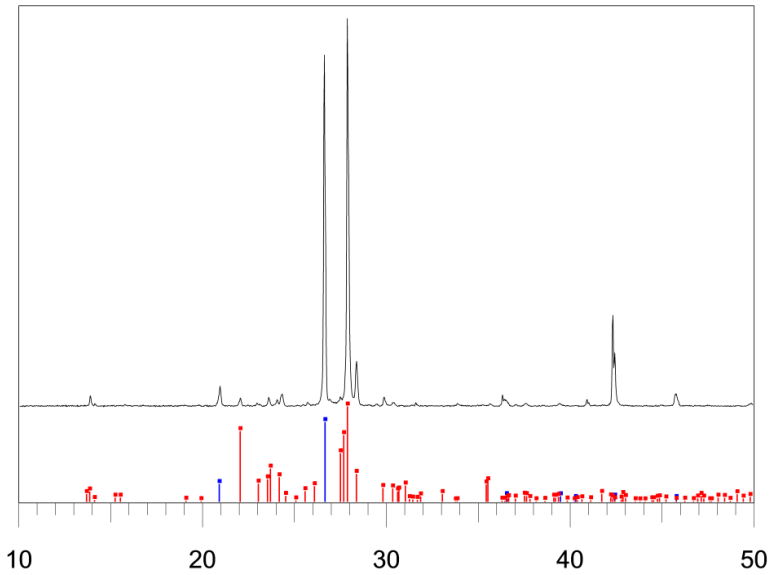

Figure D-3. DH-GAP04 399.84 m. Felsic gneiss. Red: albite, blue: quartz. Biotite was also visually observed in the sample.

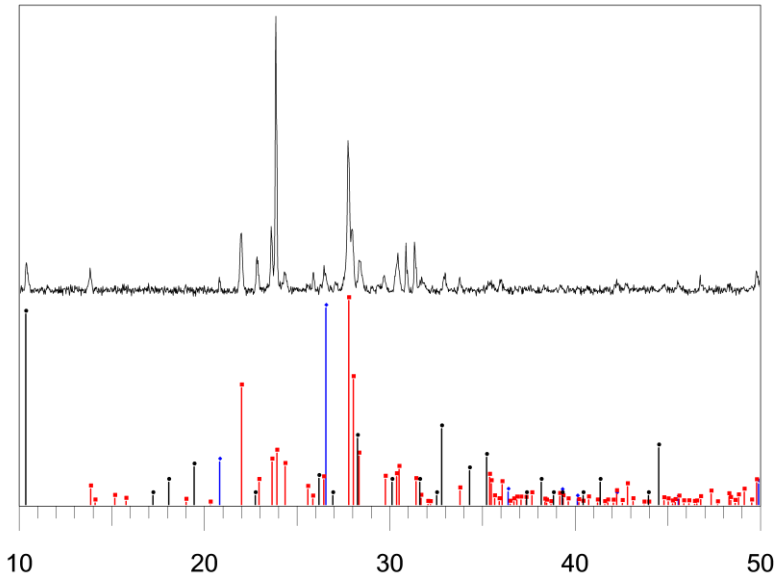

Figure D-4. DH-GAP04 557.40. Intermediate gneiss. Red: albite, blue: quartz, black: ferroactinolite.

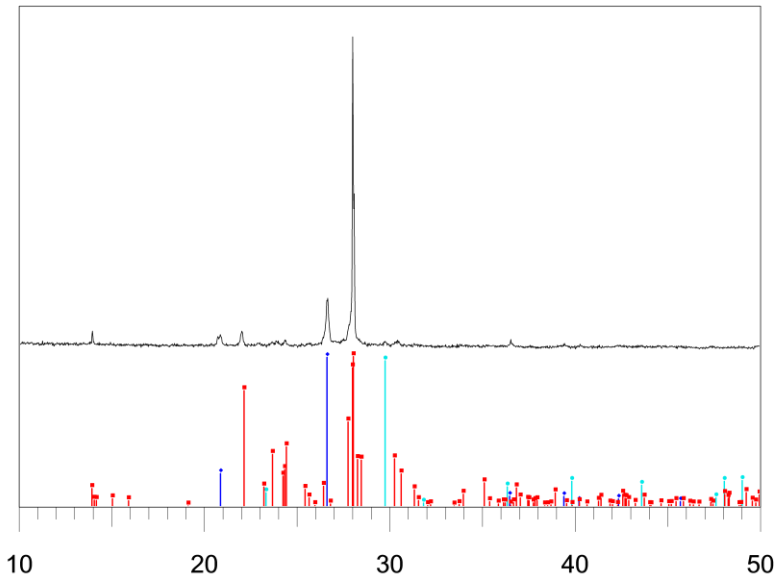

Figure D-5. DH-GAP04 570.07 m. Altered wall rock along fracture. Red: albite, blue: quartz, teal: calcite.

Figure D-6. DH-GAP04 570.07 m. Photo of alteration along fracture at 570.07m. Visually, chlorite was also present in sample.

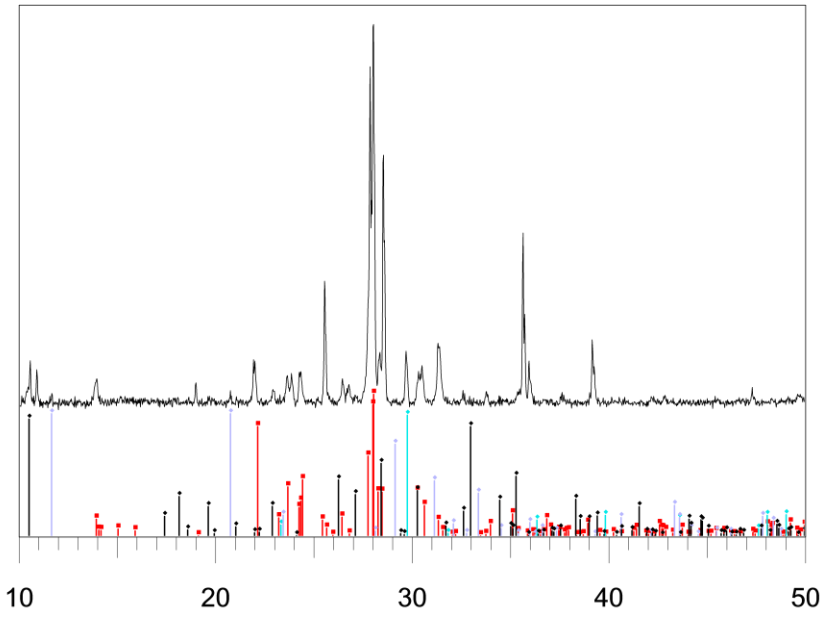

Figure D-7. DH-GAP04 570.59 m. Intermediate gneiss. Red: albite, black: ferroactinolite, teal: calcite, purple: gypsum.

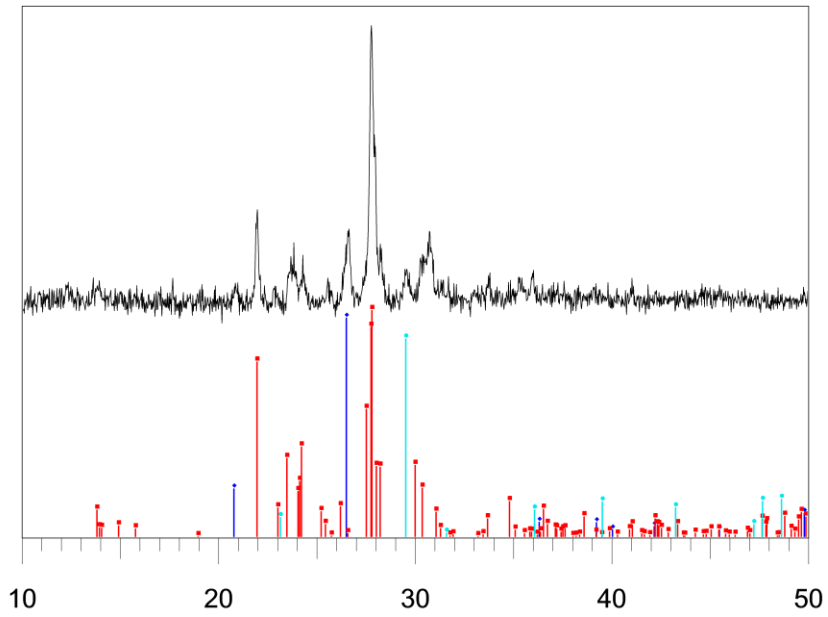

Figure D-8. DH-GAP04 638.85 m. Altered wall rock from fracture at this depth. Red: albite, blue: quartz, teal: calcite.

Figure D-9. DH-GAP04 638.85 m. Photo of alteration along fracture at 638.85 m.

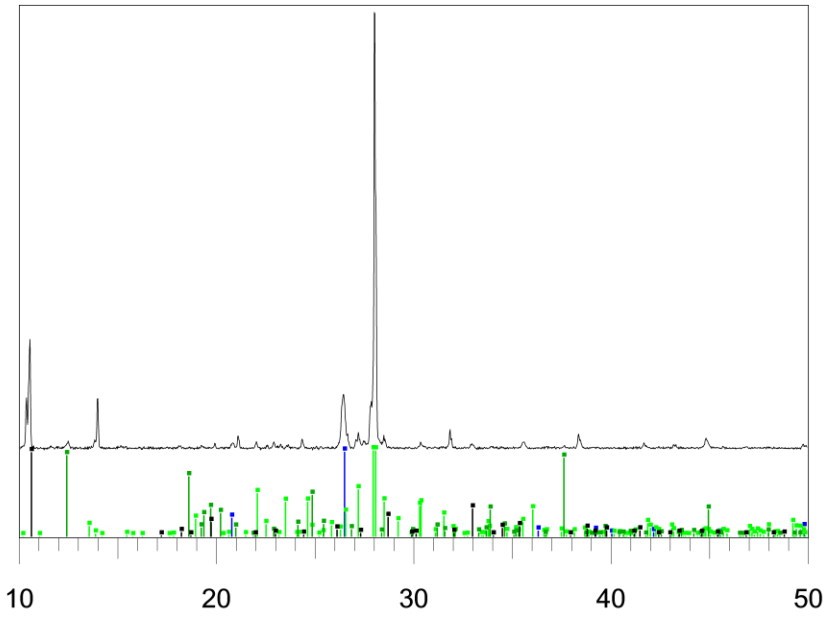

Figure D-10. DH-GAP04 670.20 m. Intermediate gneiss. Lime green: anorthite, black: ferroactinolite, blue: quartz, dark green: chlorite.

D.2. Fracture Mineral X-Ray Diffraction Patterns

Fracture mineral samples were anlayzed by XRD at the Geological Survey of Finland. From Section 4.2.2.2: Rock samples for XRD analyses were powdered in an agate mortar. Spectra were measured on a Bruker D8 Discover A25 Diffractometer over a range of 2θ 2-70° CuKα.

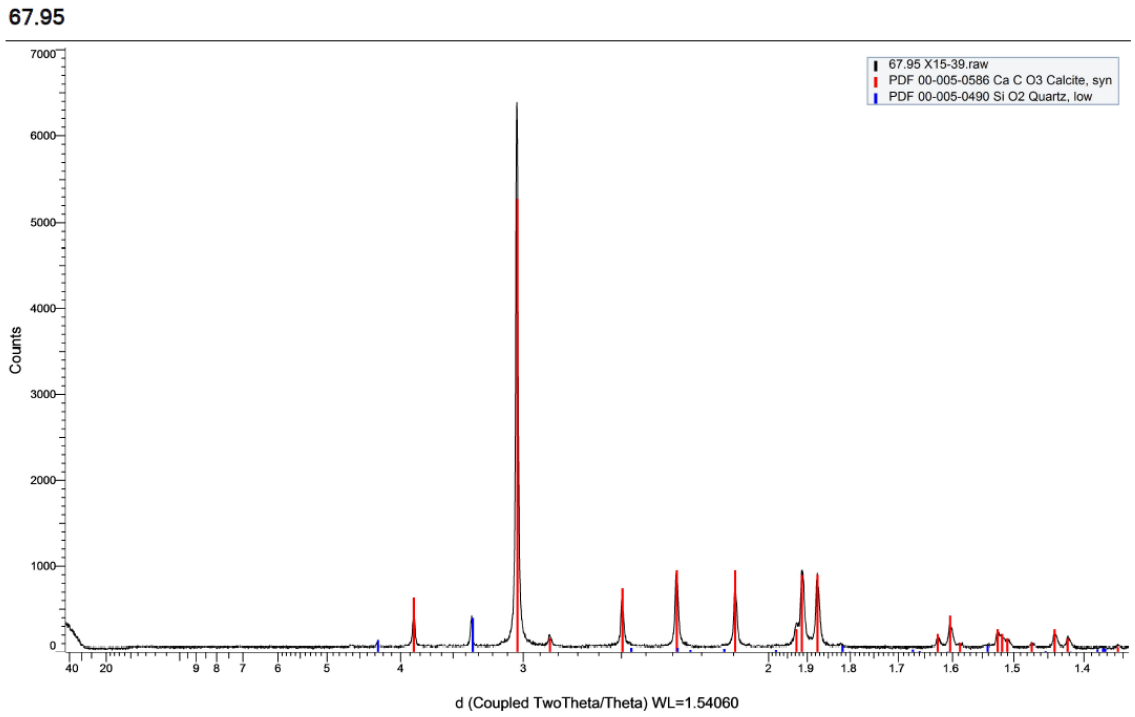

Figure D-11.DH-GAP04 67.95 m. Calcite and minor quartz.

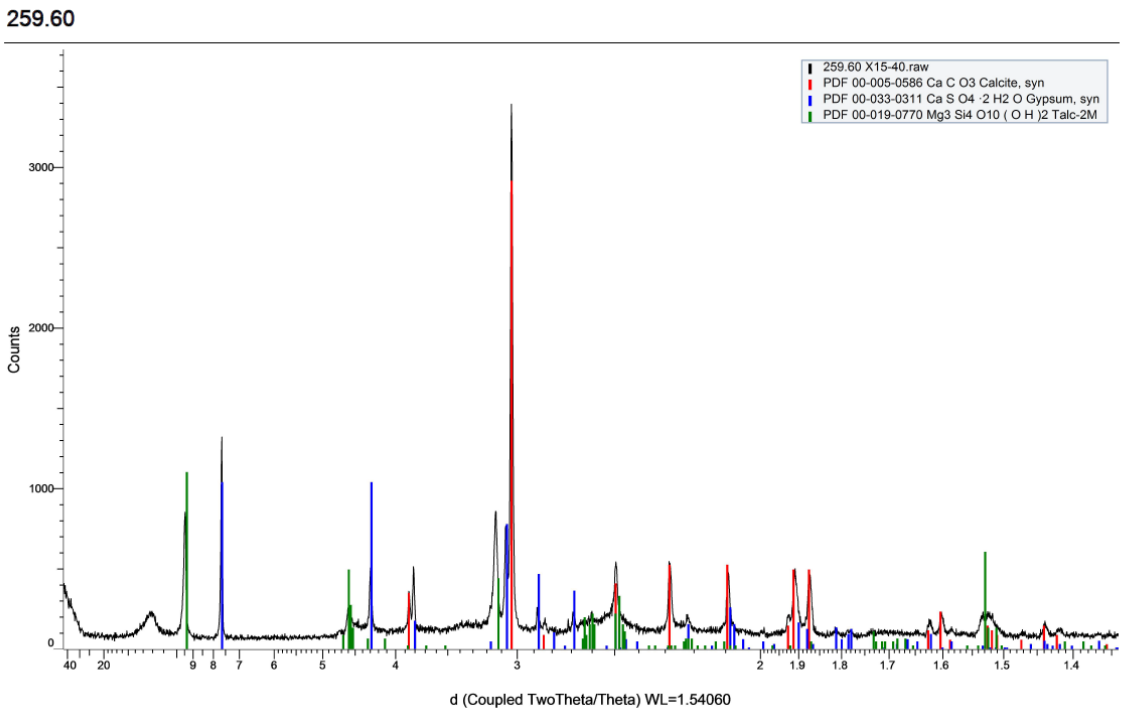

Figure D-12. DH-GAP04 259.60. Calcite, gypsum and talc.

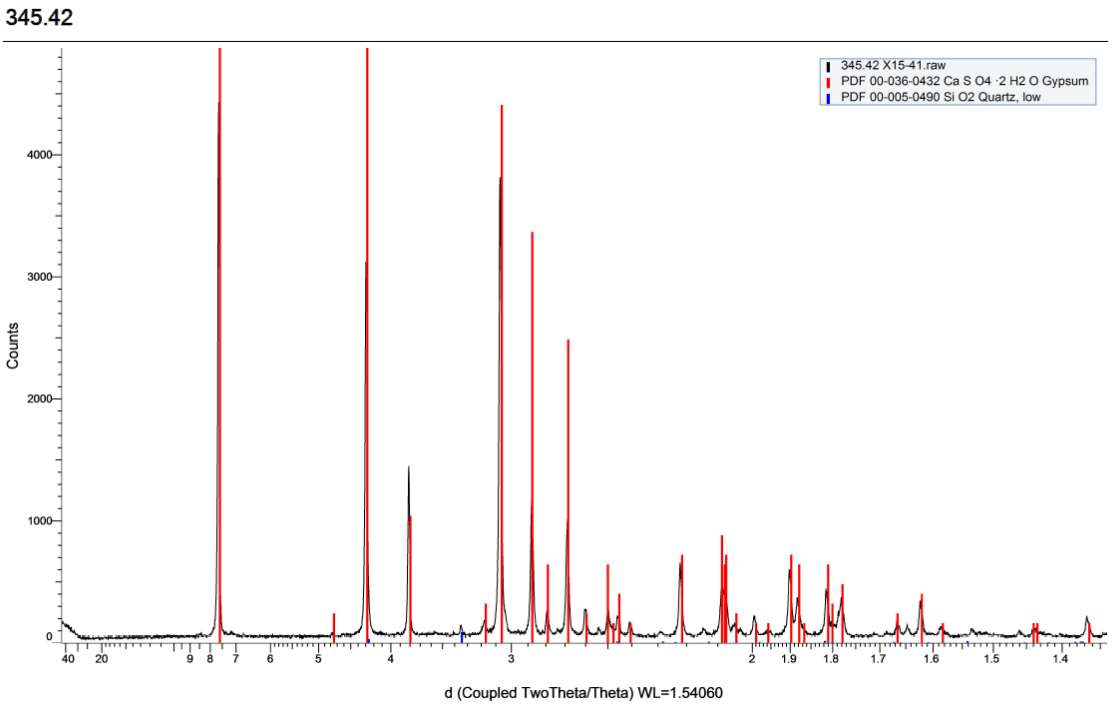

Figure D-13. DH-GAP04 345.42. Gypsum and minor quartz.

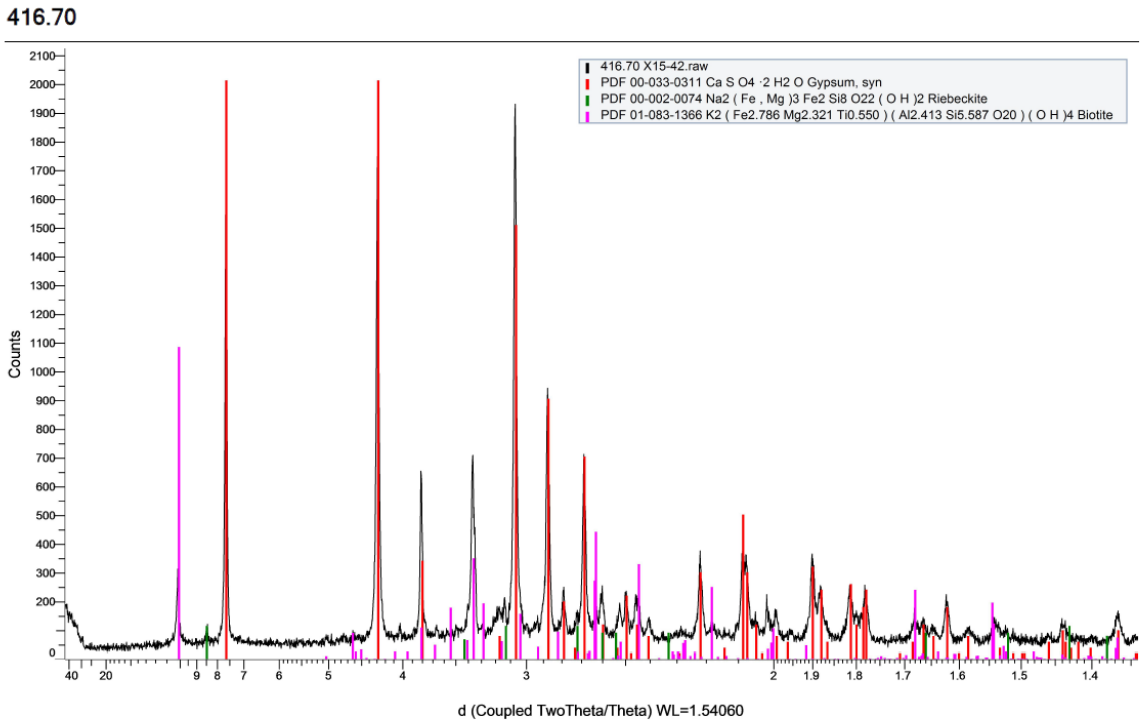

Figure D-14. DH-GAP04 416.70. Gypsum, Riebeckite and biotite.

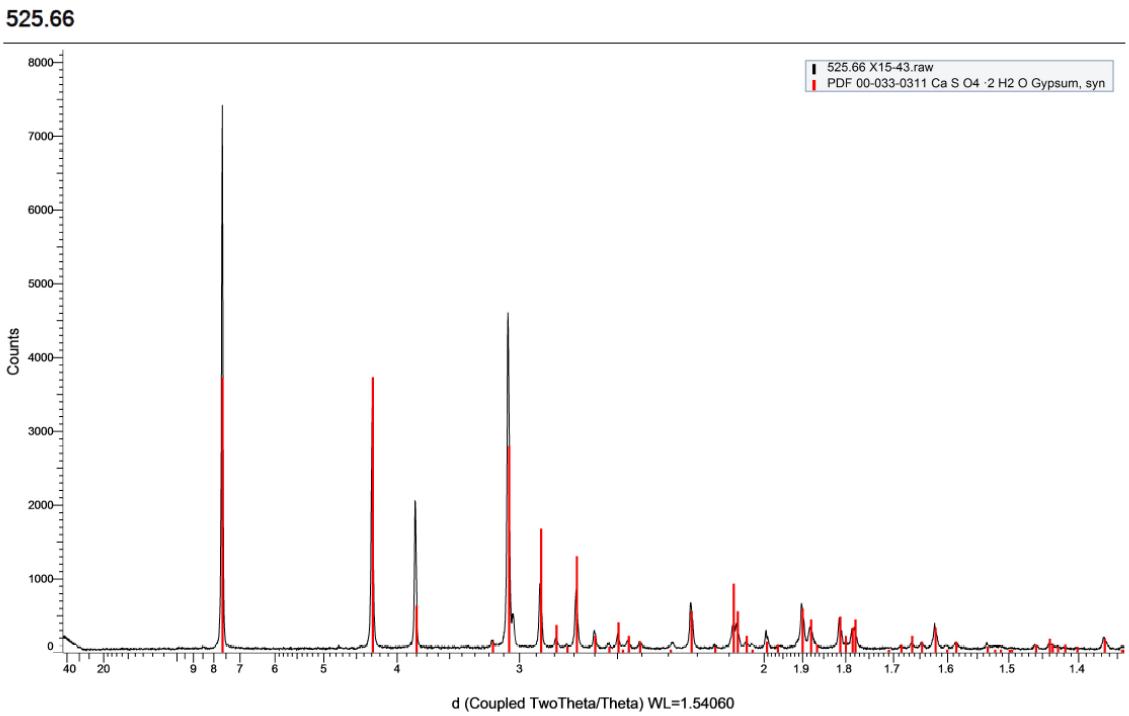

Figure D-15. DH-GAP04 525.66. Gypsum.

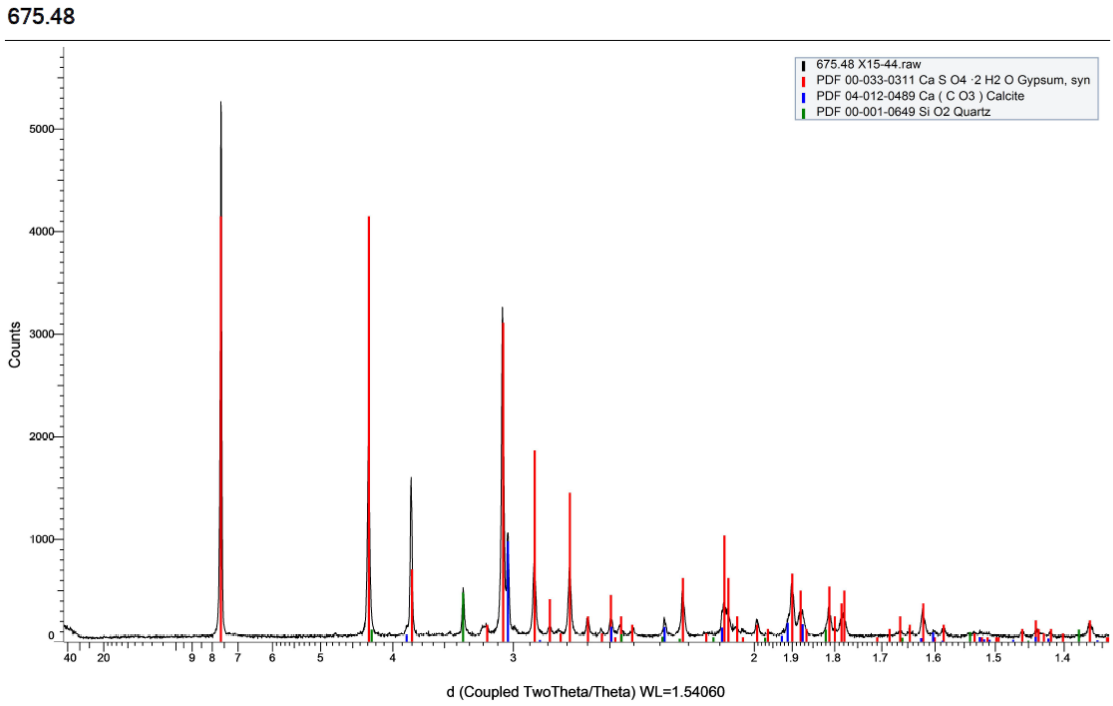

Figure D-16. DH-GAP04 675.48. Gypsum, calcite and quartz.